



UNIVERSITAT DE  
BARCELONA

## Synaptic transmission in autaptic circuits: presynaptic homeostatic plasticity and microtubule dynamics

Cecilia Velasco Domínguez

**ADVERTIMENT.** La consulta d'aquesta tesi queda condicionada a l'acceptació de les següents condicions d'ús: La difusió d'aquesta tesi per mitjà del servei TDX ([www.tdx.cat](http://www.tdx.cat)) i a través del Dipòsit Digital de la UB ([diposit.ub.edu](http://diposit.ub.edu)) ha estat autoritzada pels titulars dels drets de propietat intel·lectual únicament per a usos privats emmarcats en activitats d'investigació i docència. No s'autoritza la seva reproducció amb finalitats de lucre ni la seva difusió i posada a disposició des d'un lloc aliè al servei TDX ni al Dipòsit Digital de la UB. No s'autoritza la presentació del seu contingut en una finestra o marc aliè a TDX o al Dipòsit Digital de la UB (framing). Aquesta reserva de drets afecta tant al resum de presentació de la tesi com als seus continguts. En la utilització o cita de parts de la tesi és obligat indicar el nom de la persona autora.

**ADVERTENCIA.** La consulta de esta tesis queda condicionada a la aceptación de las siguientes condiciones de uso: La difusión de esta tesis por medio del servicio TDR ([www.tdx.cat](http://www.tdx.cat)) y a través del Repositorio Digital de la UB ([diposit.ub.edu](http://diposit.ub.edu)) ha sido autorizada por los titulares de los derechos de propiedad intelectual únicamente para usos privados enmarcados en actividades de investigación y docencia. No se autoriza su reproducción con finalidades de lucro ni su difusión y puesta a disposición desde un sitio ajeno al servicio TDR o al Repositorio Digital de la UB. No se autoriza la presentación de su contenido en una ventana o marco ajeno a TDR o al Repositorio Digital de la UB (framing). Esta reserva de derechos afecta tanto al resumen de presentación de la tesis como a sus contenidos. En la utilización o cita de partes de la tesis es obligado indicar el nombre de la persona autora.

**WARNING.** On having consulted this thesis you're accepting the following use conditions: Spreading this thesis by the TDX ([www.tdx.cat](http://www.tdx.cat)) service and by the UB Digital Repository ([diposit.ub.edu](http://diposit.ub.edu)) has been authorized by the titular of the intellectual property rights only for private uses placed in investigation and teaching activities. Reproduction with lucrative aims is not authorized nor its spreading and availability from a site foreign to the TDX service or to the UB Digital Repository. Introducing its content in a window or frame foreign to the TDX service or to the UB Digital Repository is not authorized (framing). Those rights affect to the presentation summary of the thesis as well as to its contents. In the using or citation of parts of the thesis it's obliged to indicate the name of the author.



UNIVERSITAT<sub>DE</sub>  
BARCELONA

**Synaptic transmission in autaptic circuits:  
presynaptic homeostatic plasticity  
and microtubule dynamics**

Cecilia Velasco Domínguez





UNIVERSITAT DE  
BARCELONA



Doctoral program in Biomedicine

**SYNAPTIC TRANSMISSION  
IN AUTAPTIC CIRCUITS:  
PRESYNAPTIC HOMEOSTATIC PLASTICITY  
AND MICROTUBULE DYNAMICS**

Doctoral Thesis

**Cecilia Velasco Domínguez**

Laboratory of Cellular and Molecular Neurobiology  
Department of Pathology and Experimental Therapeutics  
Faculty of Medicine and Health Sciences, University of Barcelona  
Bellvitge Biomedical Research Institute (IDIBELL)

**Author**

Cecilia Velasco Domínguez

**Thesis directors**

Artur Llobet Berenguer

Beatrice Terni

CECILIA  
VELASCO  
DOMINGUEZ -  
DNI  
47929530Z

Firmado  
digitalmente por  
CECILIA VELASCO  
DOMINGUEZ - DNI  
47929530Z  
Fecha: 2022.01.25  
12:17:46 Z





This thesis work has been supported by the predoctoral fellowship Formación de Personal Investigador (FPI) (BES-2016-076551) and sponsored by the Spanish government Ministerio de Economía y Competitividad (MINECO; SAF2015-63568-R; to A.L.), and Ministerio de Ciencia e Innovación (MICINN; RTI2018-096948-B-100; to A.L.) co-funded by the European Regional Development Fund (ERDF).

The PhD candidate Cecilia Velasco Domínguez also received support from the Institut de Neurociències of the University of Barcelona for a national congress.

The studies presented in this thesis were performed at the Laboratory of Cellular and Molecular Neurobiology under the supervision of Dr. Artur Llobet and Dr. Beatrice Terni in the Department of Pathology and Experimental Therapeutics at the Faculty of Medicine and Health Sciences of the University of Barcelona.



UNIVERSITAT DE  
BARCELONA



Institut de Neurociències  
UNIVERSITAT DE BARCELONA



*To my mum, my sister and Marc, for giving me  
the strength to take every step of the way.*

*"You must unlearn what you have learned"*

-Yoda



|   |  |           |
|---|--|-----------|
| ■ | <b>GLOSSARY OF ABBREVIATIONS</b>   | <b>1</b>  |
| ■ | <b>ABSTRACT</b>  | <b>5</b>  |
| ■ | <b>INTRODUCTION</b>  | <b>7</b>  |
|   | <b>1. Principles of neurotransmission</b>  | <b>9</b>  |
|   | 1.1 The synapse  | 10        |
|   | 1.1.1. The Presynaptic terminal  | 11        |
|   | 1.1.2. The postsynaptic terminal   | 16        |
|   | 1.2 Modes of synaptic transmission   | 17        |
|   | 1.3 Quantification of synaptic transmission                                      | 20        |
|   | <b>2. Synaptic plasticity</b>  | <b>23</b> |
|   | 2.1 Short-term synaptic plasticity   | 24        |
|   | 2.2 Homeostatic synaptic plasticity  | 26        |
|   | 2.2.1 Synaptic scaling   | 27        |
|   | 2.2.2 Presynaptic homeostatic plasticity   | 29        |
|   | <b>3. Synapses and development</b>   | <b>32</b> |
|   | 3.1 Synapse formation  | 32        |
|   | 3.2 Synapse elimination  | 36        |
|   | 3.3 Role of SPARC in synapse elimination   | 41        |
|   | 3.4 Homeostatic synaptic plasticity during development                           | 45        |
|   | <b>4. Role of the cytoskeleton in synaptic transmission</b>                      | <b>46</b> |
|   | 4.1 The synaptic actin cytoskeleton  | 46        |
|   | 4.2 Synaptic microtubules  | 50        |
|   | 4.2.1 Localization of microtubules in the synapse                                | 52        |
|   | 4.2.2 Dynamic microtubules and cargo transport                                   | 53        |
|   | 4.2.3 Microtubules and synaptic transmission                                     | 53        |
|   | 4.2.4 Manipulations of the microtubule cytoskeleton                              | 54        |
|   | <b>5. Use of autaptic neuronal cultures to investigate synaptic transmission</b> | <b>62</b> |
|   | 5.1 Autaptic connections <i>in vivo</i>  | 62        |
|   | 5.2 Autaptic neurons <i>in vitro</i>   | 64        |
| ■ | <b>OBJECTIVES</b>  | <b>67</b> |
| ■ | <b>MATERIALS AND METHODS</b>   | <b>71</b> |
|   | <b>1. Cell culture</b>   | <b>73</b> |
|   | 1.1 Single Cell Microcultures  | 73        |
|   | 1.1.1 Materials  | 73        |
|   | 1.1.2 Procedure for establishing SCMs  | 75        |
|   | 1.1.3 SCM maintenance and treatment  | 79        |
|   | 1.2 Cell lines culture   | 81        |
|   | 1.2.1 HEK293T cells  | 81        |

|  |            |
|--|------------|
| 1.2.2 CHO cells  | 81         |
| <b>2. Production of high-titer HIV-1-based vector lentivirus</b>             | <b>82</b>  |
| 2.1 Materials and reagents   | 82         |
| 2.1.1 Material   | 82         |
| 2.1.2 Solutions  | 82         |
| 2.1.3 Plasmids   | 83         |
| 2.2 Precautions  | 83         |
| 2.3 Procedure  | 83         |
| 2.4 Infection of SCMs with SyGCaMP6f lentivirus                              | 86         |
| 2.4.1 Procedure  | 86         |
| <b>3. Electrophysiological recordings</b>                                    | <b>87</b>  |
| 3.1 Instruments and solutions  | 87         |
| 3.1.1 Instruments for Patch-Clamp experiments                                | 87         |
| 3.1.2 Solutions for Patch-Clamp experiments                                  | 91         |
| 3.2 Patch clamp techniques   | 92         |
| 3.2.1 Voltage clamp  | 92         |
| 3.2.2 Current clamp  | 94         |
| 3.3 Analysis of voltage clamp recordings                                     | 94         |
| 3.3.1 Evoked neurotransmission   | 94         |
| 3.3.2 Functional RRP measurement   | 94         |
| 3.3.3 Spontaneous neurotransmission  | 95         |
| <b>4. Simultaneous electrophysiological recording and imaging</b>            | <b>97</b>  |
| 4.1 Analysis of imaging data simultaneous to electrophysiological recordings | 98         |
| <b>5. Immunocytochemistry</b>  | <b>99</b>  |
| 5.1 Confocal microscopy  | 99         |
| 5.1.1 Immunocytochemistry of SCMs  | 99         |
| 5.1.2 Correlative electrophysiology and immunocytochemistry                  | 100        |
| 5.1.3 Immunocytochemistry of CHO cells                                       | 101        |
| 5.2 STED microscopy  | 102        |
| 5.2.1 Actin-ring like structures in SCMs                                     | 102        |
| 5.2.2 Identification of microtubule plus-ends in SCMs                        | 103        |
| 5.2.3 STED microscopy image acquisition                                      | 104        |
| <b>6. Transmission electron microscopy</b>                                   | <b>105</b> |
| 6.1 Materials and protection equipment                                       | 105        |
| 6.1.1 Material   | 105        |
| 6.1.2 Protection equipment   | 106        |

|   |            |
|---|------------|
| 6.2 Solutions and reagents  | 106        |
| 6.3 Procedure   | 107        |
| 6.4 Sample processing   | 110        |
| 6.5 Segmentation and 3D modelling   | 110        |
| <b>7. Photopharmacology</b>   | <b>111</b> |
| 7.1 Photoswitchable molecules   | 111        |
| 7.1.1 Photostatins  | 111        |
| 7.1.2 SBTubs  | 112        |
| 7.2 Handling and storage  | 112        |
| 7.3 Experimental protocol and conditions  | 113        |
| 7.3.1 Incubation  | 113        |
| 7.3.2 Experimental protocol   | 113        |
| 7.3.3 Illumination set up   | 113        |
| <b>8. Statistics and reproducibility</b>  | <b>114</b> |
| <b>RESULTS</b>  | <b>115</b> |
| <b>1. Characterization of the capability of SPARC to eliminate synapses in an autaptic circuit</b>              | <b>117</b> |
| 1.1 Time course of the effect of the SPARC-derived peptide p4.2 in synaptic strength                            | 118        |
| 1.2 Characterization of synapse markers to evaluate changes in synapse numbers                                  | 119        |
| 1.3 Evaluation of changes in synaptic connectivity during exposure to p4.2                                      | 123        |
| <b>2. Compensation of synapse elimination by a mechanism of homeostatic synaptic plasticity</b>                 | <b>126</b> |
| 2.1 Changes in RRP size as part of the presynaptic homeostatic response   | 126        |
| 2.2 Characterization of presynaptic calcium influx in individual autaptic contacts using the SyGCaMP6f reporter | 127        |
| 2.3 Changes in presynaptic calcium influx as part of the presynaptic homeostatic response                       | 127        |
| 2.4 Study of the effect of peptide p4.2 on the density of cholinergic postsynaptic receptors                    | 130        |
| <b>3. Study of the action of peptide p4.2 in the neuronal F-actin cytoskeleton</b>                              | <b>133</b> |
| 3.1 Study of the ability of peptide p4.2 to reorganize the F-actin cytoskeleton in cell lines                   | 133        |
| 3.2 Study of the effect of p4.2 on the periodic actin skeleton present in neurites                              | 135        |



|  |            |
|--|------------|
| 3.3 Time course of presynaptic F-actin reorganization induced by peptide p4.2  | 136        |
| 3.4 Stabilization of the F-actin cytoskeleton and its effect on the action of peptide p4.2                             | 138        |
| <b>4. Distribution of microtubules at synaptic terminals</b>   | <b>141</b> |
| 4.1 Location of microtubules in dendrites and presynaptic terminals of autaptic neurons                                | 141        |
| 4.2 Study of the presence of microtubule plus-ends at presynaptic terminals  | 143        |
| <b>5. Effect of microtubule polymerization on synaptic transmission</b>  | <b>146</b> |
| <b>6. Effect of microtubule depolymerization on synaptic transmission</b>  | <b>150</b> |
| 6.1 Study of the effect of MT depolymerization induced by photo controllable molecules on synaptic transmission        | 150        |
| 6.2 Effect of MT depolymerization on postsynaptic function   | 158        |
| 6.3 Study of the effect of MT depolymerization produced by KIF18A activity on synaptic transmission                    | 159        |
| <b>7. Characterization of the nature of synaptic vesicles released spontaneously upon microtubule depolymerization</b> | <b>161</b> |
| <b>DISCUSSION</b>  | <b>165</b> |
| <b>CONCLUSIONS</b>   | <b>179</b> |
| <b>REFERENCES</b>  | <b>183</b> |
| <b>ANNEXES</b>   | <b>221</b> |
| Annex 1. Collagen production   | 223        |
| Annex 2. Solutions   | 225        |
| <b>PUBLICATIONS</b>  | <b>227</b> |



# **GLOSSARY OF ABBREVIATIONS**



**A**

A: amp, unit for measuring current (nA, nanoamp; pA, picoamp)  
 ABP: actin-binding protein  
 Ach: acetylcholine  
 AchR: cholinergic receptor  
 ADBE: activity-dependent bulk endocytosis  
 ADP: adenosine diphosphate  
 AMPA:  $\alpha$ -amino-3-hydroxy-5-methyl-4-isoxazolepropionic acid  
 AP: action potential  
 ATP: adenosine triphosphate  
 AZ: active zone

**B**

BafA1: bafilomycin A1  
 BDNF: brain-derived neurotrophic factor  
 BSA: bovine serum albumin

**C**

CA-4: combrestatin A-4  
 $Ca_{local}$ : local calcium  
 $Ca_{residual}$ : residual calcium  
 CaMKII: calcium calmodulin kinase II  
 CAZ: active zone cytomatrix proteins  
 CCA: common carotid artery  
 CDK5: cyclin-dependent kinase 5  
 CHO: Chinese hamster ovary  
 CME: clathrin-mediated endocytosis  
 CNS: central nervous system  
 CNTF: ciliary neurotrophic factor

**D**

DIV: days in vitro  
 dLGN: dorsal lateral geniculate nucleus  
 DMEM: Dulbecco's Modified Eagle Medium  
 DMSO: Dimethyl sulfoxide

**E**

EB: microtubule end-binding protein  
 EB3: microtubule end-binding protein 3  
 EC: EF-hand calcium binding site  
 EC: effective concentration  
 ECA: external carotid artery  
 ECM: extracellular matrix  
 EDTA: ethylenediaminetetraacetic acid  
 EM: electron microscopy  
 EPSC: excitatory postsynaptic current  
 EPSP: excitatory postsynaptic potential

**F**

F-actin: filamentous actin  
 FBS: foetal bovine serum  
 FS: follistatin-like

**G**

GABA:  $\gamma$ -aminobutyric acid  
 G-actin: globular actin (monomeric)  
 GFP: green fluorescent protein  
 GluRIIA: glutamate receptor IIA  
 GTP: guanosine triphosphate  
 GDP: guanosine diphosphate

**H**

HEK: human embryonic kidney  
 Hz: hertz, unit for measuring frequency

**I**

ICA: internal carotid artery  
 ICC: immunocytochemistry  
 IPSP: inhibitory postsynaptic potential

**K**

KIF18A: Kinesin Family Member 18A

**L**

Lat-A: latrunculin-A  
 LTD: long-term depression  
 LTP: long-term potentiation

**M**

MAP: microtubule-associated proteins  
 MBP: microtubule bound pool  
 MEM: Minimum Essential Medium Eagle  
 mEPSC: miniature excitatory postsynaptic current  
 MOI: multiplicity of infection  
 MQ: mili-Q  
 MT: microtubule

**N**

N: release site  
 nAChR: nicotinic acetylcholine receptors  
 NA: numerical aperture  
 ND: neutral density filter  
 NG: nodose ganglion  
 NGF: nerve growth factor  
 NGS: normal goat serum  
 NMJ: neuromuscular junction

**P**

Pr: probability  
 P/S: penicillin/streptomycin  
 P#: postnatal day #  
 PBS: phosphate buffered saline

PFA: paraformaldehyde  
 PHP: presynaptic homeostatic plasticity  
 PhTx: philanthotoxin  
 PNS: peripheral nervous system  
 PP: paired pulse  
 PPR: paired pulse ratio  
 PSD: postsynaptic density  
 PST: photostatin  
 PTP: posttetanic potentiation  
 PV: precursor vesicle

**Q**

q: quantal size

**R**

RGC: retinal ganglion cell  
 ROI: region of interest  
 RP: recycling pool  
 RRP: readily releasable pool  
 RS: rat serum  
 RT: room temperature  
 RtP: resting pool

**S**

SEM: standard error of the mean  
 SBT: styrylbenzothiazole  
 SBTab: styrylbenzothiazole-based micro-  
 tubule inhibitor  
 sCAMs: cell-adhesion molecules  
 SCG: superior cervical ganglia  
 SCM: single cell microculture  
 SPARC: secreted protein acidic and rich  
 in cysteine  
 STED: stimulated emission depletion  
 microscopy  
 STP: short-term potentiation  
 SV: synaptic vesicle  
 SV40T: SV40 large T antigen  
 SyGCaMP6f: synaptophysin-GCamp6f  
 Syt1: synaptotagmin 1

**T**

TEM: transmission electron microscopy  
 TGF- $\beta$ : transforming growth factor  $\beta$   
 TIP: plus-end tracking protein  
 TOR: target of rapamycin  
 TRP: total recycling pool  
 TSP: thrombospondin  
 TTX: tetrodotoxin  
 TX-100: triton X-100

**U**

UV: ultraviolet

**V**

V: volts, unit for measuring electric poten-  
 tial (mV, millivolt)  
 VAMP-2: vesicle associated membrane  
 protein 2  
 vATPase: vacuolar H<sup>+</sup>-ATPase  
 v/v: volume per volume  
 VGCC: voltage-gated calcium channel  
 vGLUT: vesicular glutamate transporter  
 V<sub>m</sub>: membrane potential

**W**

w/v: weight per volume

**Y**

YFP: yellow fluorescent protein



# ABSTRACT

Synapses are the contact sites where the transfer of information from the presynaptic to the postsynaptic site occurs. Correct processing of information requires that synapses continuously adapt their properties to an ever-changing environment. Here, we describe novel aspects that help understand the function of presynaptic terminals in the context of a simple neuronal network.

The exuberant number of synaptic contacts formed during the development of the nervous system is selectively refined by a process of synapse elimination. In the current thesis we have exploited the action of peptide p4.2, a 20 amino acid fragment located in the C-terminus of the glial secreted protein SPARC, which promotes synapse elimination in an autaptic circuit. We found that neurons forming autaptic synapses sense and compensate for synapse elimination by activating a mechanism of presynaptic homeostatic plasticity driven by presynaptic potentiation and rapid assembly of new synaptic contacts. Both actions occur concomitantly, indicating that the formation of novel synapses is associated to an overall increase in presynaptic calcium influx. To further investigate the molecular mechanisms underlying this compensatory response, we moved our interests to the participation of microtubules in the maintenance of synaptic connectivity and synaptic strength. This question could only be addressed by gaining a better understanding of the participation of microtubules in presynaptic terminal function.

By providing ultrastructural, morphological, and physiological evidence we have shown that microtubule plus-ends transiently invade presynaptic boutons and that microtubule instability is directly involved in the regulation of spontaneous neurotransmitter release probability. Microtubule polymerization is also important to postsynaptic function, indicating microtubule dynamics might be involved in forms of postsynaptic plasticity.

Altogether, the development of this project has allowed to identify yet unknown mechanisms key for better understanding the cell biology of presynaptic terminals. These findings should not only be considered in the context of a simple neuronal network, chosen because of its unique experimental possibilities, but as fundamental neuronal properties. Yet, future research in complex systems are required to further validate our findings.



# RESUMEN

Las sinapsis son los sitios de contacto donde ocurre la transferencia de información desde el terminal presináptico al postsináptico. El correcto procesamiento de información requiere que las sinapsis adapten continuamente sus propiedades bajo un entorno de constante cambio. En esta tesis describimos aspectos novedosos que ayudan a comprender la función de los terminales presinápticos en el contexto de una red neuronal simple.

El número exuberante de contactos sinápticos formados durante el desarrollo del sistema nervioso se refina selectivamente mediante un proceso de eliminación sináptica. En la presente tesis hemos explotado la acción del péptido p4.2, un fragmento de 20 aminoácidos situado en el extremo C-terminal de la proteína de secreción glial SPARC, que promueve la eliminación de sinapsis en un circuito autáptico. Hemos descubierto que las neuronas que forman sinapsis autápticas detectan y compensan la eliminación sináptica activando un mecanismo de plasticidad homeostática presináptica impulsado por la potenciación presináptica y el rápido ensamblaje de nuevos contactos sinápticos. Ambas acciones ocurren de manera concomitante, lo que indica que la formación de nuevas sinapsis está asociada con un aumento general en el flujo de entrada de calcio presináptico. Para investigar más a fondo los mecanismos moleculares que subyacen a esta respuesta compensatoria, trasladamos nuestro foco de investigación a la participación de los microtúbulos en el mantenimiento de la conectividad y fuerza sináptica.

Proporcionando evidencia ultraestructural, morfológica y fisiológica, hemos demostrado que los extremos positivos de los microtúbulos invaden transitoriamente los botones presinápticos y que la inestabilidad de los microtúbulos está directamente involucrada en la regulación de la probabilidad de liberación espontánea de neurotransmisores. La polimerización de microtúbulos también es importante para la función postsináptica, lo que indica que la dinámica de los microtúbulos podría estar involucrada en formas de plasticidad postsináptica.

El desarrollo de este proyecto ha permitido identificar mecanismos aún desconocidos que son clave para entender la biología celular de los terminales presinápticos. Estos hallazgos no solo deben considerarse en el contexto de una red neuronal simple, elegida por sus posibilidades experimentales únicas, sino como propiedades neuronales fundamentales. Sin embargo, futuras investigaciones en sistemas complejos son necesarias para validar nuestros hallazgos.



# INTRODUCTION





# 1 Principles of neurotransmission

The brain is formed by more than a hundred billion neurons and glial cells. As firstly described by Santiago Ramon y Cajal in 1888 (López-Muñoz et al., 2006), neurons are the signalling units of the nervous system, and communicate through electrical signals. Neurons are uniquely polarized cells for receiving and transmitting information and due to their morphological asymmetry, information flow is unidirectional: the dendrites are the receptive part, and the axon is the transmitting element (Fig. 1).

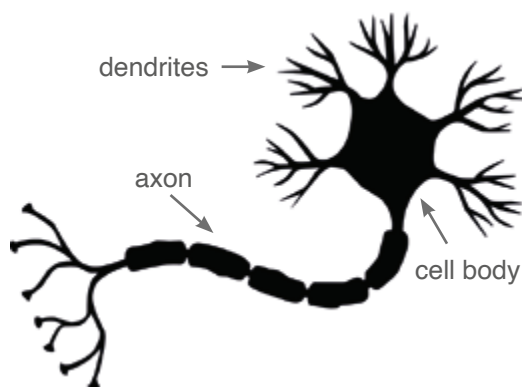


**Figure 1. Schematic representation of a neuron.**

Each neuron can be organized in three regions with specific roles. The cell body contains the nucleus, endoplasmic reticulum and Golgi apparatus, and is where metabolic processes and protein synthesis take place. The dendrites, branching out in a tree-like fashion from the soma, receive input signals from other neurons. The axon, extending from the cell body, carries information to other nerve cells.

The brain receives, analyses, and transmits information using signals in the form of **action potentials** (APs). The AP, first recorded in the squid giant axon by Hodgkin and Huxley in 1939 (Hodgkin & Huxley, 1939), is a highly cooperative all-or-none signal whose initiation depends on surpassing a voltage threshold. The ability of neuronal cells to generate an AP relies on their electrical properties. The neuron's plasma membrane acts as a diffusion barrier between two conducting solutions, the cytoplasm and the extracellular media. The different concentration of charges across the membrane, being more negative in the inside, gives rise to a difference of voltage, called membrane potential ( $V_m$ ). Changes in the resting membrane potential generate neuronal signals in the form of depolarizations (less negative potential) or hyperpolarizations (more negative potential). These changes are caused by the flow of ions across the cell membrane through ion channels. Two important types of ion channels conducting  $K^+$ ,  $Na^+$  or  $Cl^-$  control the membrane voltage: i) **leak channels**, responsible for maintaining the resting membrane potential, commonly at -60 to -70 mV and ii) **voltage-gated channels**, closed during resting conditions and open upon membrane depolarization or hyperpolarization.

Depolarization of the plasma membrane by the entrance of cations such as  $Na^+$  or  $Ca^{2+}$  to values above the AP threshold generates an AP that propagates from the initial

segment of the axon to the synapse in a very efficient manner. APs can travel as fast as 100 m/s.

## 1.1 The synapse

First coined by Charles Sherrington in 1897 (Foster & Sherrington, 1897), the synapse is the specialized site where one neuron communicates with another. Neurons can form and receive thousands of synaptic contacts. Synapses can be electrical (Furshpan & Potter, 1958) or chemical (Dale et al., 1936) depending on their form of synaptic transmission. At **electrical synapses**, the cytoplasm of the pre- and postsynaptic cells is directly connected through gap junction channels, by which the presynaptic cell sends rapid depolarizing signals to the postsynaptic cell. On the contrary, at **chemical synapses**, the cytoplasm of both cells is separated by a narrow space called synaptic cleft (20–40 nm) and synaptic transmission is mediated by the release of neurotransmitters from the presynaptic to the postsynaptic terminal. Although electrical synapses operate faster than chemical synapses, the latter involve the amplification of the chemical signal: one single vesicle containing thousands of neurotransmitters can activate thousands of postsynaptic receptors and produce a large response in the postsynaptic cell. Chemical neurotransmission is predominant in the nervous system and has been the object of study in this thesis.

In addition to the discovery of the AP by Hodgkin and Huxley, Bernard Katz and colleagues developed the **quantal theory** of transmitter release positing that neurotransmitters are released in discrete “quanta” at chemical synapses (del Castillo & Katz, 1954; Fatt & Katz, 1952). In their studies at the frog neuromuscular junction, they observed the presence of miniature end-plate potentials that differed from nerve evoked end-plate potentials by their smaller amplitude and spontaneity (Fatt & Katz, 1951).

The kinetics and pharmacology, however, were strikingly similar (Fatt & Katz, 1952), suggesting that miniature end-plate potentials were the building blocks of nerve evoked end-plate potentials (Fig. 2). To strengthen this hypothesis, del Castillo and Katz reduced the release probability of the evoked response by decreasing the extracellular calcium concentration. By

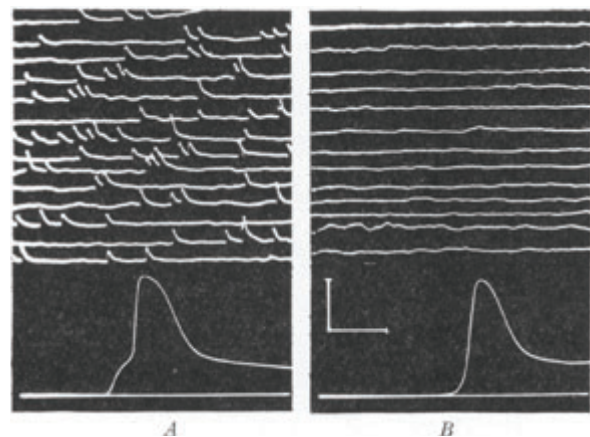


**Figure 2. Intracellular recordings showing miniature end-plate potentials at A) the end-plate of the frog neuromuscular junction and B) at a distance of 2 mm away in the same muscle fibre. Upper scale: 3–6 mV and 47 ms. Lower scale: 50 mV and 2 ms. (Adapted from Fatt & Katz, 1952).**

doing so, they were able to bring the amplitude value of the evoked end-plate potential close to the miniature end-plate potential (del Castillo & Katz, 1954), thus reinforcing the quantal theory. These findings, alongside the first electron micrographs of synaptic contacts (Couteaux & Pécot-Dechavassine, 1970; Gray, 1963; Palay, 1956), established the basis for chemical neurotransmission demonstrating that neurotransmitters are packed into **synaptic vesicles** (SVs) clustered at an electron-dense zone of the presynaptic plasma membrane called the **active zone** (AZ), and released after the arrival of an action potential. Exactly opposing this presynaptic density is aligned the **postsynaptic density** (PSD), a specialized region in the membrane of the postsynaptic cell where postsynaptic receptors are also clustered (Fig. 3).

During this thesis project, we have focused on the biology of the presynaptic terminal.

### 1.1.1 The Presynaptic terminal

The arrival of the action potential to the presynaptic terminal causes the opening of **voltage-gated  $\text{Ca}^{2+}$  channels** (VGCCs), which raises intracellular calcium levels and triggers the exocytosis of the release ready synaptic vesicles into the synaptic cleft (C. Li et al., 1995). Subsequently, neuro-

transmitters diffuse across the synaptic cleft and bind to synaptic receptors on the postsynaptic cell, leading to changes in the membrane potential and occasionally triggering the production of an AP. This process needs to be exquisitely controlled to allow rapid information transfer. Upon depolarization, fusion of SVs with the plasma membrane occurs in less than one millisecond (Llinás et al., 1981) and is precisely targeted towards postsynaptic receptors (Fig. 4). This is possible thanks to the AZ machinery.

AZs were initially proposed to be the sites where action potential-evoked synaptic vesicle fusion occurs (Couteaux & Pécot-Dechavassine, 1970). This hypothesis was later reinforced by John Heuser and Thomas Reese where after stimulating and freezing nerve terminals, exocytosis of SVs was mainly observed at this specific area (Heuser & Reese,

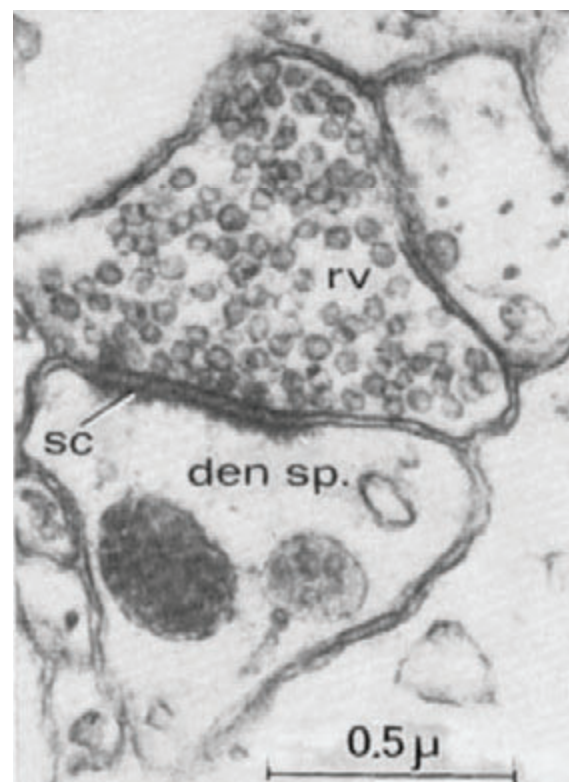


**Figure 3. Micrograph showing a synapse from the cat cerebral cortex.** Both, pre- and postsynaptic terminals can be recognized. Abbreviations: rv, round vesicles; sc, synaptic cleft; den sp, dendritic spine. (Image from Colonnier, 1968, adapted from the revision of Gray, 1969).

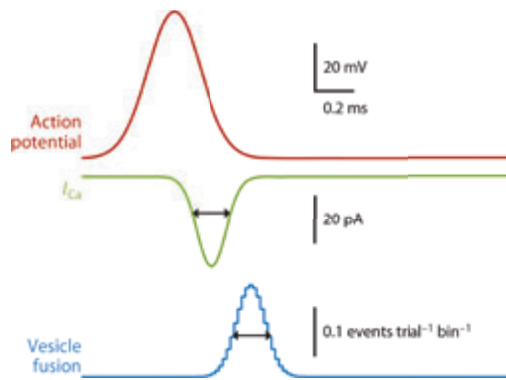


**Figure 4. Synaptic transmission.** Illustration of the rapid and precise sequence of events triggered by the arrival of an AP to the presynaptic terminal. Brief presynaptic calcium influx ( $I_{Ca}$ ) results in immediate synaptic vesicle fusion. (Adapted from Kaeser & Regehr, 2014)

1973). Thus, the AZ was defined as the key element of the presynaptic terminal responsible for transforming an action potential signal into a neurotransmitter release signal.

AZ sophisticated protein machinery accounts for the effectiveness and precision of this process, which is essential for ensuring: i) the tight **coupling** between synaptic vesicles and voltage-gated  $Ca^{2+}$  channels, and ii) the **docking** and **priming** of these vesicles to a small membrane patch, exactly opposite to where postsynaptic receptors are clustered. The specific sites of the active zone at which SVs dock, prime and fuse are called **release sites** (Pulido & Marty, 2017).

Five evolutionarily conserved proteins, RIM, RIM-BP, Munc13, Liprin- $\alpha$  and ELKS, interact with each other to form a large protein complex and constitute the AZ, with bassoon and piccolo also associated to this area (Fig. 5; reviewed in T.C. Südhof, 2012). During synaptic transmission, however, the number of SVs ready to be released upon

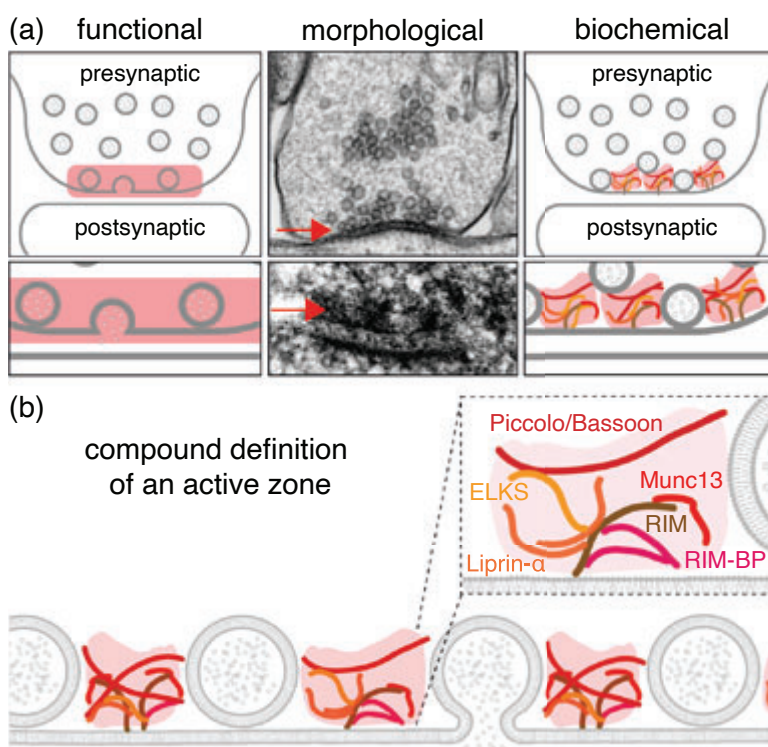


**Figure 5. Characterization of the active zone. A)** The AZ is defined functionally (left) by the area of the presynaptic membrane where vesicles fuse; morphologically (middle) through electron micrographs as the electron dense material opposite to the PSD (arrows); and biochemically (right), by the purification of proteins belonging to this area. **B)** Zoom-in of the biochemical characterization of the AZ showing the proteins that form the AZ complex (Adapted from Empeador-Melero & Kaeser, 2020).



stimulation needs to be maintained during repeated rounds of stimulation, requiring a constant supply of neurotransmitter-filled vesicles. Since *de novo* synthesis of SVs from the soma to synapses through axonal transport may be too slow to support high rates of release, synaptic vesicles undergo a dynamic cycle of fusion and retrieval, known as **synaptic vesicle cycle** (Fig. 6; Heuser & Reese, 1981; Südhof, 2004). Several modes of synaptic vesicle recycling, characterized by different molecular mechanisms and speed, have been described over the years. These include clathrin-mediated endocytosis (CME), “kiss-and-run”, ultrafast endocytosis and activity-dependent bulk endocytosis (ADBE). CME was the first mode of recycling to be uncovered (Heuser & Reese, 1973) and was shown to involve the retrieval of SV components from the plasma membrane by the formation of clathrin-coated pits at the periphery of AZs. This mode of endocytosis is relatively slow (10-30 s) and requires a set of molecules such as the clathrin adaptors AP-2 or AP180 (Milosevic, 2018; Saheki & De Camilli, 2012). An alternative faster pathway of recycling (<1-2s) named “kiss and run” produced by the reversal of an exocytic fusion pore was later reported (Ceccarelli et al., 1973; Fesce et al., 1994), opening a debate about how SVs are recycled. More recently, far from resolving this issue, two other modes of SV retrieval, ultrafast endocytosis and ADBE, emerged. The first is characterized by its speed (50 ms; Delvendahl et al., 2016; Watanabe et al., 2013) and occurs upon low- and high- frequency stimulation (Soykan et al., 2017; Watanabe et al., 2014). During ultrafast endocytosis, large endocytic vesicles (~80 nm) are formed from the plasma membrane and fused with endosomes. SVs are then reformed in a clathrin-dependent manner and filled with neurotransmitters after clathrin uncoating. In contrast, ADBE is triggered by intense bursts of activity and has been shown to retrieve large areas of membrane (~150 nm) and form endosomes in less than 2 s without the requirement of clathrin (Kononenko & Haucke, 2015).

It is likely that all four mechanisms coexist in nerve terminals and are used differently depending on activity levels, temperature or synapse type (Chanaday et al., 2019). Regardless of the recycling mode used, reformed vesicles need to be **rapidly reacidified** and **loaded with neurotransmitters** to become fully functional (Burger et al., 1989; Riveros et al., 1986). This process is mediated by the **vacuolar H<sup>+</sup>-ATPase** (vATPase), which pumps protons into the SV lumen (T. H. Stevens & Forgac, 1997; Toei et al., 2010), thus generating an electrochemical gradient that is used to shuttle neurotransmitters into SVs by vesicular neurotransmitter transporters (Blakely & Edwards, 2012). Although SVs contain many copies of vesicular neurotransmitter transporters, **only 1-2 copies of the vATPase** have been found at isolated vesicles, highlighting the tight regulation of the recycling process (Takamori et al., 2006).

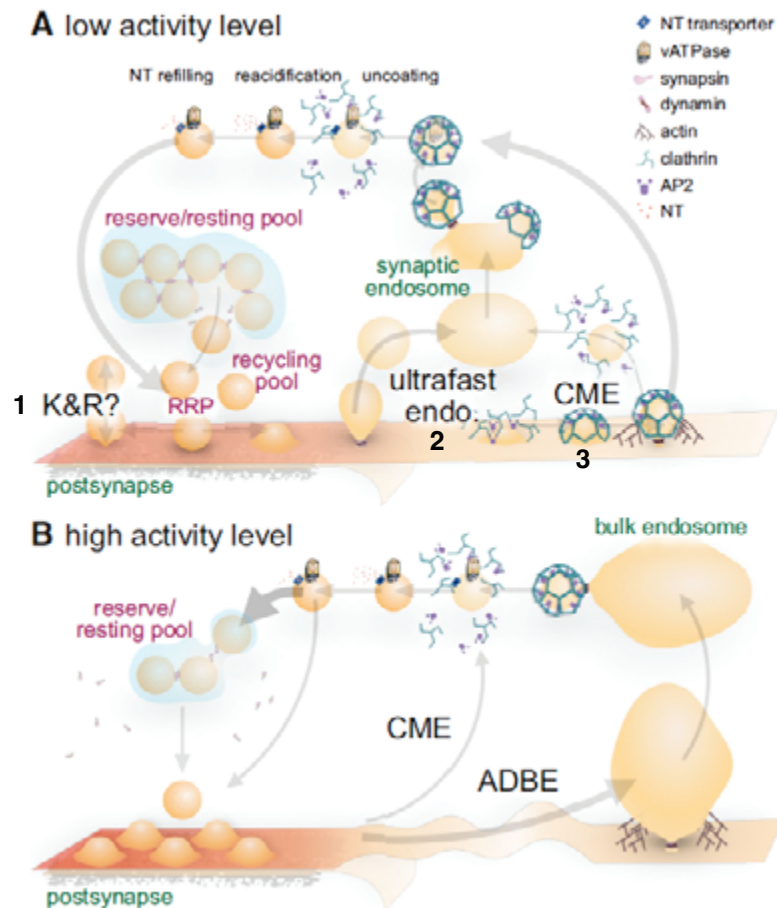


**Figure 6. The synaptic vesicle cycle. A)** During low activity levels, synaptic vesicles are retrieved via one of several mechanisms: (1) the fusion pore may reclose by kiss-and-run, (2) ultrafast endocytosis at the periaxial zone can retrieve endocytic vesicles that rapidly fuse with synaptic endosomes from which SVs regenerate in a clathrin-dependent manner, or (3) CME can generate SVs from the plasma membrane. Vesicle uncoating is necessary for the vATPase to acidify the lumen triggering concurrent neurotransmitter refilling by transporters. After refilling, SVs can be recruited back to the cluster, where they are segregated into functional pools. **B)** At high activity levels, many SVs are mobilized and exocytosed by full-collapse fusion. This activates ADBE, which retrieves large areas of membrane generating bulk endosomes from which SVs regenerate. (Adapted from Chanaday et al., 2019).

A prototypical presynaptic terminal from the central nervous system contains 100 to 200 synaptic vesicles (Harris & Sultan, 1995), with variations depending on the type of synapse. Even though vesicles appear morphologically indistinct at electron micrographs, not all vesicles are functionally equivalent. It is well-established that synaptic vesicles differ in their kinetics of release and subcellular location, prompting classification into different **SV pools** (Schikorski & Stevens, 1997). There are, however, multiple ways of pooling vesicles. The use of different experimental approaches and synapse types have led to controversial results in the identification and terminology of synaptic pools. The classical view (Denker & Rizzoli, 2010; Rizzoli & Betz, 2005) postulates that synaptic vesicles are arranged into three main pools, mobilized for release in sequential

order: 1<sup>st</sup>) the **readily releasable pool (RRP)**, 2<sup>nd</sup>) the **recycling pool (RP)** and 3<sup>rd</sup>) the **reserve pool**. The RRP is defined by those vesicles docked at the AZ and primed for immediate release upon stimulation (Kaeser & Regehr, 2017; Rosenmund & Stevens, 1996). It is the only pool that has been shown to correlate function and morphology, the size of the RRP corresponding to the number of synaptic vesicles docked at the AZ (Murthy et al., 2001). The RP is thought to serve as a source of vesicles, replenishing the RRP when it has been expended under moderate stimulation. Typically, the RP contains ~10-20% of all vesicles. In contrast, the reserve pool is formed by SVs reluctant to undergoing fusion upon stimulation, only recruited when the RP has been depleted upon high-frequency stimulation.

More recent studies, however, have given new insights in the classification above mentioned, categorizing SVs functionally, depending on whether they are capable of engaging in activity-dependent neurotransmitter release or not (Alabi & Tsien, 2012). In this approach, the total vesicle population capable of engaging in stimulus-evoked recycling form the **total recycling pool (TRP)** composed of the RRP and RP. The reserve pool is replaced by the **resting pool (RtP)** hosting synaptic vesicles that do not undergo fusion upon stimulation, even under saturating conditions (Fig. 7; Harata et al., 2001).

Although the TRP has been well characterized given their implications in synaptic strength and plasticity, the function of the RtP, which contains the majority of vesicles within the terminal (~50-85%; Fernandez-Alfonso & Ryan, 2008; Harata et al., 2001), is less well understood. Due to its large size and presumable inactivity, the RtP has been subject of speculation for many years.

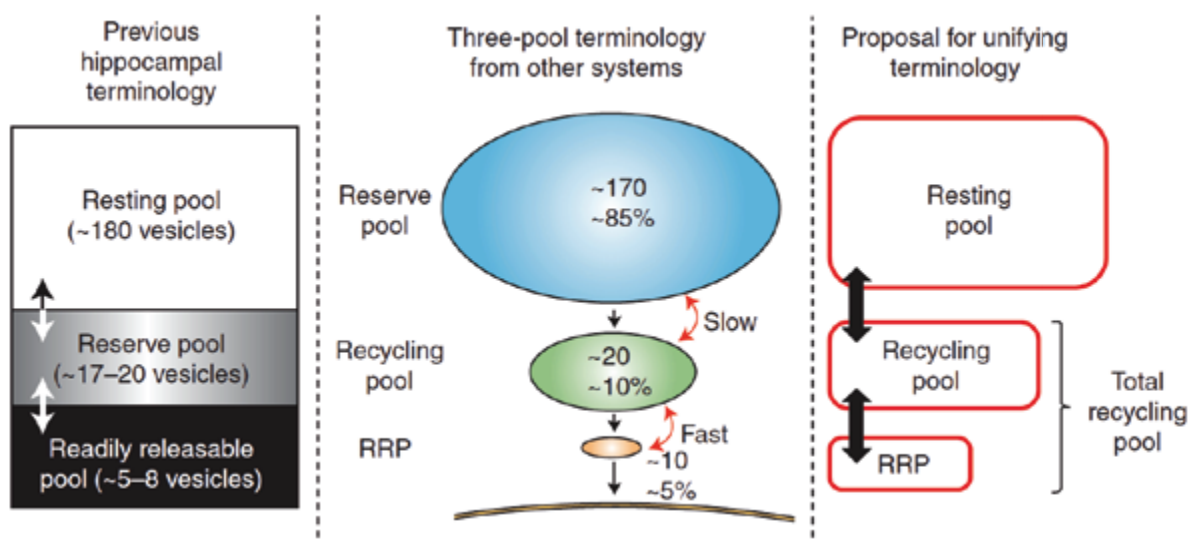


**Figure 7. Classification of SV pools.** Model from Südhof, 2000 (left), Rizzoli and Betz 2005 (middle) and Alabi and Tsien, 2012 (right). The last comes from the unification of the two first models (Adapted from Alabi & Tsien, 2012).



During the last decade, several studies using advanced imaging techniques and electrophysiology have started to shed light on the physiological role of the RtP. One possibility is that the RtP is used as a **buffer for soluble accessory proteins** involved in vesicle recycling, (Denker et al., 2011), this set of vesicles previously named as the stranded pool (Wienisch & Klingauf, 2006). Another suggestion is that vesicles from the RtP are recruited to the TRP, for example by changes in cyclin-dependent kinase 5 (CDK5) activity, the RtP thus operating as a **vesicle donor** and contributing to **presynaptic homeostatic plasticity regulation** (Jung et al., 2014; S. H. Kim & Ryan, 2011). Of importance, increasing evidences have started to link **spontaneous release** to a subset of vesicles that do not undergo activity-driven fusion (Sara et al., 2005), identified as the RtP (Fredj & Burrone, 2009). Finally, a new pool called the “super pool” has emerged over the last few years (Herzog et al., 2011; Krueger et al., 2003; Staras et al., 2010). This pool of vesicles is thought to transit SVs rapidly between neighbouring synapses along axons as far as 30 mm away by free diffusion or dependent on actin or microtubule motors. Imaging of fluorescently labelled vesicles have suggested that vesicles of the super pool are recruited from the RP and the RtP (Darcy et al., 2006; Fernandez-Alfonso & Ryan, 2008). Despite all this evidence, to what extent do vesicles from the RtP participate in evoked and spontaneous neurotransmission is still obscure.

### 1.1.2 The postsynaptic terminal

The postsynaptic terminal is defined as the receiving element of the synapse. It is specialized in transforming the chemical signal sent by the presynaptic terminal into electrical and biochemical changes in the postsynaptic neuron.

The binding of neurotransmitters to postsynaptic receptors leads to the opening or closing of ion channels either directly or indirectly, prompting the classification into two classes of synaptic receptors. Generally, receptors gating ion channels directly are referred to as ionotropic or ligand-gated channels and contain an extracellular domain that binds to the neurotransmitter and a transmembrane domain that forms an ion conducting pore. Changes in the conductance of ion channels as a result of this gating, alter the membrane potential of the postsynaptic neuron producing an **excitatory postsynaptic potential (EPSP)** or an **inhibitory postsynaptic potential (IPSP)** in excitatory or inhibitory synapses, respectively. In contrast, postsynaptic receptors controlling the opening of ion channels indirectly are referred to as metabotropic and are usually composed of seven transmembrane domains.

Whereas the activation of ionotropic receptors occurs in the order of milliseconds, that of metabotropic receptors can last seconds to minutes. Accordingly, the former are involved in the **processing of rapid transmission** and the latter play important roles in synaptic plasticity by modulating the excitability and strength of synaptic connections. The action of a released neurotransmitter from SVs depends on the properties of the

postsynaptic receptors with which it interacts, rather than the properties of the neurotransmitter itself. For example, acetylcholine (ACh) can exert its excitatory action at the neuromuscular junction by binding to nicotinic receptors or, on the contrary, function as an inhibitory transmitter to slow the heart rate through the activation of muscarinic receptors. Similarly, the type of synapse is also determined by the postsynaptic receptor present at the postsynaptic cell.

The postsynaptic terminal of excitatory and inhibitory synapses differs not only in the type of receptors expressed but also in their morphology and organization. In the mammal central nervous system, the postsynaptic side of excitatory synapses (glutamatergic) is shaped in the form of tiny protrusions called dendritic spines (Bourne & Harris, 2008). On the contrary, inhibitory synapses (generally GABAergic) and connections formed by neurons of the **peripheral nervous system** occur on dendritic shafts, cell bodies or axon initial segments and **do not form spines**.

In parallel to the AZ, the **PSD** is important for clustering postsynaptic receptors, coupling the activation of receptors to signalling pathways and mediating the apposition of the pre- and postsynaptic membranes through adhesion molecules (Sheng & Kim, 2011). Even though the composition of the PSD varies considerably between brain regions and neuron types (Cheng et al., 2006; Tashiro & Yuste, 2003; Wandong Zhang et al., 1999), different PSD proteins have been identified over the years. The best studied PSD protein is the scaffold PSD-95 and its family members (Cho et al., 1992), whose main function is to bind to and tether several proteins of the PSD such as adhesion molecules, synaptic receptors and signalling proteins (E. Kim & Sheng, 2004). Adhesion has been shown to be mediated by heterophilic transsynaptic adhesion proteins such as neuroligins (presynapse) and neuroligins (postsynapse) and the homophilic binding of N-cadherins (Tai et al., 2008).

Even though it was initially thought that the robustness of synaptic transmission relied on the stability of the number of receptors present at the synapse, it was soon hypothesized that learning and memory could be coded by changes in glutamate receptors (Lynch & Baudry, 1984). It was later confirmed that the number of neurotransmitter receptors is tightly regulated and that it can vary by **undergoing turnover through exo-/endocytosis** (Bredt & Nicoll, 2003; Collingridge et al., 2004; Nishimune et al., 1998) and by mechanisms of **lateral diffusion** (Borgdorff & Choquet, 2002; Dahan et al., 2003; Tardin et al., 2003).

## 1.2 Modes of synaptic transmission

Three modes of neurotransmitter release, synchronous, asynchronous and spontaneous, can be distinguished in synapses according to their  $\text{Ca}^{2+}$ -dependence and time course (Fig. 8A and B; Kaeser & Regehr, 2014). Synchronous release occurs during

evoked neurotransmission and lasts several milliseconds. This mode of release has been extensively characterized and constitutes the basis of fast synaptic transmission: the arrival of the action potential to the presynaptic terminal leads to a rapid and local rise of calcium levels (Neher & Sakaba, 2008) that triggers the **synchronous** exocytosis of synaptic vesicles docked at the AZ. Right after, **asynchronous** release of SVs persists for milliseconds to seconds due to residual calcium (Chirwa & Sastry, 1988; Goda & Stevens, 1994; Lu & Trussell, 2000). In contrast, **spontaneous** release is produced in the absence of any activity, when the membrane potential is at rest and presynaptic calcium levels are low (Fatt & Katz, 1952; Bernard Katz, 1969).

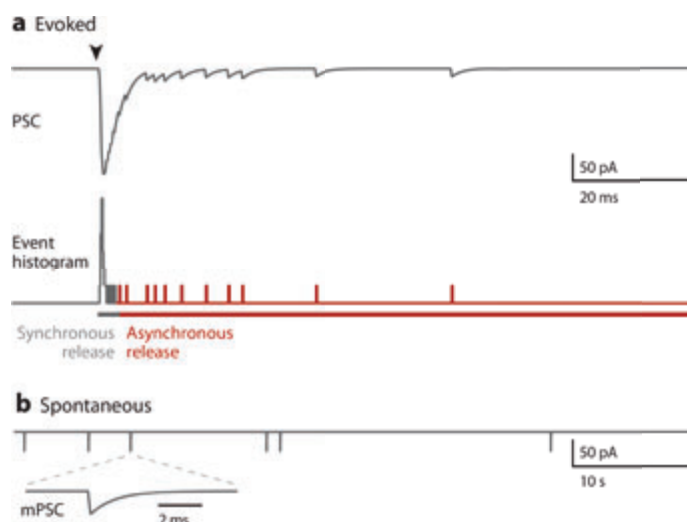


**Figure 8. Modes of synaptic transmission.** **A)** Illustration of evoked (arrowhead) synchronous and asynchronous release. **B)** Spontaneous neurotransmitter release. The inset zooms in one mPSC. Abbreviations: PSC, postsynaptic current; mPSC, miniature PSC. (Adapted from Kaeser & Regehr, 2014).

Although the classification of these three modes of neurotransmission is based on functional differences characterized by electrophysiological studies, recent studies have started to shed light on the contribution of molecular differences among synaptic vesicles in the distinction of these three forms of neurotransmitter release. For example, synaptic vesicles that fuse synchronously and asynchronously are thought to belong to the same recycling pool (Otsu et al., 2004) and to be preferentially released on one mode release or the other depending on their content of SNAREs and  $\text{Ca}^{2+}$  sensors (Raingo et al., 2012; Bacaj et al., 2013; Luo et al., 2015). Less is known, however, about the mechanisms underlying spontaneous neurotransmitter release.

Typically, spontaneous fusion of SVs with the plasma membrane occurs at a very low rate, 1-2 vesicles per minute per release site (Geppert et al., 1994; Murthy & Stevens, 1999), and produces **miniature postsynaptic events** (mEPSCs) or also called minis, which reflect the release of neurotransmitters from a single vesicle. The traditional assumption that synaptic vesicles released spontaneously and those released upon stimulation share a common identity has been questioned during the last decades. Synaptic vesicles released spontaneously are morphologically indistinguishable from those released during activity. Thus, synaptic vesicle depletion, using

the proton pump inhibitors folimycin or bafilomycin, as well as optical techniques to monitor the uptake and release of styryl dyes during spontaneous or evoked activity, have been used to uncover this issue. Controversial results have raised from studies claiming that SVs released during spontaneous and evoked neurotransmission **belong to the same SV pool** (Groemer & Klingauf, 2007; Hua et al., 2010; Ikeda & Bekkers, 2009; Prange & Murphy, 1999; Wilhelm et al., 2010), and others finding that SV released in these two modes are **drawn from different pools** (Afuwape et al., 2017; C. Chung et al., 2010; Fredj & Burrone, 2009; Koenig & Ikeda, 1999; Mathew et al., 2008; Ramirez et al., 2012; Sara et al., 2005).

Consistent with the idea of spontaneous and evoked neurotransmission operating separately, Kavalali and colleagues posited a model wherein SVs released spontaneously cause the activation of a specific set of postsynaptic receptors located at extrasynaptic patches of the postsynaptic dendrite in glutamatergic synapses (Atasoy et al., 2008; Sara et al., 2011) and use different fusion machinery and recycling pathways (Fig. 9A and B; Kavalali, 2015).

Finally, another important issue remained to be clarified is the functional significance of spontaneous synaptic transmission in the processing of information. Even though spontaneous mode of release has often been regarded as noise, recent studies have challenged this view and demonstrated spontaneous release to play important roles in **synaptic development, plasticity, homeostasis, and excitability** (Andreae & Burrone, 2018; Kavalali, 2015; Truckenbrodt & Rizzoli, 2014). The molecular mechanisms underlying spontaneous neurotransmission, however, are still unclear.

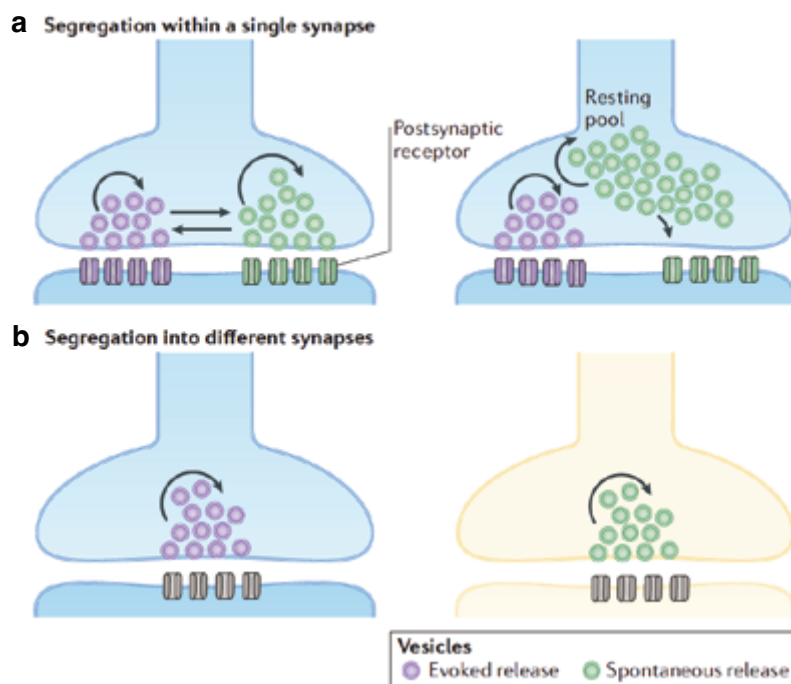


**Figure 9. Schematic representation of different models for vesicle pool segregation during evoked and spontaneous neurotransmission. A)** Spontaneous and evoked release are mediated by separate vesicle pools within the same synapse and activate distinct receptor populations (left). Spontaneous release may originate from the resting pool (right). **B)** Alternatively, synapses may be more prone to one mode of release or the other, for example depending on the developmental stage (Adapted from Kavalali, 2015).

### 1.3 Quantification of synaptic transmission

The properties of the synapse determine the efficacy of neurotransmitter release during synaptic activity. As first posited by Bernard Katz (Bernard Katz, 1969), quantal release is a stochastic process that depends on the number of independent release sites (**N**), and the probability (**Pr**) of these vesicles to be released. Thus, the number of synaptic vesicles released after the arrival of an AP is equal to  $N \times Pr$  and determines synaptic strength. Accordingly, by means of electrophysiological recordings, synaptic strength can be measured in the form of **Excitatory Postsynaptic Currents** (EPSCs) and can be defined as **EPSC** =  $N \times Pr \times q$ , where (**q**) is the quantal size.

**Release probability** is modulated by intracellular calcium concentration evoked by synaptic activity, which in turn depends on the properties of calcium channels, their coupling to synaptic vesicles and calcium buffers (Dittman & Ryan, 2019). **Quantal size** can be measured from the amplitude of mEPSCs since it reflects the release of a single vesicle. According to the **release site model** (Vere-Jones, 1966), either **none or one** synaptic vesicle are released at each release site depending on Pr. Fluctuation analysis of synaptic transmission using the variance-mean approach can be used to determine N and Pr (Sakaba et al., 2002).

Whereas changes in **q** generally rely on the number and sensitivity of **postsynaptic receptors**, **presynaptic properties** account for variations in **N** and **Pr**. For that reason, separating the contribution of pre- and postsynaptic components in EPSCs is not straightforward. Variations in these quantal parameters give rise to synaptic plasticity mechanisms (Regehr, 2012; Sakaba et al., 2002), which will be discussed in the following chapter. Presynaptic calcium influx is a key determinant of neurotransmitter release probability. Measurements of intracellular local calcium at the active zone by photolytic calcium uncaging and optical techniques have shown that high local calcium concentration ( $Ca_{local}$ : 10-100  $\mu M$ ) near release sites triggers SV release (Schneppenburger & Neher, 2000, 2005). However, the relationship between intracellular calcium influx and SV release is not lineal (Dodge & Rahamimoff, 1967). Small changes in intracellular calcium entry lead to dramatic changes in neurotransmitter release. The low-affinity calcium sensor synaptotagmin 1 (syt1) has been shown to bind  $\sim 5 Ca^{2+}$  ions (Bollmann et al., 2000; Schneppenburger & Neher, 2000, 2005). Considering that each synaptic vesicle contains  $\sim 15$  syt1 proteins, a great number of potential calcium-binding sites **modulate release probability in a cooperating manner**. Upon depolarization,  $Ca_{local}$  depends on VGCC abundance, channel gating (opening probability) and the time course of calcium entry. In turn, the amount of free calcium ions reaching SVs relies on the positioning of VGCCs and release sites, and is limited by the highly buffering environment of the cytoplasm. Therefore, the **number of VGCCs** contributing to neurotransmitter release as well as their **coupling to SVs** lar-



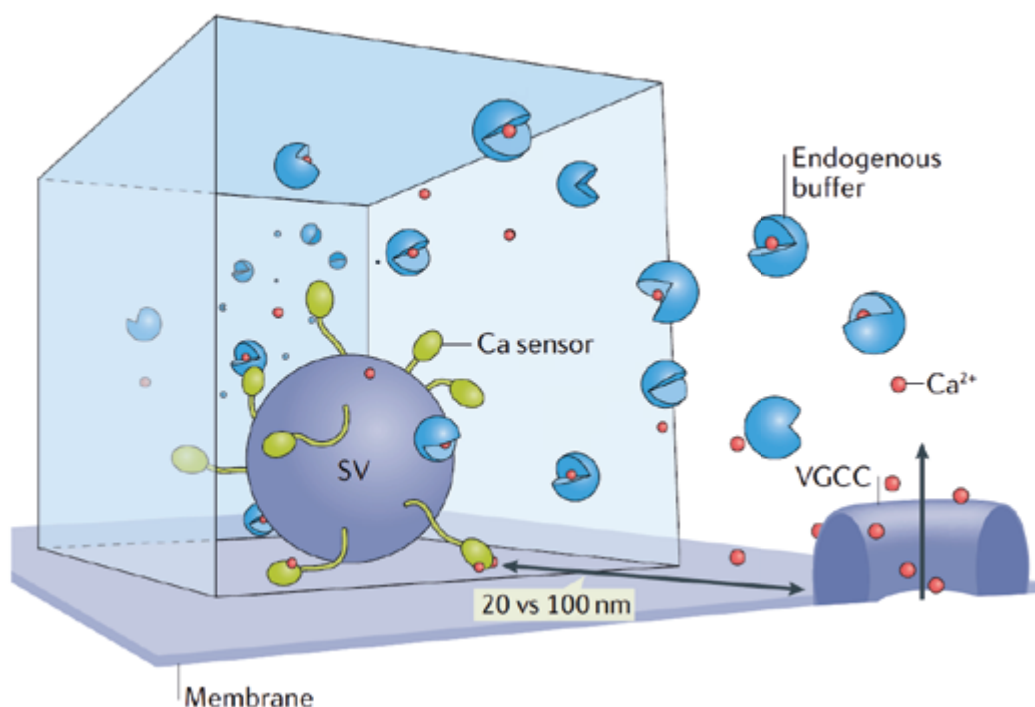
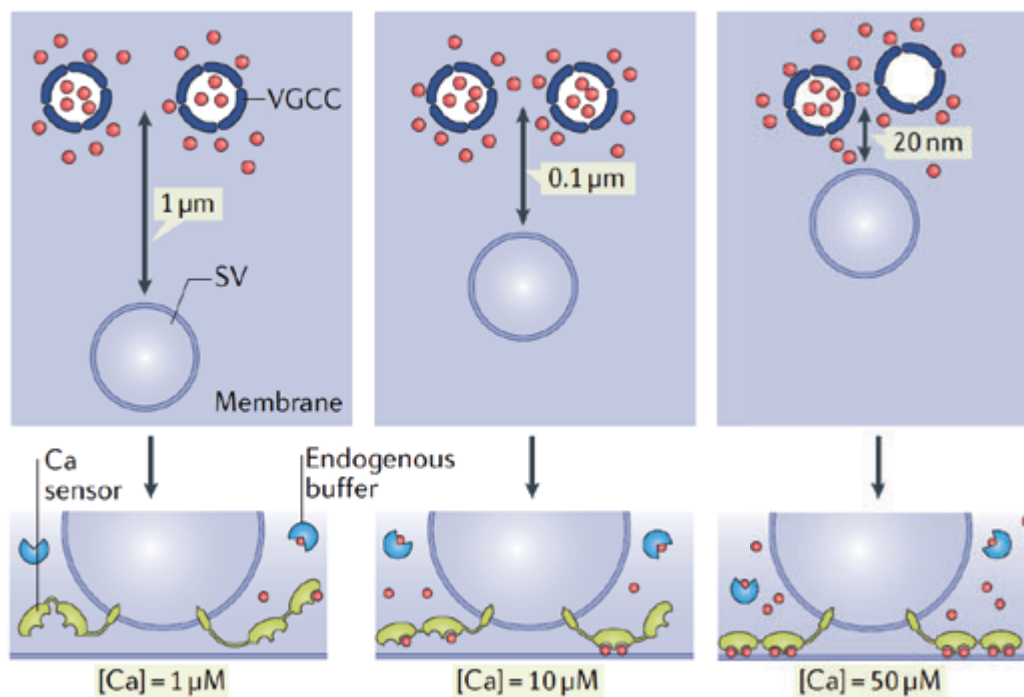
gely influences Pr and in turn **determines synaptic efficacy** (Fig. 10A and B).

Previous works have shown that the number of VGCCs per release site varies substantially depending on the type of synapse. Studies combining SDS-digested freeze–fracture electron microscopy with immunogold labelling of  $Ca_v2.1$  demonstrated that VGCCs are concentrated at the active zone and that their abundance ranges 9–30 VGCCs per release site (Althof et al., 2015; Holderith et al., 2012; Miki et al., 2017). In contrast, another study using optical fluctuation analysis at the frog neuromuscular junction (NMJ) reported a 1:1 relationship between the number of VGCCs and docked vesicles (Luo et al., 2011), suggesting that in some synapses 1 VGCC may be enough to elicit SV fusion. Despite the relevance of the number of VGCC associated to release sites, how it is regulated is not yet understood. One candidate contributing to calcium channel supply is the VGCC accessory subunit  $\alpha 2\delta$ , which influences the trafficking, localization, and biophysical properties of VGCCs (Dolphin, 2013).

After presynaptic calcium entry,  $[Ca_{local}]$  is short-lived and decreases as a function of the distance from the VGCC position. Calcium-binding proteins, such as calbindin or parvalbumin, intercept calcium before it reaches release sites (Matveev et al., 2004; Roberts, 1993), thus reducing release probability. In contrast, the remaining calcium after VGCCs have closed, called residual calcium ( $Ca_{residual}$ ), is longer-lived and can increase release probability if two stimuli are closely spaced (milliseconds). For that reason, the distance between VGCC and the fusion machinery is key for establishing initial neurotransmitter release probability, which in turn influence short-term plasticity (explained in the next chapter).

The delay between calcium entry and vesicle release has been reported to be  $\sim 200 \mu s$  (Llinás et al., 1981). Given the calcium diffusion speed, the distance between VGCCs and release sites is calculated to be 50–200 nm. A few molecules, such as RIM and RIM-BP proteins, have been shown to function as positioners to ensure the tight coupling between VGCC and release sites (Grauel et al., 2016; Han et al., 2011).

How release probability is controlled during synaptic activity is a fundamental question in neurobiology. However, despite the great advances made since the initial experiments of Katz and del Castillo, there are still gaps in our understanding of how changes in quantal parameters modulate neurotransmission and mediate synaptic plasticity.

**A 3D view****B En face view**

**Figure 10. Calcium sensing and synaptic vesicle release.** Detection of local free calcium by the fusion machinery is limited by four factors represented here in 3D (A) or 2D (B). First, the distance between VGCCs and release machinery. Second, endogenous buffers leave small numbers of free calcium ions available. Third, the number of calcium sensors at each vesicle is limited. And fourth, the time window for detection is very brief as VGCC opening is in the order of submilliseconds (Adapted from Dittman & Ryan, 2019).

# 2 Synaptic plasticity

One of the most important brain's properties is its capacity to modify neural circuit's function according to previous experience. This process is called synaptic plasticity and refers to modifications of synaptic transmission and/or structure in response to activity.

Considering the nature and duration of changes in synaptic transmission, several mechanisms of synaptic plasticity have been described over the years (Fig. 11). Synaptic plasticity can last milliseconds to minutes (**short-term plasticity**) or even hours to days (**long-term plasticity**) and can lead to either **potentiation** or **depression** of synaptic weight.

In addition, **homeostatic synaptic plasticity** maintains synaptic transmission levels to a baseline by compensating for perturbations that unbalance neuronal activity, including changes in connectivity during development, Hebbian plasticity and pathological conditions. Here, I will focus on short-term plasticity and homeostatic synaptic plasticity mechanisms.

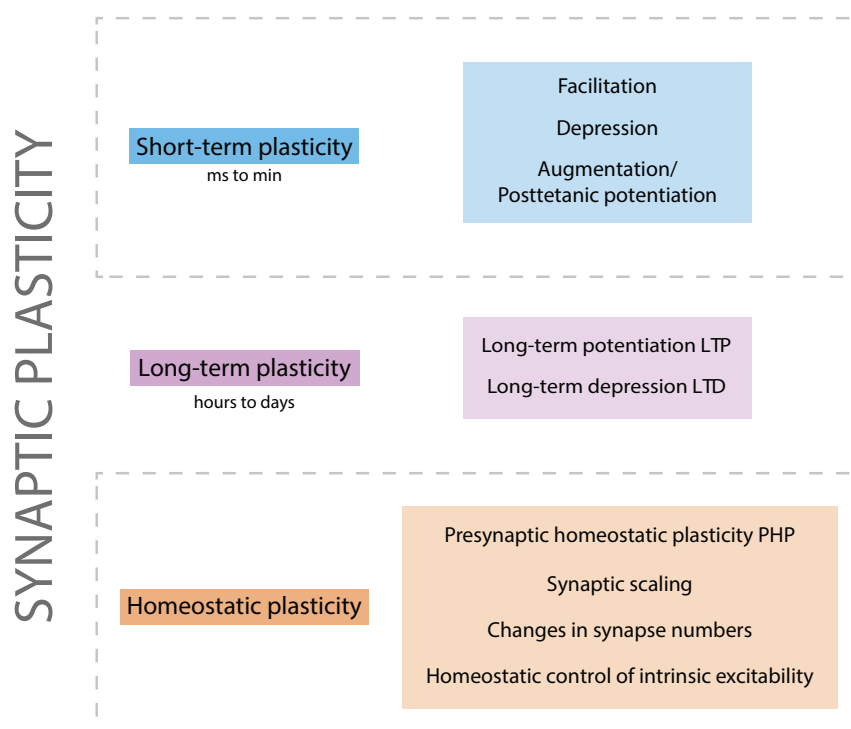


**Figure 11. Classification of synaptic plasticity mechanisms.** Diagram showing the different types of synaptic plasticity. Dotted lines indicate the mechanisms I will focus on in this chapter.



## 2.1 Short-term synaptic plasticity

Short-term plasticity is observed in virtually all organisms, ranging from invertebrates to mammals, and almost in all synapse types. It is key in transient sensory adaptations, behavioural changes, and short-term memory (Anwar et al., 2017; S. Chung et al., 2002; Motanis et al., 2018). Generally, short-term plasticity can be classified into 3 different categories: **depression**, **facilitation** and **augmentation/posttetanic potentiation** (PTP; Fig. 12; Regehr, 2012).

When two closely spaced stimuli are evoked, the second stimulus can be either depressed or enhanced depending on the release probability of the first stimulus (B. Katz & Miledi, 1968). Thus, synapses exhibiting low release probability tend to facilitate whereas those showing high release probability usually depress. Accordingly, short-term depression or facilitation can be experimentally achieved by changing extracellular calcium concentration. Multiple forms of short-term plasticity can occur in a single synapse, the result being reflected in synaptic strength (Dittman et al., 2000; Pan & Zucker, 2009).

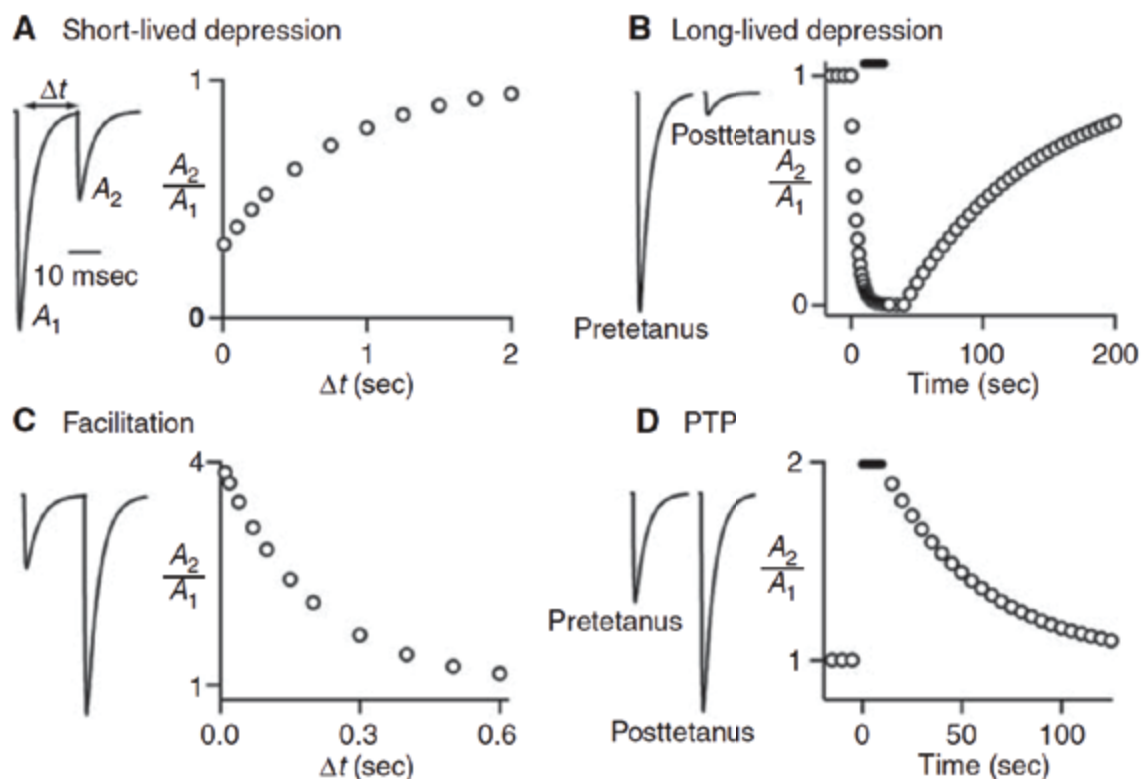


**Figure 12. Forms of short-term plasticity.** **A)** Short-lived depression is observed when the response of the second of two closely evoked stimuli is smaller. **B)** Long-lived depression occurs when high-frequency stimulation leads to a depression that persists for tens of seconds. **C)** Paired-pulse facilitation is observed when the response of the second of two closely evoked stimuli increases. **D)** Augmentation or posttetanic potentiation (PTP) lasting seconds to minutes is displayed in some synapses after tetanic stimulation. (Adapted from Regehr, 2012).

Activity-dependent changes of synaptic strength can be produced by i) **presynaptic factors**, including variations in neurotransmitter release probability and modulation of RRP size, ii) **postsynaptic factors**, driven by postsynaptic receptor saturation (Wadiche & Jahr, 2001) or desensitization (Otis et al., 1996; Scheuss et al., 2002; Trussell et al., 1993; Xu-Friedman & Regehr, 2004), which can limit evoked responses, and iii) **glial cells activity**, glia can interfere with postsynaptic receptor activation by controlling the extent and speed of neurotransmitter clearance and affect synaptic efficacy by releasing modulatory substances (Bergles et al., 1999; Danbolt, 2001).

Here, I will focus on the mechanisms underlying **presynaptic short-term plasticity**.

### *Depression*

In synapses exhibiting synaptic depression, the second of two closely spaced stimuli (milliseconds to seconds) displays a smaller response than the first one (Fig. 12A). Generally, synaptic depression can be explained by the **simple depletion model**, which posits that the reduced response of the second stimulus is based on the transient depletion of the RRP evoked by the first stimulus (Betz, 1970; Zucker & Regehr, 2002). Hence, the more vesicles are initially released, the greater is the paired-pulse depression. Depression recovery occurs within seconds, when the RRP is replenished with vesicles from the recycling pool.

Similar to synaptic depression elicited by paired-pulses, sustained stimulation causes long-lasting depression (tens of seconds to minutes) that recovers more slowly (Fig. 12B; Betz, 1970; del Castillo & Katz, 1954b; Eccles & O'Connor, 1941; A. M. Thomson et al., 1993). Trains of high-frequency stimulation deplete the recycling pool and the slower recuperation is due to longer times required for RRP replenishment (C. F. Stevens & Wesseling, 1999).

Other models, such as release site inactivation and calcium channel inactivation have also been raised to explain synaptic depression. The first is based on the interference of synaptic vesicle fusion at the active zone until vesicular membrane proteins are cleared through endocytosis or diffusion (Hosoi et al., 2009; Kusano & Landau, 1975). The second explains synaptic depression by the regulation of VGCC opening probability mediated by calcium-sensing proteins such as calmodulin (Amy et al. 1999; A. Lee et al. 2002; Peterson, DeMaria, and Yue 1999; Mochida et al. 2008).

### *Facilitation*

In synapses exhibiting synaptic facilitation, the second of two closely spaced stimuli (milliseconds to seconds) displays a greater response than the first (Fig. 12C). According to the **residual calcium model**, after the first stimulus, local calcium persists at lower concentrations in the terminal in the form of residual calcium ( $Ca_{\text{residual}}$ ; B. Katz & Miledi, 1968). Consequently,  $Ca_{\text{residual}}$  participates in increasing release probability

when a second stimulus is evoked in a short time interval ( $Ca_{local} + Ca_{residual}$ ). Similarly, sustained activity applied at high frequencies can lead to longer-lasting forms of facilitation (tens of seconds to minutes), such as augmentation or posttetanic potentiation (Fig. 12D; Magleby & Zengel, 1976; Regehr, 2012). In these cases, each stimulus of the train contributes to the buildup of  $Ca_{residual}$ , thus increasing release probability, and consequently synaptic strength.

Another model to explain facilitation is the calcium buffer model, which is based on the decrease of initial release probability by high concentrations of fast calcium-binding proteins, which limit  $Ca_{local}$  concentration at release sites (E. M. Adler et al., 1991; Roberts, 1993). Consequently, large calcium concentrations can result in saturation of calcium-binding proteins and lead to facilitation when a second stimulus is evoked, since more free calcium can reach release sites (Blatow et al., 2003; Felmy et al., 2003; Matveev et al., 2004; Neher, 1998; Rozov et al., 2001).

Like in short-term depression, calcium channel regulation has also been shown to mediate facilitation by increasing presynaptic calcium influx through VGGCs (Catterall & Few, 2008; González Inchauspe et al., 2004; Mochida et al., 2008).

## 2.2 Homeostatic synaptic plasticity

During learning and development, neural circuits change their number of synaptic contacts and undergo modifications in synaptic strength. Such flexibility allows the nervous system to store information and adapt to an ever-changing environment. Nevertheless, the computational power of a neuronal network relies on its ability to **maintain synaptic activity at a baseline**.

As Walter Cannon could observe more than 50 years ago, physiological systems keep key parameters, such as temperature or blood glucose levels, to stable set points in order to maintain the system's stability or "**homeostasis**" (Cannon, 1932). Strong evidence has shown that neuronal activity is also a key parameter that needs to be actively adjusted at basal levels when facing destabilizing forces. This process is referred to as homeostatic synaptic plasticity and relates to **compensatory adjustments of synaptic function** to accurately restore baseline function towards a set point in the continued presence of a perturbation (Fig. 13; Davis, 2006; H.-K. Lee & Kirkwood, 2019; Marder & Prinz, 2003; Pozo & Goda, 2010; Gina G. Turrigiano & Nelson, 2004; Gina G Turrigiano, 2012).

However, for a plasticity mechanism to be considered truly homeostatic, three criteria need to be satisfied. First, it should regulate a **key parameter**, for example synaptic strength or firing rate, at an established value. Second, it requires **sensors** to detect changes in basal activity caused by external perturbations. And third, it generates an **error signal** that is used to finely adjust synaptic activity back towards the set point through homeostatic effectors (Davis & Müller, 2015).

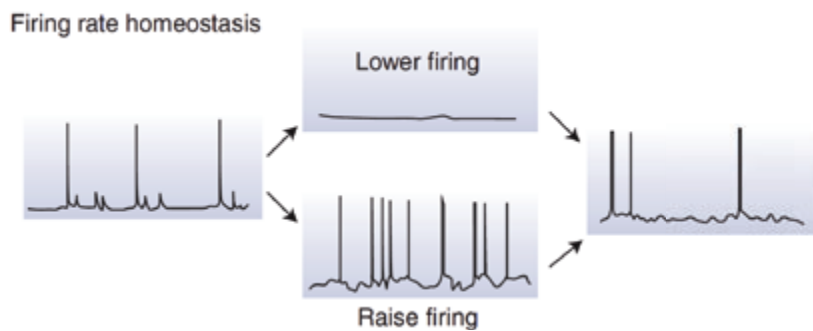


**Figure 13. Homeostatic synaptic plasticity.** Illustration of firing rate homeostasis. Perturbation of firing in either direction is restored to the baseline by homeostatic mechanisms. (Adapted from G. Turrigiano, 2012).

Given the diversity of cell-types embedded in synaptic networks, it is not surprising to find that a specific perturbation can be compensated by a rich variety of homeostatic mechanisms which either involve changes in pre- or postsynaptic function. Differences in the **locus of homeostatic control** have been shown to operate in a **neuron type- and developmental stage-specific manner** (Bartley et al., 2008; J. Kim & Tsien, 2008; Wierenga et al., 2006).

Accordingly, homeostatic plasticity mechanisms can be classified by the way in which a neuron responds to a perturbation, namely i) **synaptic scaling**, driven by the regulation of postsynaptic neurotransmitter receptors (Ibata et al., 2008; O'Brien et al., 1998; Gina G. Turrigiano et al., 1998; Gina G Turrigiano, 2008), ii) **presynaptic homeostatic plasticity (PHP)**, which involves the modulation of neurotransmitter release (Davis & Müller, 2015; Delvendahl & Müller, 2019), iii) **compensatory changes in synapse numbers** (Kirov & Harris, 1999; Wierenga et al., 2006) and iv) **homeostatic control of intrinsic excitability** (Fig. 11; Davis, 2013; Nerbonne et al., 2008; Parrish et al., 2014; Temporal et al., 2012; Gina G Turrigiano et al., 1994).

Here, I will focus on synaptic scaling and PHP. Homeostatic synaptic mechanisms to compensate changes in synaptic connectivity during synapse formation and elimination will be discussed in chapter 3.

### 2.2.1 Synaptic scaling

It is well established that one of the mechanisms by which neural circuits counterbalance destabilizing forces is the **regulation of postsynaptic receptor trafficking** and its **abundance** at postsynaptic sites. This cell-autonomous mechanism is known as synaptic scaling (Fig. 14) and has been observed in a variety of cell-types, both *in vitro* and *in vivo* (Gina G Turrigiano, 2008, 2012).

First reports of what would be defined as synaptic scaling came from the denervation supersensitivity phenomenon (Berg & Hall, 1975; Sharpless, 1975). It was observed that rat muscle denervation, driven by acetylcholine receptor (AChR) blockade with  $\alpha$ -bungarotoxin, resulted in increases of muscle excitability through changes in the number of postsynaptic receptors.

During synaptic scaling, changes in mEPSC amplitude are used as a readout of postsynaptic function (Desai et al., 2002; Gainey et al., 2009; Gina G Turrigiano et al., 1998). A study in cultured neocortical neurons showed that blocking AP-firing with tetrodotoxin (TTX) led to increases in AMPA receptor abundance accompanied with scaling up of mEPSC and EPSC amplitudes. This process was shown to require a drop in somatic calcium, decreases in CaMKIV activation and enhanced transcription (Ibata et al., 2008). In contrast, elevated synaptic activity resulted in scaling down postsynaptic receptors and required enhanced calcium influx, CamKK/CaMKIV activation and gene transcription (Goold & Nicoll, 2010).

Other molecules have been found to somehow contribute to synaptic scaling. These include Arc, involved in AMPA receptor trafficking regulation (Chowdhury et al., 2006; Shepherd et al., 2006), the scaffold proteins PSD-95 and PSD-93 (Sun & Turrigiano, 2011) and  $\beta 3$  integrins (Cingolani et al., 2008). Although significant advances have been made since its discovery, the specific **molecular mechanisms underlying synaptic scaling** are not completely understood.

**Hebbian plasticity**, described by Donald Hebb in the 1940s (Bliss & Lomo, 1973; Hebb, 1949) accounts for fast and lasting activity-dependent changes of synaptic strength based on positive feedback mechanisms, including some forms of short-term potentiation (STP), long-term potentiation (LTP) and long-term depression (LTD). Consequently, Hebbian plasticity is considered to be the mechanism by which information is coded and retained in the brain, enabling processes such as learning and memory (Bear, 1996; C. Chen & Tonegawa, 1997; Klintsova & Greenough, 1999).

However, in the absence of physiological constraints, neural circuits undergoing positive feedback mechanisms that potentiate or depress synaptic strength, would lead to instability and saturation of synaptic strength in one direction or the other. To prevent

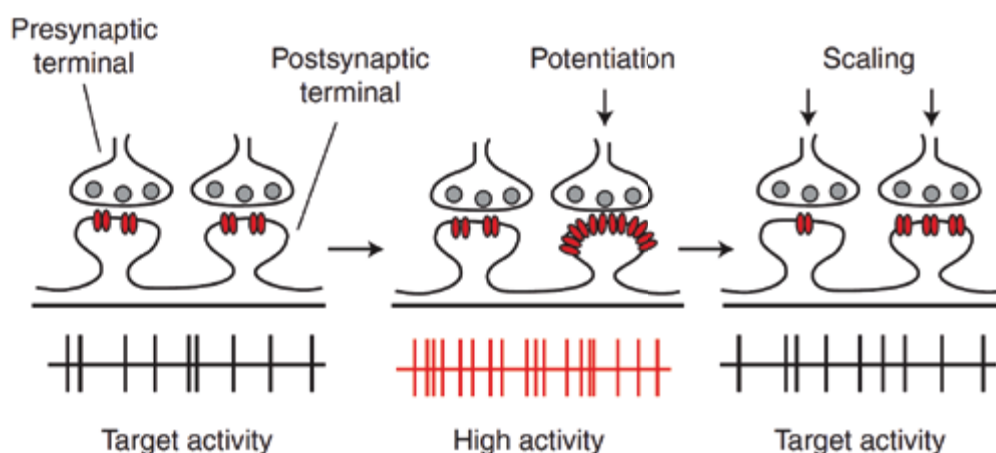


**Figure 14. Synaptic scaling.** Perturbation of synaptic activity for example by potentiation through Hebbian mechanisms triggers a homeostatic response in the form of synaptic scaling that proportionally reduces synaptic strength at all synapses to return firing to basal levels. (Adapted from Gina G Turrigiano, 2012).



this from happening, homeostatic synaptic plasticity mechanisms, such as synaptic scaling, provide negative feedback that return synaptic transmission back towards its original state (Fox & Stryker, 2017; Galanis & Vlachos, 2020). Accordingly, synaptic scaling cooperates with Hebbian plasticity to allow neuronal networks to encode information (Miller & MacKay, 1994).

Although both forms of plasticity, synaptic scaling and Hebbian plasticity, arise from **changes in postsynaptic receptor accumulation**, whether they share molecular mechanisms and how they might be interconnected, is still unclear.

### 2.2.2 Presynaptic homeostatic plasticity

First observations of what today is defined as PHP appeared in patients suffering from myasthenia gravis a few decades ago. In these patients, decreases of Ach receptors at the NMJ were compensated by increases in Ach release (Cull-Candy et al., 1980). Similarly, rat models of myasthenia gravis, generated by administration of the AchR antagonist  $\alpha$ -bungarotoxin, also showed a compensatory increase in neurotransmitter release to overcome AchR insensitivity and bring EPSPs to basal levels (Plomp et al., 1992). Further, genetic modifications using Drosophila NMJ (Davis & Goodman, 1998; Paradis et al., 2001; Petersen et al., 1997) as well as studies in mammalian neuronal cultures (Bartley et al., 2008; J. Kim & Tsien, 2008; Mitra et al., 2012) also demonstrated that perturbations in postsynaptic function leads to increases in neurotransmitter release.

Altogether, these findings revealed a common presynaptic homeostatic mechanism based on **increases of neurotransmitter release** to precisely **restore synaptic activity** after loss or impairment of postsynaptic receptors.

PHP can be activated in response to various types of perturbations in mammalian central synapses, including alterations in target innervation, postsynaptic excitability, sensory deprivation or chronic inhibition of synaptic activity (Davis & Müller, 2015).

Compensation of synaptic strength upon a continued perturbation through PHP mechanisms can take from **seconds to days** and induce little or great changes in presynaptic release (10-200%; Frank et al., 2006; Plomp et al., 1992). For example, impairing muscle-specific glutamate receptors with philanthotoxin (PhTx) at the Drosophila NMJ results in a rapid (~30 s) decrease of mEPSCs and EPSC amplitudes which are brought back to basal levels in ~10 min in the presence of PhTx (Frank et al., 2006). Yet, the specific mechanisms by which neurons modulate synaptic activity levels in response to external perturbations have just begun to be unravelled.

To that end, genetic screenings looking for potential candidates contributing to PHP have been performed in the Drosophila NMJ using the PhTx method explained above (Dickman & Davis, 2009; Müller et al., 2011, 2012; Younger et al., 2013). These studies helped to establish the bases of PHP by identifying key mutations that selectively

abolished PHP.

It is currently accepted that increases in release probability observed during PHP occur via two processes operating in parallel (Delvendahl & Müller, 2019): i) **increases in presynaptic calcium influx** through  $Ca_v2.1$  channels and ii) **increases in RRP size**:

i) *Increases in presynaptic calcium entry*: Presynaptic homeostatic plasticity is in part mediated by changes in presynaptic calcium influx which in turn modulate release probability (Fig. 15A; Müller & Davis, 2012). Although it is not clear whether control of presynaptic calcium entry is mediated by changes in channel number, function or both, a previous genetic study demonstrated the involvement of the presynaptic DEG/ENaC sodium leak channel during PHP and its coupling to homeostatic control of presynaptic calcium influx. Blocking DEG/ENaC channels with its antagonist benzamil at the NMJ, was found to obliterate the homeostatic response (Younger et al., 2013). According to these findings, it was proposed that DEG/ENaC channels are stored in synaptic vesicles at the synaptic bouton and that upon PHP activation, DEG/ENaC channels are inserted onto the presynaptic membrane and **control membrane resting potential** by modulating sodium leak. Consequently, presynaptic calcium influx is enhanced. Despite this evidence, whether PHP also involves the **insertion of  $Ca_v2.1$  channels at release sites** is still unknown.

ii) *Increases in RRP size*: Quantification of RRP size at the *Drosophila* NMJ revealed that PHP activation increases the number of vesicles ready to be released to compensate decreases in synaptic strength (Weyhersmüller et al., 2011). A further study

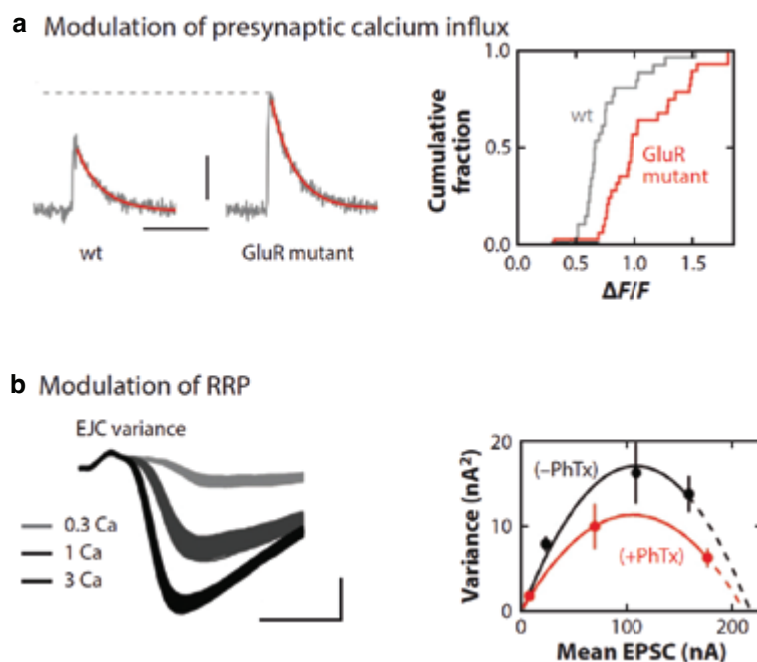


**Figure 15. Mechanisms of presynaptic homeostatic plasticity (PHP) at the *Drosophila* NMJ.** **A)** Left, example traces of evoked presynaptic calcium influx at baseline and upon induction of PHP. Scale bar 0.5  $\Delta F/F$ , 0.5 s. Right, cumulative frequency distribution of calcium transient peak amplitudes. **B)** Changes in the RRP based on variance-mean analysis. Left, example of excitatory junctional currents (EJC) at different calcium concentrations (mM). Right, parabolic fits to EJC amplitude variance-mean data that indicate an increase in RRP size after treatment with PhTx. (Adapted from Davis & Müller, 2015).

using fly RIM mutants showed that loss of RIM blocked PHP by impeding homeostatic increases in RRP size, whereas presynaptic calcium influx potentiation was unaffected (Fig. 15B; Müller et al., 2012). Same results were observed in mammalian central synapses where calcium influx and vesicle release were simultaneously imaged by the use of fluorescent reporters (Zhao et al., 2011).

Hence, these studies validated that increases in calcium entry and RRP size are both required for the homeostatic synaptic response to succeed.

Even though PHP compensation mechanisms are well understood, the molecular **signalling pathways** underlying changes in presynaptic calcium influx and RRP size are less clear. CDK5 has been proposed to be a potential candidate for controlling PHP, since its loss potentiates calcium entry and enhances RRP replenishment (S. H. Kim & Ryan, 2010, 2013). Also, as mentioned above, RIM has been proven essential for PHP, since its deletion erases the homeostatic response.

Importantly, for homeostatic control to be effective, **synaptic activity needs to be constantly monitored**. One possibility is that EPSC amplitude be somehow sensed such that changes in baseline activity initiate feedback signalling until it is well balanced. However, PHP has been shown to occur in the absence of evoked activity (Frank et al., 2006; X. Wang et al., 2010), suggesting **spontaneous neurotransmission** to provide enough information for monitoring synaptic transmission levels.

Efforts have been focused on finding sensor candidates at the postsynaptic level that detect the extent of the perturbation and relay the information to the presynaptic side through transsynaptic signalling. In this line of research, CaMKII (Haghighi et al., 2003) and TOR/S6K (Penney et al., 2012) signalling pathways have been found essential for the activation of the homeostatic response at the NMJ of *Drosophila* glutamate receptor IIA (GluRIIA) mutants.

Despite the remarkable progress made on PHP characterization during the last decades, too little is still known about **how synaptic strength is sensed and adjusted** in neural circuits.



# 3 Synapses and development

During embryonic development there is a massive formation of synapses that need to be refined during postnatal development in a process of synaptic elimination to ensure proper neural circuit connectivity. Formation and elimination of synaptic contacts also persist in mature neural circuits through experience-dependent synaptic plasticity (Gan et al., 2003; Holtmaat & Svoboda, 2009; Trachtenberg et al., 2002). Hence, changes in the number of synapses are important not only to shape neural circuits during development but also to modulate synaptic plasticity in response to experience.

Here, I will explain what is currently known about **synapse formation** and **elimination** with special emphasis on the role of **neuron-glia interactions** contributing to these processes.

## 3.1 Synapse formation

During the development of the nervous system, billions of neurons migrate to specific positions to form synaptic networks. The process of synapse formation, occurs between the end of the axon (presynaptic terminal) or along the length of the axon (*en passant* presynaptic bouton) of a given neuron and the dendrites or cell body of another, resulting in the pairing of pre- and postsynaptic specific partners. Many efforts have been made to determine where, when, and how synapses are formed and the manner in which this process is orchestrated during development.

Although synapse formation is a continuum process, it is generally divided into three major steps: i) axon guidance, ii) synaptic specificity, and iii) synaptic assembly (Fig. 16; Colón-Ramos, 2009; J. R. Sanes & Zipursky, 2020).

i) *Axon guidance*: after cells from the neuroepithelium turn into neuronal precursors by cell fate specification, neurons adopt a particular identity and migrate to a precise localization determined by the expression of morphogens and transcription factors (S. Y. Chen & Cheng, 2009). At this point, neurons extend projections that will become their axon and dendrites. Axons can travel long distances before reaching their postsynaptic partner (Debanne et al., 2011). To do that, the growth cone at the tip of the axon acts as a sensing device expressing multiple guidance receptors that are used to navigate and search for appropriate target areas. During the trajectory, the growth cone is guided by axon “**guideposts**” defined as environmental cues that can either act as long-range (diffusible) or short-range (surface) chemoattractant or chemorepellents, such as netrin or ephrin (C. E. Adler et al., 2006; Kennedy & Tessier-Lavigne, 1995).

Glial cells have been shown to direct innervation and serve as guideposts. For example, stellate cells of the cerebellum, that exclusively innervate Purkinje neurons, follow glial processes of Bergmann glia to reach Purkinje neurons (Ango et al., 2008). Once the axon finds its target area, it starts branching and searching for synaptic partners by extending long thin protrusions called filopodia, which are mainly composed of F-actin bundles (Fiala et al., 1998; Jontes et al., 2000). While the outer edge of the **growth cone** is directed by the **actin cytoskeleton**, which has been shown to be crucial during synapse formation (W. Zhang & Benson, 2001), **axonal growth** is supported by the **extension of microtubules**.

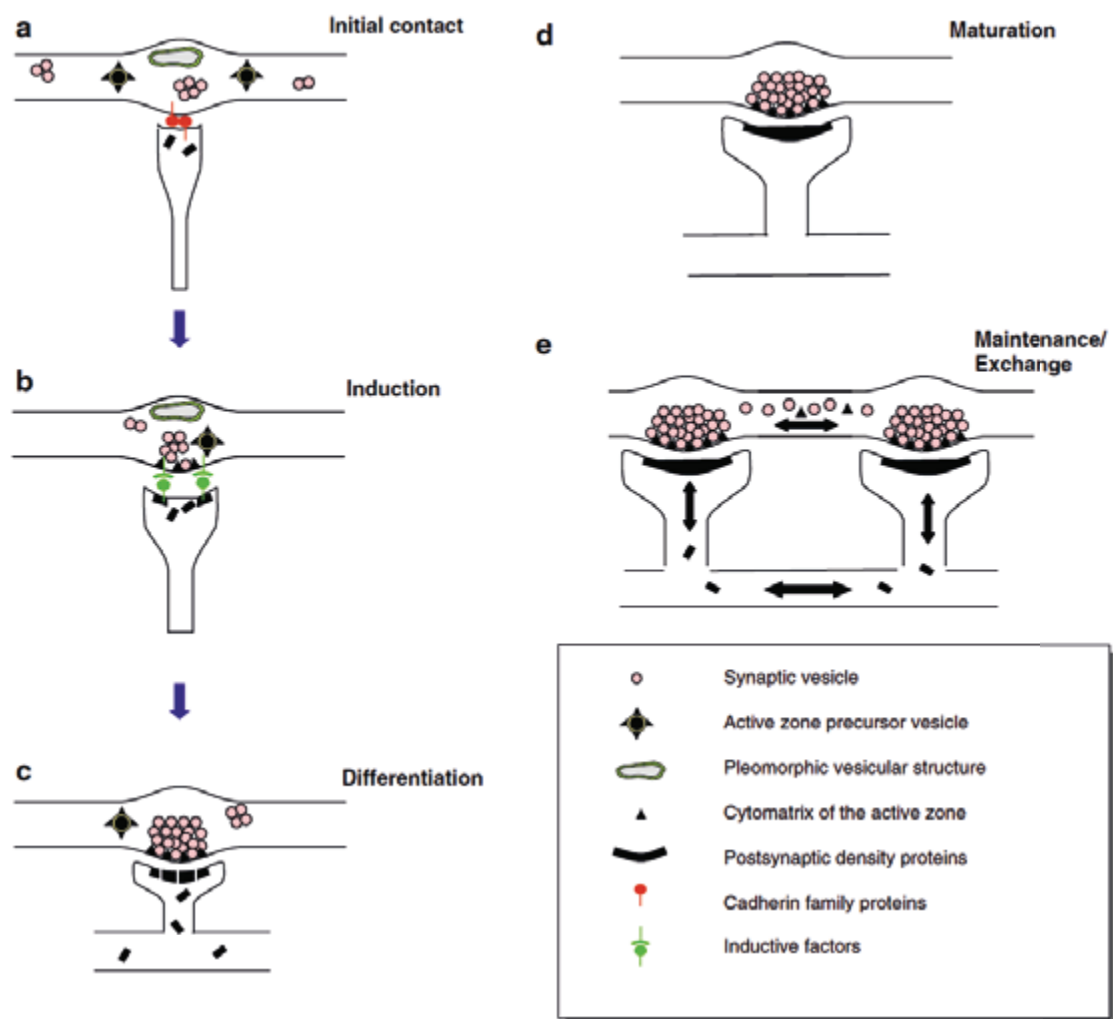


**Figure 16. Stages of synaptogenesis. A-B)** Synaptic specificity is mediated by initial contact between neurites through cell-adhesion molecules (sCAMs), which induce the formation of synaptic specializations and the recruitment of synaptic components. **C-D)** Synapse assembly is achieved by synaptic differentiation and maturation, which results in the stabilization of the nascent synapse to become fully functional. **E)** Finally, synapses need to be maintained over long periods of time by replacing and exchanging pre- and postsynaptic proteins. (Adapted from Garner et al., 2006).

ii) *Synaptic specificity*: at this point, neurites (neuronal processes of the axon or dendrites) initiate the recognition of potential targets available to them through the establishment of initial contacts mediated by **cell-adhesion molecules** (sCAMs) such as cadherins (Yamagata et al., 2018), NCAMs (Thiery et al., 1977) or neuroligin/neurexin (Scheiffele et al., 2000), among others (Fig. 16A and B).

Genetic studies have shown that this process does not depend on neurotransmitter release, but it is rather a **cell-autonomous program** (Sigler et al., 2017). Although it has been generally thought that synaptic contact occurs prior to synapse assembly, presynaptic (Prokop et al., 1996) and postsynaptic (Kummer et al., 2006) specializations have been reported to form in the absence of its partner, suggesting that synaptic specificity and assembly are **governed by two separate molecular pathways**.

iii) *Synaptic assembly*: whereas synaptic specificity determines where synapses form, synaptic assembly describes how synapses are formed (Fig. 16C and D). Both processes are part of what is known as **synaptogenesis**.

Since the neuronal biosynthetic machinery is restricted to the cell body, presynaptic components need to be synthesized in the soma, packed into **precursor vesicles** (PV), and **actively transported along the axon through microtubules** to nascent presynaptic specializations in a timely and spatially defined manner. Studies using cultured neurons have estimated that 1-5 PVs containing presynaptic components are enough to assemble a functional AZ (Ahmari et al., 2000; Shapira et al., 2003). Thus, the low abundance and transient nature of PV, diminishes the likelihood of visualizing these organelles during developmental studies and poses great challenges for characterizing its nature.

Synapse assembly requires AZ cytomatrix proteins (CAZ), exo- and endocytosis SV machinery,  $Ca_v$ s and SVs to be recruited and accumulated at nascent presynaptic compartments. Based on electron microscopy (EM) studies, different types of PVs including dense core vesicles (70-80 nm), pleiomorphic small vesicles (40–300 nm) and tubulovesicular structures have been identified as transport packets in axons. How these **presynaptic components are assembled**, in which **temporal order** (Emperador-Melero & Kaeser, 2020) and what is the **content carried** by each precursor organelle (Rizalar et al., 2021) is still contentious.

Another intriguing question about synapse formation not yet resolved is how somatic synthesis and **axonal trafficking** to nascent synapses is coordinated to ensure **stoichiometric amounts** of presynaptic material to assemble functional synapses (Ahmari et al., 2000; Goldstein et al., 2008; Shapira et al., 2003). It is possible that presynaptic biogenesis is **regulated by axonal transport** exerted by the motor proteins kinesins (Guedes-Dias & Holzbaur, 2019). The critical role of kinesins in the transport of PVs comes from studies in which mutants of KIF1A were reported to have fewer SVs and smaller AZs together with mislocalization of AZ proteins to the soma and dendrites

(Hall & Hedgecock, 1991; Pack-Chung et al., 2007; Yonekawa et al., 1998).

Once transported, synaptic vesicle precursors need to be delivered at nascent presynaptic compartments. Early studies proposed that SVs formed in the cell body are delivered as mature vesicles (40 nm; Yonekawa et al., 1998). However, given the diverse morphologies of precursor vesicles observed along axons during synapse formation, the idea of SVs being transported as immature precursors and undergoing maturation during transport or upon arrival at synaptic sites, seems more likely (Tao-Cheng, 2007; Vukoja et al., 2018). Although it is clear that precursor vesicles are transported along microtubules, how exactly is their **delivery** to the presynaptic terminal regulated and how new SVs may **enter the SV cycle** is yet to be uncovered.

Finally, each synapse type exhibits particular features that define its synaptic strength. Thus, a steady-state point of synaptic weight needs to be **set and adjusted** at nascent synapses within a given neuronal network. As explained in the previous chapter, this process is mediated by **homeostatic mechanisms**, which should involve **feedback control from the soma** to regulate presynaptic biogenesis. However, how it might be accomplished is largely unknown.

Growing evidence has revealed **glial cells** to be involved in **synapse formation and elimination**. Although most neurons in the mouse cerebral cortex start developing a few days after birth, massive synapse formation and maturation occurs during the second and third postnatal weeks. This period coincides with astrocyte maturation and differentiation, suggesting that the onset of synapse formation may be dependent on glial signals. In agreement with that idea, early studies revealed that neuronal cultures require glial cells or glial-conditioned media for neuronal survival and differentiation (Banker, 1980; Meyer-Franke et al., 1995), suggesting a **trophic role of glia** in synapse development. Consistently, later *in vivo* studies showed that if gliogenesis is blocked in the mouse cortex, neurodegeneration and altered synaptogenesis is observed (X. Li et al., 2012). Similarly, ablation of Schwann cells in tadpole developing NMJs resulted in reduced synapse formation and nerve terminal retraction (Reddy et al., 2003).

It has been well characterized that glial cells promote synapse formation by the **release of different factors** (Fig. 17). The first synaptogenic glia-derived secreted factors to be identified were thrombospondins 1-5 (TSPs; Christopherson et al., 2005). TSPs are expressed by immature astrocytes exclusively during the first week of postnatal development, coinciding with synapse formation initiation (Christopherson et al., 2005). Another important synaptogenic glial-secreted protein is hevin, also known as SPARC-like 1 (Kucukdereli et al., 2011). Similar to TSPs, hevin increases synapse numbers. However, the effect of hevin on synapse formation is balanced by the expression of another glial-secreted protein known as **SPARC** (Secreted Protein Acidic and Rich in Cysteine; Sage et al., 1984), which promotes synapse elimination (explained below). Accordingly, hevin mutants showed impaired formation and maturation of

synaptic contacts whereas SPARC mutants displayed accelerated formation of synapses (Kucukdereli et al., 2011). Since hevin and SPARC expression peaks during the second and third weeks of postnatal development, when strengthening or elimination of synapses occur, it is plausible that TSPs initiate synapse formation and **hevin and SPARC participate in either stabilizing or refining neuronal circuits** (W.S. Chung et al., 2015).

Additionally, microglia has also been shown to participate in synapse formation by the release of BDNF. Genetically inhibiting microglia or its conditioned release of BDNF showed decreases in spine formation and neurotransmission (Parkhurst et al., 2013). Finally, other glia-secreted factors such as glypcans 4 and 6 (N. J. Allen et al., 2012) or TGF- $\beta$  (Diniz et al., 2012; Fuentes-Medel et al., 2012) have also been identified to participate in synapse formation.

Although the molecular mechanisms of **neuron-glia interactions** during development are still limited, these findings indicate that glial cells are critical for synapse formation.

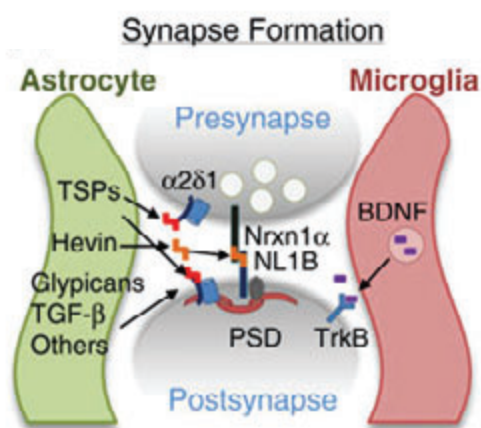


**Figure 17. Modulation of synapse formation by perisynaptic glia.** Synapse formation and maturation is controlled by several secreted astrocytic factors which bind to neuronal receptors (for example  $\alpha 2\delta$ -1 for TSPs and Nrnx1 $\alpha$ /NL1B for hevin). BDNF released by microglia also control synapse formation presumably by binding to the TrkB receptor. (Adapted from Stogsdill & Eroglu, 2017).

### 3.2 Synapse elimination

The exuberant number of synaptic contacts formed during development of the nervous system is selectively refined by a process of synapse elimination, also called **synaptic pruning**, during the first postnatal weeks. Although it is not known why this excess of connections initially form, or **how neurons adjust a correct number of synapses** by balancing synapse formation and elimination, it is clear that synaptic refinement is vital for the precise maturation of synaptic circuits (L. Katz & Shatz, 1996; Riccomagno & Kolodkin, 2015). In fact, deficits in synaptic pruning have been linked to pathological disorders such as autism (Tang et al., 2014; Tsai et al., 2012) and schizophrenia (Hoffman & McGlashan, 1997).

Compared to synapse formation, however, much less is known about the process underlying synaptic pruning. Important questions such as, how synapses are tagged



for elimination, which molecules are involved or how their disassembly and removal is accomplished, have been investigated during the last decades. A model for synapse elimination involving the following three sequential stages has been proposed (Fig. 18; Terni et al., 2017): i) **tagging**: inputs that will be removed are selected for elimination based on their synaptic strength, ii) **irreversible disassembly**: synaptic terminals lose their functional structure and disassemble. And iii) **elimination of synaptic remnants by phagocytosis**: synapses are finally removed by glial engulfment.

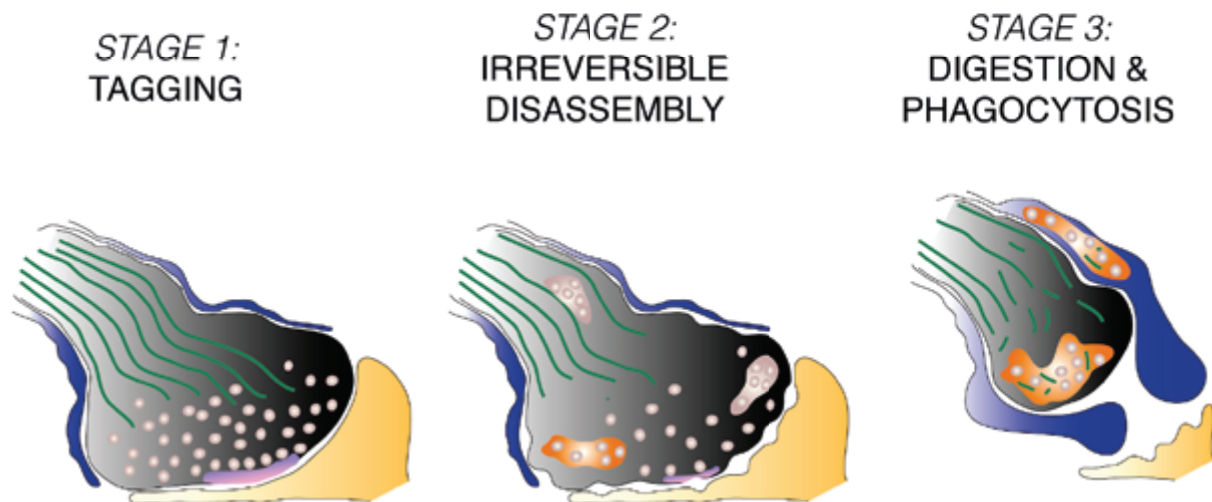


**Figure 18. Three-stage model of synaptic elimination.** In the first stage, selection of synapses for elimination is driven by neuronal activity or by the expression of molecules of the immune system. Subsequently, tagged synapses enter an irreversible program of disassembly characterized by cytoskeletal integrity loss (green) and formation of multivesicular bodies (orange). Finally, synapse elimination is completed by digestion via lysosomes or engulfment by glial cells. (Adapted from Terni et al., 2017).

### *Molecular mechanisms controlling synapse elimination*

**Glial cells**, which include astrocytes, microglia and oligodendrocytes in the central nervous system (CNS), and Schwann cells and satellite cells in the peripheral nervous system (PNS), are in tight association with synapses and are also important during synaptic development. Morphological and functional studies revealed that glial processes wrap neuronal axons, dendrites, somas and synapses (Halassa et al., 2007) and actively participate in the regulation of synaptic activity (Fig. 19; Araque et al., 1999). These findings led to the concept of the **tripartite synapse**, composed by two neurons and a glial cell as a functional unit.

Neuronal activity has been proven to be critical for selecting synapses for removal (Barber & Lichtman, 1999; Sengpiel & Kind, 2002) by a process of **activity-dependent competition** in which presumable “weak” synapses are selected for elimination whereas “strong” synapses undergo further maturation (Balice-Gordon & Lichtman,

1994; Busetto et al., 2000; Ridge & Betz, 1984).

Emerging evidence indicates that glial cells, microglia, astrocytes and Schwann cells, participate in synaptic pruning, either directly by **phagocytosis**, or indirectly by **secreting molecules** that elicit terminal disassembly and subsequent elimination (Neniskyte & Gross, 2017; Terni et al., 2017; Wilton et al., 2019).

Astrocytes can sense and modulate synaptic transmission levels. Synaptic activity elicits the elevation of intracellular  $\text{Ca}^{2+}$  in neighbouring astrocytes and triggers the release of gliotransmitters such as ATP (Fields & Burnstock, 2006) or D-serine (Henneberger et al., 2010) that in turn regulate synaptic efficacy. A similar mechanism responsible for activity-dependent synapse elimination mediated by glial cells has been proposed (Yang et al., 2016).

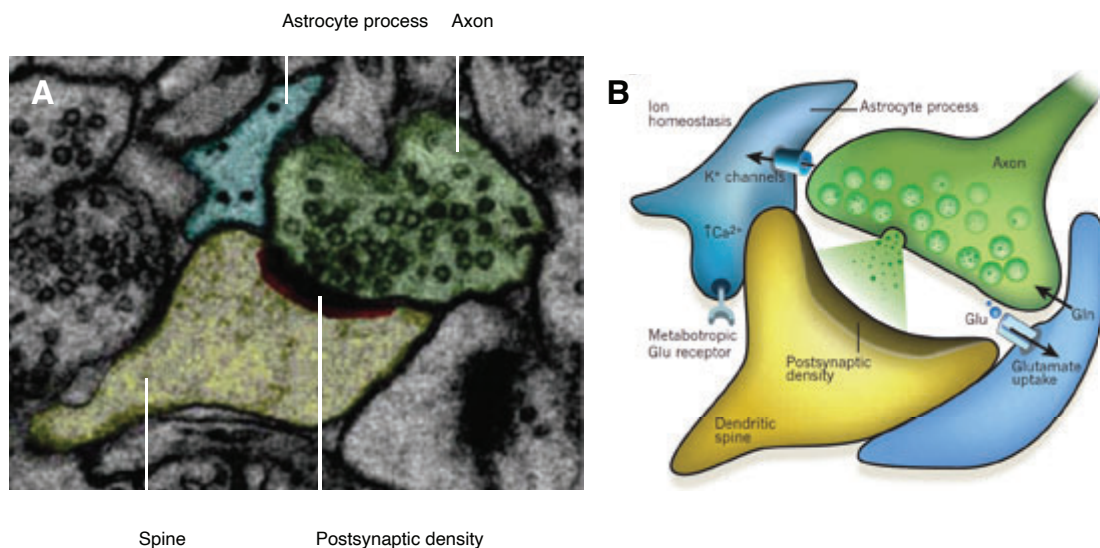


**Figure 19. The tripartite synapse.** Astrocyte processes are intimately associated with synapses both structural and functionally. **A)** Electron micrograph showing a tripartite synapse in the hippocampus. **B)** Schematic representation of a tripartite synapse. Through neurotransmitter receptors and transporters glial cells can monitor and modify synaptic neurotransmission. (Adapted from Eroglu & Barres, 2010).

The contribution of glial cells in synapse elimination has been demonstrated in diverse model systems ranging from peripheral synapses such as those at the NMJ to the central nervous system, such as the retinohthalamic system.

Here, I will revise the mechanisms of synapse elimination that have been found in these neuronal circuits to illustrate the role of **activity-dependent** and **glia-mediated synaptic refinement** (Fig. 20).

a) *Neuromuscular junction*: Given its simplicity, accessibility, and large size, the NMJ is the best studied example of synapse elimination at the PNS. During embryonic development, motor end-plates are innervated by multiple axons (~10). Over the first post-natal weeks, however, all but one of these inputs are withdrawn through activity-de-

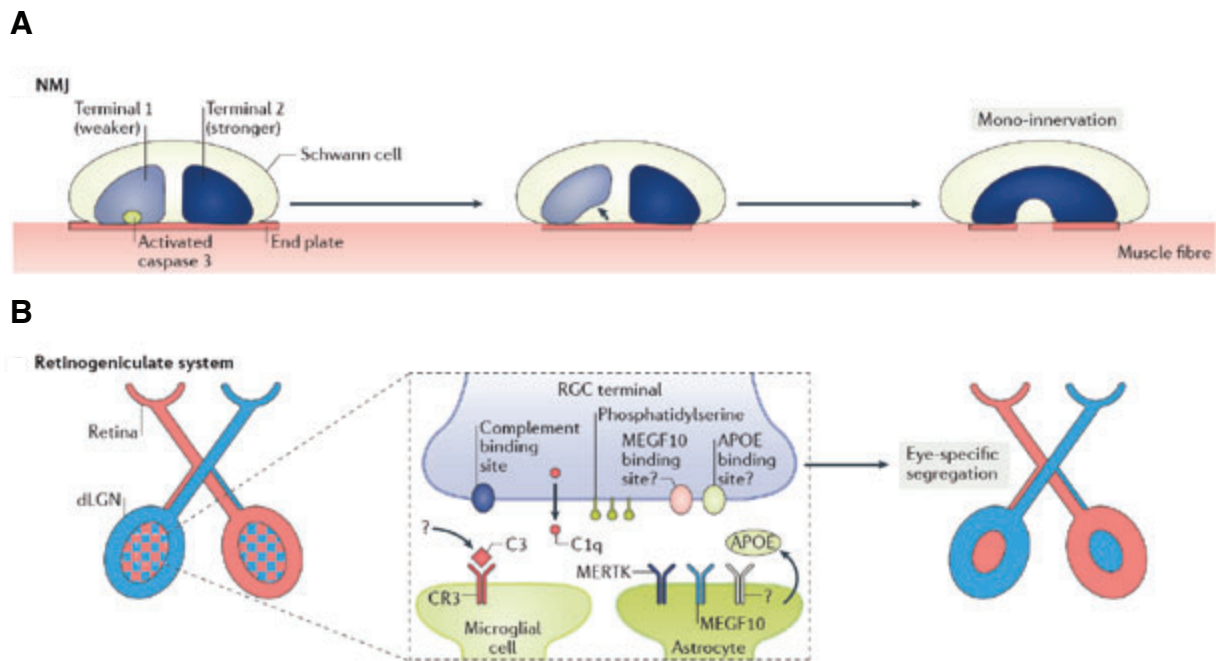


**Figure 20. Molecular mechanisms of synaptic pruning by glial cells. A)** At the developing NMJ, Schwann cells envelop multiple synaptic terminals onto the motor endplate. Weaker inputs are retracted and engulfed by Schwann cells resulting in mono-innervation of the muscle fibre. **B)** During development, RGCs in the eye send projections to both the contralateral and ipsilateral dorsal lateral geniculate nucleus (dLGN). Eye-specific segregation is achieved by synapse elimination mediated by microglia and astrocytes. (Adapted from Neniskyte & Gross, 2017).

pendent competition, which results in the disassembly and axon retraction of weaker motor inputs leaving each NMJ innervated by a single motor neuron that shows high synaptic efficacy (Fig. 20A; Colman & Lichtman, 1993; R. J. Sanes & Lichtman, 1999). Of interest, increasing or decreasing activity of individual synaptic inputs, for example by genetic manipulation of choline acetyl transferase in subsets of motor inputs (Buffelli et al., 2003), has clearly demonstrated the key role of **synaptic activity** in NMJ pruning. Additionally, combination of time-lapse imaging of fluorescent axons and electron microscopy has shown that “weaker” axons are retracted (Fig. 21; Walsh & Lichtman, 2003) and eliminated by shedding membrane remnants that are eventually engulfed by Schwann cells in the form of “**axosomes**” (Bishop et al., 2004). These findings have been indirectly confirmed by subsequent studies in which increased **lysosomal activity** was observed in retracting axons as well as in Schwann cells during synaptic elimination (Song et al., 2008). Besides, coupling of glial  $\text{Ca}^{2+}$  imaging together with electrophysiological recordings of NMJs have revealed the presence of intracellular  $\text{Ca}^{2+}$  spikes in **Schwann cells** in response to the release of Ach from motor neurons (Darabid et al., 2013), suggesting that decoding of synaptic strength of competing nerve terminals by Schwann cells may be used as a mechanism for selection of weak terminal inputs that will be subsequently engulfed and eliminated.



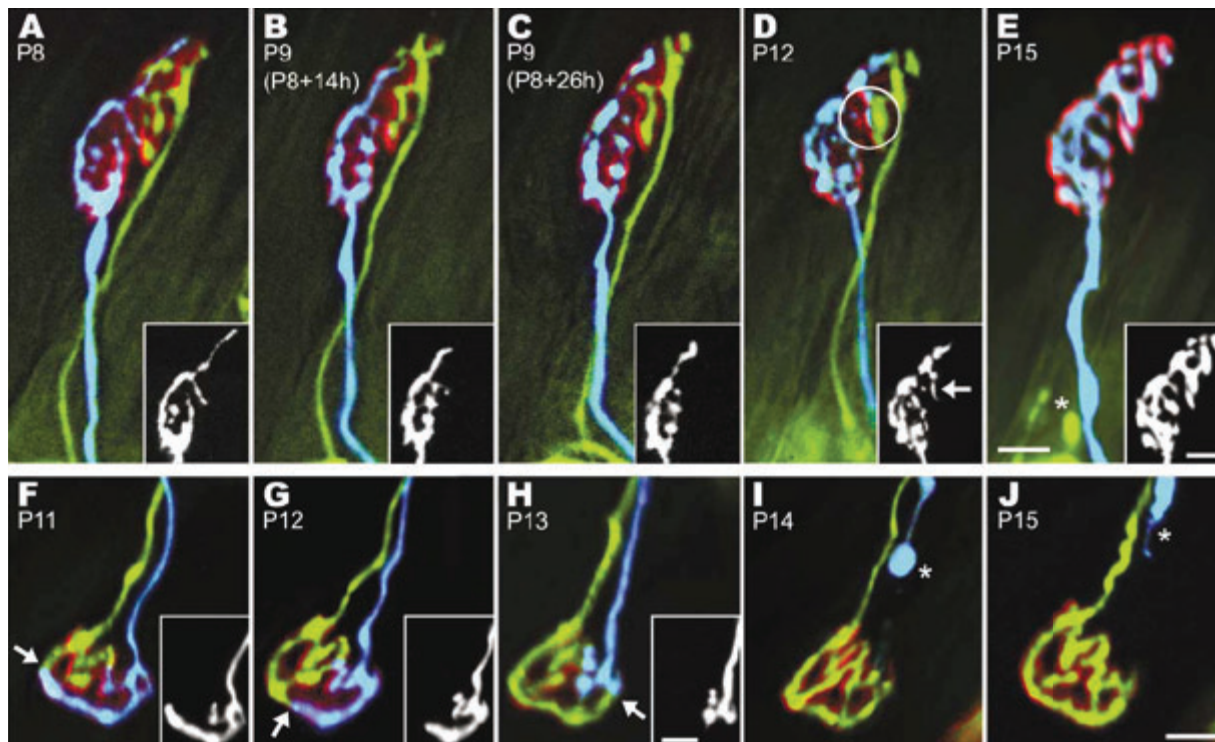


**Figure 21. Synaptic pruning at the NMJ.** In vivo imaging of 2 multi-innervated junctions between P8-P15 (A-E) and P11-P15 (F-J). In the first NMJ (A-E) the blue axon ends up occupying the sites in the upper part of the junction (D, circle) where the yellow axon was, which is consequently retracted (E, asterisk). In the second NMJ (F-J), the blue axon, which initially occupied a greater terminal area is progressively withdrawn (F, G and H, arrows) from the junction until it is retracted (I and J, asterisks). Insets, 70% size reduction. Scale bars equal 10  $\mu$ m. (Adapted from Walsh & Lichtman, 2003).

b) *Retinothalamic system*: Synaptic refinement in the visual system is vital for input segregation of each eye to the thalamus. Initially, retinal ganglion cell (RGC) projections from both eyes (ipsilateral and contralateral) form multiple, overlapping connections in neurons of the dorsal lateral geniculate nucleus (dLGN). Eye-specific segregation is achieved during the first postnatal week, before eye opening, by the elimination of overlapping connections such that each dLGN cell receives only 1-2 DRG inputs from a specific eye (Huberman et al., 2008). Although it is well established that this is an **activity-dependent** process driven by spontaneous retinal activity (Penn et al., 1998), strong evidence indicates that **phagocytosis** by glial cells (microglia and astrocytes) plays a key role during synapse elimination in the retinothalamic system (Fig. 20B). First evidence came from a study of Stevens et al. where it was found that during synaptic pruning, components of the **classical complement cascade**, C1q and C3, tag RGC presynaptic terminals for subsequent phagocytosis by microglia expressing the C3R receptor (Schafer et al., 2012; B. Stevens et al., 2007). Genetic ablation of C1q, C3 or CR3 was shown to result in reduced eye-segregation and partial overlapping of DRG inputs in the dLGN, indicating phagocytosis mediated by the complement pathway to be important for synaptic refinement in the retinothalamic system. However,

because segregation and synaptic loss were not completely prevented, it was proposed that other mediators must complete the action of microglial cells.

In parallel, astrocytes in the dLGN at the end of the first postnatal week were reported to actively engulf synaptic material, possibly complementing the action of microglia (W.S. Chung et al., 2013).

Finally, as mentioned above, retinal activity drives selective elimination of weaker DRG inputs. Consistently, pharmacological blockade of spontaneous activity on P4 was shown to reduce phagocytosis by astrocytes and microglia (W.S. Chung et al., 2013; Schafer et al., 2012).

Altogether, these findings illustrate the importance of both synaptic activity and phagocytosis by glial cells during synapse elimination. However, increasing evidence indicates that the role of glial cells is not limited to debris clearance, but also involves the **secretion of factors** that contribute to synaptic refinement. This is the case of ATP (Yang et al., 2016) and **SPARC** (López-Murcia et al., 2015; Vincent et al., 2008). Here, I will focus on SPARC, since it was used during this thesis to promote synaptic elimination.

### 3.3 Role of SPARC in synapse elimination

SPARC, also referred to as osteonectin (Romberg et al., 1985; Termine et al., 1981) or BM-40 (Dziadek et al., 1986) is a **matricellular protein** which **expression peaks during development** and decreases upon tissue differentiation. In adults, its expression is restricted to tissues undergoing extracellular matrix (ECM) **remodelling**, such as bone, in response to injury and in disease conditions such as cancer. Accordingly, SPARC has been shown to participate in the organization of the ECM and in cell migration and proliferation (Bradshaw & Sage, 2001). Given its high expression in different malignant tumours and metastasis, SPARC has attracted great interest from the cancer research community (Ledda et al., 1997; Salvatierra et al., 2015). Interestingly, strong evidence has shown that SPARC participates in the synaptic refinement of the nervous system (explained below).

SPARC's structure consists of 286 residues divided into three domains: an acidic N-terminal segment, a follistatin-like (FS) domain and an  $\alpha$ -helical domain containing two EF-hand calcium-binding sites (EC domain; Fig. 22; Hohenester et al., 1997; Maurer et al., 1995). Although it can also be found in its full-length form, SPARC has been shown to be **processed by metalloproteases** (Sasaki et al., 1997, 1998, 1999) and **bind to collagen** in a calcium dependent manner (Kaufmann et al., 2004; Mayer et al., 1991; Sasaki et al., 1997, 1998). Interaction of SPARC with other components of the ECM, such as thrombospondin 1 (Clezardin et al., 1988) and vitronectin (Rosenblatt et al., 1997), as well as with growth factors, such as PDGF (Raines et al., 1992) or VEGF (Kupprion et al., 1998) has also been reported.

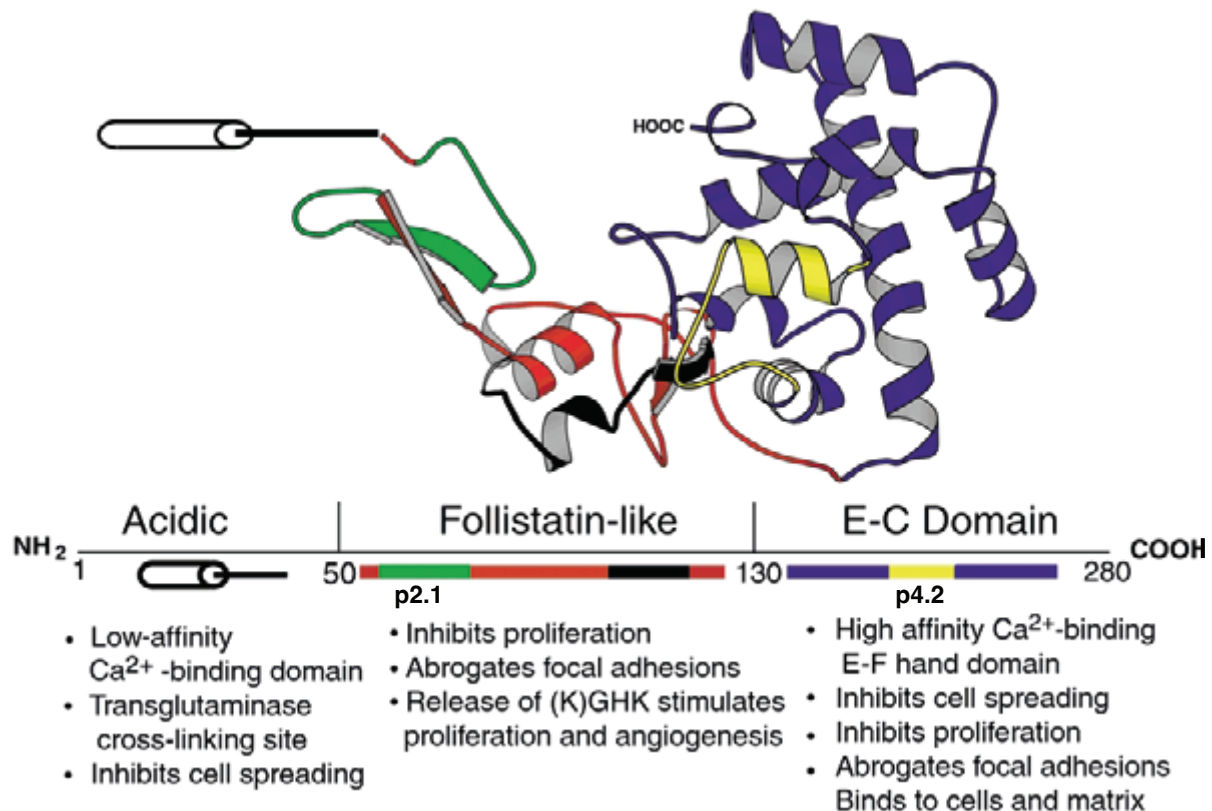


**Figure 22. Structure of SPARC.** Diagram derived from crystallographic data shows the three SPARC domains. Activities attributed to each domain are stated below. The peptides p2.1 in the follistatin-like domain (green) and the p4.2 in the EC-domain (yellow) are represented. (Adapted from Bradshaw & Sage, 2001).

The biological activity of SPARC to inhibit cell spreading (Sage et al., 1989), modify cell shape (Lane & Sage, 1990) and promote loss of focal adhesions (Murphy-Ullrich et al., 1995) characterizes SPARC as a **counteradhesive protein**. The effect of SPARC in abrogating focal adhesions was shown to be linked to **redistribution of F-actin** to the periphery in endothelial cells. In order to determine which of the SPARC domains mediated this action, peptides from the four regions of SPARC were tested (Fig. 23A and B). Only the cysteine-rich **peptide 2.1** (amino acids 54-73) and the  $\text{Ca}^{2+}$ -binding EF-hand-containing **peptide 4.2** (amino acids 254-273) were shown to disassemble focal adhesions (Murphy-Ullrich et al., 1995).

In the **nervous system**, SPARC's expression peaks during **postnatal development** and is exclusively expressed by glial cells (Vincent et al., 2008), where it is enriched in the **processes of astrocytes** (Sakers et al., 2017). A relevant study on astrocyte gene expression profiling revealed that SPARC and hevin, two proteins with high sequence affinity, are highly expressed in the **developing brain** (Kucukdereli et al., 2011). As explained before, hevin was identified as an inducer of synapse formation, while SPARC was shown to antagonize its action in RGC cultures.

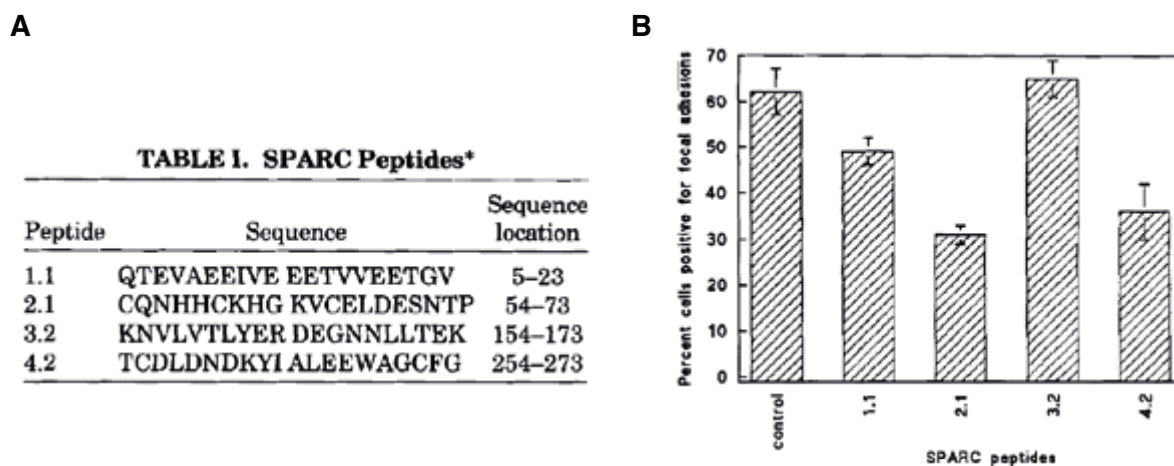


**Figure 23. Effect of SPARC peptides on abrogating focal adhesions. A)** Sequences of murine SPARC peptides (Mason et al., 1986). Numbers refer to the position of amino acids after removing the signal sequence. **B)** SPARC peptides 2.1 and 4.2 (0.2 mM) incubated for 1h at 37°C cause focal adhesion disassembly in endothelial cells. Results are expressed as the mean percentage of cells positive for focal adhesions (n=3-8). (Adapted from Murphy-Ullrich et al., 1995).

Nonetheless, the view that SPARC has an antagonistic role of hevin was challenged by our group in a previous study which showed that SPARC triggers a **cell-autonomous program of synapse elimination** in autaptic cultures (López-Murcia FJ et al., 2015). Decreases in the number of synaptic contacts and evoked postsynaptic responses were observed together with the presence of retracting axons after treatment with the active SPARC-derived peptide p4.2 (Fig. 24A-J; López-Murcia FJ et al., 2015). These data showed that the action of SPARC is hevin-independent, and therefore, that SPARC is not a mere hevin antagonist. Additionally, in agreement with previous findings demonstrating the ability of SPARC to redistribute F-actin in endothelial cells (Murphy-Ullrich et al., 1995), the disassembling effect of peptide p4.2 observed in autaptic cultures was abolished if neurons were treated with the F-actin stabilizer jasplakinolide (Fig. 24D; López-Murcia et al., 2015), indicating synapse elimination triggered by SPARC to depend on changes of the **F-actin cytoskeleton**.

Although the molecular target of SPARC is still unclear, early and recent data suggest that SPARC might be able to bind to different partners. On one hand, an early study showed that SPARC controls the number of AMPA receptor subunits during development via a  $\beta$ 3-integrin-mediated mechanism (Jones et al., 2011). On the other hand, a recent study has shown that both, SPARC and hevin, compete for the same target and are able to bind to the transsynaptic adhesion proteins neuroligins and neuroligins through their highly conserved FS domain (Fan et al., 2021). These data suggest that by the regulation of cell-adhesion molecules, **SPARC** and **hevin** might promote either the **disassembly** or **stabilization of synaptic contacts**, respectively.



Collectively, it is clear that synapse elimination is governed by synaptic activity and the contribution of glial cells. Yet, whether glial cells actively select “weak” synapses for elimination depending on activity levels, directly by phagocytosis or by the release of cues such as SPARC, or if synaptic molecular differences define “strong” and “weak” synapses by conferring resistance to synapse elimination promoted by glial cells, is still a matter of debate.

**Based on these findings, this project aims to further investigate the capability of SPARC to promote synapse elimination in an autaptic circuit and to better understand the molecular mechanisms underlying this process.**

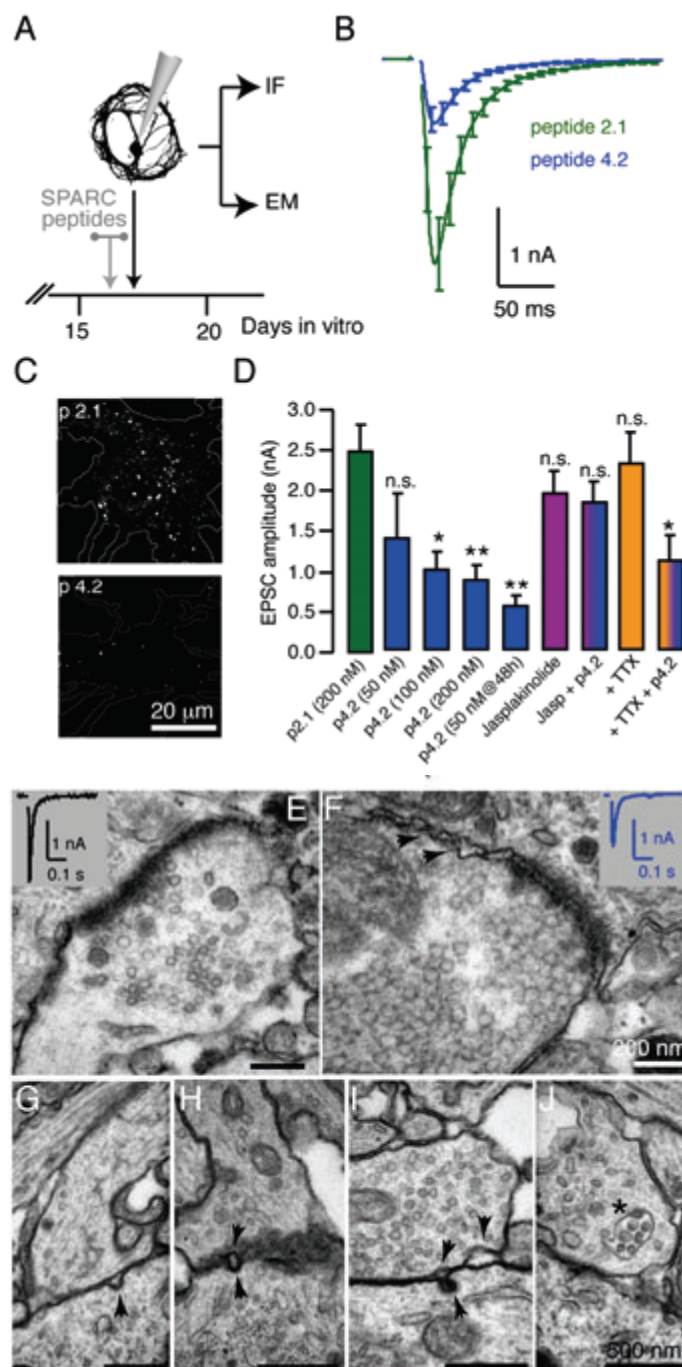


**Figure 24. The active peptide of SPARC, p4.2, triggers the disassembly of mature cholinergic synapses.** **A)** Experimental setup. Autaptic cultures were acutely incubated with different SPARC peptides for 4-6h. **B)** Average EPSCs of neurons exposed either to p2.1 (n=8) or p4.2 (n=33). **C)** p4.2 decreases the number of presynaptic terminals measured as bassoon puncta. **D)** Amplitude of postsynaptic responses assessed in different conditions. Note that the effect of p4.2 was hampered by jasplakinolide but not TTX (200 nM p2.1, n=13; 50 nM p4.2, n=18; 100 nM p4.2, n=6; 200 nM p4.2, n=16, 1 μM jasplakinolide, n=11; 1 μM jasplakinolide + 200 nM p4.2, n=12; 20 nM TTX, n=6; 20 nM TTX + 200 nM p4.2, n=8). **E-J)** Electron micrographs of cholinergic autaptic cultures. **E)** Control neuron, **F)** p4.2 treated neuron, arrows indicate membrane invaginations near an active zone, **G-J)** Images of four different p4.2 treated neurons, arrows indicate endocytic profiles and the asterisk (**J**) a multivesicular body. All averages are presented as mean ± sem. \*p< 0.01; \*\*p< 0.001. (Adapted from López-Murcia et al., 2015).

### 3.4 Homeostatic synaptic plasticity during development

As explained in the previous chapter, constant activity levels are maintained throughout development thanks to homeostatic plasticity mechanisms that balance changes in synaptic connectivity by modulating synaptic strength and intrinsic excitability. For the last few decades, pre- and postsynaptic homeostatic plasticity mechanisms have been focused on homeostatic responses triggered by experimental perturbations, such as AP-evoked activity blockade and postsynaptic receptor impairment and loss. Barely anything is known, however, about how the nervous system adapts to **synaptic pruning**.

Two evidences obtained in the refinement of visual pathways have shown the involvement of synaptic scaling during synapse elimination. In one study, decrease of mEPSC amplitude was observed together with increase of mEPSC frequencies and synapse numbers (Desai et al., 2002), indicating the **scaling down** of receptors to **compensate massive synapse formation** (Fig. 25). Another example of developmental homeostatic regulation in the retinogeniculate circuit comes from a study showing **strengthening** of selected connections to compensate synapse loss (Hooks & Chen, 2006), thus reflecting the involvement of homeostatic synaptic plasticity mechanisms in **response to synapse elimination**. Despite this evidence, how neural circuits may **sense** activity and **adjust** synaptic strength to changes in synapse numbers is still unknown.

**In this thesis, we have taken advantage of the ability of SPARC to promote synapse elimination to investigate how neural circuits respond and adapt to synapse loss.**

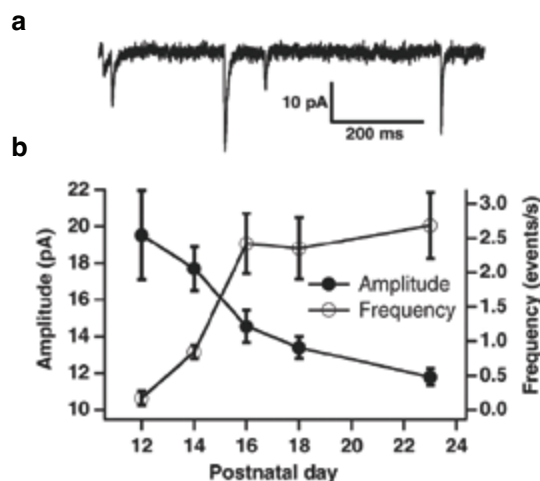


**Figure 25. Homeostatic response triggered by changes in connectivity. A)** Example of mEPSCs recorded from a neuron in layer 4 at P16. **B)** Average mEPSC amplitude (dots) and frequency (circles) in layer 4 neurons as a function of postnatal day. While mEPSC frequency increased during the second and third postnatal weeks due synapse formation, mEPSC amplitude decreased to maintain baseline activity. (Adapted from Desai et al., 2002).

# 4

## Role of the cytoskeleton in synaptic transmission

The cytoskeleton is composed of three types of filaments: actin, microtubules (MTs), and intermediate filaments, and plays important roles in cell division, motility, shape, and intracellular trafficking of all eukaryotic cells. In neurons, the cytoskeleton is essential for the formation of axons and dendrites during development, and in mature synapses it provides a structural backbone that maintains complex and branching structures and controls dynamic synaptic functions. Here, I will focus on what is currently known about the role of **actin filaments** and **microtubules** in synaptic transmission.

### 4.1 The synaptic actin cytoskeleton

Actin is the major component of pre- and postsynaptic terminals at mature synapses and drives structural changes associated to synaptic plasticity. The actin cytoskeleton is **highly dynamic** and can be found in two states within the cell: as monomers (**G-actin**) or as asymmetric two-stranded helical filaments (**F-actin**). Rapid actin dynamics (assembly/disassembly) is possible thanks to the weak, non-covalent interactions of actin monomers. At steady-state, F-actin polymerizes preferentially at the barbed end, while depolymerization occurs at the pointed end, the difference resulting in the net turnover of filaments (Fig. 26A). This process is modulated by a variety of actin-binding proteins (ABPs; reviewed in [Revenu et al., 2004](#)).

Generally, studies into the synaptic functional role of the actin cytoskeleton have relied on genetical and pharmacological approaches. Permeable drugs that either promote the **disassembly** of F-actin by sequestering G-actin monomers, such as latrunculin-A or cytochalasin B, or that **stabilize** F-actin filaments, such as jasplakinolide and phalloidin, have contributed to the current understanding of the actin cytoskeleton in synaptic transmission.

As mentioned in chapter 3, actin and microtubules play a fundamental role during synapse formation ([Dent & Gertler, 2003](#)). Specifically, actin is highly enriched in axonal and dendritic growth cones and its disruption inhibits filopodial motility and synaptogenesis ([Dunaevsky et al., 1999](#); [Wong et al., 2000](#); [W. Zhang & Benson, 2001](#)). Interestingly, a study in hippocampal cultured cells showed that the requirement of the actin cytoskeleton for maintaining the structure and localization of presynaptic proteins depends on the developmental stage. Treatment of young neurons (6 days in vitro, DIV) with latrunculin-A resulted in the loss of presynaptic proteins, such as sy-

naptophysin and bassoon, and ultrastructural synaptic morphology. In contrast, mature synapses (20 DIV) became increasingly resistant to the effect of latrunculin-A (W. Zhang & Benson, 2001), suggesting that the **actin cytoskeleton** is a candidate target for **maintaining or eliminating synaptic contacts during postnatal development**.

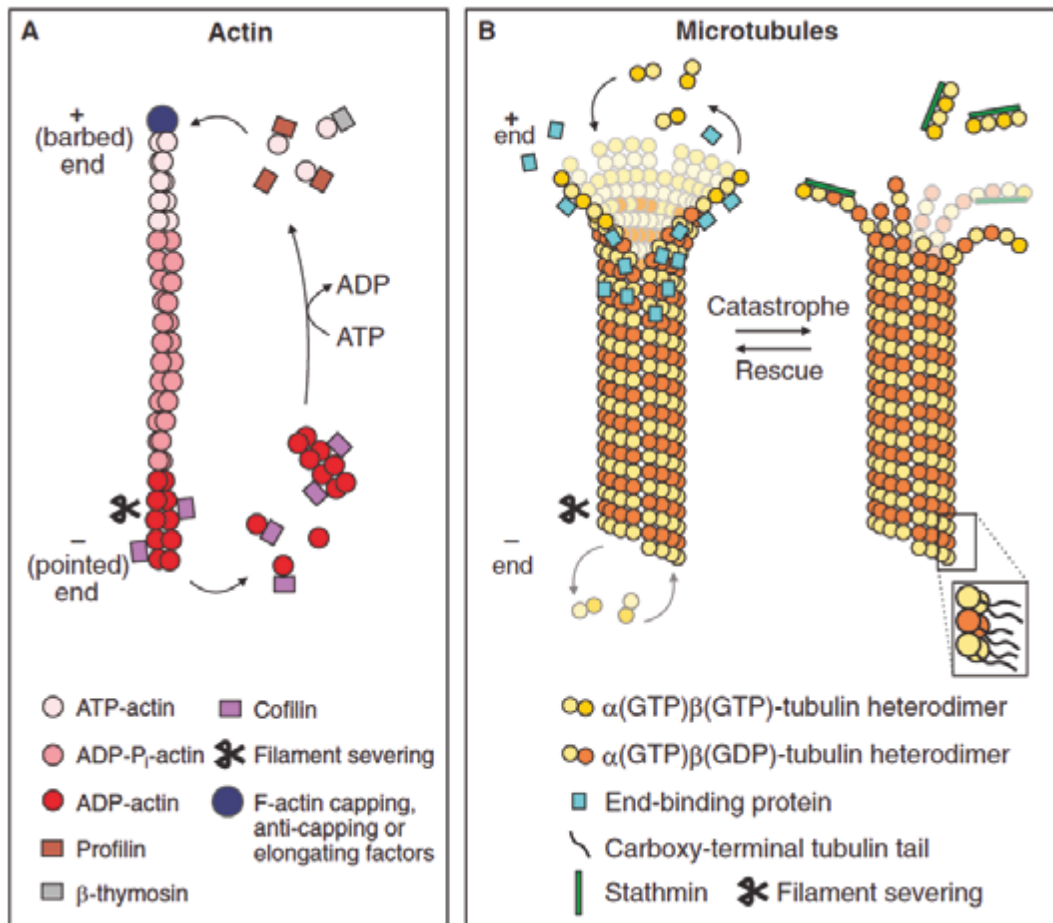


**Figure 26. Actin filaments and microtubules polymerization dynamics. A)** Actin filaments are elongated by the addition of ATP-actin monomers to the barbed end (+ end) mediated through profilin and barbed-end-bound elongating factors such as formins. ADP-actin monomers or F-actin fragments are removed from the pointed end (- end) of the filament by the action of depolymerising or severing factors such as cofilin. The detached actin can exchange its ADP for ATP and be recruited once more to the growing filament barbed end. **B)** Representation of microtubule rescue and catastrophe. Left, polymerisation occurs mostly at the plus(+)-end through the addition of  $\alpha/\beta$ -tubulin heterodimers. After incorporation into the microtubule filament, hydrolysis of the  $\beta$ -tubulin-bound GTP takes place. End-binding (EB) proteins can transiently bind to the plus end, influencing polymerisation dynamics. Right, reduction in the concentration of free  $\alpha/\beta$ -tubulin heterodimers, for example due to stathmin-mediated sequestration, is one way to induce microtubule catastrophe, leading to filament shrinkage. (Adapted from Coles & Bradke, 2015).

### *The presynaptic actin cytoskeleton*

Despite the fact that the presynaptic compartment becomes independent of F-actin disruption by latrunculin-A as development proceeds (as explained above), the presy-



naptic terminal remains highly enriched with actin in mature neurons, constituting the 2% of total protein content (Wilhelm et al., 2014).

In the presynaptic terminal, the actin cytoskeleton is organized in branched networks of F-actin (Korobova & Svitkina, 2010) that surround the SV cluster and associate to the active zone (Colicos et al., 2001; Y. C. Li et al., 2010; Morales et al., 2000; Sankaranarayanan et al., 2003), while G-actin is distributed throughout the terminal to maintain the F-actin pool (Fig. 27; Wandong Zhang & Benson, 2002).

Synaptic vesicle pools need to be physically segregated at rest to impede uncontrolled release of SVs and mobilized upon synaptic activity either by active movement or diffusion. Morphological studies have revealed the localization of **actin filaments surrounding the cytoplasmic vesicle pool** with very little actin found within the cluster

itself (Dunaevsky & Connor, 2000; Richards et al., 2004; Sankaranarayanan et al., 2003; Shupliakov et al., 2002). Actin association to SVs occurs via short filaments (~30 nm) of **synapsin-I**, which interlink and stabilize synaptic vesicles (Bloom et al., 2003; Gotow et al., 1991; N. Hirokawa et al., 1989; D. M. D. Landis et al., 1988; L. Li et al., 1995; Pieribone et al., 1995). Although the synaptic role of actin may vary among synapse types, it has been proposed that the actin-synapsin meshwork maintains and regulates the cytoplasmic pool by constituting a **physical barrier to restrict SV mobility** (Dillon & Goda, 2005). In addition to the role of actin in corralling synaptic vesicles, long actin filaments connecting the cytoplasmic vesicle pool with the AZ have been observed (Evans et al., 1998; Prekeris & Terrian, 1997), suggesting that actin may provide **cytoskeletal tracks** to facilitate the transfer of SVs to refill the RRP.

Furthermore, F-actin has also been

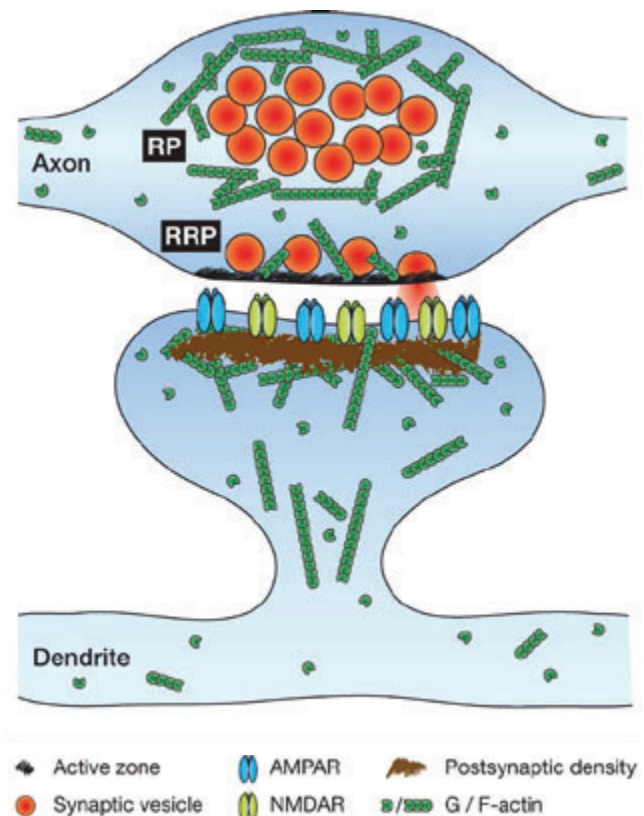


**Figure 27. Distribution of the synaptic F-actin cytoskeleton in a glutamateric synapse.** In the presynaptic terminal, actin filaments surround the cytoplasmic pool of vesicles where they act as a physical barrier. Actin is also present at the active zone in association to vesicles belonging to the RRP. In the postsynaptic terminal, F-actin is present throughout the spine and contacts the postsynaptic density. Actin monomers are homogeneously distributed throughout both synaptic compartments. (Adapted from Dillon & Goda, 2005).

shown to be involved in the positioning of recycled SVs adjacent to the AZ (Marra et al., 2012).

Collectively, these findings indicate that the actin cytoskeleton is involved in the **mobilization of SVs** which is particularly relevant to sustained neurotransmitter release (Fig. 28A).

Several lines of evidence from biochemical (Phillips et al., 2001), ultrastructural (Bloom et al., 2003; N. Hirokawa et al., 1989; Phillips et al., 2001; Rostaing et al., 2006), and functional (Morales et al., 2000) studies indicate that actin filaments are present at the AZ. It is not completely understood, however, to what extent dynamic actin participates in modulating synaptic transmission. Aside from the role of actin in regulating the size of the RRP by facilitating its replenishment, changes in neurotransmitter release following pharmacological disruption of the actin cytoskeleton have also been reported (Cole et al., 2000; C. H. Kim & Lisman, 1999; Kuromi & Kidokoro, 1998; Richards et al., 2004; Sankaranarayanan et al., 2003; X. H. Wang et al., 1996). Hence, it has been suggested that actin may control SV exocytosis by forming a physical barrier that acts as a **brake to prevent synaptic vesicle fusion** (Fig. 28B). In support to this suggestion, blocking F-actin polymerization by latrunculin-A treatment resulted in increased release probability in hippocampal cultures together with increases in the frequency of mEPSCs, without affecting RRP size (Morales et al., 2000). Likewise, the speed of evoked SV exocytosis, assessed using the styryl dye FM1-43, was enhanced upon latrunculin-A treatment (Sankaranarayanan et al., 2003), thus highlighting the role of actin in presynaptic plasticity.

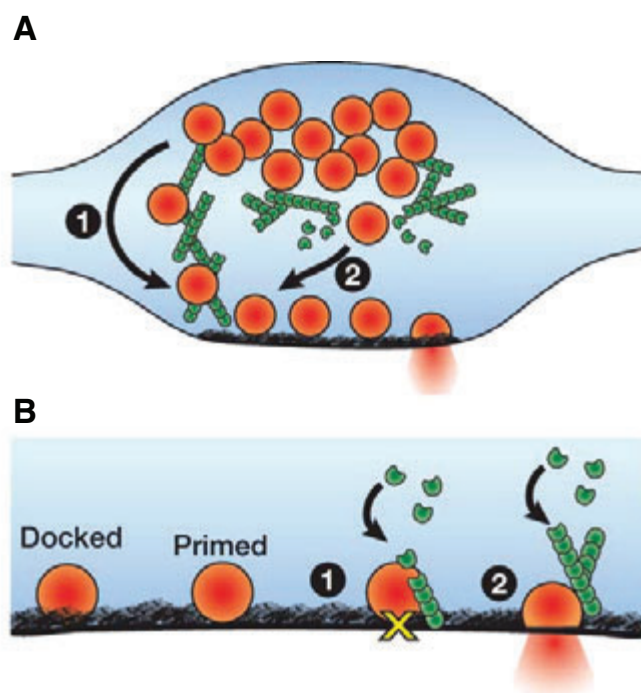


**Figure 28. Putative functions for actin at the presynaptic terminal.** **A)** Vesicle recruitment. Two models for the participation of actin in recruiting vesicles from the cytoplasmic pool to the RRP are illustrated. 1) Molecular motors such as myosin transport SVs to the RRP along actin tracks. 2) actin filaments act as a barrier and permit vesicles to replenish the RRP via diffusion or active transport. **B)** Neurotransmitter release. F-actin can regulate SV exocytosis negatively or positively either by (1) clamping SV fusion or (2) facilitating the release by coupling to the fusion machinery (Adapted from Dillon & Goda, 2005).

### *The postsynaptic actin cytoskeleton*

Actin is also enriched at the PSD (Fig. 27). Early studies already showed that changes in spine shape are driven by actin polymerization (reviewed in Bonhoeffer & Yuste, 2002). For that reason, the postsynaptic actin cytoskeleton has been best studied in dendritic spines of central excitatory synapses (Fischer et al., 1998).

At the PSD, actin has been found to anchor postsynaptic receptors and interact with scaffolding proteins (Allison et al., 1998; Kirsch & Betz, 1995; Kuriu et al., 2006). Furthermore, several studies have also highlighted the role of actin in regulating receptor mobility by internalization and trafficking (Osterweil et al., 2005; Zhou et al., 2001). Interestingly, an imaging study using fluorescent actin has elucidated that 85% of actin in dendritic spines is dynamic (Star et al., 2002).

Altogether, these data show that the actin cytoskeleton participates in the regulation of postsynaptic morphology and plasticity.

## 4.2 Synaptic microtubules

While it is well established that actin filaments are the major structural components of synapses and are involved in neurotransmitter release regulation, microtubules are believed to be restricted to active cargo transport by providing long intracellular railways (Nobutaka Hirokawa et al., 2009), with apparently no role in synaptic function (Dillon & Goda, 2005). Recent evidence, however, indicates a role for dynamic MTs in dendritic spines and axonal boutons (Parato & Bartolini, 2021).

Microtubules are polarized components of the cytoskeleton formed by polymers of  $\alpha/\beta$ -tubulin that assemble in a head to tail fashion, resulting in plus- and minus-ends. This structural polarity of MTs is recognized by motor proteins responsible for the active transport of cargo along MTs. Generally, dynein walks towards the MT minus-end (retrogradely), and members of the kinesin superfamily towards the MT plus-end (anterogradely).

Whereas the minus-end is fairly stable, the plus-end is dynamically unstable, undergoing stochastic bouts of growth and shrinkage by the exchange of tubulin subunits with the free-tubulin pool (Fig. 26B). This process is known as dynamic instability (Mitchison & Kirschner, 1984). At growing MT plus-ends, GTP-bound  $\alpha/\beta$ -tubulin heterodimers are added to the exposed ends of protofilaments. The switch from microtubule growth to shrinkage involves the release of  $\alpha/\beta$ -tubulin heterodimers and is known as ‘catastrophe’. Proteins such as stathmin promote **microtubule instability** by **sequestering  $\alpha/\beta$ -tubulin heterodimers**, thus inducing catastrophe events (Gupta et al., 2013).

Two pools of MTs can be distinguished within neurons: stable and dynamic (P. W. Baas et al., 1988, 1989; Peter W. Baas & Lin, 2011). MT stability is finely regulated by

different factors such as  $\alpha/\beta$ -tubulin acetylation (Sudo & Baas, 2010) or post-translational modifications of MT plus-ends that facilitate the binding of microtubule associated proteins (MAPs; Y. Song & Brady, 2015). MT plus-ends can also be stabilized or destabilized by the transiently association of “plus end-tracking proteins”, also called +TIPs (Schuyler & Pellman, 2001). One example is the **end-binding (EB) protein family**. Importantly, the discovery of EB proteins (Stepanova et al., 2003) allowed the **labelling of MT plus-ends** for the first time. Not until then had been appreciated how dynamic can MTs be in neurons. The main body of MT filaments can also be stabilized by MT-regulating proteins. For example, structural MAPs, such as MAP2 or Tau, have been shown to decorate axonal MTs offering protection from severing proteins (Qiang et al., 2006).

Compared to non-neuronal cells, where the minus-end of MTs nucleates within the centrosome, in mature neurons, MTs are generally not attached to the centrosome located in the cell body (Kapitein & Hoogenraad, 2015; Lüders, 2021; Weiner et al., 2021) and can be **locally nucleated** in axons and dendrites (W. S. Chen et al., 2017; Cunha-Ferreira et al., 2018; Nguyen et al., 2011; Ori-McKenney et al., 2012).

Whereas in dendrites MTs are not uniformly oriented, developing a mixed polarity of parallel and antiparallel arrangements, in axons, all MTs are oriented in the same direction, with the plus-end away from the soma (Fig. 29; P. W. Baas et al., 1988, 1989; Peter W. Baas & Lin, 2011). Besides, opposite to what had been long thought, MTs are **capable of branching in neurons**, being able to nucleate a new MT branch from an existing MT in axons (Basnet et al., 2018; Sánchez-Huertas et al., 2016).

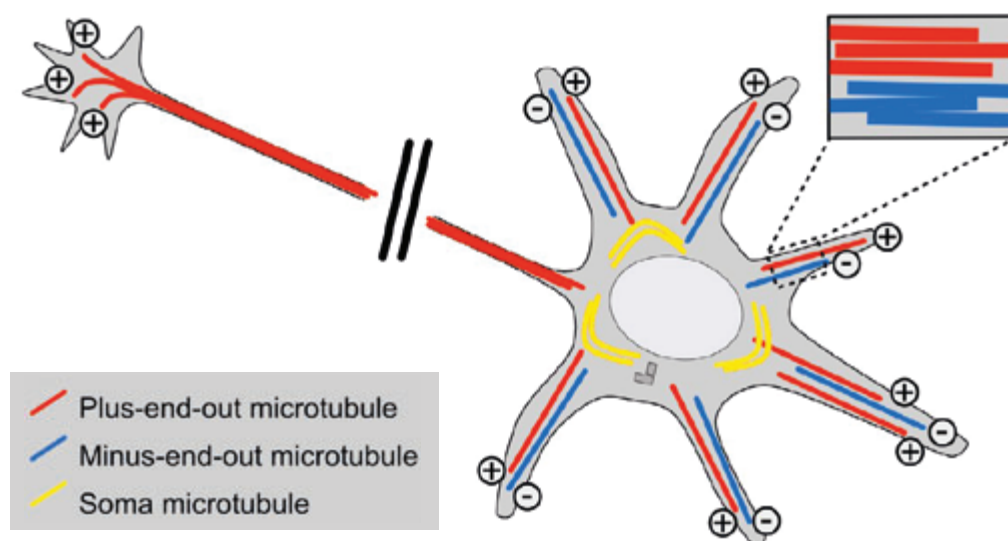


**Figure 29. The microtubule organization in neurons.** Microtubule's polarity is shown in different colours and indicated with a plus or minus symbol. Axons contain almost exclusively plus-end microtubules, whereas dendrites contain microtubules of mixed polarity. (Adapted from Lüders, 2021).



#### 4.2.1 Microtubules localization

Previous EM studies from George Gray in 1975 on the frog NMJ revealed the presence of **MTs covered by synaptic vesicles** moving towards presynaptic sites (Fig. 30A; Gray, 1975, 1978) as well as MTs in close relationship to the postsynaptic density (Fig. 30B; Westrum & Gray, 1977). According to his results, Gray claimed that MTs play a key role in the transport of SVs up to the presynaptic membrane, where SV release occurs. Unfortunately, this discovery was overlooked for decades. Instead, it had been widely accepted that actin filaments are predominantly concentrated at the distal end of presynaptic axons whereas MTs are confined to the axon. One possible reason to explain why Gray's results had not been reproduced may come from MTs lability (Gordon-Weeks et al., 1982; Westrum & Gray, 1977). In his experiments, Gray did not use conventional fixation techniques, but rather developed a novel fixation method that consisted in exposing the brain tissue to albumin before fixation to prevent labile MTs from mechanical disintegration (Gray, 1975).

Indirect evidence supporting the **relationship between MTs and SVs** at the presynapse comes from findings showing that MTs interact with SV proteins such as synapsin-I

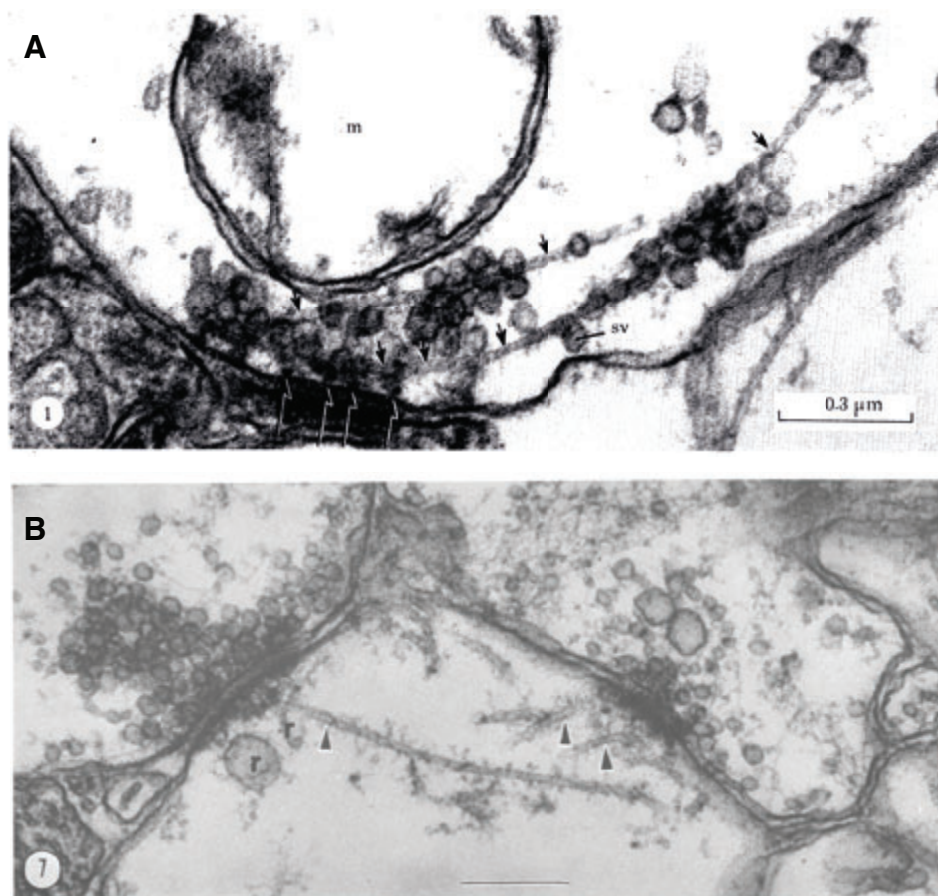


**Figure 30. Microtubules reach pre- and postsynaptic specializations.** Electron micrographs of synapses in the frog brain. Note the presence of microtubules (arrows) covered in vesicles reaching the active zone (A) and the postsynaptic density (B). (Adapted from Gray, 1975; Westrum & Gray, 1977).

(Baines AJ, 1986), synaptotagmin-I (Honda et al., 2002) and alpha-synuclein (Cartelli et al., 2016; Payton et al., 2001). Moreover, a role for MTs in the stabilization of the AZ through the Futsch protein has later been shown at the NMJ (Lepicard et al., 2014). Together, this evidence suggests that MTs lie in close relationship to presynaptic proteins and are associated to a pool of synaptic vesicles. However, the **functional role of the vesicle pool bound to microtubules** observed in electron micrographs is yet to be uncovered.

#### 4.2.2 Dynamic microtubules and cargo transport

At postsynaptic sites, it has been shown that MTs transport cargo into dendritic spines (McVicker et al., 2016), regulate spine morphology and temporally (seconds to minutes) invade dendritic spines in an activity-dependent manner (Hu et al., 2008; Jaworski et al., 2009), thereby contributing to synaptic plasticity. Some studies propose that the entry of MTs in dendritic spines is dependent on actin filaments (Merriam et al., 2013; Schätzle et al., 2018).

At presynaptic compartments, MTs are essential for the transport and delivery of synaptic elements, such as synaptic vesicle precursors (Guedes-dias et al., 2019), mitochondria (Graffe et al., 2015; Melkov & Abdu, 2018) and dense core vesicles (Bharat et al., 2017). Interestingly, a recent study combining *in vivo* and *in vitro* imaging has provided a mechanism by which synaptic vesicle precursors are transported and delivered at presynaptic sites. Kinesin-3 motor protein KIF1A transports synaptic vesicle precursors along MTs where growing plus-ends are concentrated at presynaptic sites. Given the low affinity of KIF1A for GTP-rich tubulin at plus-ends, cargo is unloaded at synapses (Guedes-dias et al., 2019). In addition, nucleation of dynamic MTs at synaptic boutons has been shown to stimulate neuronal activity and regulate interbouton transport of synaptic vesicles (Qu et al., 2019).

Although the exact mechanisms governing the sorting and unloading of cargo by motor proteins to pre- and postsynaptic sides are still obscure, these findings posit MT transport as an essential **source of newly synthesised synaptic components** for supporting synapse transmission in a fine-tuned manner (Fig. 31A-D). It is less clear, however, whether dynamic MTs are directly involved in synaptic transmission.

#### 4.2.3 Microtubules and synaptic transmission

Considering that MTs bind to SVs at presynaptic terminals, it is likely that they may participate in SV pool sorting and consequently synaptic function. Supporting this hypothesis, a recent study at the calyx of Held has linked MTs to the regulation of synaptic vesicle recycling. Electrophysiological experiments showed that MT depolymerization prolongs the slow-recovery time component of EPSCs from short-term depression during high-frequency neurotransmission, whereas F-actin depolymerization affects the

fast-recovery component (Babu et al., 2020). The exact mechanism by which dynamic MTs may impact synaptic transmission, however, awaits further investigation.

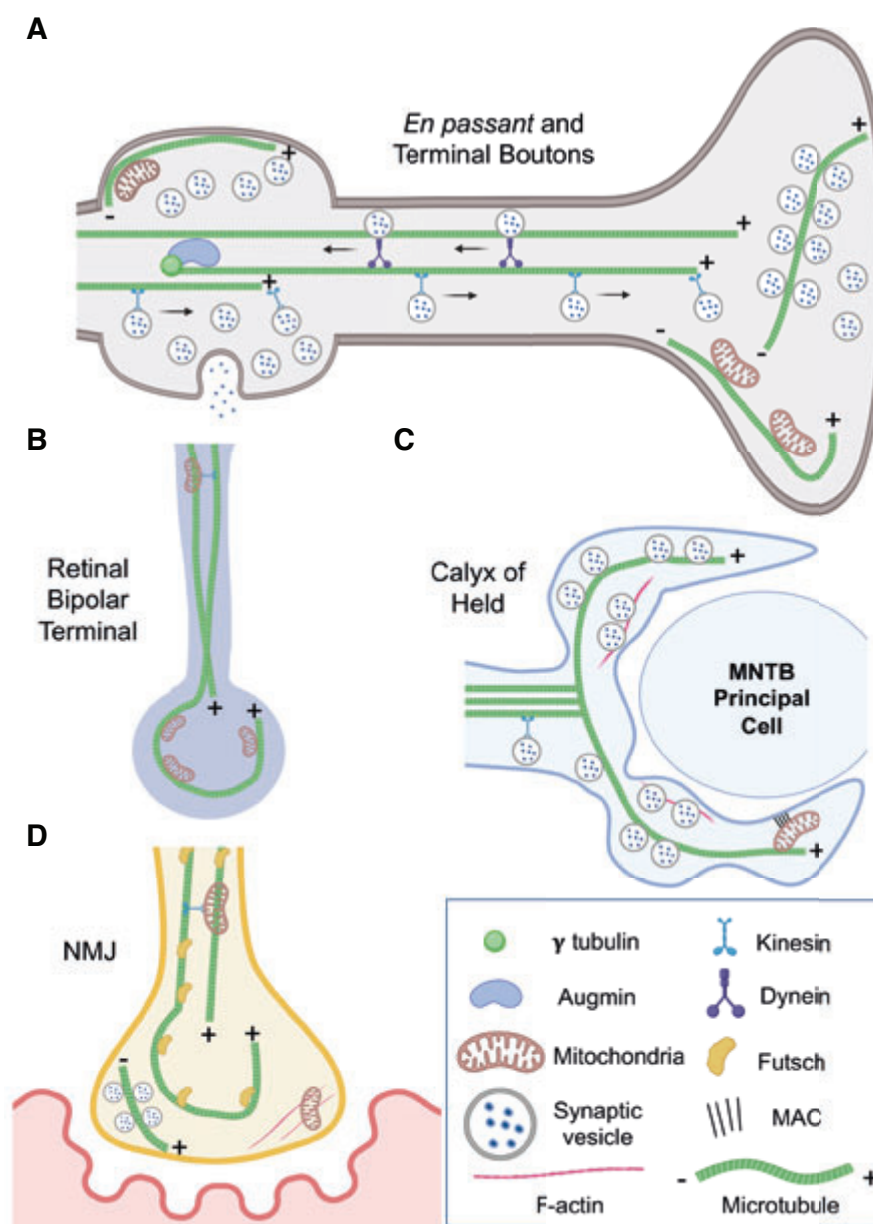


**Figure 31. Microtubule functions at different types of presynapses.** **A)** Excitatory presynaptic bouton. MTs are found associated to mitochondria and SVs close to the active zone. **B)** In goldfish retinal bipolar neurons, MTs loop into the presynaptic bouton to organize and anchor mitochondria. **C)** In the mammalian calyx of Held, presynaptic MTs extend throughout the presynaptic area and organize SVs. **D)** At the NMJ, presynaptic MTs form a loop that is stabilized by Futsch/MAP1B and have been observed to be associated to synaptic vesicles approaching the active zone. (Adapted from Parato & Bartolini, 2021).

#### 4.2.4 Manipulations of the microtubule cytoskeleton

As explained above, microtubules play key roles in cell proliferation, trafficking, morphology and motility. For that reason, many studies have been focused on understand-

ding the mechanisms underlying these biological functions. Along with genetic modifications, the development of new drugs to specifically control MTs dynamics have proven to be fundamental tools for cell biology studies.

**MT-targeted small molecules** can be classified as MT-stabilizing or destabilizing agents depending on whether they enhance or inhibit MT polymerization, respectively. To mention a few, among **MT-destabilizing drugs** are vinca alkaloids, which bind to the vinca domain of tubulin, and colchicine (and its analogues, such as combrestatins) or nocodazole, which bind to the colchicine-binding site. **MT-stabilizing drugs** include taxanes and epothilones, which bind to the taxoid-binding site (Fig 32; Steinmetz & Prota, 2018).

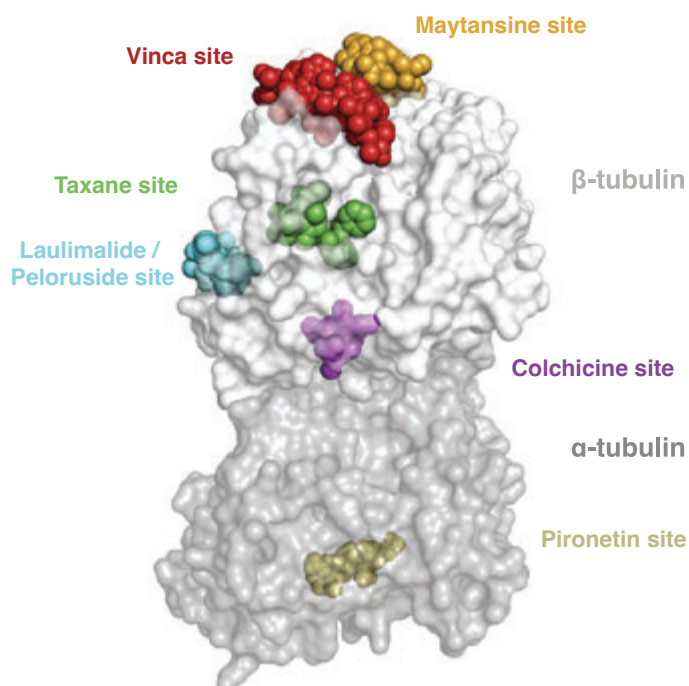


**Figure 32. Microtubule-Targeting Agent (MTA) binding sites on tubulin.** The  $\alpha/\beta$ -tubulin heterodimer is shown in dark and light gray, respectively. Bound ligands are represented in different colors: green (taxane site), cyan (lauimalide/peloruside site), magenta (colchicine site), slate (vinca site), orange (maytansine site), or yellow (pironetin site). (Adapted from Steinmetz & Prota, 2018).

Apart from their importance in anticancer therapy, the identification of small MT-disrupting chemicals are considered the most general tools for studying the MT cytoskeleton. In fact, outstanding discoveries that helped unravel the biology of microtubules would not have been possible without them (Borisy & Taylor, 1967; Taylor, 1965; Vale et al., 1985; Vallee, 1982). Additionally, over the last decade, X-ray crystallography (Prota et al., 2013; Ravelli et al., 2004) and cryo-electron microscopy (Alushin et al., 2014) studies have elucidated their mechanism of action.

Nevertheless, since MT dynamics occurs in micron- and millisecond scales, controlling the bioactivity of these drugs is necessary to investigate rapid intracellular dynamics at a mechanistic level. Unfortunately, using these MT-disrupting compounds, the desirable spatiotemporal precision is lagged far behind. In order to bridge this gap, new approaches towards photocontrol over the MT cytoskeleton have started to develop in the last decade (Velema et al., 2014).



The relatively recent arrival of **photocontrollable tools** (optogenetics and photopharmaceuticals) to manipulate biological systems with increased spatiotemporal precision has revolutionized various fields of biological research, especially those regarding rapid dynamic processes such as ion channels or the cytoskeleton (Table 1; Wittmann et al., 2020).

| Strategies to experimentally control microtubules |                               |
|---|-------------------------------|
| Low spatiotemporal precision                      | High spatiotemporal precision |
| Genetic modifications                             | Optogenetics                  |
| Bioactive molecules                               | Photopharmacology             |
|   | Photouncageable molecules     |
|   | Photoswitchable molecules     |

**Table 1.** Experimental strategies to study MT dynamics.

### *Optogenetics*

Optogenetics relies on **endogenous photoswitches**, such as retinal or flavin, and is referred to any genetically encoded protein system whose function can be light-controlled. First optogenetic experiments were performed to optically stimulate neurons through the expression of light-gated ion channels such as Channelrhodopsin-2 (Boyden et al., 2005) or “chARGe” (co-expression of *Drosophila* photoreceptor genes; Zemelman et al., 2002). These experiments shed light on the use of photochemical reactions to optically control biological systems. Since then, the scope of applications of optogenetics in biomedical research has increased steadily in a relatively short time, especially in the field of neuroscience. In the field of MTs, only one photo-inactivated fusion protein has been engineered to photocontrol the MT cytoskeleton (Van Haren et al., 2018). This optogenetic tool is based on the insertion of a blue-light-sensitive protein-protein interaction module that leads to the dissociation of EB1 from the +TIP complex upon illumination, thus impairing microtubule growth. However, this approach requires genetic manipulations, which can be limiting in some research settings.

### *Photopharmaceuticals*

Beyond optogenetics, further photocontrollable tools have been recently developed by the combination of photo-chemistry and pharmacology, which are known as photo-

pharmaceuticals. So far, two approaches, photouncageable and photoswitchable molecules, have been devised to successfully overcome the specificity issues intrinsic to bioactive compounds.

**Photouncageable molecules** are based on temporally inactivating a bioactive molecule through chemical modification with a photolabile protecting group. Most commonly, the “**caging group**” ortho-nitrobenzyl group is installed on an oxygen, sulfur or nitrogen atom, inactivating the bioactivity of the molecule. Upon exposure of the caged molecule to UV light, the compound is released from its cage and allowed to perform its biological function. Many photouncaged molecules, such as caged neurotransmitters, receptor agonists and antagonists or proteins, have been created in the recent years to photochemically modulate biological processes (reviewed in [Deiters, 2010](#)). Regarding MTs dynamics, a prodrug of paclitaxel has proven to successfully control MTs dynamics in cultured hippocampal neurons ([Skwarczynski et al., 2006](#); [Witte et al., 2008](#)).

Photouncageable molecules have made major contributions to biomedical research, however, this approach suffers disadvantages, such as irreversibility, short wavelengths and high light intensity needed for uncaging, generation of byproducts and slow illumination fragmentation ([Josa-Culleré & Llebaria, 2021](#)). Fortunately, many of these drawbacks can be avoided by photoswitchable approaches.

**Photoswitchable molecules** rely on the introduction of a **photoswitch** (synthetic molecule that can be isomerized by light) into the molecular structure of a bioactive molecule. The most common photoswitches are azobenzenes ([Beharry & Woolley, 2011](#)) and diarylethenes ([Irie, 2000](#)). New molecular scaffolds, however, such as hemithioindigos or styrylbenzothiazole (SBT), are also starting to get attention from the chemist community.

Switching the bioactivity of the compound between an on/off state is achieved by photoisomerization under light exposure with a defined wavelength, which alters the shape and polarity of the photoswitchable molecule. This isomer change results in an increase/decrease of binding affinity to its target. Normally, photoswitchable molecules can be switched between their active/inactive state using low-intensity illumination with different wavelengths.

Photocontrolling the well-studied MT-disrupting small molecules above mentioned by using photopharmacology has shown to be an elegant solution to address the need for spatiotemporal resolution in MT cytoskeleton studies. In the last 5 years, various photoswitchable analogues of the MT-stabilisers taxanes ([Müller-Deku et al., 2020](#)) and epothilone ([Gao et al., 2021](#)), together with analogues of the MT-destabilisers colchicinoids ([Borowiak et al., 2015](#); [Engdahl et al., 2015](#); [Gao et al., 2021](#); [Gao, Meiring, Kraus, et al., 2021](#); [Rastogi et al., 2021](#); [Sailer et al., 2019, 2020](#)) have been devised by using different photoswitch strategies ([Table 2](#)).

| Photoswitchable molecule | Analogue to | Photoswitch           | Reference                         |
|--------------------------|-------------|-----------------------|-----------------------------------|
| PSTs                     | CA-4        | azobenzene            | Borowiak et al., 2015             |
| azo-CA4                  | CA-4        | azobenzene            | Engdahl et al., 2015              |
| HOTubs                   | CA-4        | hemithioindigo        | Sailer et al., 2019               |
| HITubs                   | CA-4        | hemithioindigo        | Sailer et al., 2020               |
| AzTax                    | paclitaxel  | azobenzene            | Müller-Deku et al., 2020          |
| SPs                      | CA-4        | Spiropyran-merocyanin | Rastogi et al., 2021              |
| SBTub3                   | CA-4        | styrylbenzothiazole   | Gao, Meiring, Kraus, et al., 2021 |
| SBTubA4P                 | CA-4        | styrylbenzothiazole   | Gao et al., 2021                  |
| SBEpos                   | epothilone  | styrylbenzothiazole   | Gao et al., 2021                  |

**Table 2.** Photoswitchable molecules to control MT dynamics devised in the last years.

**Photostatins** (PSTs) were the first photoswitchable microtubule-inhibiting small molecules to be developed (Fig. 33A and B; Borowiak et al., 2015) by Dirk Trauner and Oliver Thorn-Seshold. PSTs are azobenzene-based analogs of combrestatin A-4 (CA-4), which can be switched on (*cis*-state) with violet light (390 nm) and off (*trans*-state) with green light (535 nm) or spontaneous relaxation, thus enabling modulation of MTs dynamics with the spatiotemporal precision of light (Fig 33D). Even though several PSTs were engineered, PST-1 was shown to have the best  $EC_{50 \text{ light/dark}}$  ratio ( $EC$ =effective concentration by assessing cell viability in HeLa cells), with *cis*-PST-1 being two orders of magnitude more potent than *trans*-PST-1 ( $EC_{50 \text{ light}}=0.5 \mu\text{M}$ , meanwhile  $EC_{50 \text{ dark}}=38 \mu\text{M}$ ; Fig 33C). This original and novel approach to assess MTs dynamics had great impact on cell biology and encouraged the chemist community to race for better generations of photoswitchable MT-modulators.

PSTs were later improved by the first generation of styrylbenzothiazole (**SBT**)-based **photoswitchable molecules** (SBTubs; Fig. 34A) by replacing the azobenzene photoswitch of PSTs with SBT (Gao, Meiring, Kraus, et al., 2021). Experiments using SBTub3 in cell culture succeeded in avoiding some of the problems inherent in azobenzenes (Fig. 34B), such as i) **metabolic instability**: azobenzenes can be reductively degraded by glutathione, thus reducing potency and increasing off-target effects and ii) **orthogonal photocontrol and imaging**: isomerization of azobenzenes requires light wavelengths typically used for imaging (GFP at 490 nm and YFP at 514 nm), leaving only the 647 nm laser channel available for imaging during photoswitching experiments.

SBTubs are photoisomerized to the active state (*Z*-isomer) with high spatiotemporal precision under 405 nm light, however, they cannot be reverted to the inactive state (*E*-isomer) neither by photoisomerization, nor by spontaneous relaxation, given their

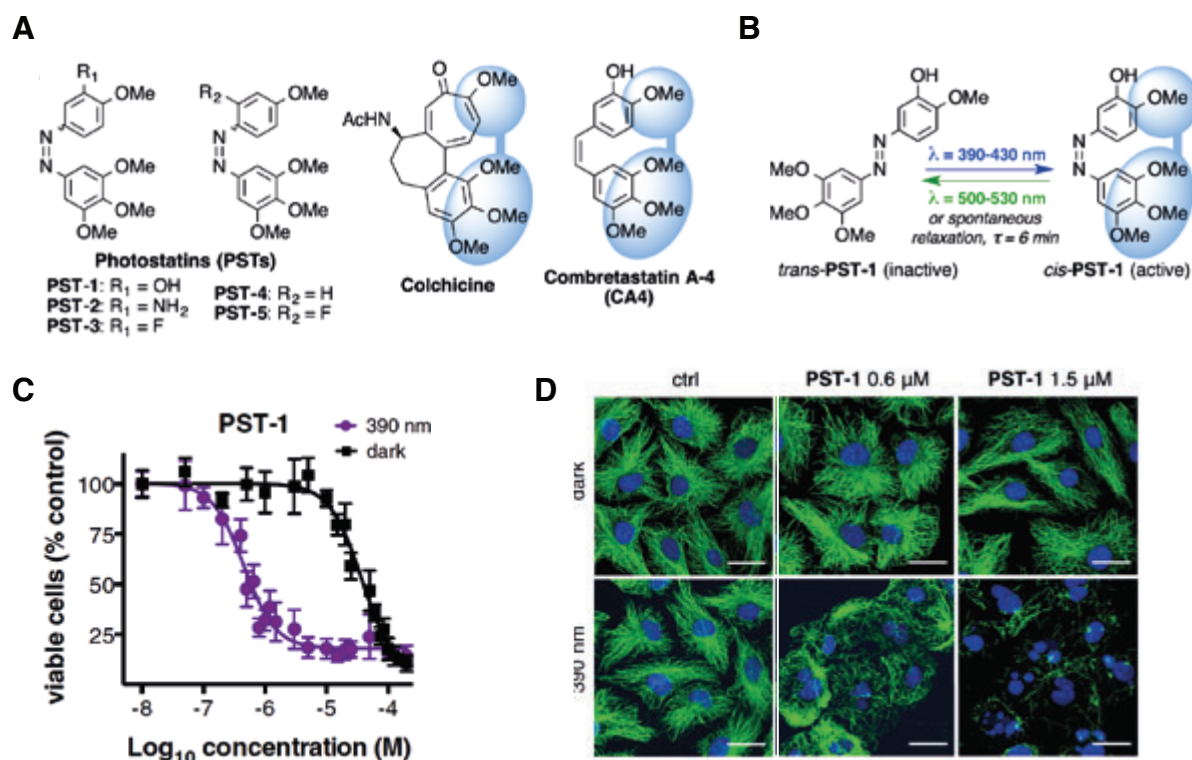


**Figure 33. Structure and biological activity of photostatins (PSTs).** **A)** Structural comparison of PSTs with colchicine and CA-4. **B)** Representative photoswitching of PST-1. **C)** Dose-response curve of cell viability for PST-1 under 390 nm irradiation and in the dark. **D)** PST-1 induces MT depolymerization and nuclear fragmentation in a dose-dependent manner while MT structure is unaffected under dark conditions, (cells were treated for 20 h with PST-1, then stained for  $\alpha$ -tubulin (green) and DNA (blue); scale bars equal 20  $\mu\text{m}$ ). (Adapted from Borowiak et al., 2015).

robust stability. Thus, the **unidirectional photoactivation** of SBTs is conceptually similar to that of photoncageable inhibitors. Despite their apparent behavioural similarities, SBTubs offer better performance in biological systems than photouncageable inhibitors by overcoming the slow fragmentation and byproduct generation issues that come along with these molecules. However, as in photouncaging, its effect can still be reversed by reducing the concentration of the bioactive isomer below its inhibitory threshold through either target dissociation or transmembrane diffusion.

GFP/YFP orthogonal photocontrol of SBTub3 over MT network integrity was demonstrated in HeLa cells and in subcellular regions of primary hippocampal neurons. MTs dynamics was assessed by labelling the EB3 protein, which tags the plus-ends of polymerizing MTs and can be identified as dynamic comets. Results from HeLa cells showed: i) fast membrane penetration of SBTub3, ii) fully GFP-orthogonal imaging and photoactivation (Fig 34C) and iii) cell-localized stop of MTs dynamics under 405 nm illumination (Fig. 34D).

Compared to cell lines, where rapid diffusion of small molecules is highly probable, in

complex systems such as embryos or irregularly shaped cells like neurons, diffusion of SBTub3 is less likely. The low diffusion of small molecules observed in complex systems favours subcellular patterning of SBTub3 photocontrol. For example, primary hippocampal neurons expressing EB3-GFP showed local disruption of MTs polymerization only in those neurites illuminated with violet light. These results demonstrated that the effect of SBTub3 can be finely tuned by *in situ* photoactivation at the micrometric scale.

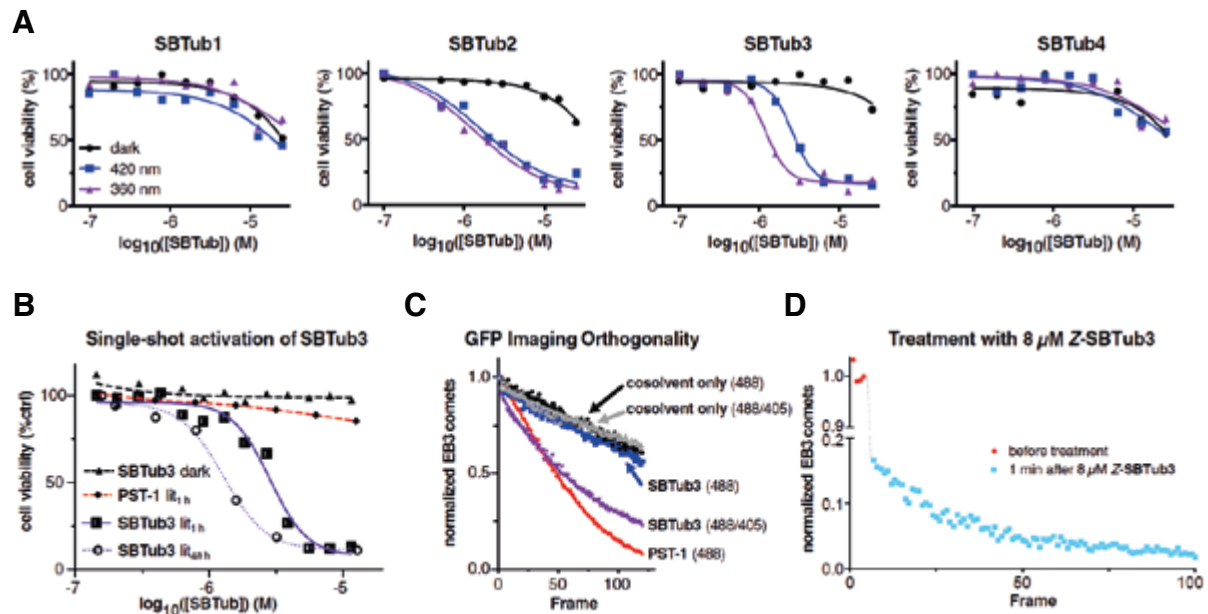


**Figure 34. Biological activity of SBTubs in HeLa cells. A)** SBTub2 and 3 give strong light-specific antiproliferative effects, while controls SBTub1/4 do not (40 h incubation). **B)** Antiproliferation assays with single-shot photoactivation (light 1 h) versus with ongoing illumination (light 48 h). Note that SBTub3 activity is sustained compared with PST-1. **C-D)** Live-cell EB3-GFP “comet” counts during GFP imaging with 488 nm. **C)** Imaging in the presence of inactive SBTub3 does not affect EB3 comets. Only additional 405 nm pulses isomerize SBTub3 to its active form and stop MT polymerization dynamics (10 mM SBTub3 or PST-1). **D)** Comet count before and after treatment with active SBTub3. (Adapted from Gao, Meiring, Kraus, et al., 2021).

Although the first generation of SBTubs tackled the main drawbacks presented in PSTs by improving metabolic stability and imaging-orthogonal photocontrol, practical limitations, such as potency and water solubility, precluded their use in *in vivo* studies. Whereas bioactivity concentration of CA-4 and PSTs in cell culture are 20 nM and 500 nM, respectively, SBTub3 has a significantly lower potency (1 mM). Given the hydrophobicity of these molecules, they usually need to be solubilized in organic cosolvents such as DMSO, which can be toxic in *in vivo* models or even in cell cultures if high doses are applied. The lower the potency of the compound, the higher is the

concentration and the amount of cosolvent needed to achieve bioactivity. For that reason, a second generation of SBTubs was developed by Thorn-Seshold and his group to optimize the potency and water-solubility of SBTub3. Successfully, SBTubA4P was reported as a potent, soluble, metabolically stable and GFP-orthogonal SBT-based photoswitchable compound to spatiotemporally control MTs dynamic *in vitro* and *in vivo* (Gao et al., 2021).

Altogether, this evidence highlights photoswitchable MT-inhibitors as **powerful tools** for the study of MTs dynamics in biological processes.

**During this project, we exploited the high spatiotemporal precision of these molecules to study the role of MTs in synaptic transmission.**



# 5 Use of autaptic neuronal cultures to investigate synaptic transmission

Given the complexity of neuronal circuits, investigation of the cell biology of the synapse and its physiology poses several challenges. Thereby, choosing an appropriate experimental model to develop a framework that help us understand the scientific question to be investigated is essential.

Among the approaches currently available to evaluate synaptic transmission, from the most complex to the simplest, are: i) *in vivo* models and acute neuronal slices, which allow the study of neuronal circuits, and ii) *in vitro* cultures, ideal to examine the cell biology of neurons. Two types of primary neuronal cultures can be established: **mass cultures**, where many neurons make connections with each other, and **autaptic cultures** (microcultures), which consist of isolated neurons making synapses with themselves. The latter method involves only one neuron, and it can be considered the most **reductionist approach**. In autaptic cultures, a given neuron is both pre- and postsynaptic, providing an accessible and direct method for studying neurotransmission.

Given the complexity of the questions attempted to investigate during this project, we took advantage of the unique scenario that microcultures offer to study synaptic transmission.

## 5.1 Autaptic connections *in vivo*

We usually think of synapses as specialized contact sites where information flows from one neuron to another. However, a single neuron can also make synapses with itself. During the seventies, apparent self-innervation connections had been sporadically observed in various brain regions and species such as cat spinal cord (Scheibel & Scheibel, 1971) and monkey neostriatum (Difiglia et al., 1976). It was not until 1972, when Van der Loos and Glaser, surprised by learning about this phenomenon, proposed the term **autapse** to describe “a synapse between a neuron and a branch of its own axon” (Van Der Loss & Glaser, 1972). In their study, aimed to perform a quantitative analysis of the rabbit cortical circuitry, autaptic contacts were found in 6 of 12 Golgi-stained pyramidal neurons from the occipital cortex.

Nowadays we are aware of the widespread existence of autapses in the central and peripheral nervous system, albeit in much smaller numbers than conventional synapses. However, in the late ninety's, they were thought to be uncommon and considered aberrant structures. Since then, anatomical, morphological and physiological evidence



for autapses *in vivo* has accumulated steadily.

**Neuroanatomical studies** using Golgi staining or intracellular markers, such as peroxidase or biocytin, revealed the presence of self-innervating connections in multiple areas of the brain including rat visual cortex and striatum (Peters & Proskauer, 1980; Preston et al., 1980), cat substantia nigra (Karabelas & Purrura, 1980) and cerebellum (King & Bishop, 1982).

It was reported that autapses presented the **typical synaptic morphology** and organization at the ultrastructural level (Cobb et al., 1997; Lübke et al., 1996; Peters & Proskauer, 1980; Tamás et al., 1997; Alex M. Thomson et al., 1996), indicating that both circuits were governed by the same principles. Interestingly, the study of Tamás, Buhl and Somogyi shed light on the **cell-type specificity** of self-innervation, showing that the likelihood of finding autaptic contacts strongly depends on the cell type (Fig. 35).

After several studies succeeding to confirm that autaptic neurons are anatomically not rare in the nervous system, **electrophysiological investigations** attempted to examine the functionality of excitatory and inhibitory autapses in intact circuits (Bacci et al., 2003; Connelly & Lees, 2010; Karayannis et al., 2010; Y. Li et al., 2010; Saada et al., 2009; Seung et al., 2000; Yin et al., 2018). Particularly, Bacci and colleagues showed that responses obtained in interneurons had the features expected for this kind of cells regarding kinetics, pharmacology, probability, and short-term plasticity. Saada et al., also performed a significant study in buccal ganglia of *Aplysia* and provided the first evidence of a function for excitatory autapses in an intact tissue by uncovering the importance of autapses to maintain persistent activation of B31/B32 neurons (Saada et al., 2009). Despite all this evidence, the functional significance of autapses in neuronal circuits is still controversial and far from being understood.

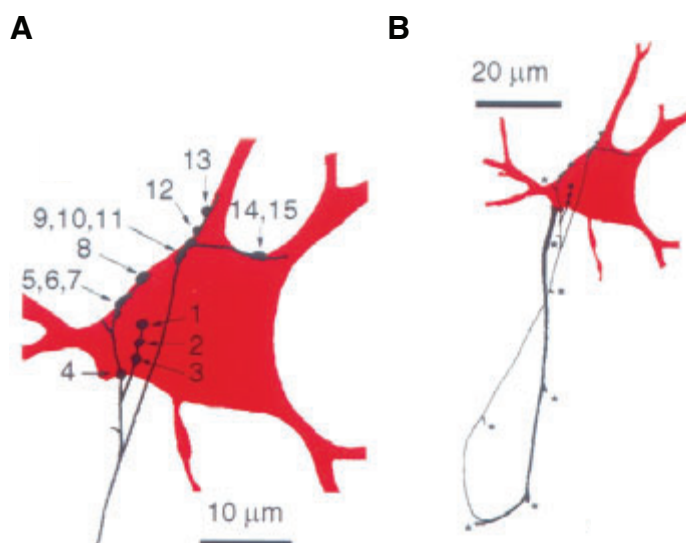


**Figure 35. Massive autaptic self-innervation in rat visual cortex by a basket cell (BC).** Light microscopic reconstructions of a large BC in layer III of area 17. **A)** The soma and dendrites are illustrated in red and axons in black. Note how the cell body is heavily innervated by axonal branches. All autaptic contacts verified by electron microscopy are numbered. **B)** Zoom out of (A), route of the axon back to the parent soma is observed. (Adapted from Tamás et al., 1997).

## 5.2 Autaptic neurons *in vitro*

Beyond the great impact entailed by the existence of functional autapses in intact tissues, the presence of autapses had been primarily reported from cultures, with comparatively **higher prevalence than *in vivo***. Unfortunately, this fact also contributed to the thought that autapses might be an artifact of neurons grown under artificial conditions. During the last decades, numerous studies have revealed that isolated neurons, constrained to grow within a small region where their axons and dendrites are giving the opportunity to intersect, are very likely to form autaptic connections. This phenomenon could be attributable to cultures being broadly 2-dimensional, with a greater likelihood of interaction between the axon and its own dendrites (Ikeda & Bekkers, 2006). A variety of autaptic contacts have been described using cells from the central and peripheral nervous system including chicken spinal ganglion cells (Crain, 1971), sympathetic ganglion cells co-cultured with myocytes (Furshpan et al., 1976; S. C. Landis, 1976) or cultured hippocampal neurons (J. M. Bekkers & Stevens, 1991).

The high prevalence of finding autapses in cultures changed from initially being a mere curiosity to emerge as a **powerful model system** for addressing important questions in neuroscience.

The first autaptic culture was developed by Reichart and Patterson together with Landis and Furshpan in the late seventies using neurons from **superior cervical ganglia** (SCG; Fig. 36A and B; Furshpan et al., 1976; S. C. Landis, 1976; Reichardt & Patterson, 1977). Experiments in mass cultures had previously revealed that most neurons from sympathetic ganglia are adrenergic and that a minority population is cholinergic (Yamauchi et al., 1973). It had also been shown that the decision to become adrenergic or cholinergic could be modulated *in vitro* by incubating the neurons with non-neuronal cells or conditioned media. Thus, in their study, Reichart and Patterson developed a technique to set up **single cell microcultures** (SCMs) in order to determine how the development of neurotransmitter function is regulated in individual neurons. Along with this study, Landis and Furshpan also made physiological and morphological observations in individual neurons using the same technique. Altogether, biochemical, electrophysiological and morphological results from SCG microcultures showed that sympathetic neurons are by default adrenergic unless they are co-cultured with myocytes or grown with conditioned medium from non-neuronal cells, in which case they become cholinergic. The “conditioned-medium factor” described in this work series was later discovered to be ciliary neurotrophic factor (CNTF; Saadat et al., 1989). These studies were the beginning of future investigations using microcultures and are the **base of the autaptic cultures established during this thesis** (Perez-Gonzalez et al., 2008).

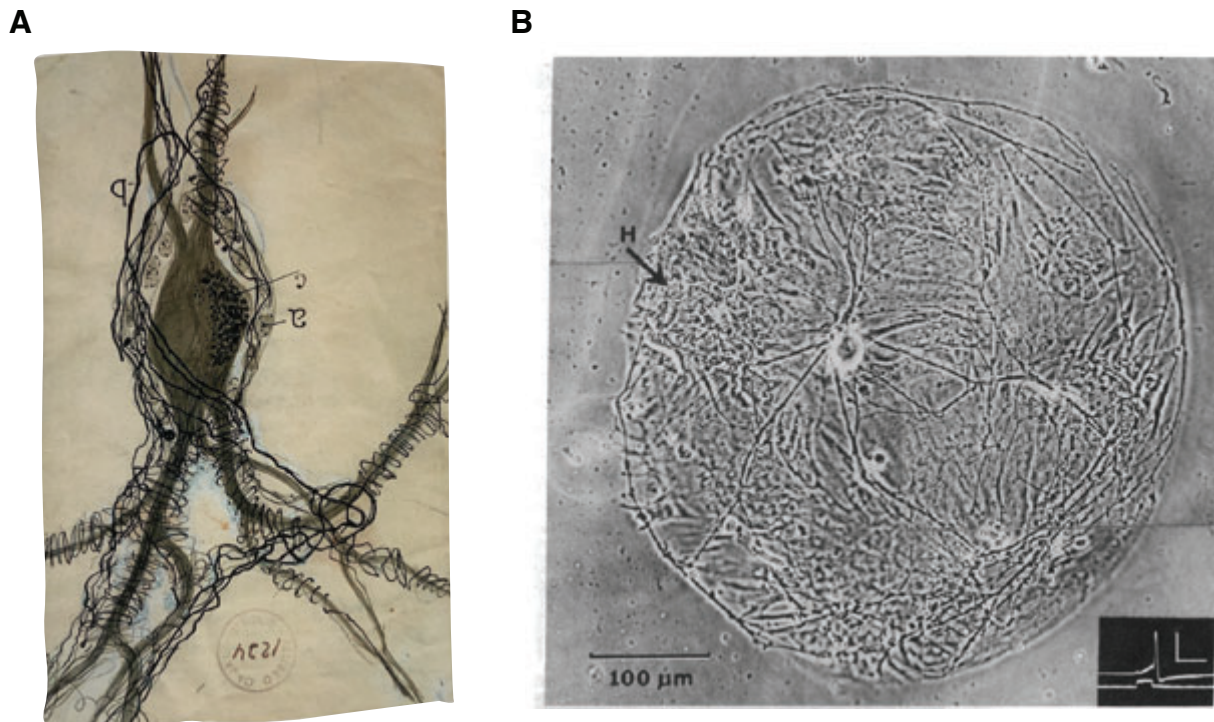


**Figure 36. Autaptic culture from rat superior cervical ganglion (SCG).** **A)** Drawing of a superior cervical ganglion neuron surrounded by axons that wrap around the neuron's cell body and dendrites (Extracted from drawings of Ramón y Cajal, E. A. Newman, et al., 2017). **B)** Microculture of a single neuron at 19 days in vitro from the rat SCG co-cultured with myocytes (arrow H). Inset shows impulse of this neuron (scale, 50 mV, 20 ms). (Adapted from Furshpan et al., 1976).

Neurons from the central nervous system can also form autapses as long as they are grown on a feeder layer of astrocytes. Bekkers and Stevens performed a remarkable study in 1991 using hippocampal microcultures and showed that both inhibitory and excitatory autapses operate in the same manner than conventional synapses of the same culture system. Synaptic and autaptic transmission appeared to be indistinguishable, upholding autaptic cultures to be a reliable tool for studying neurotransmission. Following studies reproduced this system using other cell types including the nucleus accumbens (Shi & Rayport, 1994), raphé nucleus (Johnson, 1994), ventral tegmental area (Michel & Trudeau, 2000; Sulzer et al., 1998), thalamus (Moechars et al., 2006), basal forebrain (T. G. J. Allen, 2007), or even neurons derived from human induced pluripotent stem cells (Fenske et al., 2019). Methodological papers about the establishment of microcultures have been published over the years (T. G. J. Allen, 2007; John M. Bekkers, 2020; Burgalossi et al., 2012; Fasano et al., 2008; Rost et al., 2010). However, when choosing autaptic cultures as a model system for research, it is important to bear in mind that, as reported *in vivo*, not all cells form autapses. For example,

while SCG neurons are bound to form autaptic connections in culture, neurons from dorsal root ganglia (DRG) are not.

Further differences on the establishment of SCMs using neurons from the central or peripheral nervous system have also been found. On one hand, meanwhile neurons from the CNS depend on glial secreted products to form functional autapses (Nägler et al., 2001), the survival and development of neurons from the PNS, such as sympathetic ganglia, are less dependent on trophic factors, requiring essentially nerve growth factor (NGF) to become fully functional. Finally, like in any experimental system, autaptic cultures present advantages and disadvantages needed to be considered (Table 3).

|                                   | Benefits  | Limitations  |
|-----------------------------------|---|--|
| <b>Neuronal cultures</b>          | Accessibility for electrophysiological recordings   | Axonal and dendritic morphologies are lost compared to their appearance <i>in vivo</i>   |
|                                   | Suitability for imaging experiments   | Functional properties of synapses assayed <i>in vitro</i> can also be modified and need to be subsequently confirmed in <i>in vivo</i> models  |
| <b>Autaptic neuronal cultures</b> | Simplicity: changes in neurotransmission, cellular and molecular biology caused by external factors or chemical compounds can be studied in a single neuron                                     | Pre- and postsynaptic responses are not separated, requiring specific assays to assess postsynaptic function independently   |
|                                   | Cellular homogeneity: the features and responses obtained are unequivocally from the same neuron, reducing the effect of neuronal heterogeneity   | Possible dilution or washout of intracellular components during whole-cell patch clamp experiments of both pre- and postsynaptic compartments need to be considered  |
|                                   | Practicality: in electrophysiological recordings, a single electrode gives access to the pre- and postsynaptic terminals to simultaneously stimulate and record the evoked response             | Low transfecting rates: since autaptic cultures contain only 10-15 microislands, neurons need to be transduced using more effective methods such as lentivirus infection, which need to be previously produced |
|                                   | Homogenous modifications: genetic modifications or dialysis of specific molecules from the patch pipette during whole-cell recordings are applied to all regions of the isolated neuron equally | More laborious and erratic procedure for setting up the cultures: proper preparation of the substrate is imperative and can be sometimes challenging.  |
|                                   | Control over extracellular environment: neuron-glia interactions can be accurately explored   |  |

**Table 3.** Benefits and limitations of general culture systems and single cell microcultures (SCMs) used during this thesis work compared to *in vivo* model systems.

Overall, autaptic cultures have proven to be a simple and elegant approach, invaluable for resolving many important neurobiological questions which would have not been possible to decipher using complex systems.



# OBJECTIVES





Synapse elimination is critical for the proper development of the nervous system. Yet, how neuronal circuits adapt to changes in connectivity at early developmental stages, and how the cytoskeleton participates in the disassembly and maintenance of synapses needs to be further explored.

Here, we attempt to investigate the synaptic plasticity mechanisms associated to synaptic pruning by taking advantage of the reductionist and unique scenario that autaptic cultures provide.

Accordingly, in this thesis 3 specific objectives are established:

- 1** Study the response of an autaptic circuit to synapse elimination induced by SPARC
- 2** Investigate how the presynaptic actin cytoskeleton participates in synapse disassembly
- 3** Elucidate the contribution of microtubules to presynaptic terminal function





# **MATERIALS & METHODS**



# 1 Cell culture

During this thesis, two types of cultures have been used. On one hand, neuronal primary cultures from superior cervical ganglia of postnatal day 0 (P0) to P2 Sprague Dawley rats were established as **single cell microcultures** in the absence of glial cells to study synaptic transmission. On the other hand, the **cell lines** HEK293T and CHO were used for lentivirus production and for assessment of changes in the F-actin cytoskeleton, respectively.

## 1.1 Single cell microcultures

Cholinergic SCMs were established following the previously described method ([Perez-Gonzalez et al., 2008](#)). The procedure was approved by the Department of Environment from the Generalitat de Catalunya (procedure number 9874).

SCMs are an advantageous model for studying neurotransmission and synaptic plasticity. In this culture system, an isolated neuron makes synapses with itself forming an autaptic circuit. Since the pre- and postsynaptic components of these synapses come from the same neuron (autapses), stimulation and recording of the evoked response can be performed using a single electrode. Given neurons from the SCG belong to the peripheral nervous system, they only require NGF to grow and form functional autapses. Consequently, they can be cultured in the absence of glial cells and present an ideal model to study the effect of glial secreted factors on neuronal activity ([Albrecht et al., 2012](#)).

### 1.1.1 Materials

#### *Surgical materials*

- » Dumont #55 Biology Tweezers, 11 cm long, straight, 0.05 x 0.01mm tips ([ref.14099, World Precision Instruments Inc, Sarasota, FL; Fig. 37A](#))
- » Vannas Scissors, 8 cm long, straight, 0.015 x 0.015 mm, super fine ([ref. 501778, World Precision Instruments Inc, Sarasota, FL; Fig. 37B](#))
- » McPherson Vannas Scissors, 12 cm long, curved, 8 mm blades, tips: sharp and DLC coated, stainless steel ([ref. 503364, World Precision Instruments Inc, Sarasota, FL; Fig. 37C](#))

### Coverslips

For the establishment of SCMs, different types of coverslips were used depending on the purpose of the study. Coverslips were previously sterilized by immersion in 70% ethanol and sonication (10 min).

- a)** Glass coverslips, 15 mm of diameter, num. #1 (ref. 631-1579, VWR, Germany) were used for electrophysiological and immunocytochemistry experiments.
- b)** Glass coverslips high precision, 15 mm of diameter, num. #1,5 (ref. 0117550, Marienfeld, Germany) were used for STED microscopy experiments.
- c)** Thermanox coverslips 15 mm of diameter (ref. 174969, Thermo Scientific, Germany) were used for EM experiments.



**Figure 37. Surgical material for dissection. A)** Dumont #55 Biology Tweezers, 11 cm long, straight, 0.05 x 0.01mm tips. **B)** Vannas Scissors, 8 cm long, straight, 0.015 x 0.015 mm, super fine. **C)** McPherson Vannas Scissors, 12 cm long, curved, 8 mm blades.

### Cell culture material

| Material                                | Units | Commercial brand      | Reference     |
|---|-------|-----------------------|---------------|
| Glass coverslips $\varnothing$ 15 mm    | 24    | VWR International, US | 631-1579      |
| 12-well tissue culture plate            | 2     | Sarsted, Germany      | 83.3921       |
| Tissue culture flask 25 cm <sup>2</sup> | 2     | TPP, Switzerland      | 90026         |
| Tissue culture dish $\varnothing$ 10 cm | 1     | TPP, Switzerland      | 93100         |
| Centrifuge tube 15 ml, conical          | 3     | TPP, Switzerland      | 91015         |
| Petri dish $\varnothing$ 5.5 cm         | 4     | Detalab S.L, Spain    | 200201.B      |
| Modified glass pasteur pipettes 150 mm  | 2     | Normax Lda., Portugal | 5426015       |
| 1 ml pyrogen-free syringe               | 1     | Enfa                  | JS1           |
| Hypodermic needle 26 G (0.45x12mm)      | 1     | Nipro, Belgium        | HN2613ET      |
| Neubauer chamber                        | 1     | Immune Systems        | BVS100        |
| 1.5 ml Eppendorf1                       |       | Detalab S.L, Spain    | 200400P       |
| 12 ml spray bottle                      | 1     | Muji Shop             | 4549337461475 |

**Table 4.** Tissue culture material used for the establishment of single cell microcultures.



### Solutions

- » Agarose solution 0.15% w/v (see [Annex 2](#))
- » Sterile phosphate buffered saline (PBS) 1X
- » Collagen type I (see [Annex 1](#))
- » Sterile Mili-Q (MQ) water
- » 2.5 mg/ml collagenase type IA (ref. C9891-5G, Sigma-Aldrich, St. Louis, MO) in sterile PBS 1X, passed through a 22 µm pore size filter (ref. 430624, Corning Life Sciences, US)
- » Trypsin EDTA 0.05% (ref. 25300-62, Gibco®)

### Culture medium

| Pre-plate medium   | Neuronal culture medium   |
|--|---|
| Dulbecco's Modified Eagle Medium (DMEM)/F12 [1:1], with Glutamine without HEPES (ref. 11320-033, Gibco®) | DMEM/F12 [1:1], with Glutamine, without HEPES, (ref. 11320-033, Gibco®)                 |
| 20 % (v/v) Foetal Bovine Serum (FBS; ref. 04-007-14, Biological Industries, Israel)                      | 2.5 % (v/v) FBS, (ref. 04-007-1A, Biological Industries, Israel)                        |
|  | 2.5 % (v/v) Rat serum (RS)*   |
|  | 5 nM mouse NGF-2.5S, (ref. N-100, Alomone Labs, Israel)**                               |
|  | 2 nM rat CNTF, (C-245, Alomone Labs, Israel)**  |
|  | 0.25 (v/v) Penicillin/Streptomycin (P/S), (ref. P0781, Sigma-Aldrich, St. Louis, MO)*** |

**Table 5.** Culture medium for the establishment and maintenance of single cell microcultures.

\*RS was prepared in the animal care facility of the Campus of Bellvitge, University of Barcelona.

\*\*Trophic factors were added immediately before cell spreading or medium change. CNTF was added from the first medium change and not during cell spreading.

\*\*\*During cell spreading, the dose of Penicillin/Streptomycin was reduced by a half (0.25%) until the first medium change when it was raised to 0.5% (v/v).

### 1.1.2 Procedure for establishing SCMs

#### Preparation

The first step to establish a SCM is to prepare the 12-well plates. Previously sterilized 15 mm coverslips were washed with MQ water using a ø 5.5 cm Petri dish to remove the ethanol and were placed into the 12-well plates. Coverslips were then treated with a non-permissive growing substrate of 0.15 % agarose where cells cannot get attached.

The solution of agarose with MQ-water was warmed up until the agarose was completely diluted and added to the wells. Before it became solid, agarose was removed from the wells, leaving a thin coat on the coverslips (previously described protocol, [J. M. Bekkers & Stevens, 1991](#)). 12-well plates with treated coverslips were then left to dry in the vertical laminar flow hood under UV light to sterilize the agarose coat. At the end of the procedure, collagen microdrops were sprayed onto the coverslips, providing a growing permissive substrate. Hence, only those neurons placed onto the collagen microdots were able to grow in isolation. Before the extraction of SCG, 3 Petri dishes  $\varnothing$  5.5 cm were filled with PBS 1X and left to cool. Pre-plate medium and neuronal culture medium were prepared and placed at 37°C and 8% CO<sub>2</sub> to warm up and balance the pH. Surgical material was sterilized under UV light for minimum 15 min before starting the dissection, which was performed under the stereo microscope (Leica M50, [Fig. 38](#)) in a horizontal laminar flow hood at room temperature following the next steps:

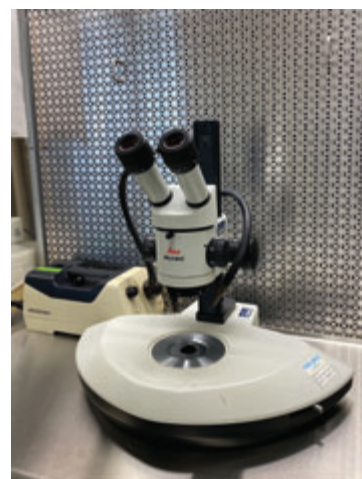


**Figure 38.** Horizontal laminar flow hood and stereo microscope used for the extraction of rat superior cervical ganglia.

#### *Extraction of SCG*

- 1) Pups were anaesthetised on ice for 15 min before undergoing surgery ([Fig. 39A](#)).
- 2) Preparing the pup: the animal was fixed with needles in crucified position on a piece of cork. During surgery, animals were continuously maintained cold by placing them on a box full of ice. This ensured anaesthesia over all the procedure ([Fig. 39B](#)).
- 3) An incision was made on the ventral part of the neck with the curved tip scissors to remove the skin of this area and expose the salivary glands (6.4X magnification; [Fig. 39C](#)).
- 4) Salivary glands were removed using the tweezers in horizontal position (up to down), so the trachea was visible. Lymphatic and glandular tissue was also set aside so we could access to the deep vascular tissue of the neck ([Fig. 39D](#)).
- 5) At this point, the bilateral muscles sternocleidomastoid, digastric and omohyoid could be observed ([Fig. 39E](#)). Pinching the middle of the sternocleidomastoid muscle with the tweezers and removing the thin omohyoid muscle allowed us to access the carotid artery (16X magnification).
- 6) The common carotid artery branches into the external and internal carotid arteries displaying a Y-like shape. Beneath the carotid artery is attached the superior cervical

ganglion (Fig. 39F). In order to extract this ganglion, the lower section of the common carotid artery was elevated and fixed with the tweezers while the two ends of the external and internal carotid artery were sectioned with the straight scissors. Finally, cutting the lower end of the common carotid artery resulted in the obtention of a dissected structure which contained the carotid artery together with the nodose ganglia and the SCG in its most dorsal part (Fig. 40A).

**7)** The obtained tissue was placed in a  $\varnothing$  5.5 cm Petri dish containing cold and sterile PBS 1X at 4°C. This process was bilateral and the ganglia of 8-12 animals were extracted for establishing SCMs in 24 coverslips (2x 12-well plates).

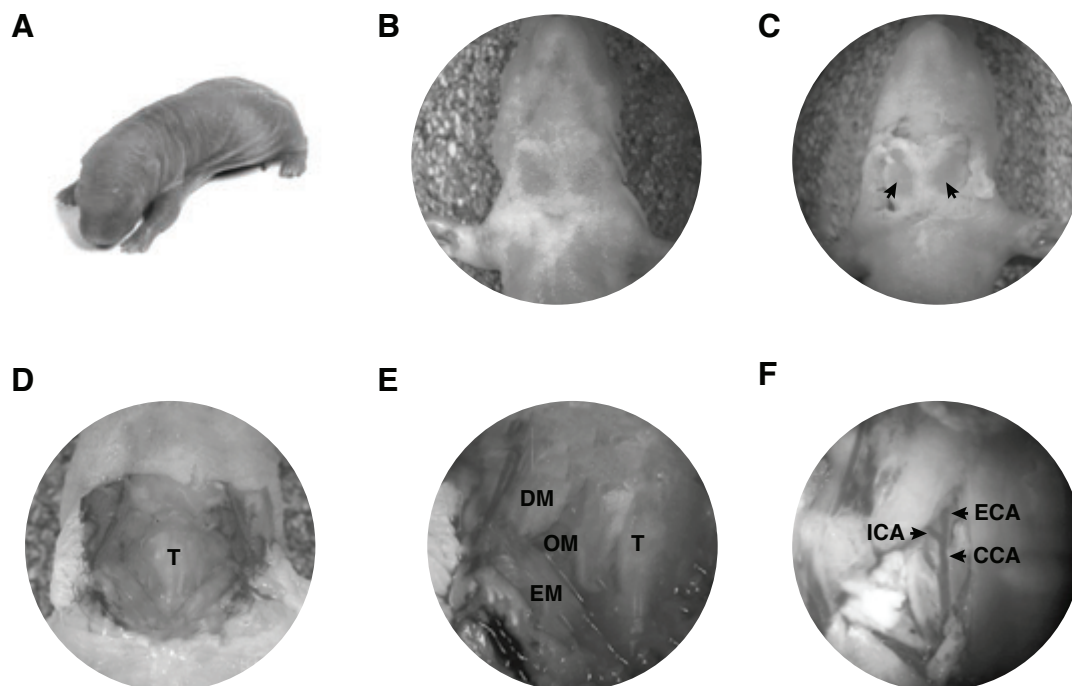


**Figure 39. Dissection and extraction of superior cervical ganglia from rat pups.** **A)** Rat pups (P0-P2) are anesthetized on ice. **B)** Fixation of the pup facing up to allow access to the ventral area of the neck. **C)** After removing the skin of this area, salivary glands are exposed (arrows). **D)** Removing the glandular tissue allows the visualization of the trachea (T) as well as **E)** the bilateral sternocleidomastoid (EM), digastric (DM) and omohyoid (OM) muscles (augmentation from **D**). **F)** View of the common carotid artery (CCA) and its external (ECA) and internal (ICA) bifurcations after removal of the sternocleidomastoid and omohyoid muscles.

**8)** After finishing the surgery of all animals, each SCG was separated from the carotid artery and nodose ganglion (25x magnification) using thin tweezers in a  $\varnothing$  5.5 cm Petri dish containing sterile and cooled PBS 1X (Fig. 40B). The connective tissue recovering the SCG was also removed to reduce the presence of fibroblasts in the culture (40x magnification).

**9)** All clean SCG (Fig. 40C) were kept in a  $\varnothing$  5.5 cm Petri dish containing sterile PBS 1X at 4°C.

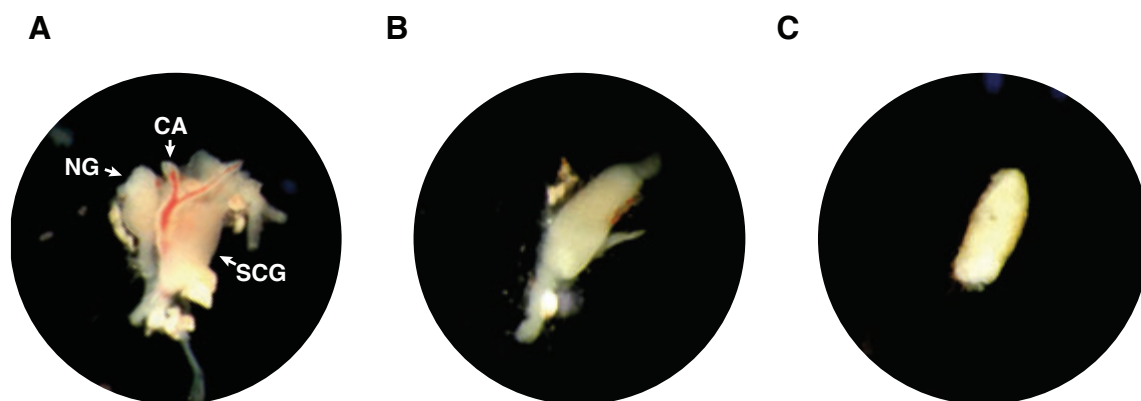


**Figure 40. Structure of the superior cervical ganglia.** **A)** Dorsal view of the resulting structure obtained from cutting the carotid artery (CA) at its internal, external, and common ends. In the dorsal part of the bifurcation of the carotid artery we find the superior cervical ganglia (SCG). The nodose ganglion (NG) is adjacent to the exterior carotid artery. **B)** SCG separated from the carotid area. **C)** Image of the extracted and clean SCG after removing the connective tissue that recovered it.

#### *Dissociation and disaggregation*

**10)** Ganglionic cells were dissociated from SCGs by enzymatic treatment:

**a)** SCG were placed in a 1.5 ml Eppendorf containing 1 ml of 2.5 mg/ml collagenase and incubated for 10 min at 37°C and 8% CO<sub>2</sub>. Collagenase was subsequently removed while ganglionic cells stayed at the bottom of the Eppendorf.

**b)** Then, 1 ml of 0.05% trypsin-EDTA was added and incubated for 20 min at 37°C and 8% CO<sub>2</sub>. After that, trypsin-EDTA was removed, and 1 ml of pre-plate medium was added to inactivate any remaining enzymatic activity.

**11)** Dissociated ganglionic cells were transferred into a 15 ml centrifuge tube where they were mechanically disaggregated using a diameter-modified glass Pasteur pipette. This step is critical for succeeding in the establishment of SCMs.

Glass pipettes were previously modified using a Bunsen burner to reduce the diameter of the tip and sterilized before use.

#### *Pre-plate*

**12)** In order to separate neurons from non-neuronal cells, medium containing all dissociated ganglionic cells was placed in a 10-cm-diameter culture dish for 60 min at 37 °C. At the end of this pre-plating period, ≥95% of non-neuronal cells were found to be adhered to the dish, but most neurons remained in suspension. The longer is the time of the pre-plate step, the more non-neuronal cells attach to the dish but the less is the number of neurons to be collected.

### *Spreading*

**13)** Medium was then collected in a 15 ml tube and centrifuged for 3 min at 1800 g. Then, the supernatant was carefully removed, and 1 ml of culture medium was added to the tube containing the pellet of neurons.

**14)** Using a glass-modified Pasteur pipette, neurons were again dissociated and transferred into a 1.5 ml Eppendorf.

**15)** The total number of neurons was manually counted under the microscope using a Neubauer chamber.

**16)** Medium containing the neurons in suspension was passed through a 26G needle connected to 1 ml syringe 5 times. The required amount neurons were then resuspended in pre-warmed and pH balanced culture medium to achieve a final concentration of 2500 neurons/ml. At this point, 5 nM 2.5 NGF was added to the culture medium.

**17)** Collagen microdots: immediately before plating the neurons, the 15 mm coverslips previously covered with a thin agarose layer were sprayed with collagen to obtain 10-20 collagen microdrops of 100-400  $\mu\text{m}$  diameter per coverslip (Fig. 41B). To do that, ~5 ml of collagen were well mixed with RPMI 10x culture medium (see Annex I) in a 15 ml centrifuge tube and transferred into an atomizer (Fig. 41A). The collagen mix was then sprayed onto the 12-well plates, which were positioned at a horizontal distance of 30-40 cm from the atomizer and ~5 cm lower.

**18)** Right after spraying the coverslips, neurons were seed at low density by adding 1 ml of neuronal medium onto each well. The time between collagen spray and cell spreading is critical because too dry or too wet collagen might result in wrinkled or detached microdrops, respectively.

**19)** Finally, plates were kept in the incubator at 37°C and 8% CO<sub>2</sub> until the first medium change.

### **1.1.3 SCM maintenance and treatment**

#### *Maintenance of SCMs*

After 1-2 days of culture establishment, partial replacement of culture medium was performed by removing 400  $\mu\text{l}$  of old medium and adding 500  $\mu\text{l}$  of fresh medium (considering slight medium evaporation). Trophic factors were added in the pre-warmed and pH balanced fresh media to achieve a final concentration of 5 nM 2.5 NGF and 2 nM CNTF.

Medium change was performed every 2-3 days until 18-22 DIV, when neurons were functionally mature. After this period, we could find single cell microcultures displaying



multiple neuronal processes (Fig. 41C and D) as well as collagen isles containing more than one neuron (Fig. 41E), or isles occupied by glial cells (Fig. 41F). For experiments, only SCMs were selected.

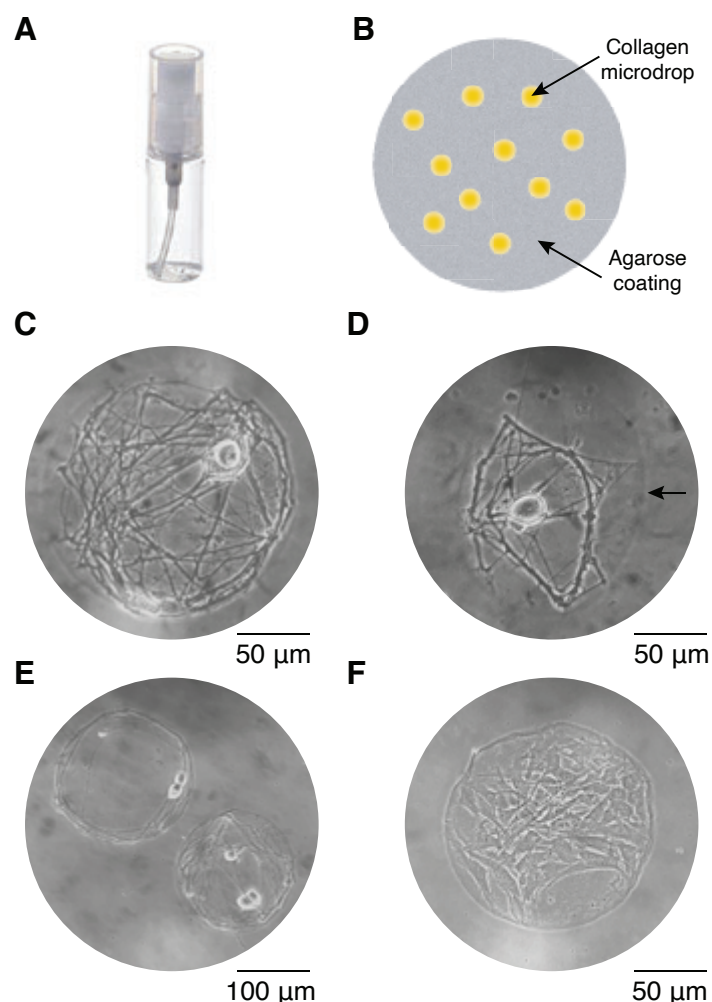


**Figure 41. Establishment of single cell microcultures by the production of collagen microdrops.** **A)** 12 ml spray bottle used to generate collagen microdrops on the coverslip where neurons will be seeded. **B)** Representation of the substrate used for generating isolated neurons. Agarose acts as a non-permissive growing substrate whereas collagen allows neuronal growing and development. **C-F)** Phase contrast images of different types of microcultures obtained using a 10X or 20X objective. **C)** and **D)** Images of single cell microcultures showing the presence of an isolated neuron growing on a collagen microdrop. Arrow indicates the outline of the collagen microdrop. **E)** Two microcultures containing more than one neuron. **F)** Non-neuronal cells grown on a collagen microdrop.

### *Treatment of SCMs*

SCMs were exposed for the indicated time intervals (ranging from 0 to 30 h) to 200 nM of the SPARC-derived peptides: p2.1 (CQNHHCKHKGKVCELDESNTTP) or p4.2 (TCDLDNDKYIALEEWAGCFG). Peptides p2.1 and p4.2 were synthesized by GL Biochem (Shanghai, China). Stocks were prepared at 2 mM using MQ water and aliquots were stored at  $-80^{\circ}\text{C}$ . Peptide solutions were thawed and diluted in culture medium. When indicated, 1  $\mu\text{M}$  jasplakinolide (ref. 2792, Tocris, UK), previously diluted in DMSO to a stock concentration of 1 mM, was added to SCMs together with 200 nM p4.2.



## 1.2 Cell lines culture

### 1.2.1 HEK293T

Lentivirus infection was used in a set of experiments as a transduction method to genetically modify SCMs. For that purpose, HEK 293T cells were used as a platform for lentivirus production.

HEK293 cell lines are derived from Human Embryonic Kidney cells. An important derivative of this cell line is the 293T (or HEK 293T) cell line, that expresses the SV40 large T antigen (SV40T) and allows transfected plasmid DNAs containing the SV40 origin of replication to be amplified, thus producing a high copy number of recombinant proteins/lentiviruses from these cells.

HEK293T cells were maintained at 37°C and 5% CO<sub>2</sub> in culture medium containing:

- » DMEM/F12 [1:1] culture medium, with Glutamine, without HEPES
- » 10% (v/v) FBS
- » 1% P/S

Cell cultures for lentivirus production were established from 1 ml of liquid N<sub>2</sub> frozen HEK293T cells which contain 10% (v/v) DMSO for cryopreservation. The aliquot was quickly thawed, and cells were seed in a 10-cm-diameter petri dish containing 10 ml of culture medium. Cell passages were performed using Trypsin/EDTA when 90-95% of cellular confluence was reached. For lentivirus production (see below), the day before transfection, 11·10<sup>6</sup> cells were seed onto five 15-cm-diameter tissue culture dishes to obtain ~80% confluence the day of transfection. Only cells with less than 30 passages were used for lentivirus production.

### 1.2.2 CHO cells

CHO cells are an epithelial cell line derived from the ovary of the Chinese hamster. Given their flattened morphology, these cells were used in this project to assess the effect of the SPARC-derived peptide p4.2 on the actin cytoskeleton.

CHO cells were maintained at 37°C and 5% CO<sub>2</sub> in:

- » F12 Ham culture medium (ref. N4888, Sigma-Aldrich, St. Louis, MO)
- » 10% (v/v) FBS
- » 1% P/S

# 2 Production of high-titer HIV-1-based vector lentivirus

During this project, infection of neurons with lentivirus was used to genetically modify SCMs. The VSV G- pseudotyped vector is the best choice for most gene-delivery experiments, both *in vitro* and *in vivo*. These second-generation lentiviruses only need two constitutive vectors (explained below), and the vector containing the gene of interest. Lentivirus production is achieved by transfecting these vectors into HEK293T cells (see Cell culture in [section 1.2.1](#)).

Here, production of lentivirus expressing synaptophysin::GCaMP6f (SyGCaMP6f) was performed as described by Didier Trono (<http://tronolab.epfl.ch/lentivectors>), Lausanne, Switzerland.

This protocol is adjusted to produce lentivirus from five 15-cm-diameter tissue culture dishes containing HEK293T cells at a confluence of 80% (which has been shown to give the best efficiency). If higher amounts of lentivirus are needed, it is recommended to increase the number of culture dishes, solutions, and reagents by 5.

## 2.1 Materials and reagents

### 2.1.1 Material

- » Laminar flow hood biosecurity level 2 with UV light for sterilization
- » Incubator at 37°C and 5% CO<sub>2</sub> exclusive for viral material
- » Five 15-cm-diameter tissue culture dishes ([ref. 93150, TPP, Switzerland](#))
- » 15 ml sterile centrifuge tubes ([ref. 91015, TPP, Switzerland](#))
- » 50 ml sterile centrifuge tubes ([ref. 91050, TPP, Switzerland](#))
- » 22 µm pore size vacuum filters ([ref. 99250, TPP, Switzerland](#))
- » Tissue culture flask 75 cm<sup>2</sup> ([ref. 90076, TPP, Switzerland](#))
- » Glass Pasteur pipette 150 mm ([ref. 5426015, Normax Lda., Portugal](#))
- » Electronic pipette controller
- » HEK293T cells ([Cat# SD-3515, ATCC](#))

### 2.1.2 Solutions

- » DMEM/F12 [1:1] culture medium containing 10% (v/v) FBS and 1% (v/v) P/S
- » Trypsin/EDTA 0.05%
- » Tris-EDTA buffer (TE), pH 8, stock 1x (see [Annex 2](#))
- » Buffered water (see [Annex 2](#))

- » 2.5 M CaCl<sub>2</sub> (see [Annex 2](#))
- » Saline solution buffered with HEPES (HeBS) 2× (see [Annex 2](#))
- » 70% (v/v) ethanol in spray bottle
- » Bleach, in a liquid waste container

### 2.1.3 Plasmids

- » pMD2G ([Addgene plasmid #12259, Didier Trono Lab](#)): encoding the VSV G envelope protein
- » pCMVR8.74 ([Addgene plasmid #22036, Didier Trono Lab](#)): encoding HIV-1 Gag, Pol, Tat and Rev proteins
- » pWPXL-syGCaMP6f: transfer vector containing the gene of interest. The synaptophysin::GCaMP6f construct was kindly provided by Dr. Leon Lagnado ([Dreosti et al., 2009](#); [Johnston et al., 2019](#)). The coding sequence of SyGCaMP6f was previously cloned into pWPXL ([Addgene plasmid #12257, Didier Trono Lab](#)) by replacing EGFP using BamHI and NdeI.

## 2.2 Precautions

This protocol requires that open tubes always be handled in the laminar flow hood. Tubes can be taken out of the laminar flow hood only when they are closed and have been sprayed with 70% ethanol.

Solid waste and plasticware must be discarded in a trash bin specific for infectious material and all liquids must be aspirated into a liquid waste bottle containing fresh bleach. Liquid waste bottle must be refilled with fresh bleach when the colour of the liquid is no longer yellow.

It is recommended that the laminar flow hood is cleaned with ethanol 70% several times during use.

Wearing double gloves is recommended. The lab coat, exclusive for the handling of viral material, must be washed and autoclaved at the end of the process.

It is advisable to use a cleanroom to produce lentivirus and a specific incubator for maintaining viral material.

## 2.3 Procedure

*1st day: Preparation of HEK293T cells for transfection*

**1)** To obtain a ~80% confluence on the day of transfection, cells were either seeded Friday for Monday (3 days before transfection), by spreading 2.5·10<sup>6</sup> cells/15 cm dish, or Monday for Tuesday (the day before transfection), by plating 11·10<sup>6</sup> cells/15 cm dish.

**2)** HEK293T cells were maintained in DMEM/F12 [1:1] culture medium containing 10% (v/v) FBS and 1% (v/v) P/S at 37°C and 5% CO<sub>2</sub>. Cells that were in culture for more than 30 passages were not used.

*2nd day: Co-transfection of plasmids through the calcium phosphate method*

**3)** A couple of hours before transfection, culture medium was replaced with 22.5 ml of fresh preheated DMEM medium containing 10% FBS without antibiotics. Remains of the old medium containing P/S were washed 3 times with PBS 1x carefully.

**4)** For five 15-cm plates to be transfected, DNA concentration of all plasmids was adjusted to 1 mg/ml in TE buffer, pH 8 (Table 6). The transfection mix (here called tube A) was prepared in a sterile 50-ml conical tube. After addition of CaCl<sub>2</sub> 2,5 M, tube A was well mixed by pipetting or vortexing. Another tube containing 5.7 ml of 2x HeBS was prepared (here called tube B).

**5)** To form a fine precipitate of CaCl<sub>2</sub> optimal for transfection, addition of the content from tube B to tube A was made under vigorous vortexing. To get agitation into tube A, a sterile glass Pasteur pipette was adapted to an electronic pipette controller and positive pressure into tube A was emitted. While agitating the transfection mix, 2x HeBS was added dropwise.

**6)** The precipitate was left at room temperature under the laminar flow hood for at least 5 min but without exceeding 30 min.

**7)** CaCl<sub>2</sub> precipitate was added to the cells dropwise (2.25 ml/dish) and mixed by gently swirling until the medium has recovered a uniformly red colour (drops generated a whitish colour).

**8)** Cells were incubated overnight at 37°C and 5% CO<sub>2</sub> in an incubator specific for viral material.

| Tube A (add in this order)   | Tube B            |
|--|-------------------|
| Plasmids:<br>39,5µg pMD2G<br>73 µg pCMVR8.74<br>112,5 µgp WPXL-SyGCaMP6f (transfer vector plasmid)<br>3.3 ml TE buffer 0.1x<br>1.75 ml buffered water<br>565 µl CaCl <sub>2</sub> 2,5M | 5.7 ml of 2x HeBS |

**Table 6.** Solutions used for HEK293T transfection following the calcium phosphate method.

*3rd day: Harvesting vector stocks*

**9)** Early the next morning, culture medium was changed (approximately 16 h after the addition of the DNA). Old medium was aspirated, and 14 ml of prewarmed fresh DMEM culture medium containing 10% FBS and 1% P/S were slowly added. This step needs to be done carefully, since HEK293T cells show high tendency to detach.

**10)** At this point, transfection efficiency could be checked under the microscope if the transfer plasmid containing the gene of interest had a fluorescent reporter. To test the reagents it is recommended to perform a transfection using a GFP encoding lentiviral vector.

**11)** Cells were incubated for 8 hours.

**12)** Culture medium from each plate was harvested to a 50-ml centrifuge tube. Tubes were closed and sprayed with 70% ethanol before taking them out of the laminar flow hood. The supernatant was stored at 4°C over the collecting period.

**13)** 14 ml of fresh prewarmed culture medium were added to the cell monolayer and incubated for another 8-12 h. Supernatant was harvested 2-3 times, every 8-12 h. During this thesis work, supernatant collection for the first time was made in the evening, around 8 h after medium replacement. The second harvest was done the next morning, around 12 h later, and the third was made in the afternoon of the same day after 8 h.

*4th day: Aliquots and storage*

**14)** Supernatant was centrifuged for 5 min at 500 g, 4°C, to pellet detached cells and debris.

**15)** Cleared supernatants were collected and filtered using a 0.22-µm pore size filter unit. Supernatant can be kept at 4°C for 5-7 days, but no longer.

**16)** Supernatant containing lentivirus were distributed in 1 ml aliquots and stored at -80°C. Freeze/thaw cycles strongly reduce the lentivirus titer. It is recommended to use the total content of the thawed aliquot or discard the remains in a container specific for infectious material.

**Note:** Supernatants can be used directly or concentrated if needed. Given the low density of neurons in SCMs, it was not necessary to concentrate the vector stock for the development of this thesis. However, when a more concentrated lentivector suspension is needed, lentiviral titer of concentrated supernatants are measured to find the optimal MOI (Multiplicity Of Infection), which corresponds to the number of viral particles that can infect each cell in the tissue culture dish. By adjusting a specific level of infection, variability among experiments is reduced.

## 2.4 Infection of SCMs with SyGCaMP6f lentivirus

To genetically modify SCMs to express Synaptophysin-GCaMP6f, lentiviral infection was performed at 12-14 DIV during a 1:2 overnight incubation of the appropriate viral stock (0.5 ml/well). Alternatively, neurons could also be incubated with greater amounts of lentiviral stock (up to 0.8 ml) during shorter time periods over day (6-8h). Fluorescence was evident at 4–6 days after infection, coinciding with the time when neurons were ready to be recorded (18-22 DIV).

Inter and intra culture variability in the expression of SyGCaMP6f infected SCMs as well as among neurons within the same well could be observed even when infection was performed with the same viral stock and incubation conditions.

### 2.4.1 Procedure

Infection of SCMs needs to be performed under the same precautions and security measures required for lentivirus production.

*1st day: (ideally in the late afternoon)*

- 1) Aliquots containing 1ml of lentiviral stock were kept at -80°C. The proper number of aliquots were left to thaw under the laminar flow hood considering 1 aliquot is used to infect 2 wells.
- 2) Overnight 1:2 incubation was performed by removing 500  $\mu$ l of culture medium and adding 500  $\mu$ l of lentiviral stock.
- 3) The tissue culture plate was kept in an incubator specific for viral material at 37°C and 8% CO<sub>2</sub> overnight.

*2nd day: (preferably in the early morning)*

- 4) The next morning, all the content from each infected well (culture medium + viral stock) was discarded in a container with bleach and 1 ml of fresh prewarmed and pH balanced neuronal culture medium was added to each well.
- 5) Once viral stock medium was replaced, the 12-well tissue culture plate could be again maintained in the regular incubator specific for primary cultures at 37°C and 8% CO<sub>2</sub>.



# 3 Electrophysiological recordings

SCMs form autaptic neuronal circuits so that the pre- and postsynaptic components belong to the same neuron. Hence, during electrophysiological recordings, a single electrode placed in the cell body is used to stimulate (generate an action potential) and record the evoked response.

During this thesis, we have taken advantage of this culture system to perform patch-clamp experiments in whole cell configuration. This technique is based on the generation of a hole on the cellular membrane of the neuronal soma that gives access to the interior of neuron. By means of an electrode contained within a glass pipette filled with internal solution (see the [Solutions section](#) below) we can record current and voltage changes ([Fig. 42](#)). Although most experiments have been carried out in the voltage-clamp modality, current clamp experiments have also been performed. Both techniques will be explained in this chapter.

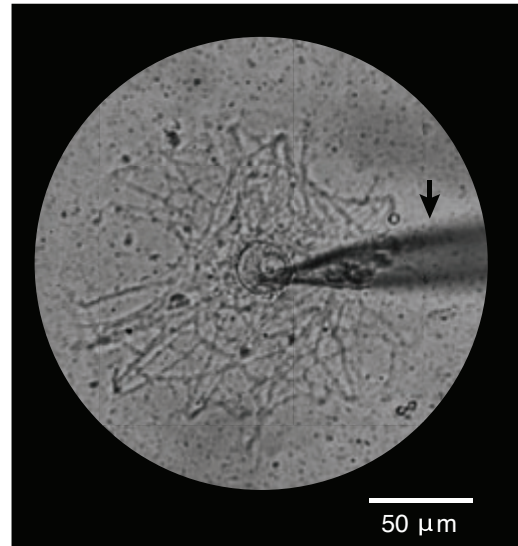


**Figure 42. Electrophysiological set up.** Phase contrast image of a recorded single cell microculture obtained with a 60X air objective. Access to the interior of the neuron through the soma is made by means of a glass pipette filled with intern solution and containing an electrode (arrow). A patch is generated on the cell membrane and successive suction allow to pierce the membrane and access to the cell interior.

## 3.1 Instruments and solutions

### 3.1.1 Instruments for Patch-Clamp experiments

#### *Recording stage*

For electrophysiological recordings, 15-mm diameter glass coverslips containing SCMs (18-22 DIV) were placed on a RC-25F recording/perfusion chamber ([Fig. 43A](#); [Cat # 64-0233, Warner Instruments, Hamden, US](#)) which has a hole of smaller diameter than that of the coverslip to allow visualization of the cells under the microscope. This chamber has an inlet and an outlet hole that facilitate the perfusion with external solution. A manifold placed in the inlet hole ([model ST-3R, Cat# 64-1407, Warner Instru-](#)

ments, US) was used to add external solution into the chamber whereas a right-hand suction tube (model ST-1R, Cat# 64-1400, Warner Instruments, US) placed in the outlet hole and connected to the vacuum system was used to withdraw the solution. A reference electrode is assembled in the perfusion compartment (see the [Electrodes and wires section](#) below). The recording chamber was mounted on a chamber platform (Fig. 43B). Depending on the type of experiment, two chamber platforms were employed. For standard electrophysiological recordings, the P-1 chamber platform (Cat# 64-0277, Warner Instruments, Hamden, US) was used. A 24x50 mm cover glass of thickness #1 (ref. 631-0146, VWR, Germany) was mounted onto the chamber platform right underneath the coverslip to prevent leakage of external recording solution. For electrophysiological recordings coupled to imaging, the P-4 chamber platform (Cat# 64-0280, Warner Instruments, Hamden, US) was used instead, and no cover glass was needed. High vacuum grease (ref. Z273554-1EA, Dow Corning®, Sigma-Aldrich, St. Louis, MO) was used to seal and secure both the glass coverslip under the recording chamber and the cover glass onto the platform (when needed). To complete the assembly and place it onto the Olympus IX-50 inverted microscope the chamber platform was mounted onto a Series 20 stage adapter of 11 cm of diameter (Fig. 43C; model SA-OLY/2, ref. 64-2411, Warner Instruments, Hamden, US).



**Figure 43. Recording stage set up used for electrophysiological recordings of autaptic neurons.** **A)** RC-25F recording chamber with the perfusion and suction tubes connected to the chamber's inlet and outlet, respectively. These tubes allow external solution to enter and leave the chamber, thus providing a continuous flow. The coverslip was mounted beneath the middle of the chamber (hole) and sealed with vacuum grease. **B)** P-4 chamber platform to hold the recording chamber. **C)** SA-OLY/2 stage adapter to assemble the chamber platform onto the objective of the inverted microscope.

### *Suction circuit*

To achieve whole cell configuration of SCMs during recording, the patch pipette needs to pass through 3 stages: bath, on-cell and whole-cell. A suction circuit was set for opening the cell after the seal (patch) was made on the cell membrane. Connected to the suction tube of the holder (Fig. 44A) was placed a tube that allowed direct suction from the mouth to generate vacuum in the patch pipette.

### Headstage

The headstage is a device with built-in circuitry that is placed above the recording stage and holds the patch pipette by means of an electrode holder. The headstage transmits electrical signals from the patch pipette onto the amplifier, thus acting as a pre-amplifier (CV-4 Headstage, Gain X1/100, Axon Instruments, US).

The electrode holder (Fig. 44A) was used to hold the patch pipette, which was filled with internal solution, contained a chlorinated silver electrode (see [Electrodes and wires section](#) below) and was in contact with the holder through a gold pin.

The headstage was mechanically controlled by a water hydraulic micromanipulator (Fig. 44B; model MHW-3, Narishige, Japan) that allowed the movement of the patch pipette with nanometer precision along the X, Y, and Z axes. Maintaining the micromanipulator in good conditions without drift is critical for successful recordings.

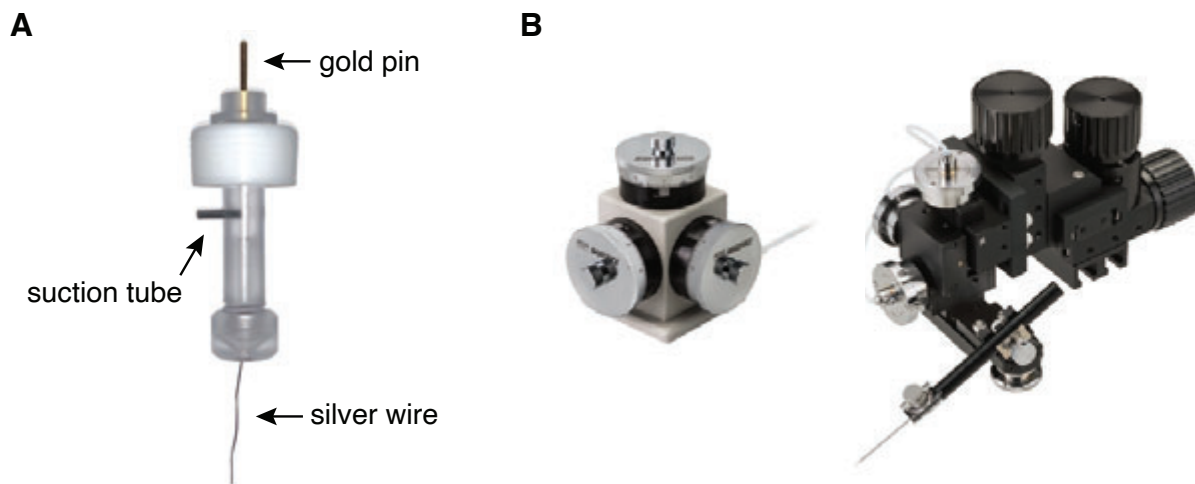


**Figure 44. Micromanipulation of the patch pipette. A)** Electrode holder used to hold the patch pipette. **B)** Water hydraulic micromanipulator (left) that connects to the macromanipulator (right) to move the patch pipette through the X, Y, Z axes with nanometer precision.

### Electrophysiological setup

To measure changes in current or voltage during electrophysiological recordings, the headstage was connected to an amplifier that contains the circuitry required to measure and magnify electrical currents.

During this thesis, recordings were made using an Axopatch-1D patch-clamp amplifier (Fig. 45A; Molecular Devices, San Jose, CA) under the control of an ITC-18 board (Fig. 45B; Instrutech Corp, Port Washington, NY) driven by WCP software (Dr. John Dempster, University of Strathclyde, UK) or mafPC (IgorPro-based software developed by Matthew Xu-Friedman, University of Buffalo, US).

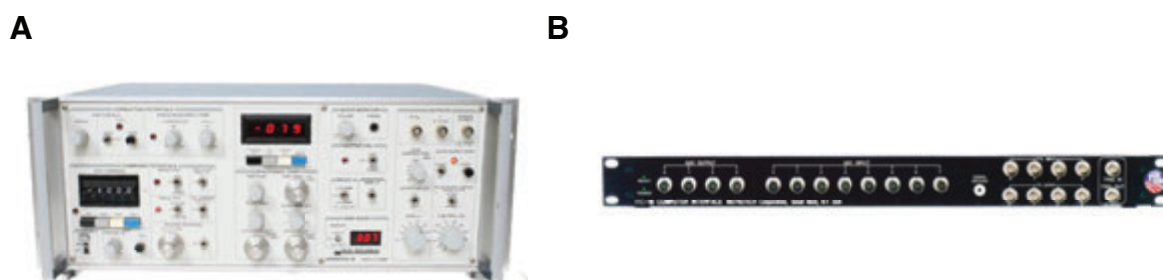


**Figure 45. Amplifier and interface.** A) Axopatch-1D patch-clamp amplifier. B) Instrutech ITC-18 interface that allows the conversion of analog signals provided from the amplifier to digital signals into the software.

### *Electrodes and wires*

Patch electrodes were obtained from chlorinated (by immersion in bleach for 2 days) silver wire 0.25-mm-diameter (ref. AG548511, ADVENT, UK)

Reference electrodes were obtained from chlorinated silver wire 0.5-mm-diameter (ref. AG548609, ADVENT, UK) and were soldered to a socket contact (ref. SA3347/1, Bulgin Limited, Switzerland). The reference electrode was connected to the headstage through two crimp contacts soldered in a wire, one connecting to the reference electrode (SA3348/1, Bulgin Limited, Switzerland) and another to the headstage (ref. SF-7QP2000, Phoenix contact, Germany).

### *Patch pipettes*

Patch pipettes or micropipettes used for electrophysiological recordings were obtained from pulling borosilicate glass capillaries (1.2 OD x 0.69 x 100 L mm, ref. 30-0044, Harvard Apparatus) by means of a horizontal forging Micropipette puller (Fig. 46A, model P-97, Sutter Instruments, Novato, CA) containing a trough filament, 3 mm wide (ref. FT330B, Sutter Instruments, Novato, CA). A protocol of 5 pull steps was used for shaping patch pipettes.

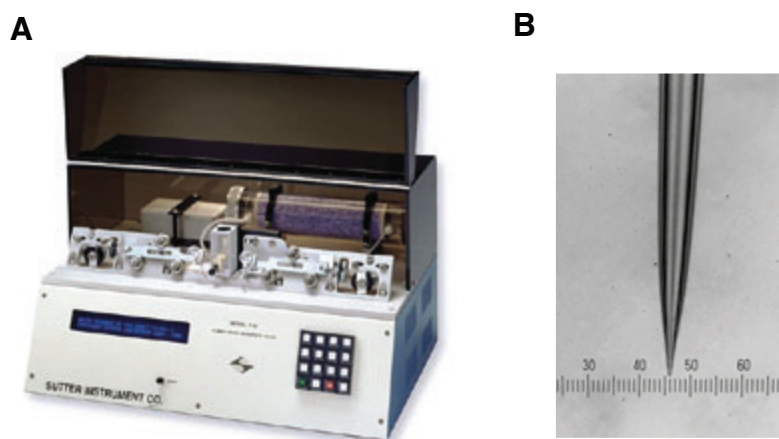


**Figure 46. Micropipette puller and patch pipette.** A) Horizontal forging micropipette puller to make patch pipettes. B) Example of the tip of a patch pipette. The tip shape is crucial for making a successful patch, piercing the cell membrane, and maintaining the series resistance throughout the recording. Values are expressed in mm.

Optimal shape of the micropipette tip is crucial for establishing the patch on the neuronal membrane and for its reliable maintenance throughout recordings.

For experiments in whole-cell configuration, outwardly convex tips are preferred over concave tips because they hold pressure more optimally. Typical resistances of pipettes used for recordings were 3–5 M $\Omega$  when filled with internal solution (Fig. 46B).

### 3.1.2 Solutions for Patch-Clamp experiments

During electrophysiological recordings, neurons were continuously perfused with extracellular solution and the patch pipette was filled with internal solution to resemble physiological ion concentrations (Table 7). Experiments were performed at room temperature (23 °C).

| External solution (mM)      | Internal solution (mM)   |
|-----------------------------|--------------------------|
| NaCl 130 mM                 | K-gluconate 130 mM       |
| KCl 5 mM                    | HEPES 10 mM              |
| HEPES-hemisodium salt 10 mM | EGTA 1 mM                |
| MgCl <sub>2</sub> 2 mM*     | Na <sub>2</sub> ATP 3 mM |
| -----                       | NaGTP 1 mM               |
| Glucose 10 mM               | MgCl <sub>2</sub> 4 mM*  |
| CaCl <sub>2</sub> 2mM*      |                          |

**Table 7. External and internal solutions for electrophysiological recordings.** External solution is adjusted to pH 7.4 with NaOH and to 290 mOsm/kg before the addition of glucose and CaCl<sub>2</sub>, which increases osmolarity to ~300 mOsm/kg. Dotted line separates the stock solution (kept at 4°C) from the addition of glucose and CaCl<sub>2</sub> that is made before starting the experiment (room temperature). Internal solution is adjusted to pH 7.2 with KOH and to 290 mOsm/kg and is kept at -20°C in 1 ml aliquots. All salts were from Sigma-Aldrich (St. Louis, MO). \*Prepared from commercial solutions at 1 mM.

External and internal solutions were supplemented with the following components either for acute treatment or for protein dialysis, respectively.

» External solution: acute treatment of SCMs by adding compounds to the extracellular solution during electrophysiological recordings are detailed in the corresponding result sections. Aliquoting and storage is explained here.

1) **Latrunculin-A** (ref. 3973, Tocris, UK) was diluted in DMSO at a stock concentration of 2 mM and maintained at -20°C.

2) **Bafilomycin A1 from Streptomyces** (ref. B1793, Sigma-Aldrich, St. Louis, MO) was diluted in DMSO at a stock concentration of 100  $\mu$ M and maintained at -20°C.

» Internal solution:

1) **EGTA concentration** of the internal solution was increased when indicated.



2) **Tubulin (porcine) TRITC Rhodamine labelled** (ref. [TL590M](#), [Cytoskeleton](#)) was diluted in general tubulin buffer containing PIPES 80 mM, MgCl<sub>2</sub> 2 mM, EGTA 0.5 mM, GTP 1 mM to a stock concentration of 10 mg/ml and maintained at -80°C. Vials were snap frozen in liquid N<sub>2</sub>. Tubulin was added to internal solution at different concentrations for dialysis when indicated. In control conditions of dialysis, general tubulin buffer was added to internal solution (1:400, same dilution as for tubulin 25 µg/ml). Tubulin was denaturalized when indicated by warming it up at 100°C for 30 min.

3) **Recombinant Kinesin Family, Member 18A (KIF18A)** (ref. [RPF518Hu01](#), [Cloud-Clone Corp.](#)) was reconstituted in Tris 20 mM, NaCl 150 mM to a concentration of 1 mg/ml and maintained at -80°C for 4 months. It is recommended to avoid vortex and repeated freeze/thaw cycles. KIF18A was added to internal solution at different concentrations for dialysis when indicated. For control conditions, only the buffer for protein reconstitution was added (1:40, same dilution as for KIF18A 25 µg/ml).

## 3.2 Patch-Clamp techniques

Two techniques to evoke and record synaptic activity were used in this work:

- 1) **Voltage Clamp**: membrane voltage is set to a certain value, while currents associated to synaptic activity are recorded.
- 2) **Current Clamp**: current to evoke action potentials is injected, while changes in membrane voltage are recorded.

### 3.2.1 Voltage clamp

Neurons were clamped at -60 mV and stimulated by a 1–2 ms depolarization step that drove membrane potential to 0 or 10 mV. This depolarizing stimulus triggered the opening of voltage-gated Na<sup>+</sup> channels. Since recordings of SCMs display both, pre- and postsynaptic currents, the presence of functional autaptic synapses was identified by the generation of EPSCs that appeared immediately (5-10 ms) after the sodium current associated with the generation of an action potential (Campbell C et al., 1984). EPSCs were observed in ~80% of 18-22 DIV microcultures ([Fig. 47](#)). The autaptic current appeared as an inverted Gaussian bell and reflected the synchronicity of stimulated synapses. The peak of this current corresponds to the moment of maximum synaptic vesicle release ([C. F. Stevens & Williams, 2007](#)). Increases in CNTF concentration during culture maintenance enhanced EPSC amplitude. Further details of neurotransmission in SCMs are available elsewhere ([Albrecht et al., 2012](#); [Perez-Gonzalez et al., 2008](#)).

Since the patch electrode is placed on the neuronal soma and neuronal processes are prolonged and tortuous, voltage fixation is spatially limited. This phenomenon, known as space-clamp, results in the filtering of the depolarizing stimulus and evoked respon-



ses as a function of their distance from the electrode (Ulrich & Luscher, 1993). Therefore, axosomatic synapses are the main contributors to EPSCs and the participation of axodendritic synapses distally located from the soma on the evoked response is spatially limited.

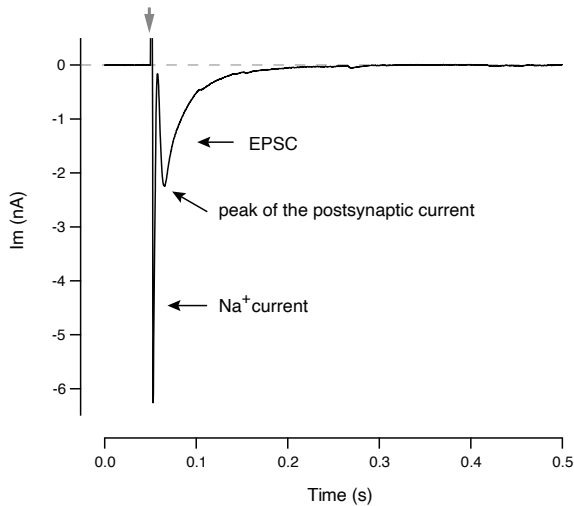


**Figure 47. Voltage clamp recording of an autaptic neuron.** The action potential generated by an electrical stimulus (gray arrow) appears as an inward current of sodium. This action potential propagates through the axon and within 10 ms generates an autaptic excitatory postsynaptic current (EPSC) that corresponds to synaptic transmission in the autaptic circuit. In our culture system, this current is due to the entry of  $\text{Na}^+$  and  $\text{Ca}^{2+}$  ions through cholinergic postsynaptic receptors.

### Chemical stimulation

Given that both, pre- and postsynaptic function, contribute to changes in EPSC amplitude, evaluating them separately is not straightforward. To test the contribution of postsynaptic nicotinic receptors, chemical stimulation was performed by applying a local puff of 50  $\mu\text{M}$  acetylcholine using a fused-silica capillary (Fig. 48; Microfil, #MF-28G, World Precision Instruments, Sarasota, FL). Timing of application was set to 30 ms using a TTL pulse.

It is important to consider that currents triggered by chemical stimulation are generated by both, synaptic and extrasynaptic cholinergic receptors. For that reason, accompanying chemical stimulation assessment with the analysis of mEPSC amplitude, provides a more accurate readout of postsynaptic function.

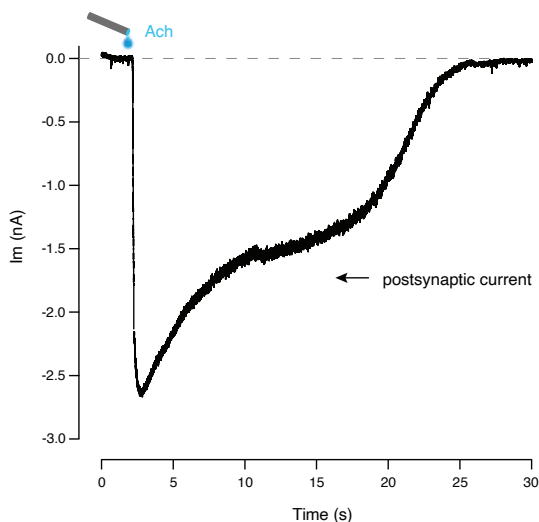


**Figure 48. Chemical stimulation triggered by a puff of acetylcholine (Ach).** To assess the contribution of postsynaptic function to excitatory postsynaptic currents (EPSCs), a puff of 50  $\mu\text{M}$  Ach was delivered onto the cell body of the autaptic neuron. The current generated by the opening of cholinergic postsynaptic receptors is illustrated.

### 3.2.2 Current clamp

Current clamp experiments were used in a specific experiment to study neuronal excitability of SCMs. In these experiments, the action potential threshold was evaluated by injecting a given amount of current.

Functionality of autaptic circuits were first validated in voltage clamp (presence of EPSCs) before changing to current clamp modality. Different amounts of current were injected (pA) while changes in membrane voltage were recorded. The value of current injected from which an action potential was generated was established as the AP threshold, which was used to compare neuronal excitability.

## 3.3 Analysis of voltage clamp recordings

Voltage clamp recordings provide information about three types of synaptic transmission present in neuronal circuits: synchronous or evoked, asynchronous and spontaneous (Kaeser & Regehr, 2014).

During this thesis, analysis of evoked and spontaneous electrophysiological data was performed using custom-made macros written in IGOR Pro 6-8 (Wavemetrics, Oregon, USA).

### 3.3.1 Evoked neurotransmission

For the analysis of EPSCs, basal current was previously subtracted, and amplitude of the current peak was measured (Fig. 49). Neurons with leak currents greater than 10% of the resulting EPSC, or greater than 500 pA, were discarded, since it indicates poor sealing and poor voltage maintenance during voltage clamp. Since our research does not focus on the analysis of  $\text{Na}^+$  currents, they have been blanked from all EPSC traces shown in this thesis.

### 3.3.2 Functional RRP measurement

During this project, we have used trains of high-frequency stimulation to estimate RRP size (Schneppenburger et al., 1999). During high-frequency stimulation, the RRP is rapidly depleted, which leads to synaptic depression until a steady state is reached (Fig. 50A). Cu-

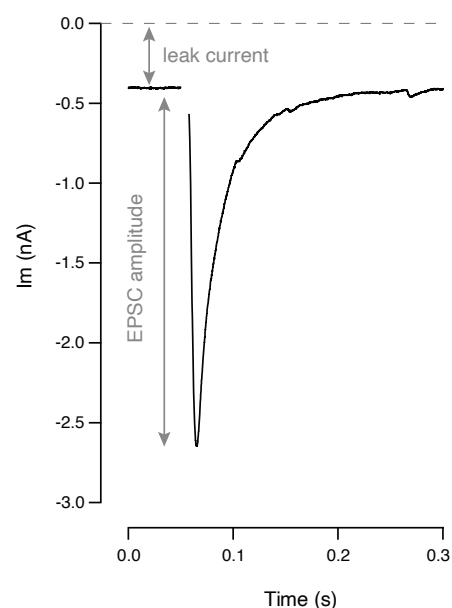


**Figure 49. Voltage clamp recordings associated to a depolarizing stimulus in an autaptic neuron.** Synaptic weight was assessed in the form of EPSC amplitude, which was measured by subtracting the basal leak current and calculating the maximum current value of the evoked response. Inward sodium current has been blanked.

mulative analysis of the amplitude of the EPSCs from the stimulus train as a function of experimental time allows the fitting of a linear function to the steady state of the depression. Extrapolation of this line with the ordinate axis provides an estimated value of RRP size (Fig. 50B). Here, trains of stimuli at 14-20 Hz were applied to estimate RRP size in autaptic neurons.

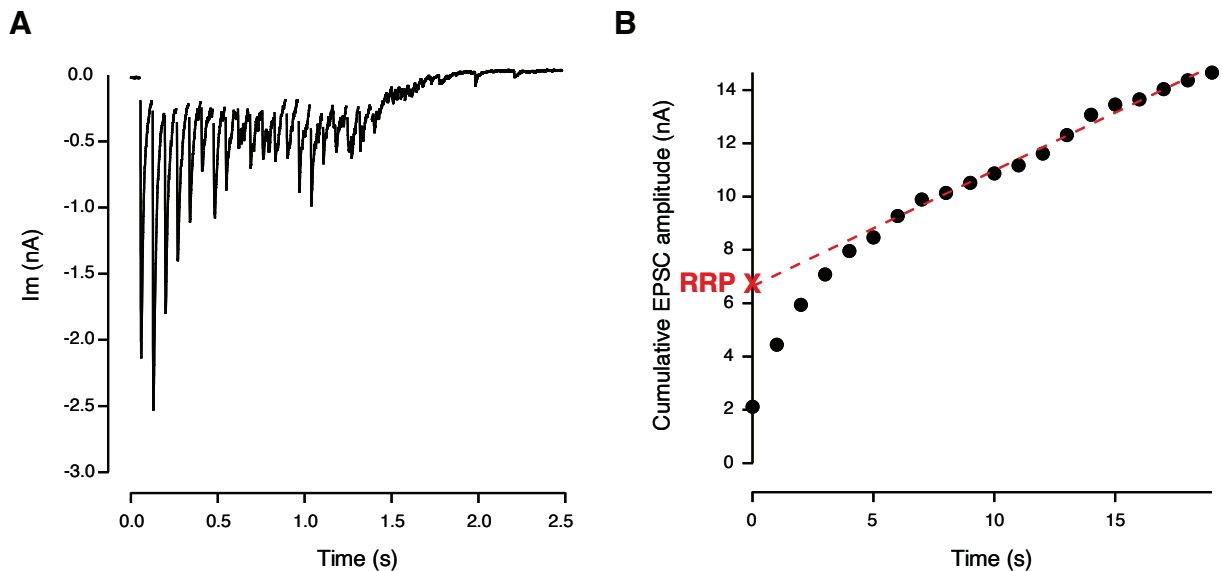


**Figure 50. Functional estimation of RRP size by high-frequency stimulation. A)** EPSCs evoked during the delivery of a train of 20 stimuli at 14 Hz in an autaptic neuron. Notice how synaptic transmission is depressed after 5-6 action potentials. **B)** Cumulative analysis of the EPSCs evoked in **(A)**. A linear function (red dotted line) is fitted to the steady state of the depression. Extrapolation of this line with the ordinate axis provides an estimated value of RRP size (red cross).

### 3.3.3 Spontaneous neurotransmission

Spontaneous neurotransmitter release occurs in the absence of neuronal activity and corresponds to the release of a single vesicle that is displayed in the form of a miniature excitatory postsynaptic current (mEPSC; Fig.51A and B).

Analysis of the amplitude of mEPSCs provides information of postsynaptic function and was performed using a macro written in IGOR Pro (Wavemetrics, Oregon, US) by Dr. Eugene Mosharov (Columbia University, US). Automatic identification of mEPSCs using this macro had to be manually revised.

Analysis of mEPSC frequency provides information of presynaptic function. An average value of 1 Hz in spontaneous neurotransmitter release has previously been reported in our culture system (Perez-Gonzalez et al., 2008). However, since spontaneous neurotransmitter release is a stochastic process, high variability in mEPSC frequency is usually observed. Thus, the longer are the recordings of mEPSC analysed, the more reliable are the data obtained.

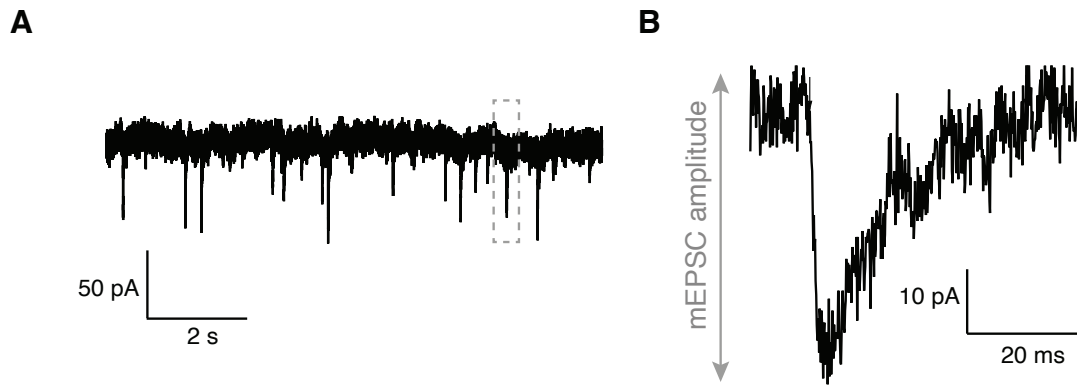


**Figure 51. Spontaneous neurotransmitter release recorded in an autaptic neuron. A)** Illustrative example of miniature excitatory postsynaptic events (mEPSCs) recorded during 10 seconds in a single cell microculture at rest. Counting the number of miniature events was used to analyse mEPSC frequency and the number of cumulative mEPSC as a function of time. **B)** Magnification of the mEPSC squared in **(A)**. mEPSC amplitude was calculated by measuring the current peak.

# 4 Simultaneous electrophysiological recording and imaging

To associate presynaptic calcium influx to neurotransmission, SCMs expressing Synaptophysin-GCaMP6f (SyGCamp6f) were imaged and simultaneously recorded electrophysiologically. SyGCamp6f is an improved version of SyGCaMP2 (Dreosti et al., 2009). The calcium reporter GCaMP6f is linked to the synaptic vesicle protein synaptophysin and therefore this construct is used to identify calcium concentration changes occurring at the presynaptic terminal. Lentivirus were used as a transduction method for obtaining SCMs expressing SyGCaMP6f (see section 2).

SyGCaMP6f accumulates at synapses showing a punctuate pattern during stimulation while diffuse fluorescence is homogeneously distributed throughout the cell at rest (Fig. 52A and B; Martínez San Segundo et al., 2020). Before starting the experiment, a region of interest of 256x256 pixels was selected on the perisomatic area and gain was adjusted to a low value to prevent fluorescence from reaching saturation during stimulation.

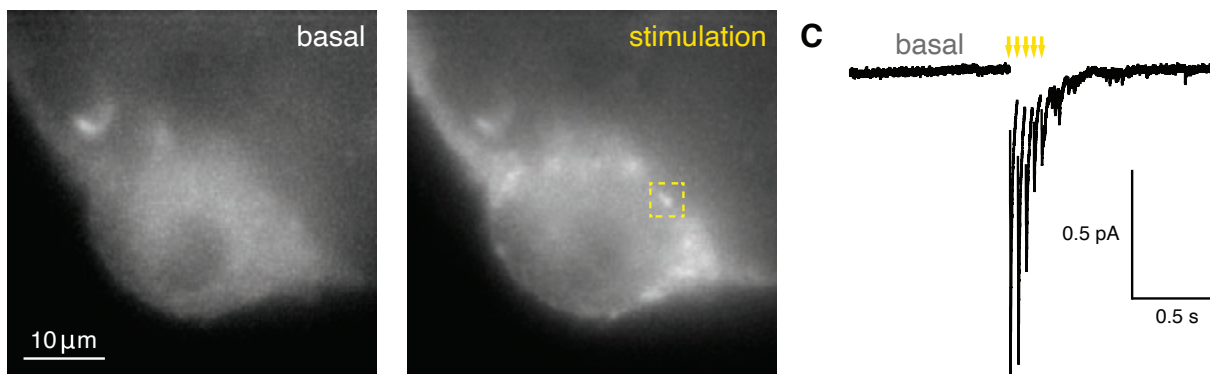


**Figure 52. Imaging of presynaptic calcium influx coupled to electrophysiological recordings.**

**A)** Axosomatic region of a single cell microculture (SCM) expressing the presynaptic calcium reporter Synaptophysin-GCaMP6f (SyGCaMP6f) in basal conditions (maximum projection). Fluorescence is homogeneously distributed throughout the neuron. **B)** SCM shown in **(A)** upon a train of 5 stimuli (maximum projection). Notice how SyGCaMP6f fluorescence increases in discrete rounded dots around the soma (yellow box), indicating the presence of axosomatic synapses. Presynaptic calcium influx of these synapses, selected as regions of interest (ROIs) in Image J, was assessed by calculating relative changes in baseline fluorescence, measured as  $(F - F_0) / F_0$ . **C)** Evoked response obtained during a train of 5 stimuli at 20 Hz coupled to SyGCaMP6f fluorescence changes shown in **(A)** and **(B)**.

Coverslips were mounted on the recording chamber using the P-4 chamber platform. Neurons were observed in an inverted Olympus IX-50 microscope and illuminated with blue light, using an ET480/20x excitation filter. Fluorescence was acquired using a q505LP dichroic and a HQ535/50 nm emission filter (Chroma Technology Corp., VT). Images were collected through a 60x UPlanFLN objective (1.25 N.A, Olympus, Tokyo, Japan) using Type F immersion liquid (Cat# 11513859, Leica, Germany) and visualised on an ImageEM camera controlled by HCImage (Hamamatsu).

Images were acquired at 40 Hz simultaneously to the application of a train of 5 stimuli at 20 Hz or a single stimulus (Fig. 52C). TTL pulses generated by mafPC controlled the exposure time of the camera, as well as the timing of light illumination, which was adjusted via a shutter (Uniblitz, NY), to minimise photobleaching.

#### 4.1 Analysis of imaging data simultaneous to electrophysiological recordings

Image analysis was carried out combining Image J and macros written in Igor Pro software. SyGCaMP6f fluorescence ( $F$ ) was obtained after subtracting the background fluorescence found in regions of interest drawn outside of the microculture. Calcium increases were reported as relative changes of SyGCaMP6f fluorescence, measured as  $(F - F_0)/F_0$ .

Putative synapses were identified on difference images that illustrated the location of stimulation dependent changes in fluorescence. Regions of interest (ROIs) of  $1.3 \times 1.3 \mu\text{m}$  were drawn on the center of mass of identified puncta, which were typically round,  $\sim 1 \mu\text{m}$  diameter structures. A given punctum was considered a synapse when exhibited a  $\Delta F/F_0$  increase above three standard deviations of baseline values recorded before stimulation. This criterion avoided the contribution of synapses found out of focus. Block of depolarization with  $1 \mu\text{M}$  TTX demonstrated that changes in SyGCaMP6f fluorescence were exclusively related to neurotransmission.



# 5 Immunocytochemistry

During this work, immunofluorescence assays of SCMs or CHO cells were performed to morphologically identify the location of proteins of interest under the confocal microscope.

Stimulated emission depletion (STED) microscopy was also used in this thesis project to obtain super-resolution images of autaptic neurons.

## 5.1 Confocal microscopy

### 5.1.1 Immunocytochemistry of SCMs

For immunocytochemistry, coverslips containing SCMs were:

- » Rinsed in PBS 1X.
- » Fixed in 4% PFA (prepared in phosphate buffer 0.1 M) for 15 min.
- » Washed 3 times with PBS 1X.
- » Permeabilized with 0,3% TX-100 for 30 minutes.
- » Blocked with 20% NGS, 0,2% TX-100 and 0,2% gelatine for 1h.
- » Incubated with a monoclonal antibody combined with a polyclonal primary antibody (Table 8) in a solution containing 1% NGS, 0,2% TX-100 and 0,2% gelatine, overnight at 4°C in a humid chamber.
- » Rinsed in blocking solution 3 times for 5 minutes.
- » Incubated for 1 hour at RT in the absence of light with appropriate secondary antibodies labelled with Alexa Fluor-488 and Alexa Fluor-555 for fluorescent staining
- » Washed 3 times with PBS 1X.
- » Incubated with DAPI 1:10000 for 2 min when indicated.
- » Washed with PBS 1X.
- » Mounted with Fluoromount (ref. F4680, Sigma-Aldrich, St Louis, MO) or ProLong Gold Antifade (ref. P36934, Invitrogen, Carlsbad, CA) and dried at RT overnight.

#### *Image acquisition*

Cells were visualized in a Zeiss LSM 880 confocal microscope (Carl Zeiss AG, Germany). Optical sections were acquired using a 63X oil immersion objective PL-APO (1.4 NA).

| Specificity                              | Host species | Concentration | Commercial brand   | Reference     |
|--|--------------|---------------|--------------------|---------------|
| Bassoon<br>(clone SAP7F407)              | Mouse        | 1:1000        | Enzo Life Sciences | ADI-VAM-PS003 |
| N-cadherin                               | Sheep        | 10 µg/ml      | R&D Systems        | AF6426        |
| VAMP-2                                   | Rabbit       | 1:500         | Synaptic Systems   | 104202        |
| Synapsin-I                               | Rabbit       | 1:1000        | Millipore          | AB1543P       |
| Nicotinic acetylcholine receptor alpha 3 | Rabbit       | 1:50          | Abcam              | ab183097      |
| PSD93                                    | Rabbit       | 1:500         | Synaptic Systems   | 124102        |
| Acetylcholine transporter (VAcHT)        | Goat         | 1:1000        | Millipore          | ABN100        |
| α-bungarotoxin                           | -            | 1 µg/ml       | Thermo Fisher      | B35451        |
| Piccolo                                  | Rabbit       | 1:1000        | Abcam              | ab20664       |
| Munc13-1                                 | Rabbit       | 1:500         | Synaptic Systems   | 126103        |
| EB3<br>(clone KT6)                       | Mouse        | 1:250         | Invitrogen         | MA1-72525     |

**Table 8.** Primary antibodies for immunocytochemistry of single cell microcultures.

### 5.1.2 Correlative electrophysiology and immunocytochemistry

To correlate the number of synapses with synaptic transmission, SCMs displaying a representative morphology were recorded, micrographed, fixed, and stained by immunocytochemistry for the expression of the presynaptic marker bassoon and the synaptic adhesion protein N-cadherin. Appropriate secondary antibodies labelled with Alexa Fluor-488 and Alexa Fluor-555 were used to visualize N-cadherin and bassoon labelling, respectively. Images of recorded SCMs were used to identify stained microcultures in a Zeiss LSM 880 confocal microscope. Confocal sections were acquired using a 63x oil immersion objective PL-APO (1.4 NA).

### *Quantification of synapse numbers*

Images were analysed in Image J. The procedure for obtaining an estimate of synapses contributing to recorded EPSCs was based on the quantification of the density of bassoon and N-cadherin puncta located in the somatic region and nearby dendritic tree. Specifically, only somatic and dendritic puncta found  $\leq 20$   $\mu\text{m}$  away from the edge of the soma were considered. Synaptic contacts more distally located were not considered because the cable-filtering properties of dendrites in cultured neurons attenuate their contribution to recorded EPSCs (J. M. Bekkers & Stevens, 1996). A punctum was considered as a putative synapse if it spanned from three to five consecutive confocal Z-sections (0.33  $\mu\text{m}$  optical thickness), had a diameter ranging from 0.2 to 0.5  $\mu\text{m}$  and was stained with bassoon or N-cadherin. Density was calculated by dividing the number of bassoon and N-cadherin puncta by the analysed area.

### **5.1.3 Immunocytochemistry of CHO cells**

To study changes in the F-actin cytoskeleton of CHO cells, simultaneous labelling of G-actin and F-actin was carried out following previously described methods (Cramer et al., 2002; Knowles & McCulloch, 1992):

- » Fixation with PFA 4% in cytoskeleton buffer (Cramer et al., 2002) for 20 minutes.
  - ◇ Stock 16% PFA (ref. 15710, Electron Microscopy Sciences, Hatfield, PA)
  - ◇ Cytoskeleton buffer: 10 mM MES, 3 mM MgCl<sub>2</sub>, 138 mM KCl, 2 mM EGTA, 0.32 M sucrose
- » Washing 3 times with PBS 1X.
- » Permeabilization with 0,5% TX-100 for 10 minutes.
- » Rinsing 3 times with 0,1% TX-100.
- » Blocking with a solution containing 2% BSA and 0,1% TX-100 for 20 minutes.
- » Incubation with phalloidin-Alexa Fluor 488 1:2000 (A12379, Thermo Fisher, Waltham, MA) and deoxyribonuclease I-Alexa Fluor 594 5  $\mu\text{g}/\text{ml}$  (D12372, Invitrogen, Carlsbad, CA) for 30 minutes at RT in blocking solution in the dark.
- » Washing 3 times with PBS 1X.
- » Incubation with To-pro 1:500 for 15 min (1 mM in DMSO, ref. T3605, Molecular Probes).
- » Mounting with Fluoromount (ref. F4680, Sigma-Aldrich, St. Louis, MO) and letting it dry overnight.

### *Image acquisition*

Cells were visualized under a Leica TCS-SL confocal microscope using a 63 $\times$  immersion oil objective PL-APO (1.4 NA).

### *Quantification of F-actin and G-actin staining*

Images were analysed in Image J. The distance among F-actin filaments was calculated using a line profile drawn along the longest cell axis estimated by Image J (Feret's diameter). Only the basal region of the cell (~1.5  $\mu\text{m}$  optical thickness) was considered for analysis. To estimate the quantity of G-actin and F-actin in a single cell, the fluorescence of all pixels found in the maximum intensity projection were summed (RawIntDen command in Image J) after background subtraction. The relationship between G-actin and F-actin was calculated by dividing values obtained in the red and green channel, respectively.

## **5.2 STED microscopy**

### **5.2.1 Actin-ring like structures in SCMs**

STED microscopy was used for visualization of actin ring-like structures in autaptic neurons using phalloidin to stain F-actin and VAMP-2 to label synapses. The immunocytochemistry protocol was performed as follows:

- » Rinsing: in PBS 1X.
- » Fixation: SCMs were immersed for 15 min in a 4% PFA solution prepared in phosphate buffer 0.1 M from a 16% PFA stock solution.
- » Washing: cells were washed 3 times with PBS 1X for >5 min.
- » Permeabilization: 0.3% TX-100 for 20 min.
- » Blocking: neurons were incubated with blocking solution containing: 20% NGS + 0.2% TX-100 for 2 h.
- » Primary antibody: overnight incubation at 4°C with a primary monoclonal antibody anti-VAMP-2 (1:1000, [Synaptic Systems 104211](#)) in 1% NGS + 0.2% TX-100.
- » Rinsing: neurons were rinsed in blocking solution 2 times.
- » Secondary antibody: cells were incubated for 1.5 h with an anti-mouse secondary antibody labelled with Alexa Fluor-488.
- » Washing: 3 times wash with PBS 1X.
- » Phalloidin staining: subsequently cells were incubated with 0.165  $\mu\text{M}$  phalloidin-Atto 647N ([ref. 65906, Sigma-Aldrich, St. Louis, MO](#)) for 2.5 h at room temperature, followed by an overnight period at 4 °C.
- » Washing: 3 times wash with PBS 1X.
- » Mounting with ProLong Gold antifade, letting to dry overnight at RT.

### *Quantification of actin ring-like periodicity*

F-actin structures present in SCMs were revealed by STED microscopy and analysed by plotting changes in fluorescence intensity along line profiles (1–3  $\mu\text{m}$  length) drawn in Image J. Values were exported to Igor Pro 8.0 to quantify periodicity. The average distance between peaks found within an analysed segment was considered as representative of a given neurite.

### **5.2.2 Identification of microtubule plus-ends in SCMs**

STED microscopy was also used to study the location of microtubule growing-ends at the synapse, which were labelled with EB3 and synapsin-I, respectively.

Material and thickness of the substrate supporting the sample constitutes a critical point in terms of optical STED performance. Since all Leica objective lenses with coverglass correction are corrected for #1.5 coverslips, SCMs for this procedure were grown on this type of coverslips (thickness:  $0.170 \pm 0.01$  mm). Preparation of the samples was performed as follows:

- » Rinsing 3x with PBS 1X
- » Fixation with PFA 2 % in PBS 1X
- » Washing 3x with PBS 1X for >10 min
- » Permeabilization with 0.1% TX-100 in PBS 1X for 10 min
- » Rinsing 3x with PBS 1X
- » Washing 3x with PBS 1X for >10 min
- » Block with BSA 2 % for 2.5 h
- » Incubation of primary antibody in BSA 2% and 0.1% TX-100 in PBS 1X, in a humid chamber overnight at 4 °
  - ◇ rabbit polyclonal synapsin-I antibody, 1:250, (ref. AB1543P, Merck Millipore, Germany)
  - ◇ EB3 monoclonal antibody, 1:100, (clone KT6, ref. MA1-72525, Invitrogen, Carlsbad, CA)
- » Rinsing with PBS 1X
- » Washing 3x with PBS 1X for 20 min
- » Incubation of secondary antibody in BSA 2% and 0.1% TX-100 in PBS 1X for 1.5 h in the dark at RT
  - ◇ anti-rabbit Atto-647N, 1:100
  - ◇ anti-mouse Alexa Fluor Plus-594, 1:100
- » Rinsing with PBS 1X
- » Washing 3x with PBS 1X for 20 min
- » Mounting with ProLong Gold antifade for at least 24 h at RT

### *Quantification of microtubule plus-ends at the synapse*

Synaptic invasion of microtubule plus-ends revealed by STED microscopy was quantified using Image J. Synapsin-I was used to locate putative axosomatic synapses and invasion of MT plus-ends was determined by co-localization analysis of synapsin-I with EB3 (Colocalization macro in Image J).

### **5.2.3 Image acquisition**

Single plane STED images were acquired on a Leica TCS SP8 STED 3× (Leica Microsystems, Mannheim, Germany) on a DMI8 stand using a 100×/1.4NA HCS2 PL APO objective. A pulsed supercontinuum light source set at 644 nm was used for excitation and a pulsed depletion laser at 775 nm was added with no pulse delay at 20% intensity. Detection was performed with a hybrid detector (HyD) between 652 and 750 nm and gating between 0, 3, and 6 ns. Scanner speed was set to 600 Hz and images were taken with 8× frame accumulation and 2× frame average. Pixel size was set according to the depletion power to 23 nm.



# 6 Transmission electron microscopy

Electron microscopy enables us to look in far more detail at cellular structures than light microscopy. During this work, transmission electron microscopy (TEM) was performed to study the location and morphology of microtubules at the synapse. TEM was performed correlative with electrophysiology by recording autaptic neurons before fixation. To recognize the recorded neuron on the EM sample, neurons were micrographed before fixation. EM samples were prepared from SCMs grown on thermanox coverslips.

**Note:** Most chemicals in this protocol are toxic or harmful to us or the environment, so local health and safety rules as well as precautions indicated for each compound need to be followed. A lab coat and double gloves were worn during the procedure.

## 6.1 Materials and protection equipment

### 6.1.1 Materials

- » Thermanox coverslips 15-mm diameter (see [Cell Culture section 1.1.1](#))
- » Surgical blade ([ref.0211, Swan-Morton, UK](#))
- » Dumont tweezers #55 ([ref. 14099, World Precision Instruments Inc, Sarasota, FL](#)) of exclusive use for this protocol
- » 12-well plates ([ref. 83.3921, Sarsted, Germany](#))
- » Glass microbeaker 2.5 ml ([Cat# 60982, Electron Microscopy Sciences, Hatfield, PA](#))
- » Porexpan container with ice
- » Vegetal Oil
- » BEEM® Embedding capsules size 3 ([Cat# 69910-01, Electron Microscopy Sciences, Hatfield, PA](#))
- » BEEM® Embedding capsule holder for size 3 ([Cat# 69917-01, Electron Microscopy Sciences, Hatfield, PA](#))
- » Laboratory stove at 60°C
- » Forceps, Rochester-Pean 7.25" ([ref. 501707, World Precision Instruments Inc, Sarasota, FL](#))
- » Liquid N<sub>2</sub> container
- » Nugent Utility Forceps, angled tip ([ref. 504473, World Precision Instruments Inc, Sarasota, FL](#))

### 6.1.2 Protection equipment

- » Lab coat
- » Double nitril gloves
- » Mask FFP3 with valve for respiratory protection (ref. Aura 9332+, 3M, UK)

### 6.2 Solutions and reagents

- » Fixation solution: 1.8% (v/v) glutaraldehyde in sodium cacodylate 0.1 M. It is prepared under the fume hood from:
  - ◇ 25% (v/v) glutaraldehyde stock solution (Cat# 16216, Electron Microscopy Sciences, Hatfield, PA)
  - ◇ 0.2 M sodium cacodylate buffer, pH 7.6 (Cat# 11650, Electron Microscopy Sciences, Hatfield, PA), 1:2 dilution with MQ-water
- » 0.1 M sodium cacodylate buffer, pH 7.6
- » 0.05 M sodium cacodylate buffer, pH 7.6
- » Solution containing 1% (v/v) osmium tetroxide ( $\text{OsO}_4$ ) and 1.5% (w/v) potassium ferricyanide in 0.1 M sodium cacodylate
  - It is prepared as follows (8 ml, for 4 samples):
    - ◇ 0.12 g of potassium ferricyanide (ref. 20150, Electron Microscopy Sciences, Hatfield, PA)
    - ◇ 6 ml of 0.1 M sodium cacodylate
    - ◇ 2 ml of aqueous 4%  $\text{OsO}_4$  (ref. 19150, Electron Microscopy Sciences, Hatfield, PA)

**Note:** *This solution is very toxic, so it needs to be handled under the fume hood, using double gloves, the lab coat and the FFP3 mask.*

- » Solution containing 1% (w/v) tannic acid diluted in 0.05 M sodium cacodylate. It is prepared as follows:
  - ◇ 0.01 g of tannic acid (ref. 21700, Electron Microscopy Sciences, Hatfield, PA)
  - ◇ 10 ml of 0.05 M sodium cacodylate

**Note:** *Vortex quickly as it clumps easily. Wear double gloves and mask.*

- » Ethanol 100% (v/v)
- » Ethanol 90% (v/v) diluted in MQ water
- » Ethanol 70% (v/v) diluted in MQ water
- » Propylene oxide solution (ref. 20410, Electron Microscopy Sciences, Hatfield, PA)

**Note:** This solution is very volatile toxic, so it needs to be handled under the fume hood, using double gloves, the lab coat and the FFP3 mask.  
Propylene oxide dissolves most laboratory plastic so EM-grade plasticware or glass was used for working with this solution.

- » Epon resin containing:
  - ◇ 8.3 ml (9.17 g) of Embed-812 resin (ref. 14900, Electron Microscopy Sciences, Hatfield, PA)
  - ◇ 5 ml (5.67 g) of Araldite-502 (ref. 10900, Electron Microscopy Sciences, Hatfield, PA)
  - ◇ 18.3 ml (18.33 g) of DDSA Special (ref. 13710, Electron Microscopy Sciences, Hatfield, PA)
  - ◇ 0.6 ml (0.57 g) of DMP-30 (ref. 13600, Electron Microscopy Sciences, Hatfield, PA)

Vortex quickly after adding all the compounds and then leave it to settle for at least 30 min.

Note: 1.2 ml (1.14 g) of BDMA is recommended, instead of DMP-30, for better penetration and stability. Slight variation of the accelerator (DMP-30 or BDMA) will drastically affect the colour and brittleness of the EM block.

In order to mount the samples on EM blocks at the end of the procedure, embedding capsules were filled with Epon resin and polymerized at 60 °C for 24-48 h in the previous days.

### 6.3 Procedure

The protocol described here is for preparing 4 samples of thermanox coverslips. Incubations with different solutions were made adding a volume of 2 ml/well in 12-well plates. All the procedure was performed under the fume hood.

- » Fixation: SCMs that have previously been recorded, were micrograph and fixed in 1.8% glutaraldehyde in sodium cacodylate 0.1 M in two steps:
  - ◇ 20 min at RT
  - ◇ 20 min at 4 °C

**Note:** Fixation is a very important step. High osmolarity solutions may lead internal membranes to collapse and increase vesicle recycling, producing artefactual images. The fixative solution used here displayed an osmolarity of 320 mOsm, which is physiologically accepted. Alternative protocols may use fixative solutions containing 1.5% paraformaldehyde / 1.5% glutaraldehyde in 0.1 M Sodium Cacodylate (650 mOsm), which show too high osmolarity values for recorded neurons.

- » Washing 3x with sodium cacodylate 0.1 M (>5min).
- » Cells were incubated with freshly made 1% Osmium tetroxide / 1.5% potassium ferricyanide for 1 hour, at 4 °C in the darkness (inside a porexpan container filled with ice).
- » As much OsO<sub>4</sub> as possible was removed and cells were washed 2x with 0.1 M sodium cacodylate.

**Note:** Osmium waste must be handled inside the fume hood and treated with vegetable oil to inactivate it. All materials containing inactive osmium must be tightly closed and placed in a container specific for toxic residues.

- » Cells were incubated with freshly made 1% tannic acid / 0.05 M Sodium Cacodylate buffer (1:2 dilution of 0.1 M sodium cacodylate solution) at RT for 45 minutes in the darkness.
- » Washing twice in 0.05 M Sodium Cacodylate.
- » Washing once for 5 minutes in MQ-water.
- » Washing 2x 5 minutes in 70% ethanol.
- » Washing 2x 5 minutes in 90% ethanol.
- » Washing 5 minutes in 100% ethanol.

**Note:** It is possible to stop the protocol here and leave the cells overnight in 100% ethanol 4 °C.

- » At this point, autaptic neurons were stained black and could be easily located under the stereo microscope (Fig. 53A). A square was drawn around the recorded and micrographed neuron using a surgical blade.
- » Cells were incubated with 1:1 Epon resin and propylene oxide (1 ml of each) for 30 min at RT in the dark.

**Note:** Since propylene oxide dissolves most laboratory plastic, glass microbeakers are placed inside the 12-well plate. To extract propylene oxide from the bottle and mix it with the resin, a previously 1ml-marked glass pipette was used.

Propylene oxide is very toxic and volatile. Handling must be quick, made under the fume hood and wearing the lab coat, double gloves and FFP3 mask.

- » As much as possible of the mix was removed and the coverslips were transferred into new wells containing fresh 100% Epon. Cells were incubated for at least 1h at RT.
- » Coverslips were placed in fresh Epon and incubated for at least an additional hour or overnight.
- » Before mounting, the embedding capsule holder was prepared (Fig. 53B). Empty embedding capsules were spatially placed in the capsule holder. Previously polymerized resin blocks were separated from their capsule and placed into the empty embedding capsules, so only half of the block was inside. Supports for the coverslips around the capsule using aluminium foil (inverted L-shape) were made and stuck onto the holder when needed.
- » Coverslips were mounted downwards on top of the resin blocks.
  - ◇ Coverslips were taken out the well using the tweezers. The square around the recorded neuron made with the blade could be seen when looking at it against the light.
  - ◇ Coverslips were mounted downwards onto the resin block, so the square was placed on the middle of the block (Fig. 53C). Residual resin from incubation was used to fill the cleft at the top of the block. Bubble formation was avoided.
- » The capsule holder with the samples was left in the preheated stove at 60 °C for 1-2 days to allow the polymerisation of Epon resin.
- » EM blocks were separated from the thermanox coverslips by immersion in liquid N<sub>2</sub>. To do that, the block was fixed with the forceps and immersed into liquid N<sub>2</sub> for 12 s. Immediately after that, the coverslip was separated from the block using the nugent utility forceps.
- » The EM block was visualised under the stereo microscope to verify that the recorded neuron was on the middle of it ready to be processed (Fig. 53D).

**Note:** It is important to make sure that there are no remains of thermanox on the block, as it may damage the diamond blade of the microtome.

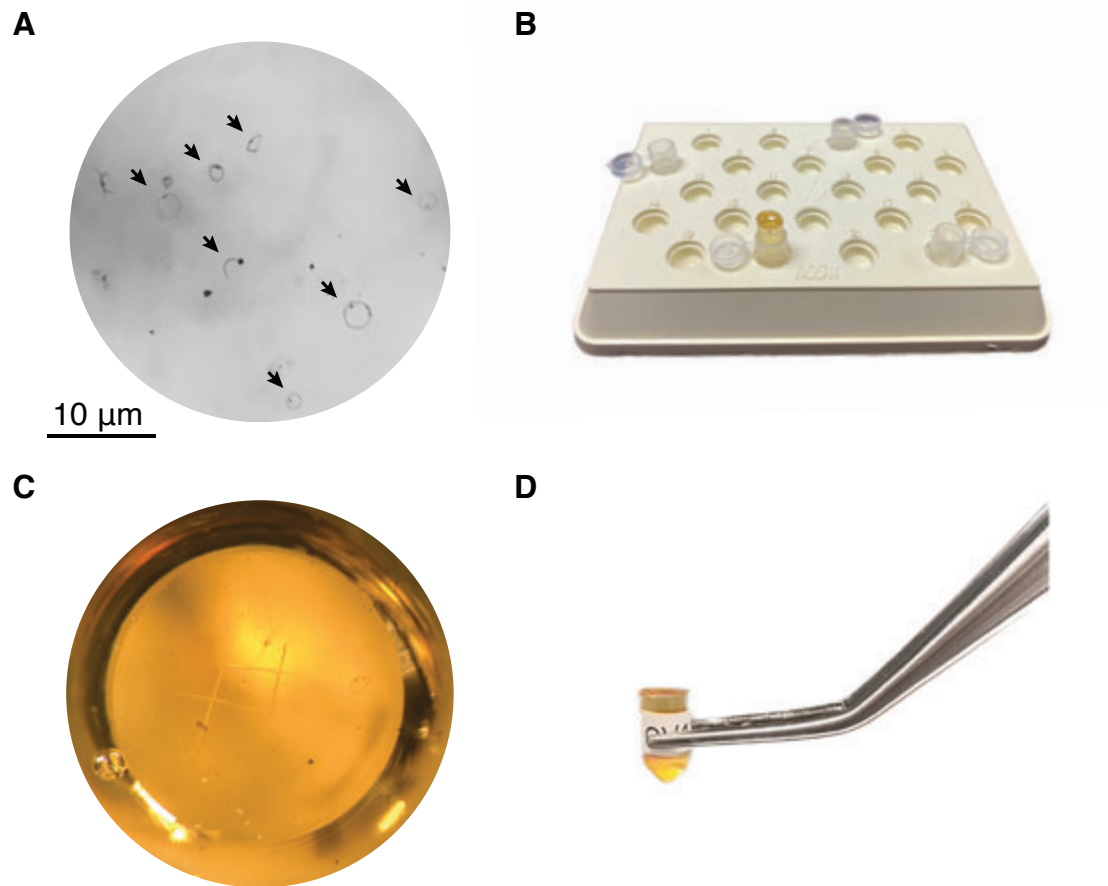


**Figure 53. Electron microscopy of single cell microcultures (SCMs).** **A)** Image of SCMs (arrows) stained black because of the osmium tetroxide, visualized under the stereo microscope. **B)** Embedding capsule holder set up. Notice how empty capsules are used as a support for resin blocks on which coverslips will be mounted. **C)** Thermanox coverslip mounted onto the resin block positioning the recorded neuron in the middle (square). **D)** Resin block after separating the thermanox coverslip with liquid  $N_2$ . The recorded neuron is contained on the resin block ready to be processed.

## 6.4 Sample processing for serial EM

EM samples were cut into serial ultra-thin slices (70 nm) with an ultramicrotome and stained with uranyl acetate and lead citrate to increase the level of contrast in the final image (in collaboration with the EMBL, Heidelberg). Sections of recorded neurons were viewed under a JEOL 1010 electron microscope (UB, Barcelona).

## 6.5 Segmentation and 3D modelling

Images obtained from serial TEM were aligned and segmented using TrackEM2 in ImageJ. Modelling was performed by importing the ImageJ segmentation files into the Blender software.



# 7 Photopharmacology

Different photocontrollable molecules have been used during this project to assess the effect of MT depolymerization on synaptic transmission. The combrestatin-derived photoswitchable molecules PST-1, PST-2 (Borowiak et al., 2015), SBTub3 (Gao, Meiring, Kraus, et al., 2021) as well as combrestatin-A4 were kindly provided by Oliver Thorn-Seshold (LMU, Munich).

## 7.1 Photoswitchable molecules

### 7.1.1 Photostatins

PSTs are light-switchable tubulin depolymerisers. They can be used to reversibly switch live cells between states of ordinary and inhibited microtubule polymerisation dynamics, with sub-second temporal and subcellular spatial resolution.

Light illuminations change PSTs between their bioactive *cis* and inactive *trans* isomer states. The PST *cis* state has similar biological effects to known tubulin inhibitors colchicine, combretastatin or nocodazole. The inactive *trans* state does not affect tubulin at all.

Upon reaching a threshold concentration of the *cis* state inside a cell, tubulin polymerisation slows then stops and microtubules start to depolymerise. When the *cis* concentration drops below this threshold, tubulin polymerisation restarts. The threshold is usually reached at an applied extracellular *cis*-concentration of ~150-1000 nM.

Illumination with a given wavelength of light shifts the balance between *cis* and *trans* isoforms towards a “photoequilibrium ratio” that is dictated by the wavelength used. Relatively low light intensities are sufficient, even unfocussed LEDs. Thus, lasers are not required.

Usually, UV and blue wavelengths generate equilibria favouring the bioactive *cis* form; and blue-green and green wavelengths generate equilibria favouring the inactive *trans* form (Table 9). The sensitivity of PSTs to light at 480-520 nm is much lower than its sensitivity at 380-420 nm. Hence, inactivating PST by applying green light may require a substantially longer pulse.

The active *cis* form spontaneously “relaxes” back to the *trans* isoform over time, eventually reaching 100%-*trans*, following first-order kinetics. None of the PSTs can be photoreverted to 100% *trans* with any wavelength of light; spontaneous relaxation is the only process to achieve it.

**Note:** For short-term experiments with normal-relaxing PSTs like PST-1 (<2 h), handling should be done in dark-room conditions for inactive control experiments. For fast-relaxing PSTs like PST-2, typically no light-blocking precautions are needed due to their faster relaxation to the inactive state.

### 7.1.2 SBTubs

SBTubs are photocontrollable colchicine binding site inhibitors, that can inhibit microtubule polymerisation at low micromolar concentrations. SBTub3 is switched on with 360 or 405 nm light/laser to the Z-state but it cannot be switched off to the E-state due to its robust stability (Table 9).

| Key parameters                                       | PST-1     | PST-2     | SBTub3  |
|--|-----------|-----------|---------|
| Wavelength for best % active, nm                     | 385       | 390       | 405     |
| Wavelength for best % inactive, nm                   | 514 (81%) | 514 (85%) | -       |
| Best wavelengths for imaging                         | >550 nm   | >550 nm   | >488 nm |
| Relaxation halflife ("fast/slow")                    | 12 min    | 0.75 min  | -       |
| Cellular toxicity IC <sub>50</sub> of active isoform | 400 nM    | 400 nM    | 1.6 μM  |
| Molecular weight, g/mol                              | 318       | 317       | 283.4   |

**Table 9.** Comparative table of the properties of the photoswitchable molecules used.

#### *Combretastatin A-4*

CA-4 (MW: 316.34 g/mol) was used as a non-photoswitchable positive reference compound (maximum bioactivity level) of microtubule depolymerization to compare its effect with the performance of its photoswitchable derivatives in our culture system.

## 7.2 Handling and storage

PST-1, PST-2 and SBTub3 were provided as powder and diluted in DMSO to a final concentration of 10 mM and stored in the dark at 4°C.

**Note:** For photostatins, stepwise dilutions into buffer (for example 3 steps) are recommended, since PSTs can precipitate if their cosolvent is changed too rapidly.

## 7.3 Experimental protocol and conditions

### 7.3.1 Incubation

SCMs were incubated with MT polymerization inhibitors for 12 min in the dark at the indicated concentrations. Dilution of 10 mM DMSO stocks in external solution were performed in 4 steps, reassuring it was properly dissolved. Abundant wash for 2 min was performed to make sure all cells had been exposed to the same amount of the compound and reduce variability among experiments.

### 7.3.2 Experimental protocol

Evoked (paired-pulse stimulation spaced 100 ms, every 30 s) and spontaneous neurotransmission (30 s periods) were assessed in basal conditions (dark) and after illumination. Light protocols for each experiment are indicated.

### 7.3.3 Illumination set up

Photoactivation was performed in an inverted Olympus IX-50 microscope using a Hg arc lamp (100 W) as light source through an air 60X objective (LCPlanFI 60X/0.7, Olympus, Tokyo, Japan). Neurons were exposed to near-UV 410 nm light (excitation filter ET410/40, Chroma Technology Corp., VT) or green 535 nm light (Fig. 54; excitation filter ET535/50, Chroma Technology Corp., VT). The timing of illumination was controlled by TTL pulses generated by mafPC adjusted via a shutter (Uniblitz, NY). To reduce light intensity that may cause phototoxicity, neutral density (ND) filters 0.4 (XB195, Omega Optical LLC, Brattleboro, VT) and ND 0.6 (XB196, Omega Optical LLC, Brattleboro, VT) were used.

Experiments were always performed under green transmission light (excitation filter ET545/25, Chroma Technology Corp., VT) to avoid photoactivation during basal conditions.

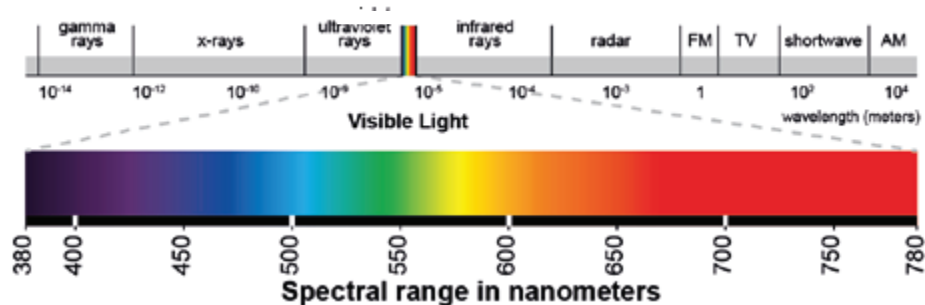


**Figure 54. Visible light spectrum.** Spectral range of light wavelengths in nanometers. Excitation filters that only allow the pass of a specific light wavelength (or wavelength range) were used to illuminate photoswitchable molecules and control their bioactivity: 410 nm light (switch on) and 535 nm light (switch off). (Image extracted from Eye Hortilux website).

# 8 Statistics and reproducibility

Control experiments were carried out for each culture, considering a culture as a group of SCMs established from a litter of rat pups. The neurons of a given culture were distributed between two or more different experimental protocols.

Experimental groups used for evaluating statistical differences passed the Kolmogorov-Smirnov normality test. Data from averages were always expressed as mean  $\pm$  s.e.m. Comparisons between two groups were established using unpaired two-tailed Student's t-test. When comparing more than two groups one-way ANOVA followed by Bonferroni multiple comparison test was applied. Differences as a function of time within one experimental group were evaluated using one-way ANOVA repeated measures followed by Dunnett's comparison test.

The number of independent observations, as well as the type of statistical test applied and the degree of significance, are indicated in the figures.



# RESULTS





# 1 Characterization of the capability of SPARC to eliminate synapses in an autaptic circuit

A previous study from our group had shown that the active SPARC-derived peptide p4.2 (20 amino acid peptide from the EC domain) activates a cell-autonomous program of synapse elimination in cholinergic single cell microcultures (López-Murcia et al., 2015). In that study, autaptic neurons established from superior cervical ganglia cultured in the absence of glial cells were acutely exposed to 200 nM p4.2 for 2-5 hours, which resulted in decreases of synaptic strength and synapse numbers together with increases in the formation of secondary lysosomes and multivesicular bodies observed by electron microscopy. Interestingly, only ~30 % of synapses were disassembled.

To investigate whether p4.2 could eliminate all synapses present in an autaptic circuit or if there were synapses resistant to the effect of p4.2, incubation time with 200 nM p4.2 was prolonged up to 30h. Synaptic strength was assessed for different time periods in the form of excitatory postsynaptic currents (Fig. 55). Given that the SPARC-derived peptide p2.1 (20 amino acid peptide from the FS-domain) did not show any effect in neurons (López-Murcia et al., 2015), it was used as a negative control.

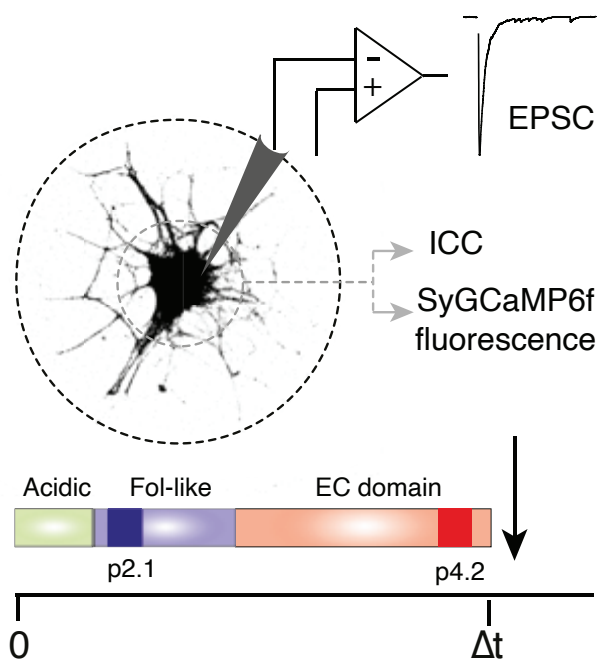


**Figure 55. Experimental setup to investigate the ability of p4.2 to promote synapse loss.** Single Cell Microcultures (SCMs) were incubated with 200 nM of p4.2, a 20 amino acid peptide derived from the SPARC EC-domain which induces a cell-autonomous mechanism of synapse elimination. The 20 amino acid peptide p2.1 derived from the follistatin-like domain of SPARC was used as a negative control. Neurons were exposed to either p4.2 or p2.1 during different time periods up to 30 h. Evoked excitatory postsynaptic currents (EPSCs) were recorded from SCMs using voltage clamp (patch clamp, whole cell configuration) to assess synaptic strength relative to immunocytochemistry (ICC) or imaging of presynaptic calcium influx using the reporter SyGCaMP6f.

## 1.1 Time course of the effect of peptide p4.2 in synaptic strength and neuronal excitability

Results confirmed previous observations demonstrating that SPARC reduces synaptic strength after 5 h of incubation with p4.2. However, after 30 h of exposure, neither a stabilization at a steady-state phase, nor a total elimination of synaptic transmission were observed. Instead, postsynaptic evoked responses showed an exponential decay that reached its minimum value after 15 h of p4.2 exposure, and that was followed by a compensatory increase within ~30 h of p4.2 incubation (Fig. 56A and B). This biphasic change of synaptic strength induced by p4.2 was well described by a parabolic fit. After the recovery phase, EPSCs amplitude was brought back to initial levels, suggesting the activation of a homeostatic compensatory mechanism in response to synapse elimination. In contrast, treatment with 200 nM peptide p2.1, did not modify EPSC amplitude at any of the incubation times.

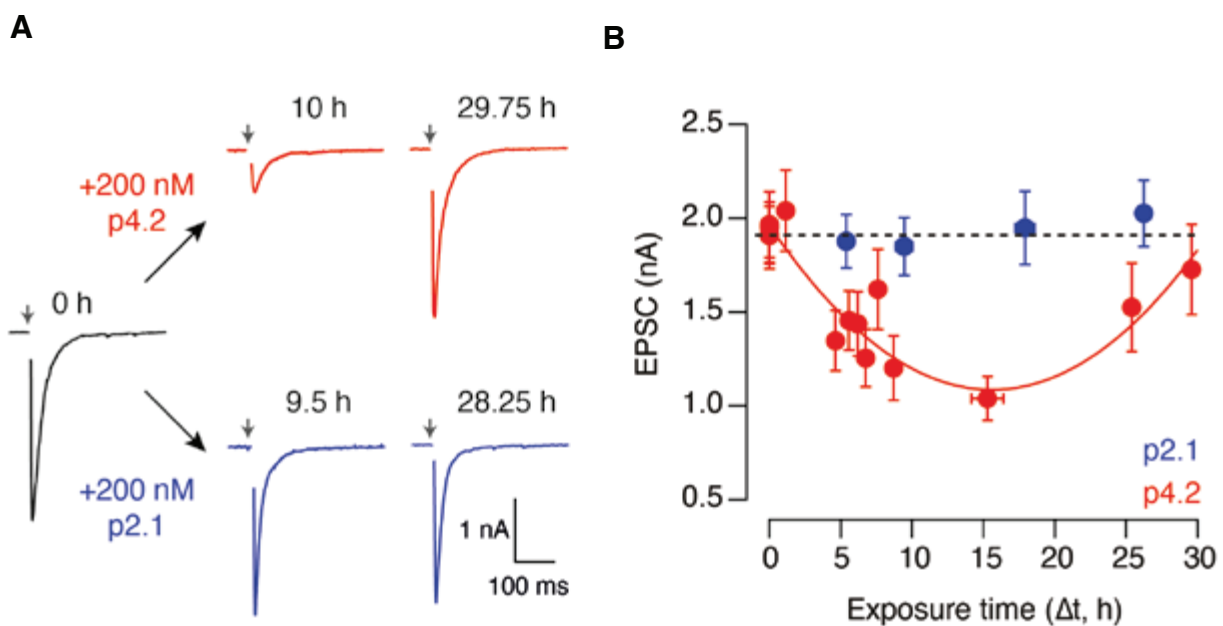


**Figure 56. Peptide p4.2 produces a biphasic change in synaptic strength.** **A)** Single cell microcultures (SCMs) were exposed to either 200 nM p4.2 or p2.1 for different time periods and synaptic strength was evaluated in the form of excitatory postsynaptic currents (EPSCs). Arrows mark the moment of the stimulus. **B)** Parabolic fit,  $EPSC(t)=3.49t^2-109.4t+1960$ , shows changes in EPSC amplitude (pA) as a function of 200 nM p4.2 exposure. Maximum EPSC amplitude decay occurred after 15.4 h of p4.2 exposure. Longer incubation times up to 30 h displayed a compensatory response that brought EPSC values to basal levels. Each bin shows the average EPSC amplitude of 10 autaptic neurons. Error bars show s.e.m. ( $n = 280$  SCMs, 50 different cultures). Exposure to p2.1 ( $n = 72$  SCMs, 9 different cultures) did not modify basal synaptic strength (dotted line). Each bin indicates the average EPSC amplitude of 18 neurons. Error bars indicate s.e.m.

EPSCs in an autaptic neuron display the summation of postsynaptic responses from all autapses in the circuit. Hence, changes in synaptic strength can be used to estimate the number of functional autapses in the neuronal network.

However, to rule out the possibility that changes in neurotransmission observed during p4.2 incubation could be related to variations in neuronal excitability rather than synapse numbers, current clamp experiments were performed to evoke APs in control neurons and in neurons exposed to p4.2 for 16h. Current injections required to trigger an AP were comparable between the two conditions, indicating that decreases in synaptic strength produced by p4.2 were not caused by changes in neuronal excitability but were the result of synapse loss (Fig. 57).

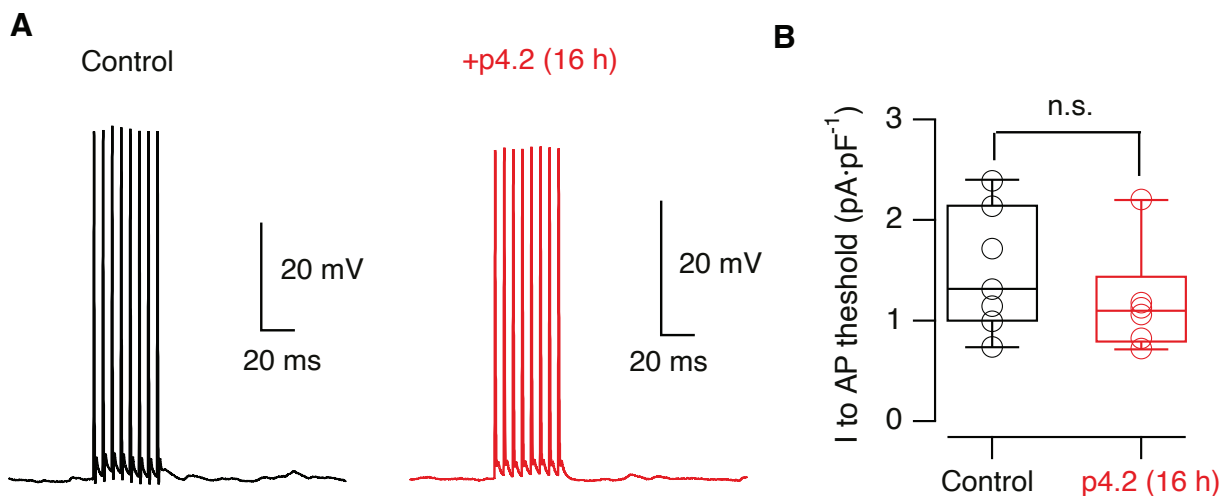


**Figure 57. Exposure to p4.2 does not alter neuronal excitability.** **A)** Examples of action potentials evoked by a train of 8 stimuli at 200 Hz in a control neuron (black) and in a neuron incubated with 200 nM p4.2 for 16 h (red). **B)** The amount of current required to elicit an action potential was comparable between control neurons ( $n = 7$ ) and neurons treated with p4.2 for 16 h ( $n = 6$ ,  $p=0.35$ ). Box plots show the median (horizontal line), 25 to 75% quartiles (boxes), and ranges (whiskers). Experimental groups were compared using the unpaired Student's t-test.

## 1.2 Characterization of synapse markers to evaluate changes in synapse numbers

The previous study from our group demonstrating the ability of p4.2 to elicit a cell-autonomous program of synapse elimination showed that decreases of synaptic strength were accompanied by the reduction of synapse numbers assessed by immunocytochemistry using the presynaptic marker bassoon (López-Murcia et al., 2015).

To further evaluate whether bassoon puncta truly reflect presynapses, and therefore can be used to estimate changes in synapse numbers triggered by p4.2, we performed colocalization assays of bassoon with additional synapse markers (Fig. 58).

As postsynaptic markers, we used the fluorescent antagonist of  $\alpha 7$  nicotinic acetyl-

choline receptors (nAChR),  $\alpha$ -bungarotoxin-Alexa 555, and also assessed antibodies against the  $\alpha$ 3 nAChR and the postsynaptic density protein PSD93. As presynaptic markers, we tested primary polyclonal antibodies against the active zone proteins piccolo and Munc13-1, the v-SNARE VAMP-2, and the presynaptic cytoplasmic protein synapsin-I. In addition, staining of N-cadherin, a synaptic adhesion protein present both pre- and postsynaptically was also evaluated. Markers displaying non-specific staining were discarded. Only those markers showing a punctate pattern of  $\sim 1 \mu\text{m}$  of diameter that spanned throughout 2-3 stacks were evaluated for colocalization with bassoon.

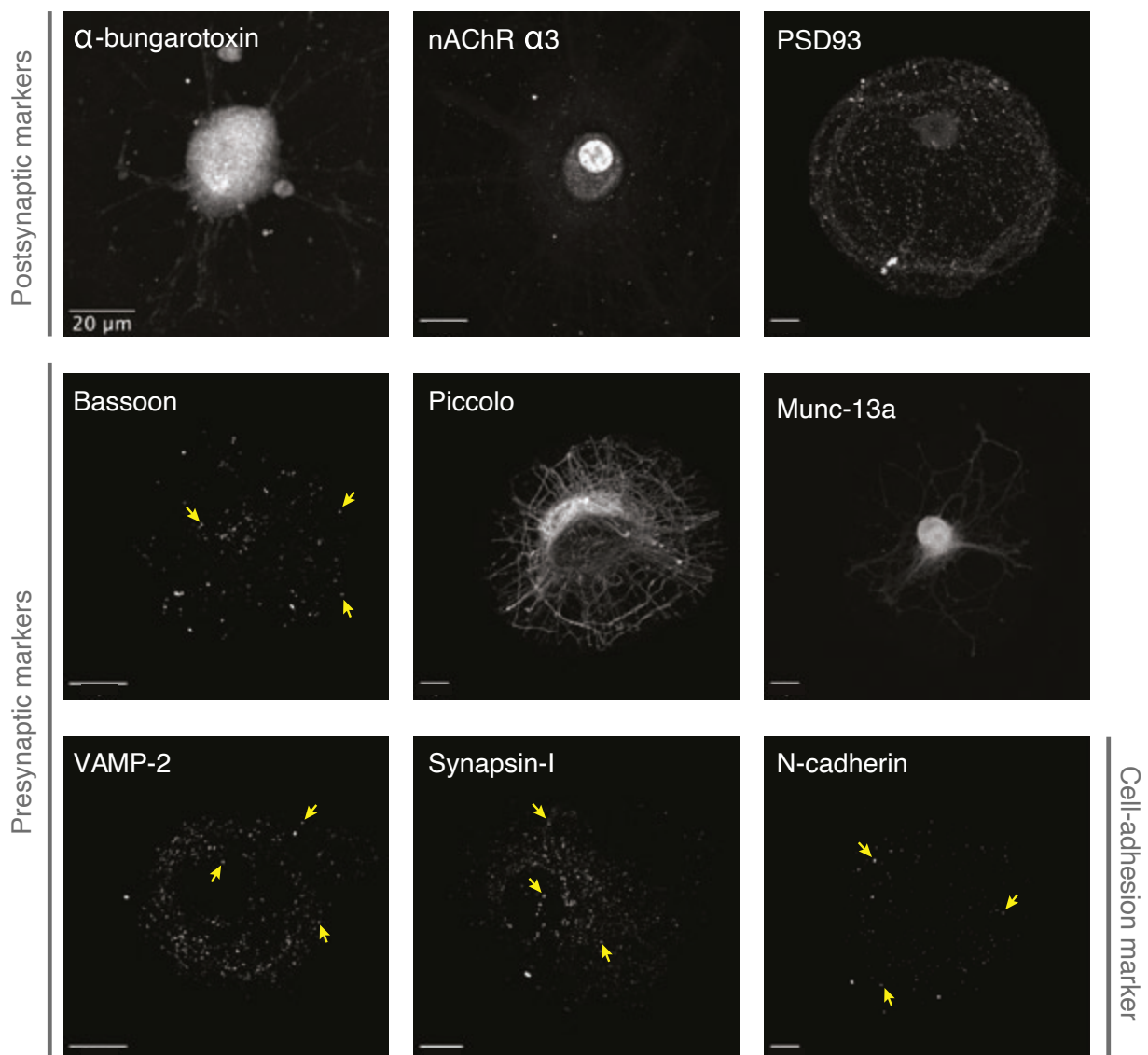
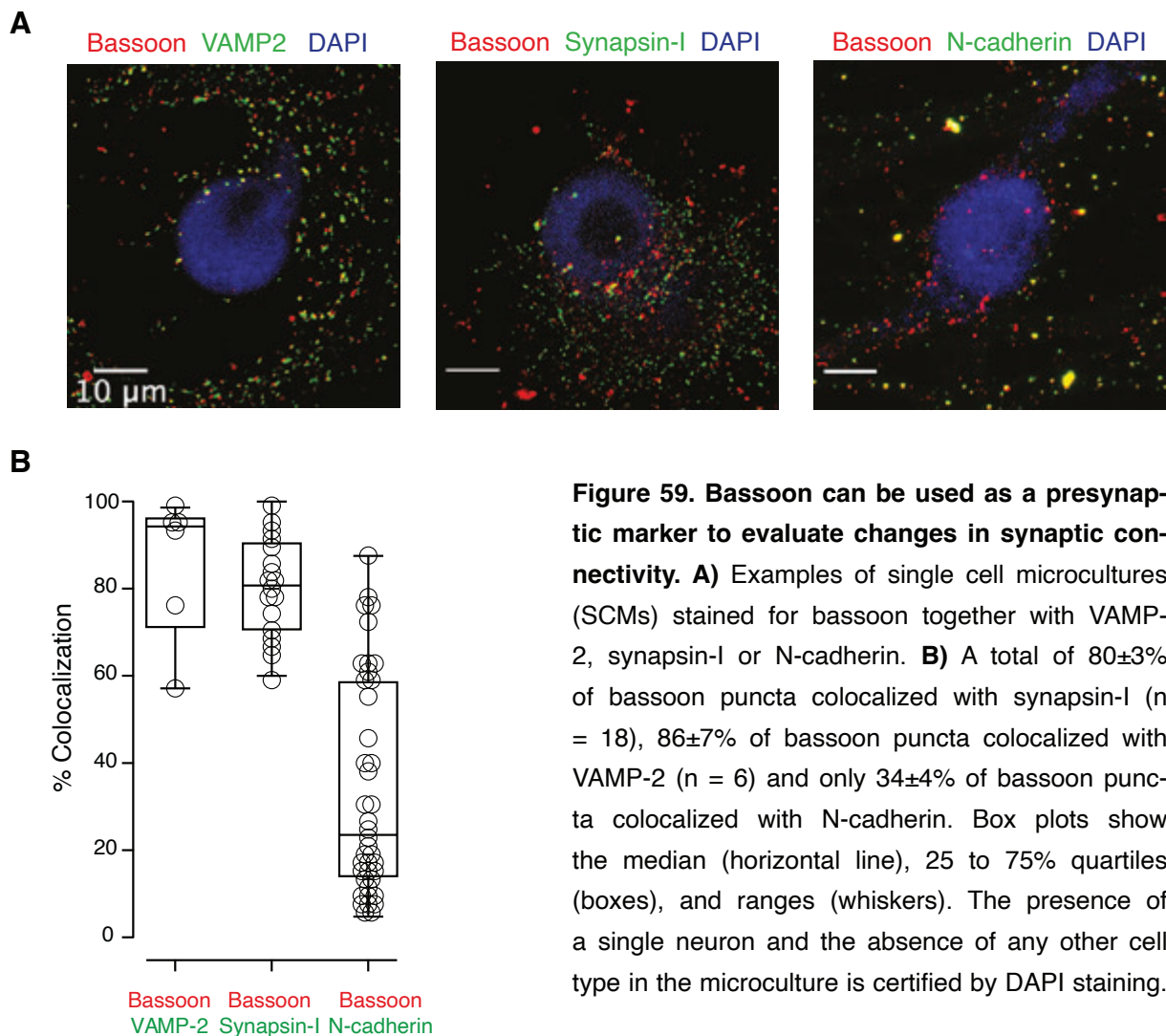


**Figure 58. Characterization of synaptic markers.** Representative examples of microcultures stained with different synaptic markers. None of the postsynaptic markers,  $\alpha$ -bungarotoxin-555,  $\alpha$ 3 acetylcholine receptors and PSD93, met the requirements for being considered good synaptic markers given their unspecificity. As for presynaptic markers, piccolo and Munc-13a showed unspecific labelling, but bassoon, VAMP-2 and synapsin-I displayed a punctate pattern that spanned throughout 2-3 stacks ( $z = \sim 350 \text{ nm}$ ). The cell adhesion protein N-cadherin also showed a characteristic synaptic punctate pattern. Yellow arrows point to putative synapses.

We did not manage to get good co-staining with any of the postsynaptic markers tested. Labelling of acetylcholine receptors with  $\alpha$ -bungarotoxin was unsuccessful because acetylcholine receptors in autonomic ganglia contain a combination of  $\alpha 3$  and  $\alpha 4$  subunits but lack  $\alpha 7$  subunits. We next tested a polyclonal antibody against  $\alpha 3$  subunits to combine it with the anti-bassoon monoclonal antibody used for staining. Labelling was completely unspecific. As an alternative we tested a polyclonal antibody against PSD-93, and again, staining was unsuccessful.

Although staining with the presynaptic active zone markers piccolo and Munc13-1 was not specific, VAMP-2, synapsin-I and N-cadherin staining met the requirements for being considered good synaptic markers.

Next, we performed colocalization assays of bassoon with VAMP-2, synapsin-I and N-cadherin (Fig. 59A). Above 80% of bassoon puncta were colocalized with VAMP-2 and synapsin-I, reinforcing the identity of bassoon puncta as synapses. Although N-cadherin also showed a punctate pattern, only 34% of bassoon staining colocalized with N-cadherin, suggesting the labelling of different structures (Fig. 59B).





To further explore the relationship between synapse markers and synaptic strength, correlative electrophysiology and immunocytochemistry experiments were performed (Fig. 60A). Recorded SCMs were fixed and stained for the previously characterized presynaptic marker bassoon and the adhesion protein N-cadherin, which was used as a control marker.

Due to the cable-filtering properties of dendrites, the contribution of each synapse to recorded EPSCs diminishes as a function of the distance between the synapse and the cell body where the electrode is. That results in attenuation of postsynaptic responses from axodendritic contacts distally located. Therefore, only puncta located in the cell body and nearby dendritic tree (<20  $\mu\text{m}$  away from the soma) were considered.

In control neurons, the number of bassoon puncta was linearly related to synaptic strength (Fig. 60B), indicating each putative synaptic contact contributed with 59 pA to the recorded EPSC (slope). Considering a release probability of 0.8, quantal size would be of approximately 70 pA, which is in line with previous observations ( $\text{EPSC} = N \times Pr \times q$ ; Perez-Gonzalez et al., 2008). Puncta identified by N-cadherin labelling, however, were not linearly related to EPSC amplitude, suggesting N-cadherin to be dispensable for mature cholinergic synapses and to be expressed in non-synaptic structures and/or immature contacts.

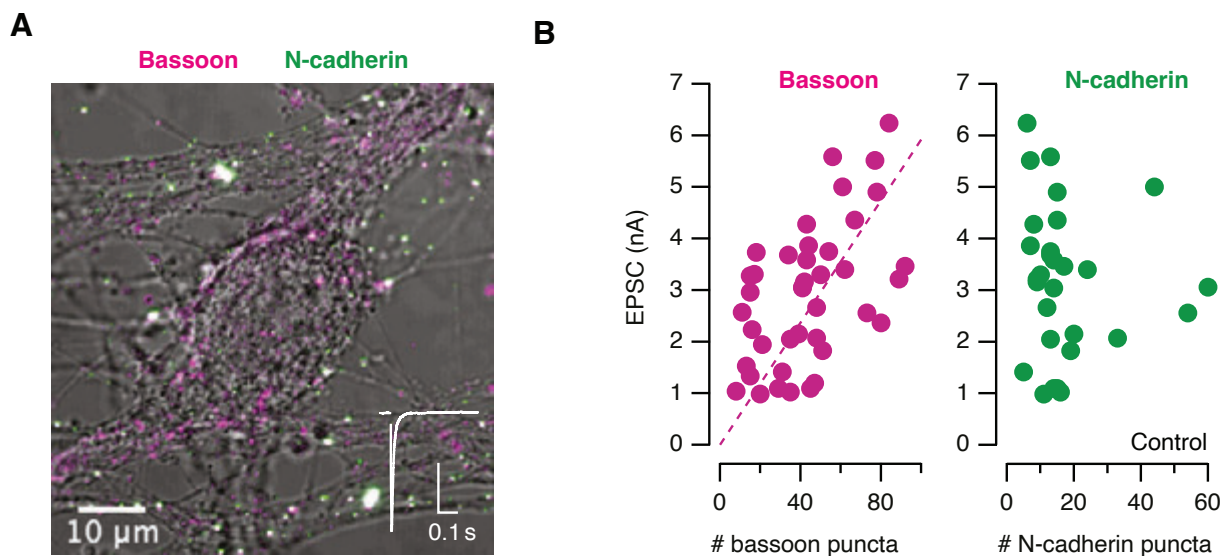


**Figure 60. Bassoon puncta are linearly related to synaptic strength.** **A)** Correlative electrophysiology and immunocytochemistry experiments were used to evaluate the relationship between the number of putative synapses and synaptic transmission. Image of the somatic and perisomatic region (soma +20  $\mu\text{m}$  radius) of an autaptic neuron stained for bassoon (magenta) and N-cadherin (green). The bassoon puncta found within the imaged area were considered putative synapses contributing to the recorded evoked response (white trace). **B)** Plots showing the relationship between excitatory postsynaptic currents (EPSCs) and the number of bassoon and N-cadherin puncta in control single cell microcultures (SCMs;  $n = 41$ ). Only bassoon puncta were linearly related to synaptic strength ( $59 \text{ pA} \cdot \text{bassoon puncta}^{-1}$ , Pearson correlation coefficient=0.54).

### 1.3 Evaluation of changes in synaptic connectivity during exposure to p4.2

Next, we evaluated changes in synapse numbers in microcultures exposed to p4.2 for distinct time intervals. In parallel to changes in synaptic strength, exposure of neurons to 200 nM p4.2 also produced a biphasic change in the density of bassoon puncta, indicating that synapse elimination was followed by rapid synapse formation to compensate synapse loss (Fig. 61A and B). According to parabolic fits, minimum values of EPSC amplitude and bassoon puncta density were reached upon 12.4 and 15 h of p4.2 exposure, respectively. Changes in synaptic strength occurred before changes in synapse numbers, revealing that compensatory synapse formation took place in a time window of ~2.5 h.

However, while synaptic strength was fully recovered after the compensatory phase, original levels of bassoon puncta density were not, suggesting the involvement of other contributors to the synaptic homeostatic response (Fig. 61B).

The slope of the linear relationship found between EPSC amplitude and the number of bassoon puncta after 24 h of p4.2 exposure showed that each synapse contributed with 72 pA to neurotransmission, a 25% more than in control conditions (Fig. 61C). These data suggested that synapses resistant to elimination had been potentiated. N-cadherin continued being unrelated to synaptic strength after treatment with p4.2. Collectively, these data indicate that in an autaptic circuit, synapse elimination triggered by p4.2 is compensated by a coordinated homeostatic response involving: i) rapid *de novo* synapse formation and ii) synapse potentiation.



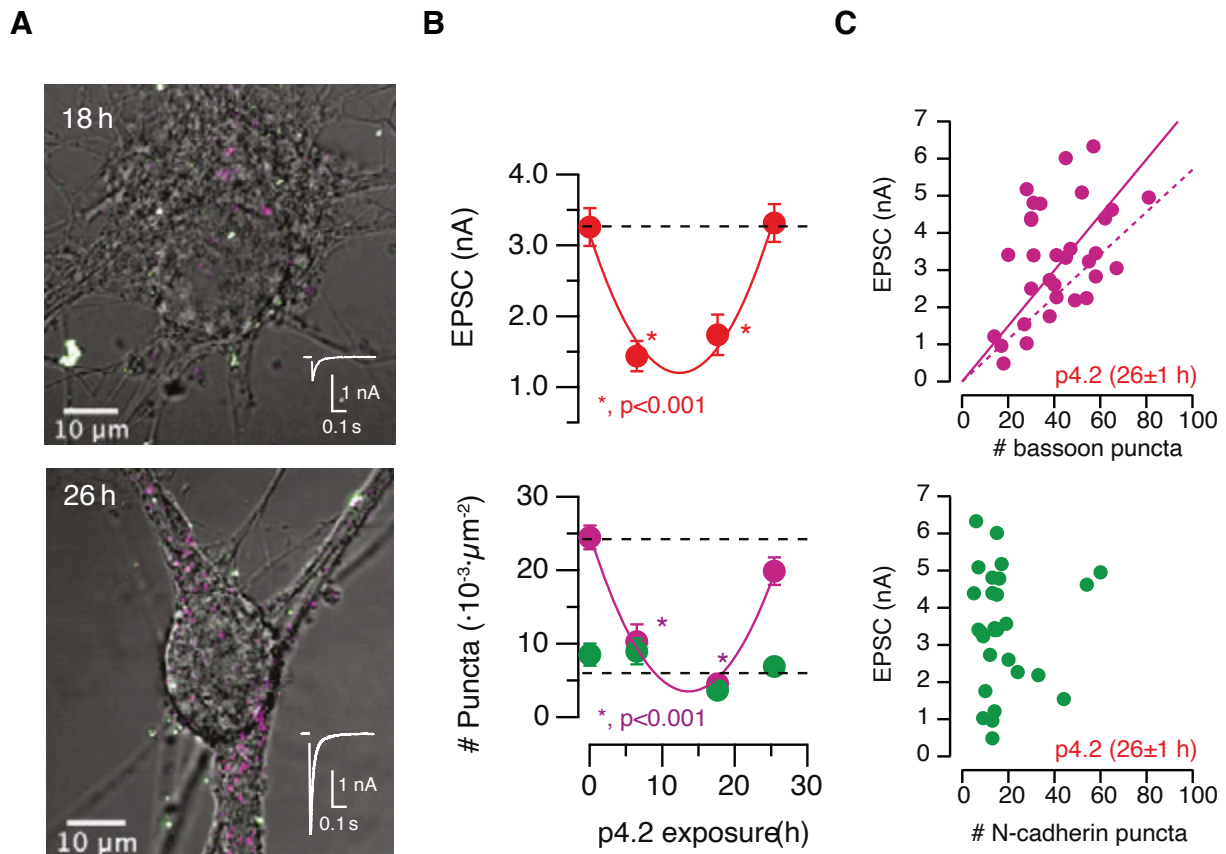


**Figure 61. Rapid synapse formation compensates synapse loss triggered by p4.2. A)** Images of the somatic and perisomatic region (soma +20  $\mu\text{m}$  radius) of two single cell microcultures (SCMs) exposed to p4.2 for 18 and 26 h, respectively. Associated excitatory postsynaptic currents (EPSCs) are displayed (white traces). **B)** Time course of the effect of p4.2 on evoked postsynaptic responses (up) and on the density of bassoon and N-cadherin puncta (down) of SCMs. Dots indicate mean  $\pm$  s.e.m. Experimental groups: 0 h p4.2 (control),  $n = 28$ ; 6 h p4.2,  $n = 19$ ; 17.6 h p4.2,  $n = 18$ ; 26 h p4.2,  $n = 33$ . Synaptic strength (expressed in pA) and the density of bassoon puncta were both related to p4.2 exposure time by two parabolic functions ( $\text{EPSC}(t) = 13t^2 - 317t + 3162$ ,  $\text{Puncta}(t) = 0.11t^2 - 3.14t + 25$ ). Minimum values were observed at 12.4 and 15 h in EPSCs and density of bassoon puncta parabolic fits, respectively. Asterisks indicate significant differences relative to control values using one-way ANOVA followed by Bonferroni multiple comparisons test. **C)** EPSC amplitude of neurons exposed to p4.2 for an average of 26 h was linearly related to the number of bassoon puncta identified by immunocytochemistry (solid line;  $n = 33$ ,  $72 \text{ pA} \cdot \text{bassoon puncta}^{-1}$ , Pearson correlation coefficient=0.45). For comparison purposes, dotted line indicates the relationship obtained in control conditions (Fig. 60). The number of N-cadherin puncta was not related to synaptic strength in SCMs exposed to p4.2 for 26 h ( $n = 33$ ).

To characterize the nature of the newly formed synapses in response to synapse elimination, we investigated short-term plasticity of autaptic cultures exposed to p4.2. According to the simple depletion model (Betz, 1970; Zucker & Regehr, 2002), depression between paired pulse (PP) stimuli occurs when most vesicles available for release are depleted during the first evoked stimulus. Thus, the lower is the number of vesicles

available for release in the second stimulus, the higher is the depression. Although paired pulse depression at 50 ms interval was not modified during the synapse elimination phase, it increased by ~25% in SCMs treated for >24 h with p4.2 (Fig. 62A and B). Generally, immature synapses contain a lower number of synaptic vesicles and tend to display short-term depression. Hence, enhanced synaptic depression could be explained by the participation of newly formed synaptic contacts.

Another possibility is that the compensatory response involved increases in neurotransmitter release probability, for example by enhancing presynaptic calcium influx, and led to greater short-term depression.

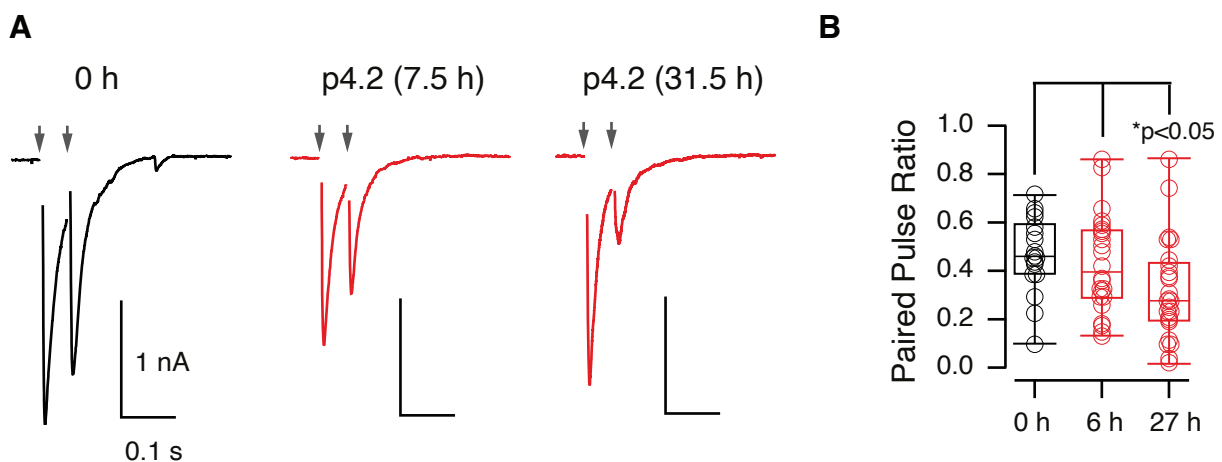


**Figure 62. Short-term depression is enhanced at the end of the compensatory response of neurons exposed to p4.2.** **A)** Paired pulse plasticity was assayed by delivering two pulses at a time interval of 50 ms in control conditions or in neurons treated with p4.2. Arrows mark the moment of the stimulus. **B)** Box plot of the paired pulse ratio in neurons exposed to p4.2 for the time periods indicated. Synaptic depression was increased at the end of the recovery phase. Box plot shows the median (horizontal line), 25–75% quartiles (boxes), and ranges (whiskers) of the paired pulse ratio obtained in control neurons ( $n = 18$ ), neurons exposed to p4.2 for  $6.4 \pm 1$  h (mean  $\pm$  s.e.m.,  $n = 26$ ) and neurons exposed to p4.2 for  $27 \pm 1$  h (mean  $\pm$  s.e.m.,  $n = 25$ ). Statistical differences were evaluated using one-way ANOVA followed by Bonferroni multiple comparisons test.

## 2 Compensation of synapse elimination by a mechanism of homeostatic synaptic plasticity

It is well described that homeostatic plasticity mechanisms activate to compensate changes in synaptic transmission. Specifically, PHP is characterized by increases in the availability of vesicles ready to be released (RRP size) and augmentation of presynaptic calcium entry that in turn increases neurotransmitter release probability. Next, we attempted to explore whether the synaptic potentiation observed after synapse elimination triggered by p4.2 was due to the activation of a PHP mechanism.

### 2.1 Changes in RRP size as part of the presynaptic homeostatic response

We started by evaluating changes in RRP size using high frequency stimulation in neurons exposed to p4.2 (Fig. 63A). Similar to the density of bassoon puncta, RRP size also experimented a biphasic change, reaching the minimum value after 16 h of p4.2 exposure that was not completely restored to basal levels (Fig. 63B). These data indicate that the number of vesicles available for immediate release had been increased in response to synapse elimination.

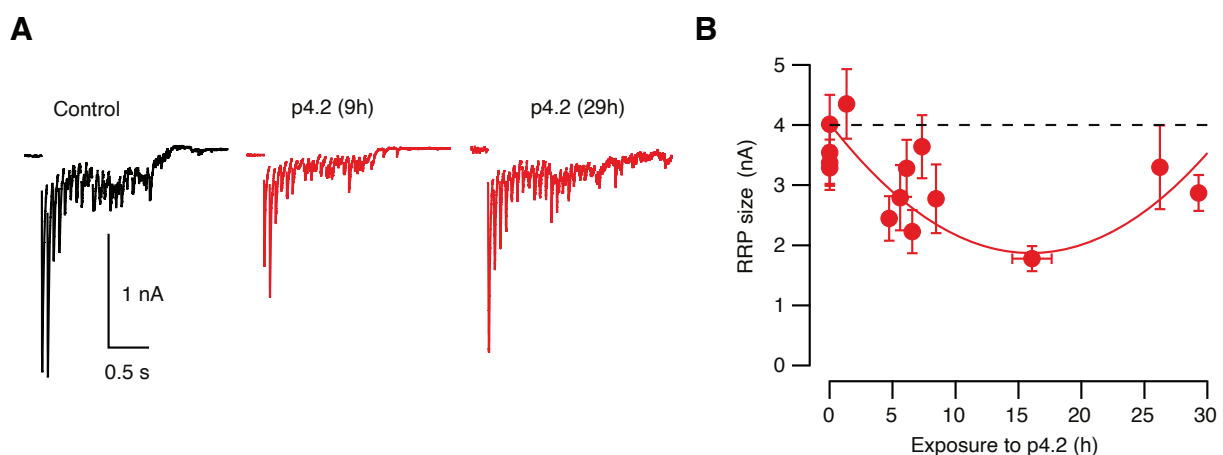


**Figure 63. The synaptic homeostatic response activated by synapse elimination involves changes in the size of the RRP. A)** Trains of 20 stimuli delivered at 14 Hz were used to calculate the size of the readily releasable pool (RRP). **B)** Changes in RRP size in neurons exposed to p4.2 during different times were biphasic and were described by a parabolic function, expressed in pA ( $RRP(t) = 8.5t^2 - 270t + 4028$ ). The minimum value was found after 16 h of p4.2 exposure ( $n = 224$ , each bin shows the mean  $\pm$  s.e.m. of 16 neurons).

## 2.2 Characterization of presynaptic calcium influx responses in individual autaptic contacts using the SyGCaMP6f reporter

To further investigate the hypothesis involving the activation of a PHP mechanism in response to synapse elimination, we measured evoked presynaptic calcium entry. To do that, EPSCs were recorded concomitantly with imaging of presynaptic calcium influx using the calcium reporter synaptophysin-GCaMP6f.

The indicator accumulated in discrete puncta and increases in fluorescence were observed after application of a train of five stimuli delivered at 20 Hz (Fig. 64A). Acute application of 1  $\mu$ M TTX abolished both, evoked postsynaptic currents and calcium responses, confirming the identity of putative synaptic contacts identified with SyGCaMP6f (Fig. 64B).

Measurement of  $\Delta F/F_0$  changes in SyGCaMP6f puncta showed a distribution of presynaptic calcium increases that was well described by three gaussian functions with mean  $\pm$  SD  $\Delta F/F_0$  changes of  $0.022 \pm 0.01$ ,  $0.100 \pm 0.05$  and  $0.277 \pm 0.02$ , respectively. These three populations of autapses were considered to represent terminals of low, medium, and high calcium influx, respectively (Fig. 64C).

To investigate whether the opening probability of calcium channels in a specific synapse could fluctuate, or if in contrast, it was an inherent property of each synapse, we evaluated the variability of SyGCaMP6f responses to a single stimulus. Since it was not possible to resolve low fluorescence increases after a single stimulus, only synapses showing medium and high presynaptic calcium influx were analyzed. Large variability was found in evoked postsynaptic responses (CV= 20%, n=3 SCMs) compared to that found in the amplitude of detected SyGCaMP6f transients, which was fairly stable (CV=8%, n= 3 SCMs). These results validated the presence of three different populations of synapses and indicated that the reliable opening of voltage gated calcium channels is independent to variations in neurotransmitter release probability (Fig. 64D).

## 2.3 Changes in presynaptic calcium influx as part of the presynaptic homeostatic response

SCMs infected with lentiviruses to express the reporter SyGCaMP6f were incubated with 200 nM p4.2 up to 20 h. The biphasic change in synaptic strength was also observed but, it occurred faster than in non-infected neurons (Fig. 56). Maximum decay was found after 9.4 h of p4.2 exposure and original levels of synaptic strength were reached after  $\sim$ 18 h (Fig. 65A). The higher concentrations of CNTF applied in infected SCMs to facilitate maximal synapse formation could account for differences in the kinetics of the homeostatic response (see [Materials & Methods](#) for details).

Exposure of autaptic neurons to p2.1 did not modify EPSC amplitude and neither the

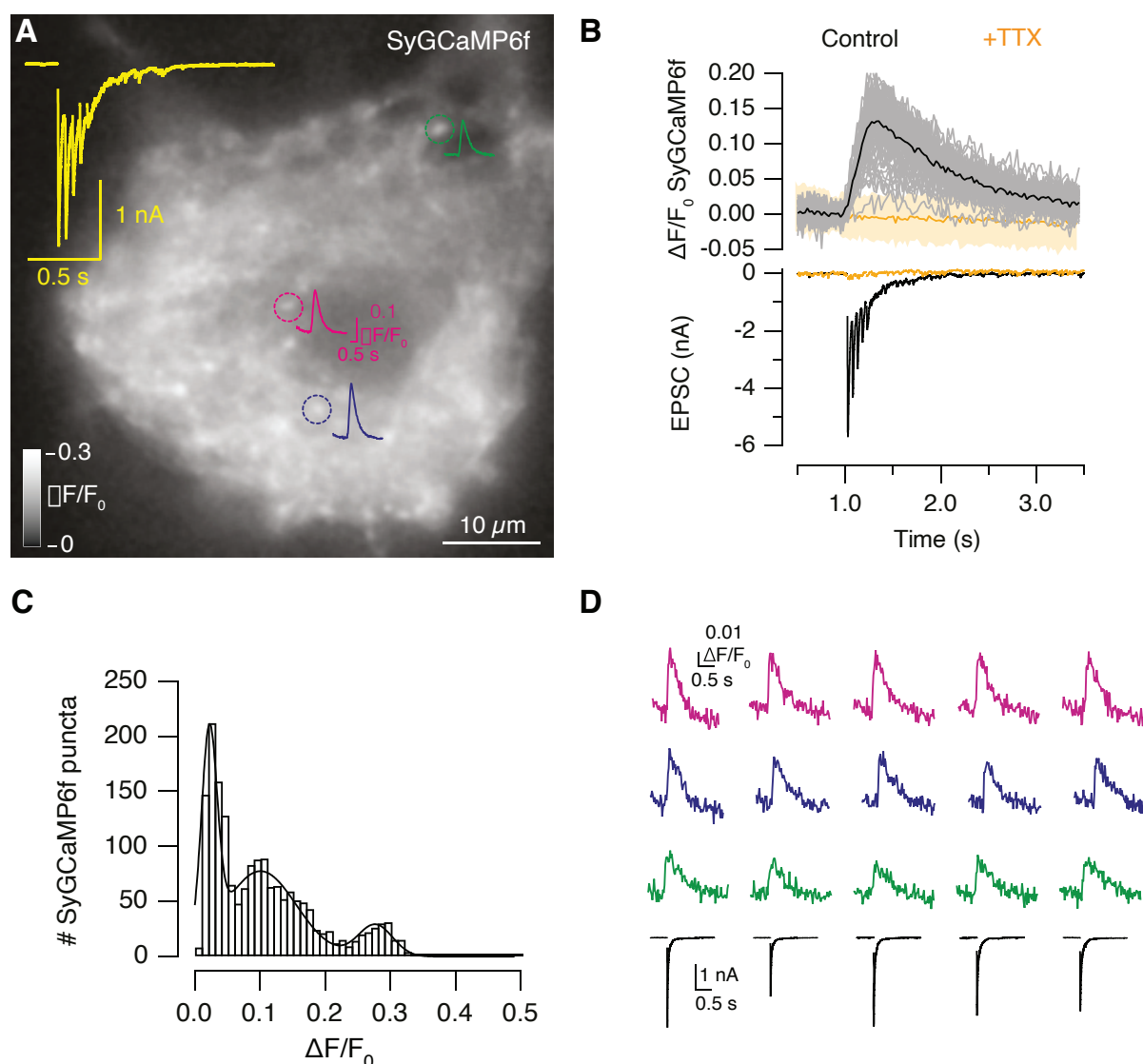


**Figure 64. Characterization of the presynaptic calcium influx reporter SyGCaMP6f.** **A)** Imaging of single cell microcultures (SCMs) infected with lentivirus to express the presynaptic calcium reporter SyGCaMP6f were performed concomitantly with electrophysiological recordings. Representative example showing SyGCaMP6f fluorescence increases in an autaptic neuron. A train of five stimuli was delivered at 20 Hz (yellow trace). The image is the average of 32 frames acquired at 40 Hz during the entire time of the experiment. During stimulation, discrete, round,  $\sim 1 \mu\text{m}$  spots that showed  $\Delta F/F_0$  changes larger than three standard deviations (SDs) of basal  $\Delta F/F_0$  fluorescence were considered functional presynaptic terminals. Dotted circles show the responses of three different functional synapses. **B)** ROIs of synapses displaying increases in SyGCaMP6f fluorescence during stimulation are shown (individual synapses, gray traces; average, black trace) together with its associated evoked response (EPSC, black trace). Acute application of  $1 \mu\text{M}$  TTX suppressed both, postsynaptic currents, and presynaptic calcium influx responses (orange trace, average). Shadowed areas in  $\Delta F/F_0$  SyGCaMP6f responses show three times the SD. **C)** Histogram showing the distribution of peak  $\Delta F/F_0$  SyGCaMP6f changes detected in individual puncta in response to a train of five stimuli ( $n = 1755$  puncta, 27 neurons). Three populations with mean  $\Delta F/F_0$  values of 0.02, 0.1, and 0.28, were identified by a gaussian function. **D)** Five consecutive single depolarizations applied at 0.03 Hz were used to assess variability. Notice that increases in SyGCaMP6f fluorescence remained constant while the amplitude of the associated excitatory postsynaptic currents varied.

probability of finding terminals with low, medium, or high calcium influx (Fig. 65B). Although the amplitude of presynaptic calcium transients in response to a train of five stimuli delivered at 20 Hz did not change after treatment with p4.2 for 6 h (Fig. 65B), it was indeed enhanced during the compensatory phase in response to synapse elimination. An overall increase in presynaptic calcium influx was observed after 19 h of p4.2 exposure (Fig. 65C). The three populations of contacts showing low, medium, and high calcium responses were identified at  $\Delta F/F_0$  changes of mean  $\pm$  SD:  $0.054 \pm 0.02$ ,  $0.177 \pm 0.04$ , and  $0.36 \pm 0.04$ , respectively (Fig. 65D).

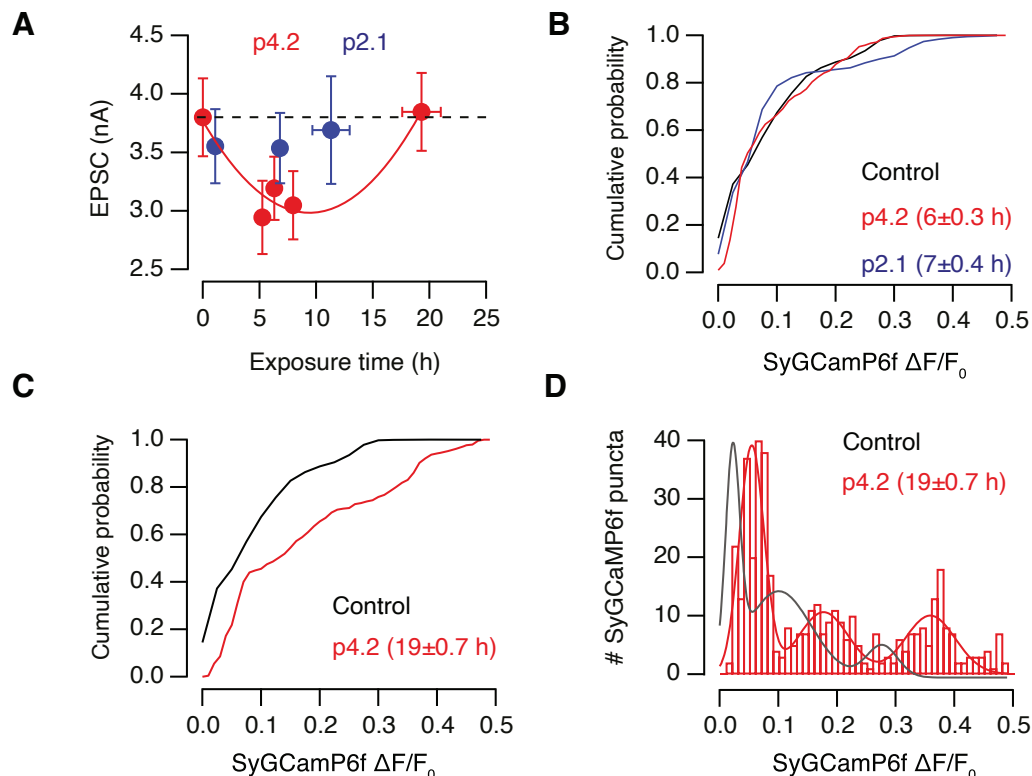


**Figure 65. Exposure to p4.2 causes an increase in presynaptic calcium influx.** **A**) Changes in excitatory postsynaptic currents (EPSCs) during exposure to 200 nM of the peptides p4.2 or p2.1 in neurons infected with lentivirus to express the presynaptic calcium reporter SyGCaMP6f. Single cell microcultures (SCMs) exposed to p4.2 showed a biphasic change in EPSCs amplitude that was well described by a parabolic function (expressed in pA,  $EPSC(t) = 3.6t^2 - 112t + 1961$ ), showing a minimum value at 9.4 h). Bins indicate mean  $\pm$  s.e.m. of 11 SCMs ( $n = 55$ ). Exposure to p2.1 did not modify synaptic strength. Bins indicate mean  $\pm$  s.e.m. of 8 SCMs ( $n = 24$ ). **B**), **C**) Cumulative probability of increases in SyGCaMP6f  $\Delta F/F_0$  found in individual puncta upon application of a train of five stimuli delivered at 20 Hz in neurons exposed to two time intervals of 200 nM p4.2 exposure: **(B)** corresponding to the minimum value of synaptic strength ( $6 \pm 0.3$  h,  $n = 847$ , 20 SCMs) and **(C)** to the end of the compensatory response ( $19 \pm 0.7$  h,  $n = 521$ , 10 SCMs). Time of exposure to p4.2 is indicated as mean  $\pm$  s.e.m. Data obtained in control conditions or in neurons treated with p2.1 for  $7 \pm 0.4$  h ( $n = 647$ ) are also shown for comparison purposes. **D**) Histogram showing the distribution of individual peak  $\Delta F/F_0$  changes obtained upon stimulation with a train of five stimuli delivered at 20 Hz in cells exposed to p4.2 for  $19 \pm 0.7$  h (mean  $\pm$  s.e.m.,  $n = 521$ , 10 SCMs). Three gaussian functions with mean  $\Delta F/F_0$  values of 0.05 and 0.18 and 0.36 were identified. Distribution of control responses (Fig. 64) is shown (gray trace) for comparison purposes.



Increases in presynaptic calcium influx were also assessed by single stimuli. [Figure 66](#) illustrates an example of a neuron exposed to 200 nM p4.2 for 19h that displayed a comparable synaptic strength to a control neuron but showed larger presynaptic calcium influx. On average, the amplitude of presynaptic calcium transients raised from  $3.8 \pm 0.4\%$  ( $n = 13$ ) to  $5.6 \pm 0.4$  (mean  $\pm$  s.e.m.,  $n = 15$ ,  $p = 0.009$ , unpaired t-test) by the end of the compensatory response, indicating a broad potentiation of synapses resistant to the effect of p4.2.

Altogether, these results indicated that in an autaptic circuit, synapse elimination activates a mechanism of presynaptic homeostatic plasticity that is driven by increases in RRP size and gain of presynaptic calcium entry.

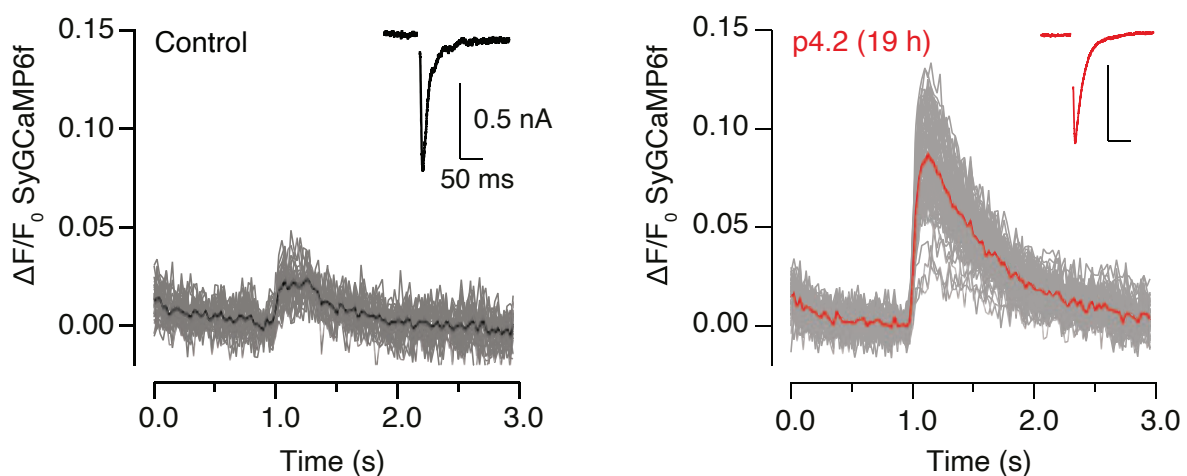


**Figure 66. Illustrative examples of SyGCaMP6f responses.** Left, control neuron (average response is shown in black). Right, neuron exposed to 200 nM for 19 h, at the end of the compensatory response to synapse loss (average response is shown in red). Notice how both neurons display comparable synaptic strength (inlets).

## 2.4 Study of the effect of peptide p4.2 on the density of cholinergic postsynaptic receptors

To study whether the compensatory increase in synaptic strength had also a postsynaptic component, we evaluated the contribution of cholinergic receptors to synaptic transmission. To do that, electrical stimulation was followed by chemical stimulation achieved by applying a local puff of 50  $\mu$ M acetylcholine ([Fig. 67A](#)). While electrical stimulation of neurons incubated with p4.2 up to 30 h showed a biphasic change in EPSC amplitude, the response to chemical stimulation was maintained throughout the period investigated. These data suggest that synapse elimination driven by p4.2 only induced the disassembly of the presynaptic terminal without altering the density of postsynaptic receptors ([Fig. 67B](#)). Exposure to peptide p2.1 did not modify the response to chemical nor electrical stimulation ([Fig. 67C](#)).



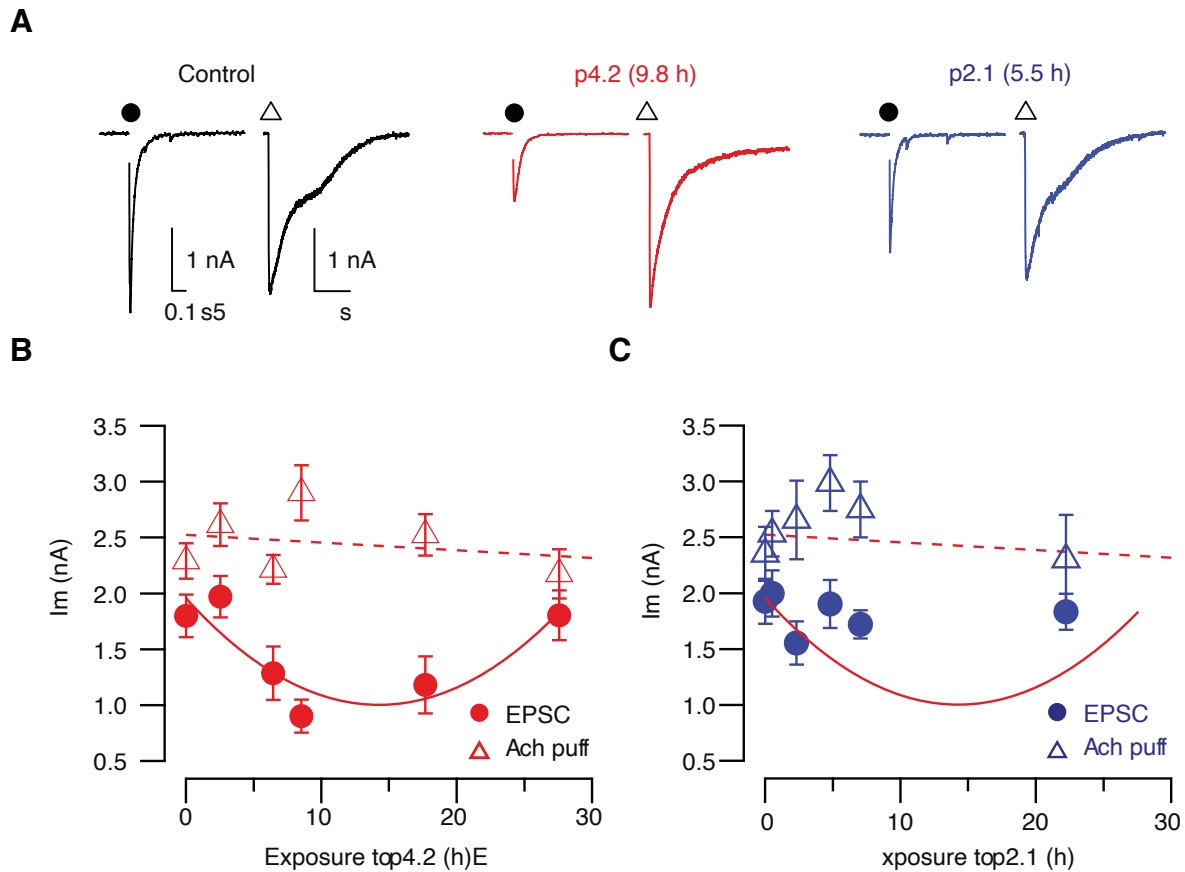


**Figure 67. Evaluation of the pre- and postsynaptic components to the action of p4.2. A)** Examples of characteristic responses obtained during sequential stimulation of single cell microcultures (SCMs) by depolarization (dot) or by addition of a local puff of 50  $\mu$ M acetylcholine (triangle) in control conditions (black) or in neurons exposed to p4.2 (red) or p2.1 (blue). Time interval between electrical and chemical stimulation was 1 min. **B)** Changes in postsynaptic responses elicited by electrical (EPSC) or chemical stimulation (Ach Puff) as a function of p4.2 time of exposure. While excitatory postsynaptic currents (EPSCs) decayed following a parabolic fit (solid line), responses to acetylcholine remained unaffected (dotted line). Each bin indicates the mean  $\pm$  s.e.m of 10 different neurons ( $n = 60$ ). **C)** Neither electrical nor chemical responses were altered in autaptic neurons upon incubation with 200 nM p2.1. Each bin shows the mean  $\pm$  s.e.m of 8 different SCMs ( $n = 48$ ). Red solid and dotted lines from **B)** are shown for comparison purposes.

Since local puffs of acetylcholine applied to SCMs activate both synaptic and extrasynaptic nicotinic receptors, next we assessed postsynaptic function by analyzing quantal size. Amplitude of mEPSCs remained unchanged in neurons exposed to p4.2 for different time intervals (Fig. 68A and B). An average quantal size of  $\sim 70$  pA, similar to previously reported values, confirmed that the number of postsynaptic receptors was not altered by p4.2 action. These results ruled out the possibility of a postsynaptic mechanism of homeostatic plasticity, for example synaptic scaling, in response to synapse elimination triggered by p4.2. Of importance, the maintenance of a constant density of cholinergic receptors in the postsynaptic plasma membrane could facilitate the assembly of newly formed contacts during the recovery phase after synapse loss.

Additionally, mEPSC frequency was also analyzed. Immature synaptic contacts are often associated with higher frequencies of mEPSCs. We wondered whether rapid synapse formation in response to synapse elimination could lead to higher mEPSC release rates. Although incubation of SCMs with p4.2 at the end of the compensatory response showed a slight increase in spontaneous neurotransmitter release (Fig. 68C), there were no significant differences in the frequency of mEPSC in neurons recorded at the end of the homeostatic response ( $p=0.7$ ) and neither during the phase of synaptic elimination driven by p4.2 ( $p=0.45$ , differences were evaluated using one-way ANOVA followed by Bonferroni multiple comparisons test).

These results indicate that the compensatory response to synapse elimination only affected evoked neurotransmitter release by changing the properties of the presynaptic terminal without altering the density of postsynaptic receptors.

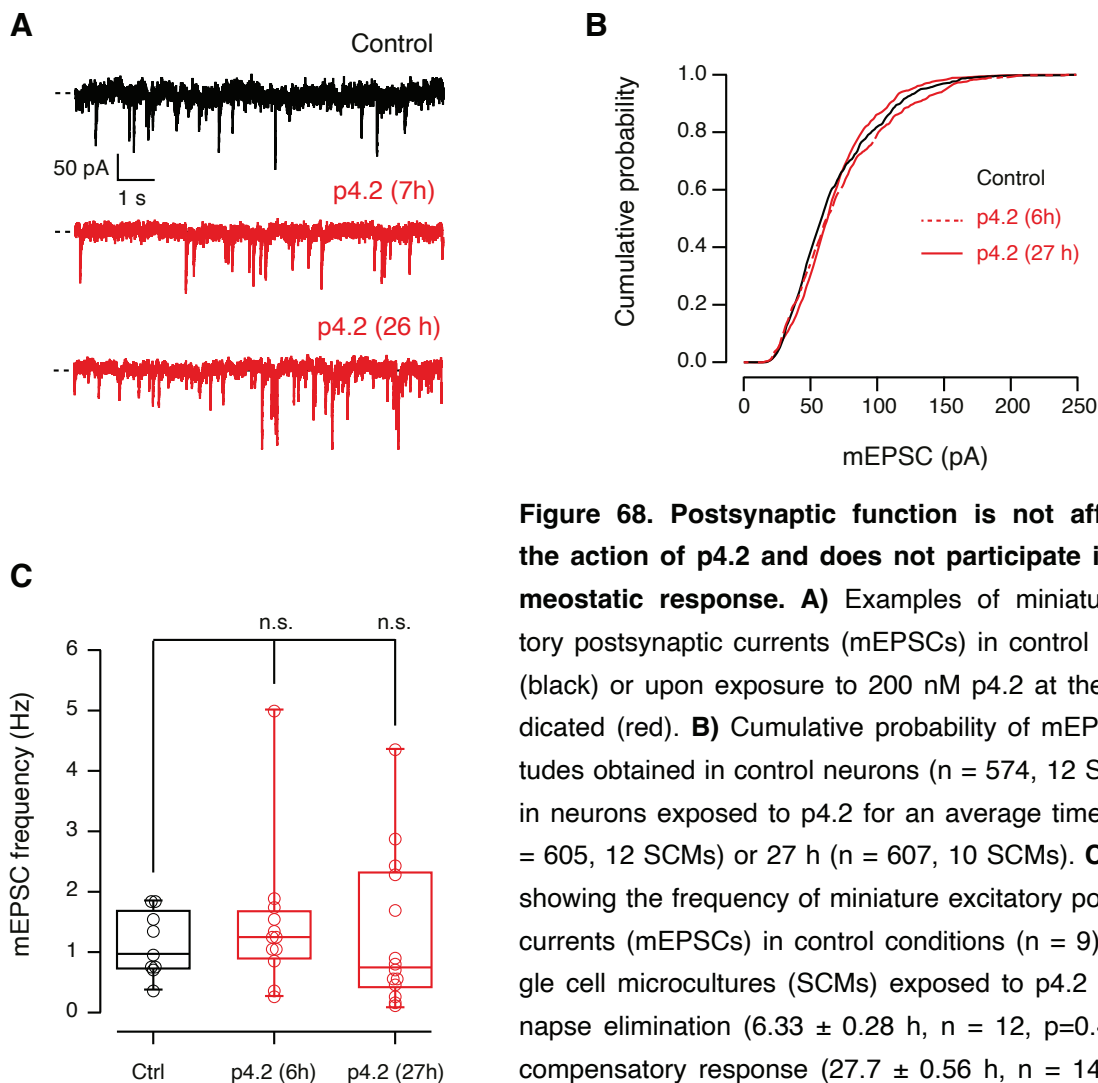
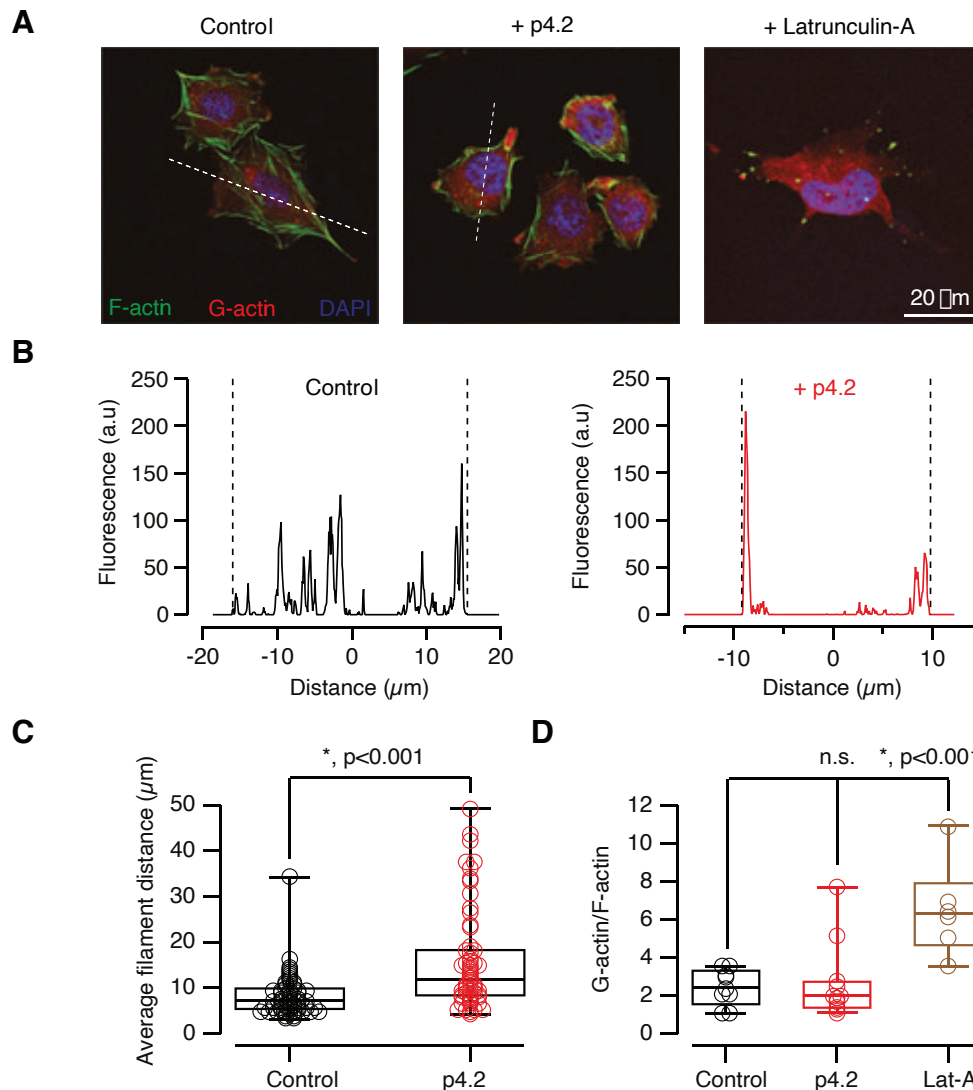


**Figure 68. Postsynaptic function is not affected by the action of p4.2 and does not participate in the homeostatic response.** **A)** Examples of miniature excitatory postsynaptic currents (mEPSCs) in control conditions (black) or upon exposure to 200 nM p4.2 at the times indicated (red). **B)** Cumulative probability of mEPSC amplitudes obtained in control neurons ( $n = 574$ , 12 SCMs) and in neurons exposed to p4.2 for an average time of 6 h ( $n = 605$ , 12 SCMs) or 27 h ( $n = 607$ , 10 SCMs). **C)** Box plot showing the frequency of miniature excitatory postsynaptic currents (mEPSCs) in control conditions ( $n = 9$ ) or in single cell microcultures (SCMs) exposed to p4.2 during synapse elimination ( $6.33 \pm 0.28$  h,  $n = 12$ ,  $p=0.45$ ) or the compensatory response ( $27.7 \pm 0.56$  h,  $n = 14$ ,  $p=0.70$ ). Experimental groups were compared using one-way ANOVA followed by Bonferroni multiple comparisons test.

# 3 Study of the action of peptide p4.2 in the neuronal F-actin cytoskeleton

## 3.1 Study of the ability of peptide p4.2 to reorganize the F-actin cytoskeleton in cell lines

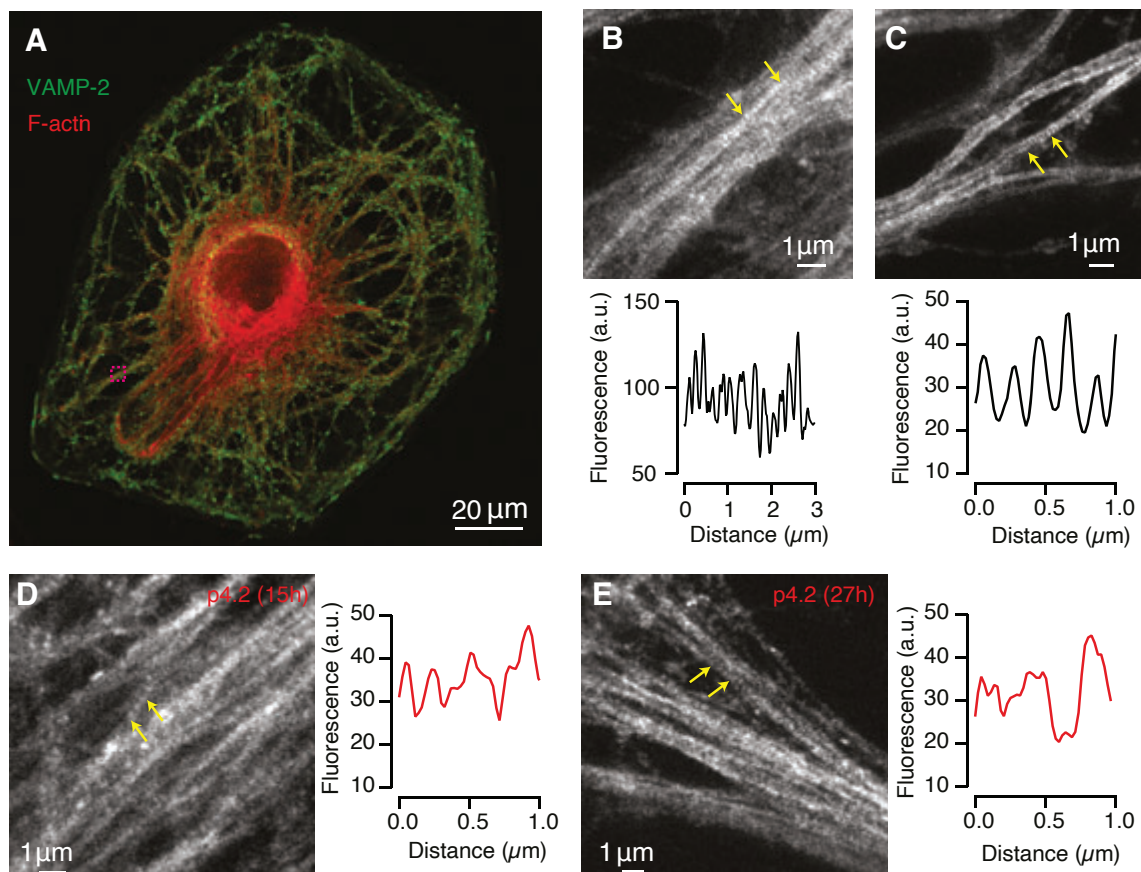
Previous studies in cultured endothelial cells had demonstrated the counteradhesive ability of p4.2 to disrupt focal adhesions by redistributing the actin cytoskeleton (Murphy-Ullrich et al., 1995). To study the capability of peptide p4.2 to alter the F-actin organization in other cell types, such as epithelial cells, we exposed CHO cells to 200 nM p4.2 for 16 h and assessed F-actin distribution by labelling the F-actin cytoskeleton with fluorescent phalloidin (Fig. 69A). Plot profiles obtained by drawing a line through the longest cell axis revealed an enrichment of filamentous actin in the periphery in cells treated with p4.2, confirming previous observations (Fig. 69B and C). To investigate whether this redistribution was linked to F-actin depolymerization, we complemented F-actin staining with the labelling of actin monomers with fluorescent DNase-I and calculated the G-actin/F-actin ratio. Results showed that the effect of p4.2 on F-actin was not related to F-actin depolymerization. In contrast, the F-actin depolymerizing agent latrunculin-A, which was used as a positive control, displayed higher G-actin/F-actin ratio, indicating the increase of soluble actin monomers in the cell cytoplasm (Fig. 69D). These data demonstrate the ability of p4.2 to reorganize the actin cytoskeleton without disrupting it.



**Figure 69. Peptide p4.2 causes reorganization of the F-actin cytoskeleton in epithelial cells. A)** Images of CHO cells labelled with phalloidin-Alexa Fluor 488 and deoxyribonuclease I-Alexa Fluor 594 show the distribution of filamentous actin (F-actin) and monomeric actin (G-actin), respectively. Cells were incubated with 200 nM p4.2 for 16 h or with 1  $\mu$ M latrunculin-A. **B)** Plot profiles obtained from drawing a line (dotted line in A) through the longest axis of the cell (see “Materials & Methods” for details). Fluorescence peaks indicate the distribution of actin filaments. The center of the cell is set to a distance of 0  $\mu$ m and cell borders are indicated by dotted lines. **C)** Distance among F-actin filaments in control cells (n = 58) and cells exposed to p4.2 (n = 60) reveals that upon p4.2 treatment, F-actin is redistributed to the periphery of the cell. Box plot shows the median (horizontal line), 25–75% quartiles (boxes), and ranges (whiskers). Statistical differences were evaluated using unpaired two-tailed Student’s t-test. **D)** The G-actin and F-actin relationship was evaluated by integrating the fluorescence of deoxyribonuclease I-Alexa Fluor 594 and phalloidin-Alexa Fluor 488 on a single cell basis. Latrunculin-A was used as a positive control for F-actin depolymerization. Box plot shows the median (horizontal line), 25–75% quartiles (boxes), and ranges (whiskers) of G-actin/F-actin in control cells (n = 9), cells exposed to p4.2 (n = 11) and cells treated with latrunculin-A (n = 6). Notice that treatment of CHO cells with p4.2 did not modify G-actin/F-actin. Evaluation of statistical differences were performed using one-way ANOVA followed by Bonferroni multiple comparisons test.

### 3.2 Study of the effect of p4.2 on the periodic actin skeleton present in neurites

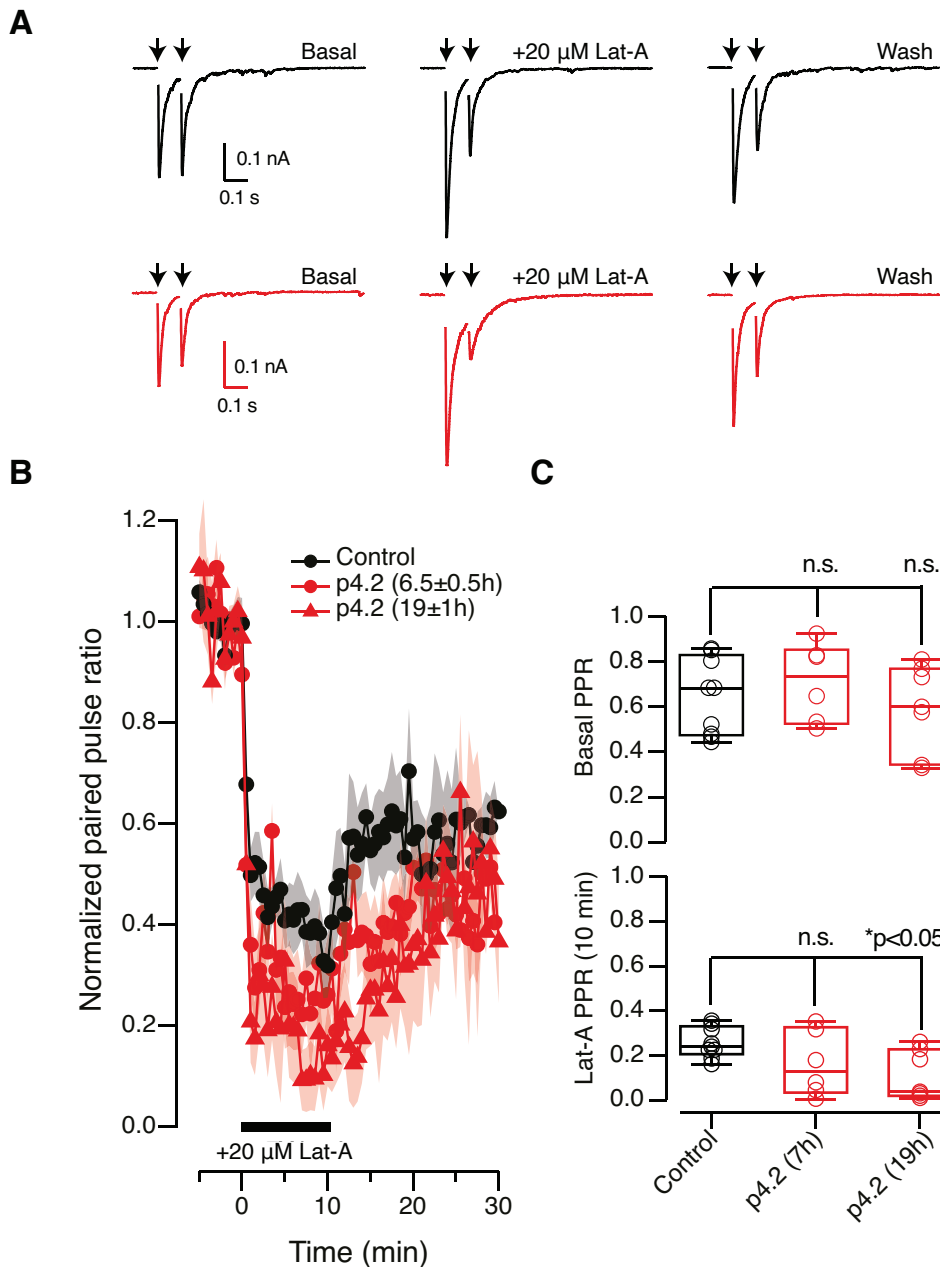
Next, we investigated whether p4.2 had a similar action on the actin cytoskeleton found in neurons. It had been previously described in hippocampal neurons that the actin cytoskeleton in neurites is organized in actin ring-like structures that appear with a periodicity of 180–190 nm (B. Han et al., 2017). STED microscopy revealed the characteristic actin skeleton in autaptic neuronal processes spaced at 195 nm (Fig. 70A-C). In neurons incubated with 200 nM p4.2 for 15 or 27 h, actin ring-like structures were disrupted and appeared distributed in patches rather than in regularly spaced bands. Some regions, however, showed periodic structures spaced at 250-300 nm, revealing the ability of p4.2 to redistribute the neuronal F-actin cytoskeleton (Fig. 70D and E).



**Figure 70. Peptide p4.2 disrupts the actin cytoskeleton present in neurites.** **A)** Image of a single cell microculture (SCM) showing the distribution of F-actin labelled with phalloidin-Atto 647N and VAMP-2. The box region was selected for STED microscopy (shown in B). **B)** and **C)** Up, example of images obtained from two different control neurons showing the actin ring-like structures present along neurites. Down, plot of line profiles drawn between arrows. Peaks of fluorescence represent the periodic actin ring-like structures regularly spaced at ~190 nm. **D)** and **E)** Representative images (left) of neurons exposed to 200 nM p4.2 for 15 h (**D**) or 27 h (**E**) and the associated plot line profiles (right). Notice how the periodic structure of the actin skeleton is altered upon p4.2 action. Most neurites do not show apparent actin-ring like structures although in some regions regularly spaced peaks appear at 250-300 nm distance.

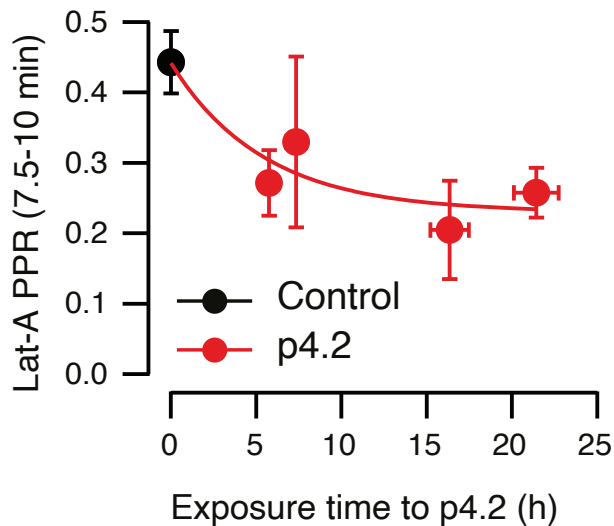
### 3.3 Time course of presynaptic F-actin cytoskeleton reorganization induced by peptide p4.2

Exposure of SCMs to peptide p4.2 results in the redistribution of the neuronal F-actin cytoskeleton. To investigate whether this reorganization of the F-actin cytoskeleton facilitates presynaptic disassembly, we evaluated the time course of p4.2 effect on F-actin changes. We took advantage of the ability of latrunculin-A to increase neurotransmitter release probability, which leads to increases of short-term depression (Morales et al., 2000). The effect of latrunculin-A on synaptic depression was used as a readout of presynaptic F-actin remodeling triggered by p4.2. Paired-pulses of 100 ms were applied to assess short-term plasticity before, during and after local application of 20  $\mu$ M latrunculin-A. In control neurons, acute addition of latrunculin-A enhanced synaptic strength and consequently increased short-term depression by ~40% (Fig. 71A). Even though neurons incubated with p4.2 showed no differences in basal paired pulse ratio (PPR), depression caused by latrunculin-A was enhanced (Fig. 71B and C). Due to a maximum increase in release probability, 3 out of 7 cells treated for  $19 \pm 1$  h (mean  $\pm$  s.e.m.) with p4.2, displayed an almost absent response in the second evoked stimulus. The time course of the depression caused by latrunculin-A as a function of p4.2 exposure showed an exponential decay with a time constant of 5.5 h (Fig. 72). Accordingly, rearrangement of the actin cytoskeleton could be expected to be completed after three time constants, which concurs with the moment of maximum synapse loss found at ~16 h (Fig. 61B). These data suggest that presynaptic disassembly and subsequent synapse elimination triggered by p4.2 relies on the reorganization of the F-actin cytoskeleton.



**Figure 71. Time course of the effect of p4.2 on the reorganization of the presynaptic F-actin cytoskeleton.** **A)** The effect of Latrunculin-A on short-term plasticity was used to assess the time course of F-actin reorganization produced by p4.2. Acute application of 20  $\mu\text{M}$  Latrunculin-A increased short-term depression in control neurons when paired pulses (PP) were delivered at a interval of 100 ms. Washing out Latrunculin-A resulted in partial recovery of depression. Black traces show PP plasticity in a control single cell microculture (SCM). Red traces show PP responses in a SCM exposed to 200 nM p4.2 for 19 h. Arrows mark the moment of the stimulus. Notice the enhanced depression induced by Latrunculin-A compared to the control neuron. **B)** Normalized PP ratio (PPR) as a function of experimental time. Depression was immediately increased upon application of Latrunculin-A. **C)** PPR recorded in basal conditions (up) and 10 min after addition of 20  $\mu\text{M}$  Latrunculin-A (down) in the indicated experimental conditions. Box plots show the median (horizontal line), 25–75% quartiles (boxes), and ranges (whiskers) of PPR values obtained in control conditions ( $n = 9$ ) and 7 h ( $n = 6$ ) or 19 h ( $n = 7$ ) after application of 200 nM p4.2. Differences were evaluated using one-way ANOVA followed by Bonferroni multiple comparisons test.

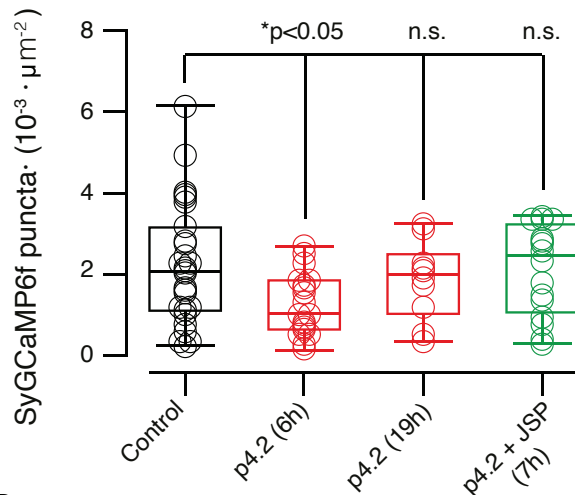
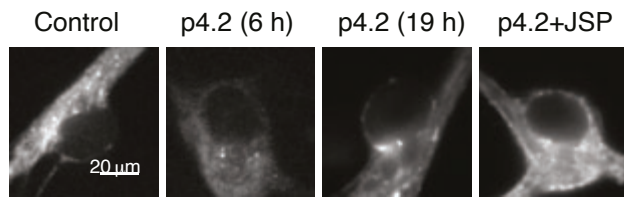
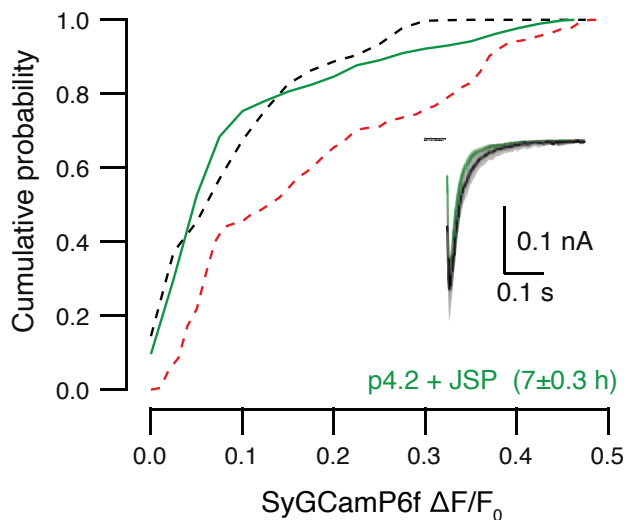




**Figure 72. Time course of the decay in PPR produced by Latrunculin-A as a function of p4.2 exposure time.** PPR values correspond to the average decrease observed after 7.5-10 min of Latrunculin-A application. PPR obtained in control neurons is indicated in black (mean  $\pm$  s.e.m,  $n = 9$ ). Each red bin shows the mean  $\pm$  s.e.m. of three different neurons exposed to p4.2 (red,  $n = 12$ ). Decay of PPR is fitted by an exponential function showing a time constant of 5.5 h.

### 3.4 Stabilization of the F-actin cytoskeleton and its effect on the action of peptide p4.2

To further investigate whether synapse disassembly and the subsequent elimination of autaptic contacts were driven by the reorganization of the F-actin cytoskeleton caused by p4.2 action, we blocked the effect of the p4.2 on the F-actin cytoskeleton by simultaneously exposing neurons to p4.2 and the F-actin stabilizing drug jasplakinolide. Quantification of the number of SyGCaMP6f puncta responding to a train of five stimuli was used to evaluate synapse loss. Control SCMs contained  $(2.23 \pm 0.30) \times 10^{-3}$  puncta  $\cdot \mu\text{m}^{-2}$  ( $n = 27$ , mean  $\pm$  s.e.m.), while neurons exposed for 6 h to p4.2 presented a lower density of  $(1.26 \pm 0.17) \times 10^{-3}$  puncta  $\cdot \mu\text{m}^{-2}$  ( $n = 20$ ;  $p < 0.05$ ; one-way ANOVA followed by Bonferroni multiple comparisons test) that increased to  $(1.86 \pm 0.30) \times 10^{-3}$  puncta  $\cdot \mu\text{m}^{-2}$  ( $n = 10$ ) after 19 h of p4.2 treatment (Fig. 73A), resembling results obtained in correlative electrophysiology and immunocytochemistry experiments (Fig. 61). In contrast, when p4.2 was applied concomitantly to jasplakinolide, neither EPSC amplitude, nor the density of  $(2.12 \pm 0.28) \times 10^{-3}$  puncta  $\mu\text{m}^{-2}$  ( $n = 16$ ) were different from control neurons (Fig. 73A and B), thus confirming the ability of jasplakinolide to prevent synapse loss. In addition, the distribution of changes in SyGCaMP6f fluorescence was also comparable to controls when jasplakinolide was added to the media (Fig. 73B), suggesting that stabilization of the actin cytoskeleton prevented synapse elimination triggered by p4.2 and consequently the presynaptic homeostatic response. Altogether, these findings indicate that synapse elimination triggered by the active SPARC-derived peptide p4.2 is mediated by reorganization of the F-actin cytoskeleton.

**A****B****Figure 73. Stabilization of the F-actin cytoskeleton prevents the action of p4.2.**

**A)** The number of functional synapses was evaluated by using the SyGCaMP6f reporter coupled to electrophysiological recordings. Example of difference images of single cell microcultures (SCMs) expressing the presynaptic calcium influx reporter obtained during stimulation with five stimuli delivered at 20 Hz at the indicated conditions. Notice how the transient decay of SyGCaMP6f puncta caused by exposure to 200 nM p4.2 for 6 h was not observed when p4.2 was incubated in the presence of 1  $\mu$ M jasplakinolide (JSP). Box plots show the median (horizontal line), 25–75% quartiles (boxes), and ranges (whiskers) of the density of SyGCaMP6f puncta in control conditions ( $n = 27$ ), after 6 h of exposure to p4.2 ( $n = 20$ ), after 19 h of exposure to p4.2 ( $n = 10$ ) and after 7 h incubation of p4.2 and jasplakinolide ( $n = 16$ ). Statistical differences were evaluated using one-way ANOVA followed by Bonferroni multiple comparisons test.

**B)** Cumulative probability of SyGCaMP6f  $\Delta F/F_0$  increases in SCMs exposed to 200 nM p4.2 concomitantly with 1  $\mu$ M jasplakinolide for  $7 \pm 0.3$  h (mean  $\pm$  s.e.m.,  $n = 1030$ , 16 SCMs). Dotted lines display the distribution obtained in control conditions (black) and in neurons incubated with p4.2 for 19 h (red) for comparison purposes. The inset shows the average of excitatory postsynaptic currents (EPSCs) obtained in control neurons (black,  $n = 12$ ) and in neurons incubated with 200 nM p4.2 and 1  $\mu$ M jasplakinolide (green,  $n = 11$ ). Solid line  $\pm$  shadowed area indicates mean  $\pm$  s.e.m.

Collectively, our data show that synapse loss in an autaptic circuit is compensated by the activation of a mechanism of presynaptic homeostatic plasticity that is driven by *de novo* synapse formation and presynaptic potentiation mediated by increases in RRP size and presynaptic calcium entry.

Neuronal protein synthesis machinery is absent in the axon and synaptic boutons. Consequently, *de novo* synapse formation observed in response to synapse elimination likely involves the recruitment of modular units of presynaptic material to nascent synaptic sites through active microtubule transport (Shapira et al., 2003).

Although assembly of functional synaptic boutons during synapse formation can be completed within 1 h of initial axodendritic contact, as shown in cultured CNS synapses (Ahmari et al., 2000; Friedman et al., 2000; reviewed in Ziv & Garner, 2004), synaptogenesis during development occurs progressively over an extended period of time that can take days to weeks until the neuron reaches a specific number of connections (S. H. Lee & Sheng, 2000; Rao et al., 1998). Here, we have shown that ~60% of autaptic synapses present in a microculture are synchronously formed in ~10 h to compensate synapse loss. Therefore, the homeostatic synaptic response observed here involves rapid synapse formation, compared to that found during synaptic development.

These observations highlight the tight control of this process and suggest that active microtubule transport of presynaptic components is determinant for maintaining the "proper" number of synapses within a neuronal network.

However, despite the essential role of microtubules during synapse formation, their involvement in homeostatic plasticity mechanisms and synapse maintenance in mature neurons is almost uncharted.

During the second part of this project, we aimed to gain new insights as how microtubules might participate in the regulation of homeostatic synaptic plasticity mechanisms necessary to keep synaptic transmission at a baseline.

Yet, because the role of microtubules at the synaptic level is not well understood, our first objective was to get a better understanding of the contribution of microtubules in synaptic function.

## 4 Distribution of microtubules at synaptic terminals

To study the role of microtubules in synaptic function, we performed electrophysiological recordings of evoked and spontaneous synaptic transmission in autaptic cultures correlative to electron microscopy, optical microscopy, or protein dialysis (Fig. 74).

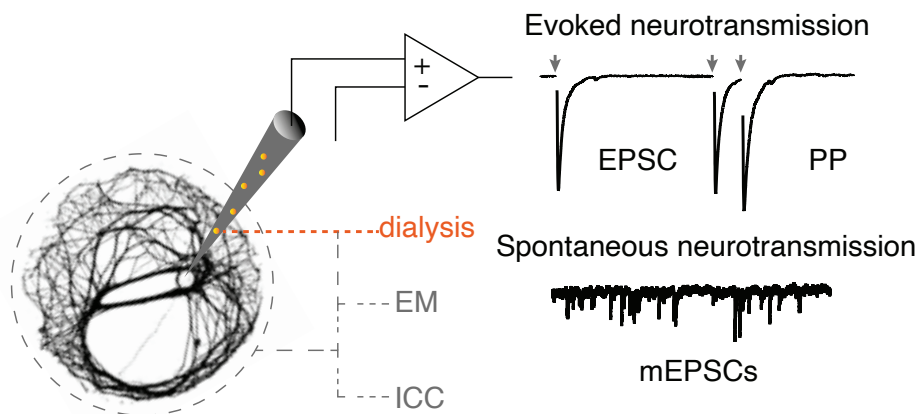


**Figure 74. Experimental setup to study the role of microtubules in synaptic transmission.** Schematic representation of the experimental setup used to investigate the role of microtubules in synaptic transmission during this project. Electrophysiological recordings of excitatory postsynaptic currents (EPSCs), Paired Pulses (PP) and miniature excitatory postsynaptic currents (mEPSCs) from single cell microcultures (SCMs) were performed correlative to either electron microscopy (EM), immunocytochemistry (ICC) or were coupled to protein dialysis through the patch pipette.

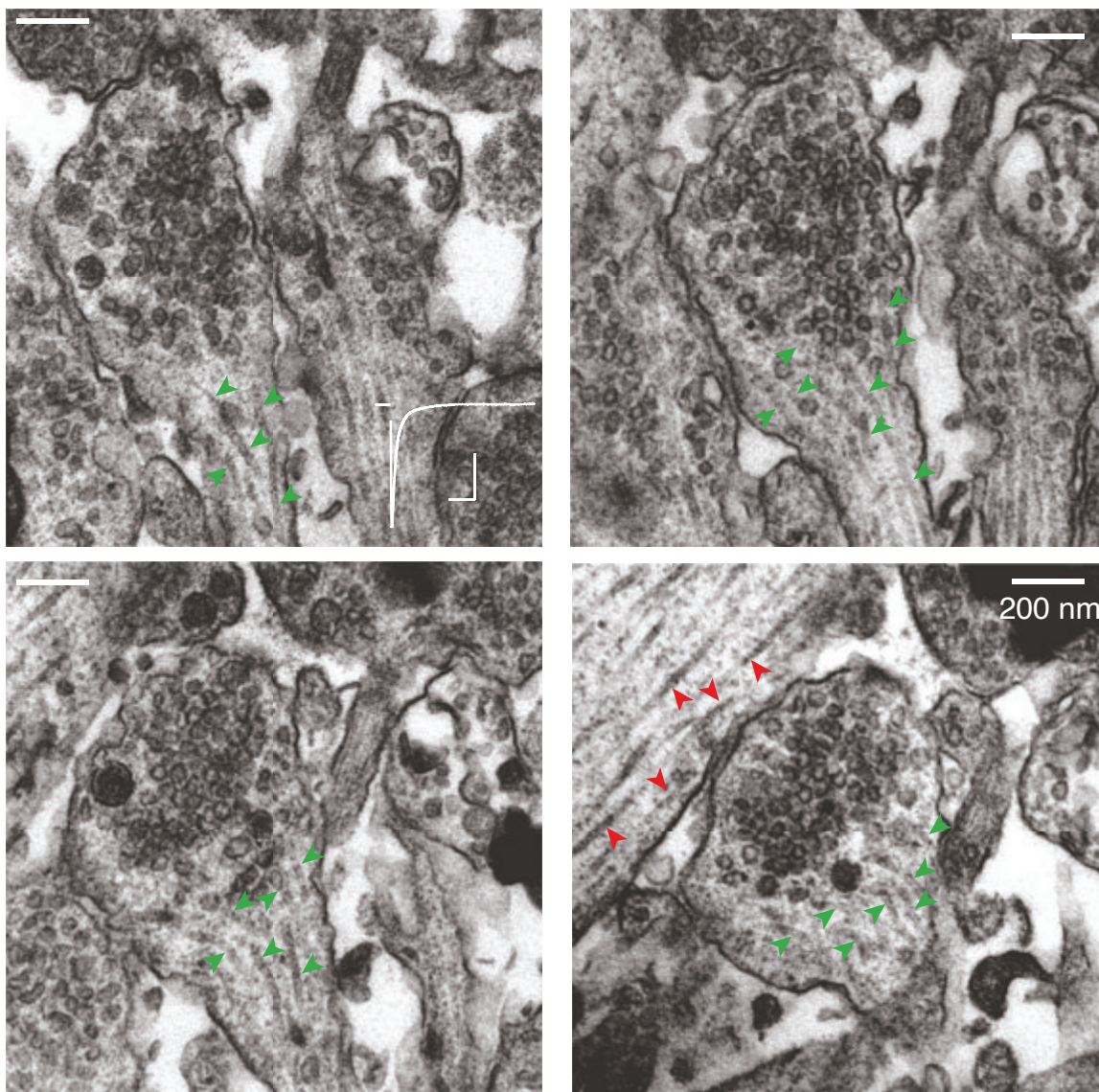
### 4.1 Location of microtubules in dendrites and presynaptic terminals of autaptic neurons

Early electron micrographs presented by George Gray (Gray, 1975; Westrum & Gray, 1977), first revealed that microtubules appear at both sides of synapses. We started by investigating whether the same scenario could also be found in our culture system. Serially sectioning EM samples of autaptic neurons revealed the presence of MTs entering synaptic boutons, often showing synaptic vesicles attached to them, both in axodendritic and axosomatic autapses. MTs were also observed in dendrites near postsynaptic specialization sites (Fig. 75A and B).

Although the presence of MTs at both sides of the synapse have been previously observed in electron micrographs, whether MTs may participate in the control of homeostatic synaptic plasticity mechanisms responsible for maintaining basal levels of neurotransmission, for example by providing regulated amounts of presynaptic material such as VGCCs or SVs, is not known.



A



B

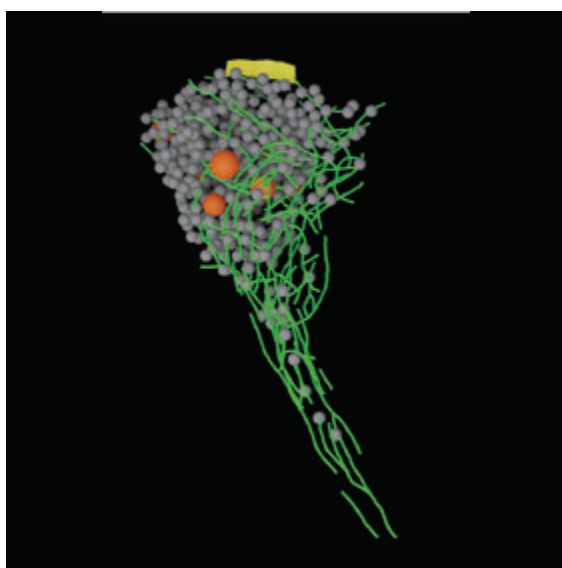


**Figure 75. Microtubules are found at the synapse both in presynaptic terminals and dendrites. A)** Serial electron micrographs from an autaptic neuron (left to right, up and down), with the corresponding EPSC (white trace). Scale bars, 1  $\mu$ m, 100 ms. Notice the presence of microtubules entering the presynaptic terminal (green arrows) and in dendrites (red arrows). **B)** 3D reconstruction of the axodendritic autapse shown in **(A)** obtained by 7 sections of serial-EM. Synaptic vesicles (gray), microtubules (green), active zone (yellow) and dense core vesicles (orange).

## 4.2 Study of the presence of microtubule plus-ends at presynaptic terminals

If microtubules were to contribute to changes in synaptic transmission, plus-ends of dynamic microtubules must be present at pre- and/or postsynaptic sites. Although our observations from serial-EM images suggested that microtubules enter the presynaptic terminal, it was not clear whether their plus-ends were contributing to the cytoskeleton of the bouton or if, in contrast, they were passing across the axon.

Dynamic microtubules are controlled by different factors such as MT-associated proteins (MAPs), MT motors and MT regulatory proteins. The latter are associated with the distal end of growing microtubules and have been used for studying MT growth dynamics (Pérez et al., 1999). Among these “plus end-tracking proteins”, also called +TIPs (Schuyler & Pellman, 2001), is the end-binding protein EB3, which is used as a marker of MT plus-ends (Stepanova et al., 2003).

Immunocytochemistry assays of EB3 and synapsin-I were used to investigate the presence of MT plus-ends at the presynaptic terminal (Fig. 76A). As shown in Fig. 59, colocalization of synapsin-I and the presynaptic protein bassoon (~80%) had proven the bona fide identification of presynaptic terminals by synapsin-I labelling. While synapsin-I showed a punctate staining under the confocal microscope, EB3 was observed throughout synaptic processes with accumulations at discrete patches, identified as EB3 comets (Fig. 76B).

Plotting a line profile throughout the center of synapsin-I puncta along neurites showed that putative synapses were associated with regions where there was a concentration of EB3 (Fig. 76C). Not all EB3 comets colocalized with synapsin-I, but were found along neuronal processes. These data suggest that MTs plus-ends are found along neurites, but are also present in synaptic boutons. However, given the resolution of confocal microscopy (~250 nm), structures smaller than 250 nm are lost in a blur. To further investigate whether MT growing-ends enter presynaptic boutons, a higher optical resolution was required.

To overcome the light diffraction limit, SCMs labelled with synapsin-I and EB3 were visualized under the STED microscope. 3D STED z-sections provided information of synaptic volumes. We centered on axosomatic synapses since they are the main contributors to recorded postsynaptic responses. On average, putative axosomatic synapses labelled with synapsin-I appeared in 7 consecutive sections (z resolution=156 nm) and displayed a diameter of ~1  $\mu\text{m}$ , which is in agreement with previous observations (see also serial EM in Fig. 75).

High-resolution images showed that MT plus-ends are indeed associated with presynaptic terminals. However, rather than total colocalization of synapsin-I and EB3 staining, invasion of MT plus-ends into a limited number of putative synapses was obser-

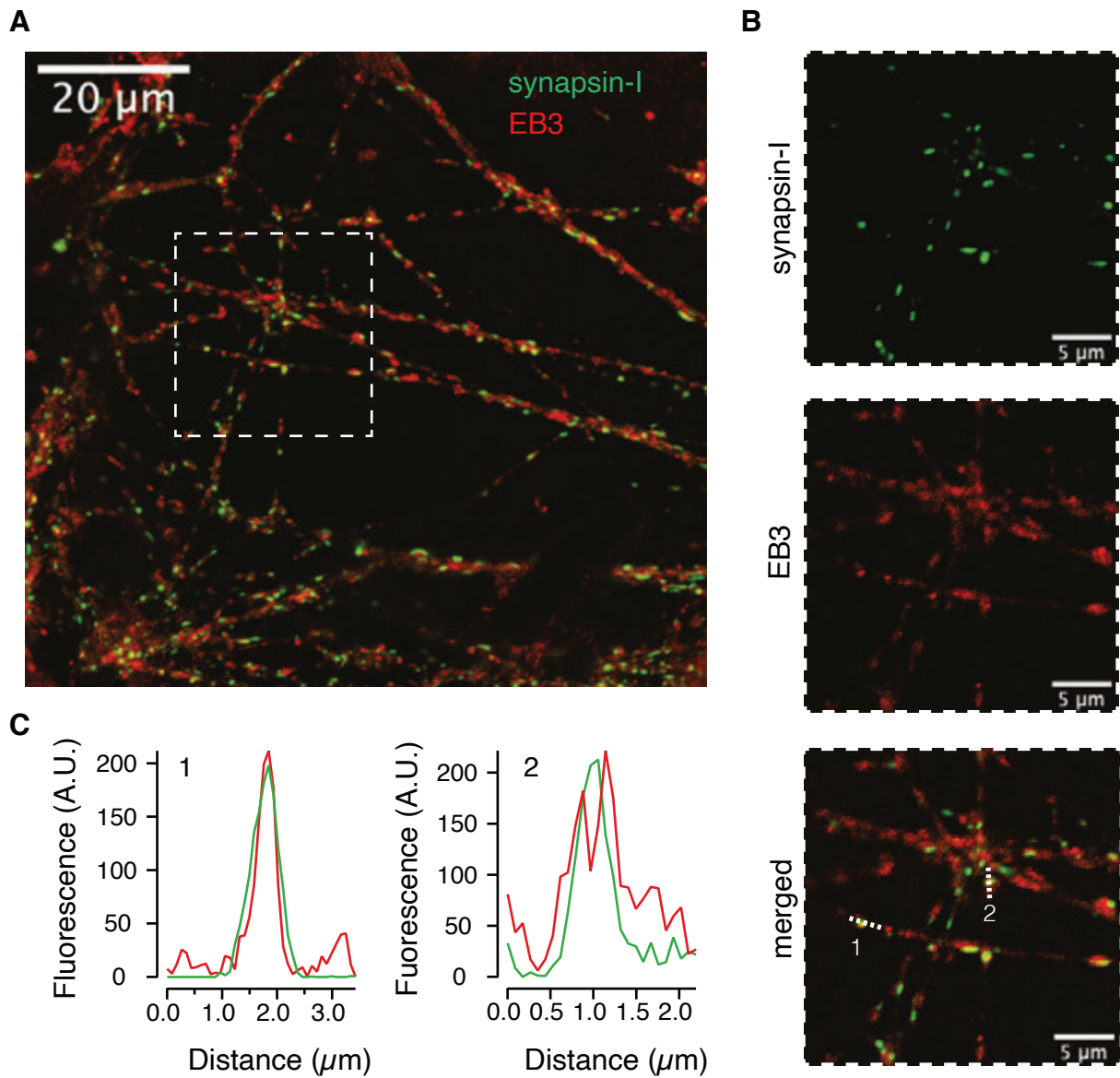


**Figure 76. Distribution of microtubule plus-ends and presynaptic terminals under the confocal microscope. A)** Neuronal processes of an autaptic neuron labelled with EB3 (red) and synapsin-I (green) showing the distribution of microtubule growing ends and putative presynaptic terminals, respectively. **B)** Images of the boxed region in A shows the punctate pattern of putative synapses labelled with synapsin-I (green), EB3 comets (red) and merged, where colocalization of EB3 and synapsin-I can be observed. **C)** Plot of line profiles from dotted lines drawn in B, showing the colocalization of EB3 and synapsin-I.

ved ( $n=317$ , Fig. 77). A total of 64% of the putative synapses analyzed were invaded by MT plus-ends at least once in the complete z-section of the synapse, with an average of 6 stacks (out of 7) presenting overlapping of the two markers. Altogether, these data indicate that MT growing-ends enter presynaptic terminals in a high number of synapses and suggest a possible dynamism of MTs at the presynaptic site.



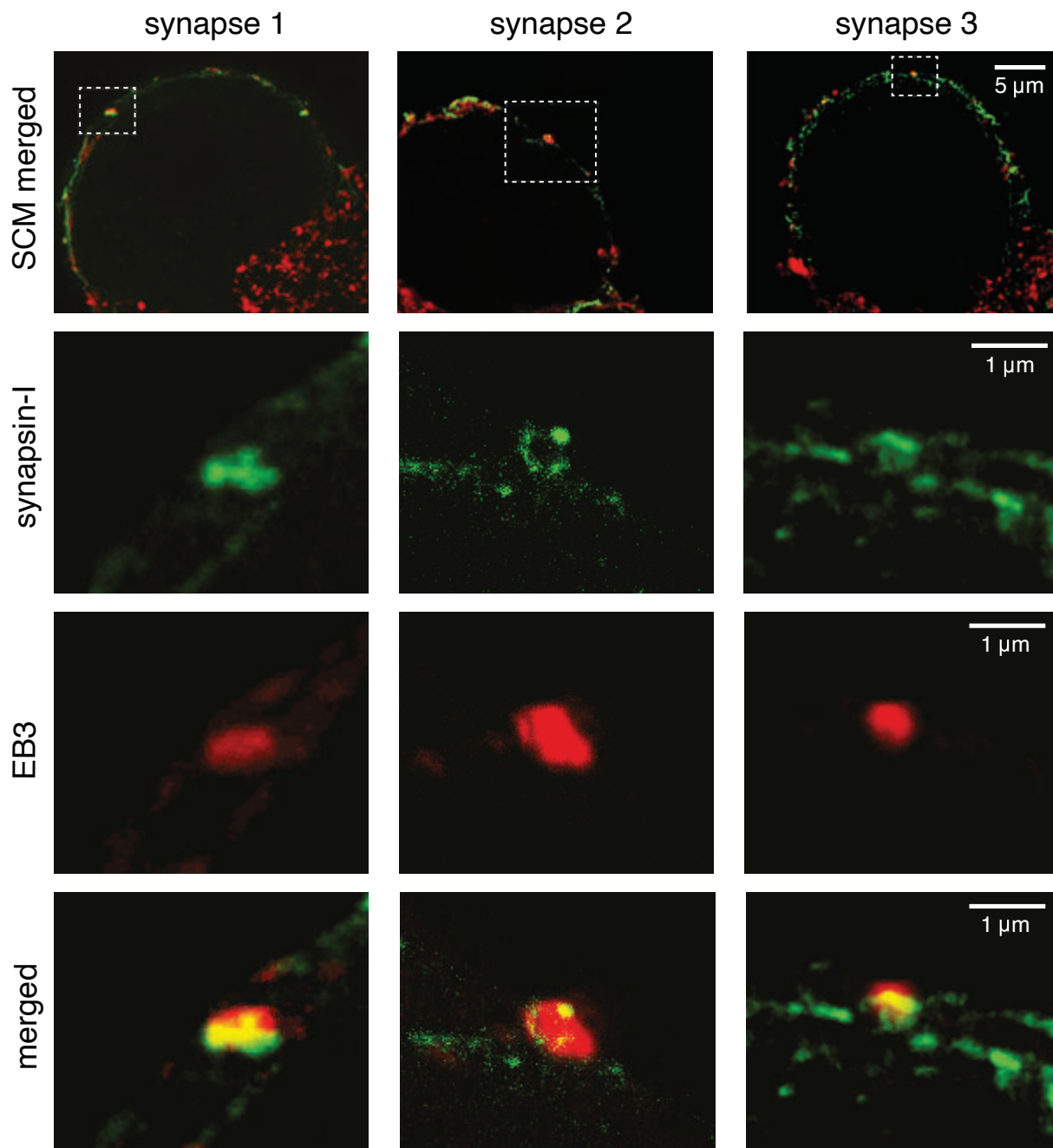


**Figure 77. Microtubule plus-ends invade presynaptic terminals.** Maximum projections of single cell microcultures (SCMs) labelled with EB3 (red) and synapsin-I (green) obtained with STED microscopy. High resolution images provide detailed visualization of microtubule plus-ends and its association to synapses (z resolution=156 nm, xy resolution=22,3 nm). Neuronal cell bodies and magnification of axosomatic synapses are shown (synapses 1-3, from dotted boxes). Overlapping of both markers in individual axosomatic synapses were analyzed across z-sections. On average, 64% of the analyzed putative synapses were invaded by microtubule plus-ends in at least one of the imaged planes. Synapsin-I staining was used to determine the whole volume of each synapse, which on average spanned across 7 sections (7 SCMs, 317 synapses).

## 5 Effect of microtubule polymerization on synaptic transmission

Dynamic microtubules are in constant polymerization/depolymerization through the addition and removal of  $\alpha/\beta$ -tubulin heterodimers at their plus-ends. To investigate whether enhancement of microtubule polymerization may be used as a mechanism for regulating synaptic strength, for example by increasing MT active transport of precursor vesicles (Guedes-dias et al., 2019), we promoted the formation of new MT polymers by increasing the concentration of free tubulin in the cytoplasm. Addition of  $\alpha/\beta$ -tubulin heterodimers in the internal solution of the patch pipette during electrophysiological recordings and its subsequent dialysis to synaptic contacts should favour MT dynamics towards a polymerizing state.

Adding 25  $\mu\text{g/ml}$  of exogenous tubulin to the cell body of autaptic neurons increased synaptic strength by  $\sim 40\%$  after 20 min of dialysis ( $2.3\% \text{ increase} \cdot \text{min}^{-1}$ ), when assessed in the form of EPSCs. In contrast, loading the internal solution with the same concentration of denatured tubulin or tubulin control buffer did not have any effect on the evoked response ( $-0.19\% \cdot \text{min}^{-1}$  and  $-0.7\% \cdot \text{min}^{-1}$ , respectively; Fig. 78A and B). Changes were assessed after 10 mins of recording to ensure proper dialysis of the internal solution. We repeated the same experiment using different tubulin concentrations and found that the effect observed was concentration-dependent. Only concentrations above 10  $\mu\text{g/ml}$  of tubulin showed a positive effect on neurotransmission (Fig. 78C).

These results suggest that enhancement of MT polymerization by means of increasing the pool of free tubulin in an autaptic neuron might be used as a mechanisms for potentiating synaptic strength.

However, the effect of MT polymerization on EPSC amplitude could be due to changes in pre- and/or postsynaptic function. To separate the contribution of pre- and postsynaptic components associated with tubulin dialysis sequential electrical and chemical stimulation was performed (Fig. 79A). Neurons loaded with 25  $\mu\text{g/ml}$  tubulin increased in  $\sim 20\%$  the responses triggered by a puff of Ach ( $p=0.0044$ , one-way ANOVA repeated measures) as well as the responses caused by depolarization ( $p<0.0001$ , one-way ANOVA repeated measures) after 20 min of recording. Nor EPSC amplitude neither the response to Ach were modified in neurons when recorded in the presence of control buffer in the internal solution (Fig. 79B-D). These results suggested that enhancement of synaptic strength triggered by enhancing MT polymerization had a postsynaptic component.

Because chemical stimulation with Ach activates both synaptic and extrasynaptic cholinergic receptors, these data were further validated by assessing the amplitude of

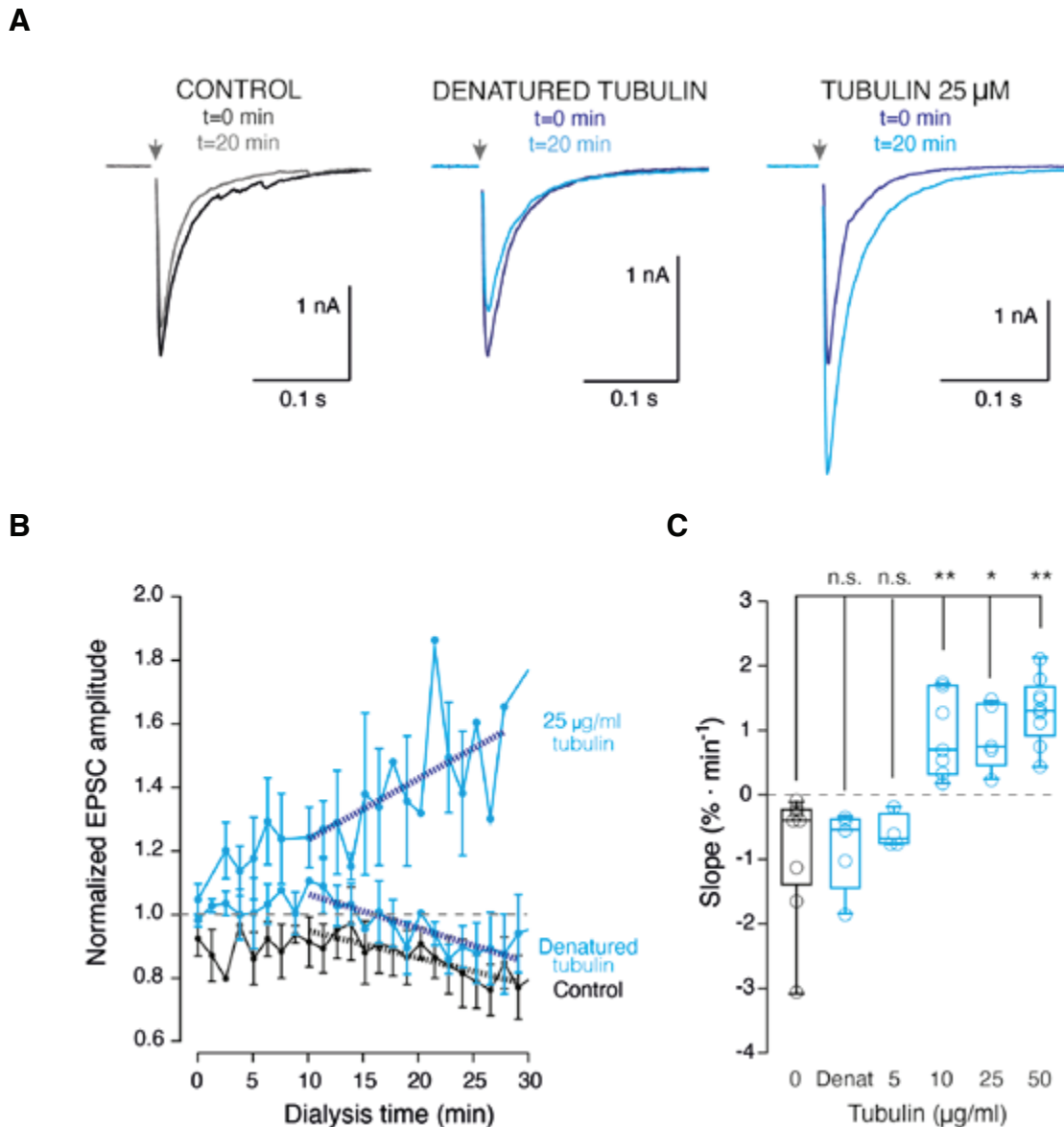


**Figure 78. Increasing microtubule polymerization by dialysis of exogenous tubulin potentiates synaptic strength in a concentration-dependent manner in autaptic circuits. A)** Representative examples of EPSCs at the start ( $t=0$ ) and end ( $t=20$ ) of the recording. SCMs were dialyzed with control buffer, denatured tubulin or 25  $\mu$ g/ml tubulin. **B)** Mean normalized EPSC amplitude as a function of dialysis time. Experimental conditions: control buffer (black,  $n = 9$ ), denatured tubulin (blue,  $n = 5$ ) and 25  $\mu$ g/ml tubulin (blue,  $n = 5$ ). Linear fittings are adjusted to each condition (time 10-30 min) to measure the slope and calculate the changing rate of the evoked responses caused by dialysis of the loaded intern solution. SCMs were stimulated at 0.8 Hz and normalized values of EPSC amplitude were decimated 2.5 times. Dots indicate mean  $\pm$  s.e.m. **C)** Box plot showing the median (horizontal line), 25-75% quartiles (boxes), and ranges (whiskers) of the slopes measured from the time course of normalized EPSC amplitude (as shown in **B**) in neurons with different tubulin concentrations (blue): 50  $\mu$ g/ml ( $n = 9$ ,  $*p < 0.0001$ ), 25  $\mu$ g/ml ( $n = 5$ ,  $*p = 0.003$ ), 10  $\mu$ g/ml ( $n = 7$ ,  $*p < 0.0001$ ), 5  $\mu$ g/ml ( $n = 5$ ,  $*p = 0.95$ ), denatured 25  $\mu$ g/ml tubulin ( $n = 5$ ,  $p > 0.99$ ) or control buffer (black,  $n = 9$ ). Slopes are expressed as percentage of change  $\cdot \text{min}^{-1}$ . Evaluation of statistical differences were performed using one-way ANOVA followed by Bonferroni multiple comparisons test.

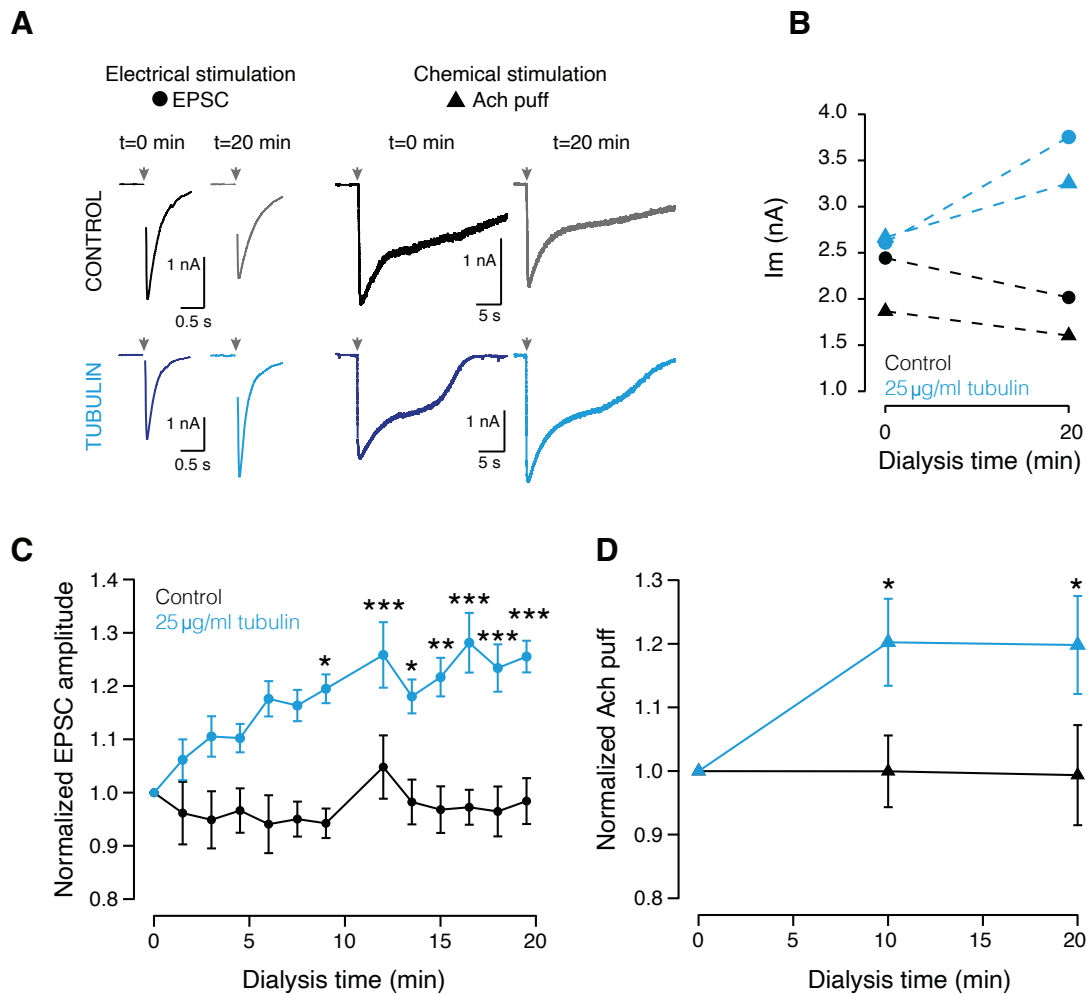


**Figure 79. Increasing tubulin availability in an autaptic circuit enhances postsynaptic function.**

**A**) Illustrative examples of recordings obtained by depolarization (dot) or chemical stimulation (triangle) with a puff of 50  $\mu$ M acetylcholine (Ach) in control conditions (black) or during tubulin dialysis (blue) at the start and end of the recording. Stimulus transients have been blanked. **B**) Quantification of the example shown in **A**). Notice the increase in both chemical and electrical responses after 20 min of tubulin dialysis through the patch pipette. **C**) and **D**) Mean normalized EPSCs and Ach puff evoked currents as a function of experimental time during dialysis of control buffer (black,  $n = 13$ ) or 25  $\mu$ g/ml tubulin (blue,  $n = 17$ ). Electrical and chemical stimulation were sequentially performed at intervals of 1.5 min and 10 min, respectively. Dots indicate mean  $\pm$  s.e.m. Asterisks indicate significant differences relative to basal values (dialysis time 0) using the one-way repeated measures ANOVA followed by the Dunnett's multiple comparisons test, \* $p < 0.01$ , \*\* $p < 0.001$ , \*\*\* $p < 0.0001$ .

miniature excitatory postsynaptic events. Changes in mEPSC amplitude are often associated with variations in the number of postsynaptic receptors, for example during synaptic scaling (G. G. Turrigiano et al., 1998). Recording of spontaneous neurotransmitter release showed that, on average, the amplitude of mEPSCs increased by more than 20% after 20 min of tubulin dialysis ( $p = 0.0293$ , one-way ANOVA repeated measures), whereas it did not change in control conditions (Fig. 80A and B). On the other hand, estimation of the number of SVs released after a single depolarization, calcula-

ted by dividing the EPSC amplitude (Fig. 80C) between the average value of mEPSC amplitude, was unchanged in tubulin dialyzed neurons or when dialysis was performed with control buffer (Fig. 80D), ruling out the contribution of the presynaptic terminal to the synaptic potentiation associated to MT polymerization.

Altogether, these results indicate that: i) enhancement of MT polymerization does not modify presynaptic function in basal conditions. Whether it may be important for regulating synaptic strength after synapse loss induce by peptide p4.2, however, should be further explored. And ii) the amount of free tubulin in a neuronal circuit is a limiting factor for postsynaptic function, suggesting that changes in MT polymerization might be used as a mechanism for controlling the number of postsynaptic receptors present at the PSD, for instance during synaptic plasticity.

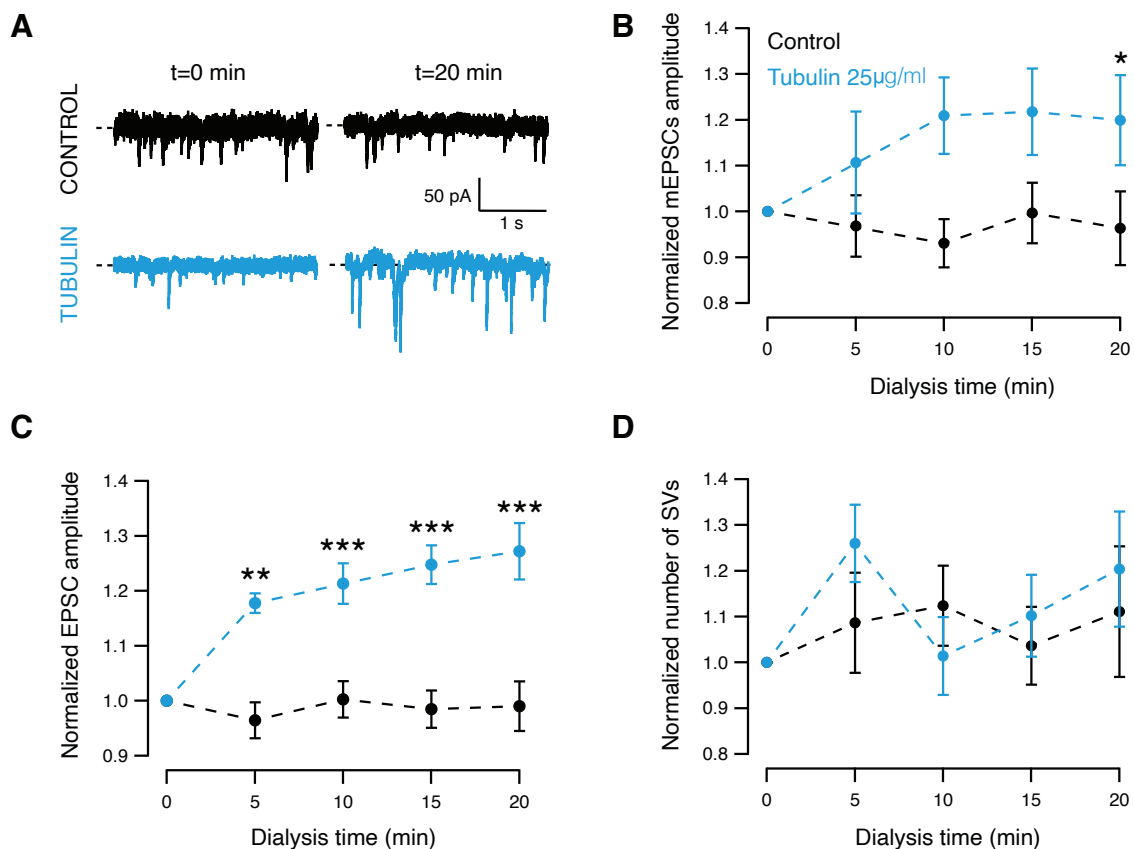


**Figure 80. Increasing tubulin availability in an autaptic circuit does not change presynaptic function.** **A)** Recordings of spontaneous neurotransmitter release in control conditions (black) or upon tubulin dialysis (blue) at t=0 min and t=20 min of recording. **B)** Mean of normalized mEPSCs amplitude averaged at 5 min intervals during 25 µg/ml tubulin dialysis (blue, n = 11) or control conditions (black, n = 14). **C)** Mean normalized evoked responses as a function of dialysis time averaged at 5 min intervals during 25 µg/ml tubulin dialysis (blue, n = 11) or control conditions (black, n = 14). **D)** Mean relative number of synaptic vesicles released after a single stimulation calculated by dividing the EPSC amplitude (**C**) between the averaged mEPSCs amplitude (**B**) at 5 min intervals during 25 µg/ml tubulin dialysis (blue, n = 11) or in control conditions (black, n = 14). Dots indicate mean ± s.e.m. Asterisks indicate significant differences relative to basal values using the one-way repeated measures ANOVA followed by the Dunnett's multiple comparisons test, \*p<0.05, \*\*p<0.001, \*\*\*p<0.0001.

# 6 Effect of microtubule depolymerization on synaptic transmission

Having assessed the effect of promoting MT polymerization on synaptic function, we next investigated the effect of enhancing MT depolymerization. Since promoting MT polymerization resulted in postsynaptic potentiation, it is possible that MT depolymerization is used to scale down postsynaptic function, for example to provide negative feedback during long-term potentiation caused by Hebbian plasticity mechanisms.

MT dynamic instability is a rapid process difficult to study by conventional techniques such as pharmacology or genetic modifications. Photoswitchable tubulin-depolymerizers are powerful tools for the study of MTs dynamics in biological processes given their spatiotemporal precision (Castle & Odde, 2015). Photostatins were the first photoswitchable microtubule-inhibiting small molecules to be developed (Borowiak et al., 2015). PSTs are azobenzene-based analogs of combrestatin A-4 with the ability to be switched on (*cis*-state) under violet light (390 nm) or switched off (*trans*-state) under green light (514 nm) or by spontaneous relaxation.

## 6.1 Study of the effect of MT depolymerization induced by photocontrollable molecules on synaptic transmission

To study the impact that MT instability might have on synaptic transmission, we exploited the properties of PST-1. First, we aimed to adjust the PST-1 concentration, incubation time, and light protocol necessary to induce a differential and reversible effect on synaptic function without causing any toxic effect on non-treated neurons.

SCMs were incubated with 150 nM PST-1 for 12 min and were abundantly washed (2 min) to ensure there were no amounts of extra-cellular compounds left that could change the concentration of PST-1 inside the cell among experiments. Recording of evoked postsynaptic responses to assess synaptic strength (EPSC) together with recording of mEPSCs were performed in the dark (basal conditions) and during alternating 8- or 12-min phases of violet (410 nm) and green (535 nm) light to switch PST-1 between its active and inactive states. Because PSTs absorb violet light better than green light, a single pulse of 2 s was used to photoswitch *trans*-PST-1 to *cis*-PST-1. Photoconversion to the inactive state was performed by giving 20 s pulses of green light for longer periods, 8 or 12 minutes, to complement photoisomerization with spontaneous relaxation of the compound.

Results showed that synaptic strength was not affected by PST-1 under these experimental conditions and neither in control conditions (DMSO) when illumination pulses were applied (Fig. 81A and B, left). Frequency of mEPSCs, however, increased as a



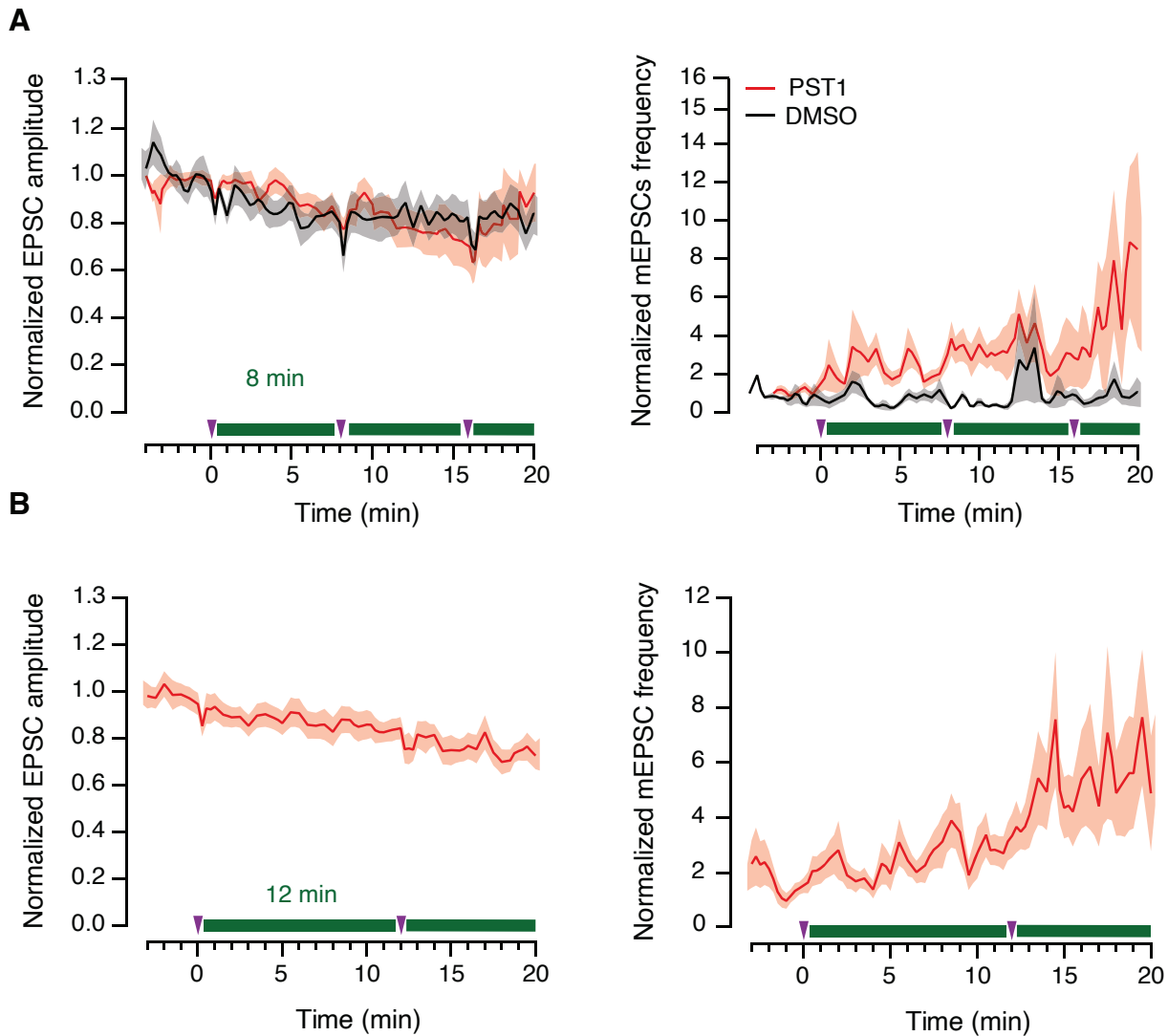


**Figure 81. Characterization of the effect of PST-1 on synaptic function.** Single cell microcultures (SCMs) were incubated with 150 nM PST-1 (red) or 0.0015% DMSO (black) for 12 min and were abundantly washed for 2 min. Excitatory postsynaptic currents (EPSCs, left) and miniature events (mEPSCs, right) were recorded in basal conditions (dark, 3 min) and during alternating 2 s pulses of 410 nm illumination followed by 8 min (A) or 12 min (B) phases of 20 s pulses of green light (535 nm). Constant green transmitted light was applied during PST-1 photoisomerization to the *trans* state. Notice how EPSC amplitude was not affected by *cis*-PST-1 whereas the frequency of mEPSCs increased as a function of experimental time in a light-independent manner. Experimental conditions: **A)** neurons incubated with 150 nM PST-1 ( $n = 13$ ) or DMSO ( $n = 6$ ) under 8 min illumination intervals. **B)** neurons incubated with 150 nM PST-1 ( $n = 17$ ) under 12 min illumination intervals.

function of experimental time upon illumination with violet light. This effect was not reversed after illumination with green light (Fig. 81A and B, right).

A total of 81% of PST-1 molecules are switched to their *trans*-isoform under green light illumination whereas the remanent 19% of *cis*-PST-1 molecules relax spontaneously to its inactive state with a half-life relaxation of 12 min (Borowiak et al., 2015; PST guideline kindly provided by Dr. Thorn-Seshold). Our results show that, even when the phase

of green light was prolonged up to 12 min, to achieve maximal spontaneous relaxation of *cis*-PST-1 (leaving ~10% *cis*-PST-1), the effect of PST-1 on mEPSC frequency was not reverted (Fig. 81B, right).

These data suggest that MT depolymerization might influence spontaneous neurotransmitter release without affecting synaptic strength. However, changes observed in mEPSC frequency were not reversible. That could be due to the **long half-life of *cis*-PST-1**. It might be that 12 min was not enough to reduce the remaining *cis*-PST-1 under its bioactivity threshold. It was also possible that increases of spontaneous neurotransmitter release were caused by **microtubule repolymerization**. Enhancement of spontaneous neurotransmission was observed during the green illumination phase, after depolymerization has been triggered by applying 2 s of violet light. Thus, it could be that repolymerization, rather than depolymerization, was what caused synaptic vesicles to spontaneously fuse with the plasma membrane. Finally, we should discard *cis*-PST-1 **off-target effects**.

To evaluate the first possibility, we assessed the effect of MT depolymerization on SCMs using Photostatin-2 (PST-2), which displays the shortest half-life (45 s) among all PSTs. To ensure that illumination of PST-2 with violet light, but not green light, was responsible for the changes observed in synaptic function, the phase of violet illumination was extended up to 3 min.

Unfortunately, enhanced spontaneous SV release and modifications in sodium currents were observed in control conditions when constant 3-min 410 nm illuminations were applied, reflecting a toxic effect of violet light. Kinetics of sodium currents evoked by depolarization presented a slower inactivation profile upon constant violet illumination (Fig. 82A). In addition, sporadic sodium spikes were observed in resting conditions, indicating the anomalous opening of sodium channels at hyperpolarized membrane potentials (-60 mV; Fig. 82B). These observations indicated that excessive illumination of neurons with violet light produces toxic effects that alter both, neuronal electrical properties, and spontaneous neurotransmitter release rates.

Different illumination patterns were applied to control neurons until we obtained a non-toxic light protocol. To differentiate the pressumable target-specific effect of photostatins on SV spontaneous release from phototoxicity artefactual effects, changes in sodium currents were used as a readout for light toxicity in non-treated neurons.

To avoid phototoxicity and still validate that the effect observed on spontaneous neurotransmission was due to MT depolymerization caused by *cis*-PST-2 (violet phase), but not MT-repolymerization (green phase), 3 s violet light pulses were applied every 30 s for 3 min. Following the PST-2 activation phase, illumination of neurons with 535 nm was applied for 4 min to photoconvert PST-2 to its inactive state (Fig. 83A). Since green light photoswitches 85% of PST-2 molecules to their inactive state, and considering PST-2 has a half-life of 45 s, virtually no *cis*-PST-2 molecules (~0.5%) should

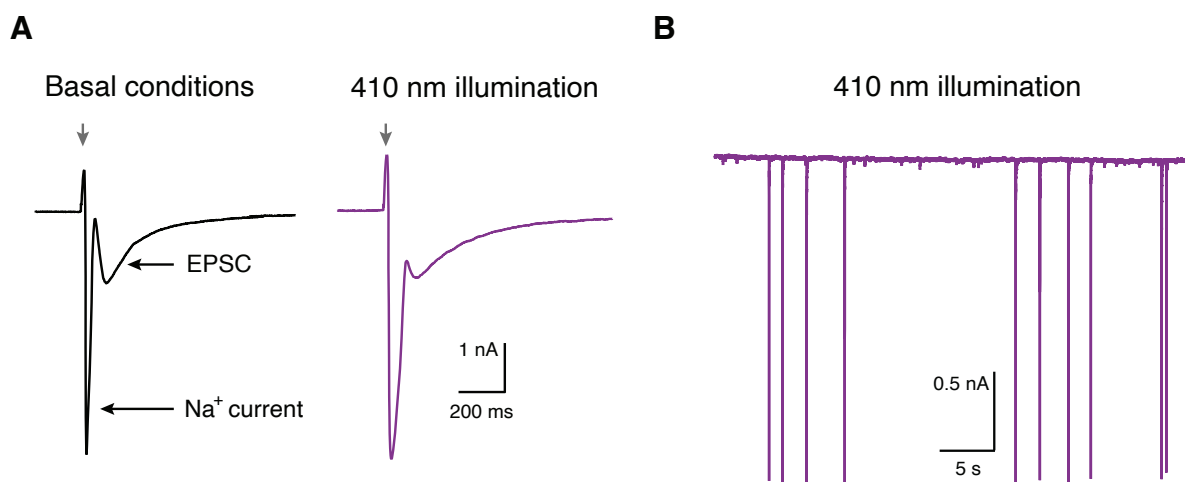


**Figure 82. Representative example of the toxic effect of violet light on sodium channels.** Neurons overexposed to violet illumination with a pulse of 3 min showed: **A)** evoked sodium current increases associated to excitatory postsynaptic currents (EPSCs) and **B)** spontaneous  $\text{Na}^+$  spikes under resting conditions, when the membrane potential was clamped at  $-60$  mV. Notice how increases in sodium current are associated to slower gating kinetics (delayed inactivation of  $\text{Na}^+$  channels).

remain at the end of the inactivation phase.

SCMs were incubated with 1 mM PST-2 for 12 min and were abundantly washed. Recording of evoked postsynaptic responses and mEPSCs were performed in the dark (basal conditions) and during alternating periods of violet and green light. As reported previously (Perez-Gonzalez et al., 2008), the averaged mEPSC frequency of cholinergic microcultures is  $\sim 1$  Hz. Thus, only neurons presenting mEPSCs frequencies below this value in basal conditions were selected for testing.

Stopping MT polymerization by activating PST-2 with 410 nm light pulses increased spontaneous synaptic vesicle release within 3 minutes (Fig. 83B), indicating that the effect was produced by violet (MT depolymerization) and not green light (MT repolymerization). However, as it occurred in PST-1 experiments, illumination with green light did not revert this effect. Neurons incubated with 0.01% DMSO and illuminated the same way as before to assess light toxicity did not show any effect on the number of cumulative mEPSCs (Fig. 83B). EPSC amplitude was not modified in neurons incubated with PST-2 and neither in control conditions (Fig. 83C).

Altogether, these observations suggest that MT depolymerization enhances spontaneous synaptic vesicle release and indicate that despite the almost complete photoisomerization of PST-2 to its inactive isoform at the end of the 535 nm illumination phase, the effect produced by MT catastrophe on mEPSC rate is not reversible.

To rule out the possibility that the more spontaneous vesicles were being released due to off-target effects caused by intrinsic instability linked to azobenzene-based molecules, we repeated the same experiments using the next generation of photocontrollable

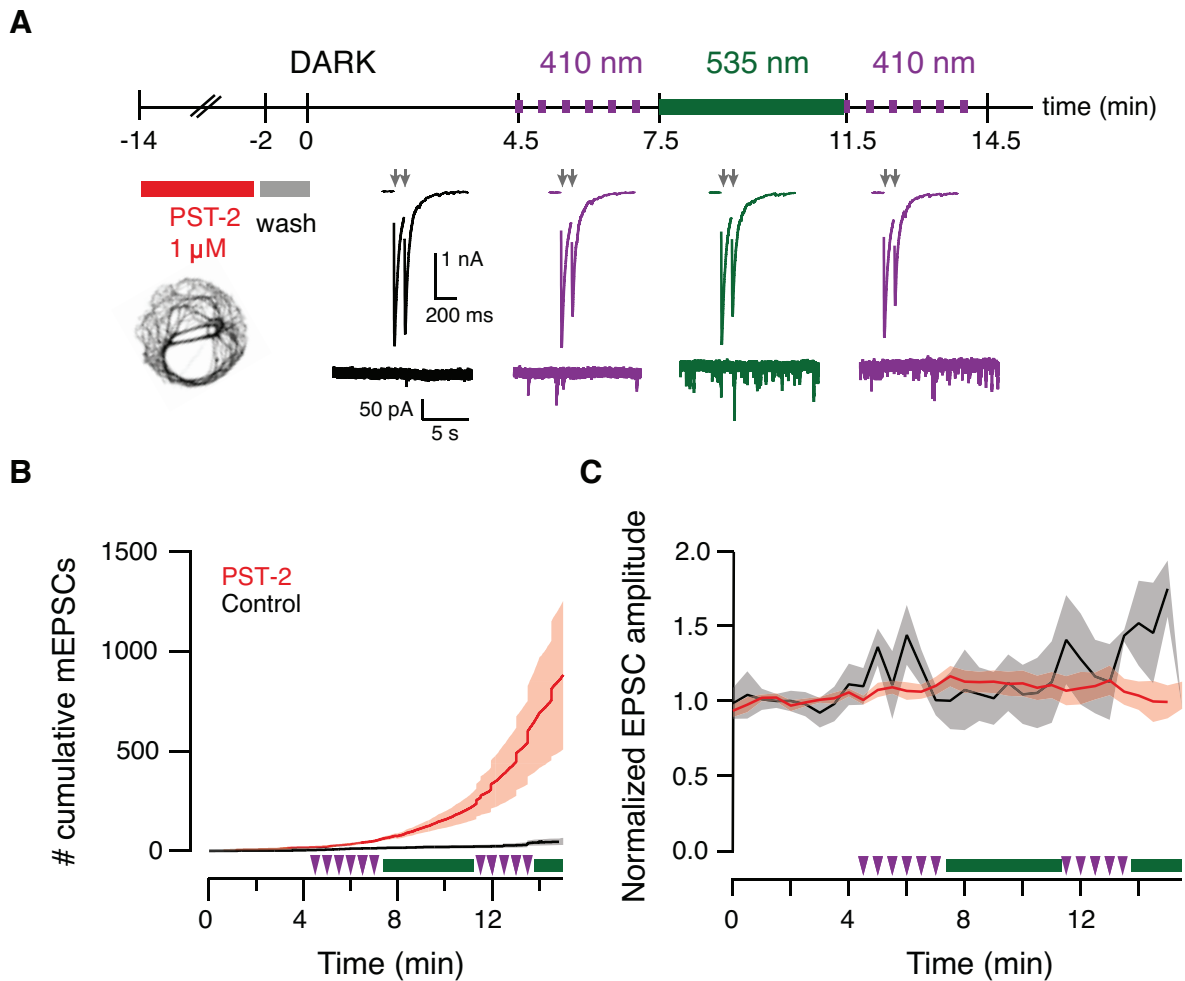


**Figure 83. Microtubule depolymerization by PST-2 causes irreversible increases in spontaneous synaptic vesicle release without altering synaptic strength. A)** SCMs were incubated with the photoswitchable molecule PST-2 at 1  $\mu$ M or 0.01% DMSO for 12 min and were abundantly washed for 2 min before recording. EPSCs and mEPSCs were recorded for a basal period of 4.5 min in the dark. Sequential periods of violet (3 s every 30 s for 3 min) and green light (constant 4 min illumination) were used to photoswitch PST-2 between its active and inactive state, respectively. **B)** and **C)** Mean number of cumulative mEPSCs and normalized EPSC amplitude as a function of experimental time in neurons treated with PST-2 (red,  $n = 14$ ) or DMSO (black,  $n = 8$ ). Notice how increases in the number of cumulative mEPSCs were well described by a power function in neurons incubated with PST-2 and illuminated ( $mEPSC(t) = 0.01 + t^{4.18}$ ) while mEPSCs accumulated linearly in control conditions ( $mEPSC(t) = 2.12t$ ). Spontaneous release was constantly assessed throughout the experiment while single stimuli were recorded every 30 s. Solid lines and shadowed areas indicate mean  $\pm$  s.e.m. Light patterns are indicated by violet arrows and green lines.

MT-inhibitors, SBTubs, which are styrylbenzothiazole-based tubulin-inhibitors (Gao, Meiring, Kraus, et al., 2021). SBTubs are photoisomerized to the active state (Z-isomer) under 405 nm light, however, they do not revert to the inactive state (E-isomer) neither by photoisomerization nor by spontaneous relaxation, given their robust stability. Thus, the unidirectional photoactivation of SBTubs is conceptually like that of photouncageable inhibitors and was used as positive control of irreversible photoswitching.

Electrophysiological recordings of paired pulses to evaluate synaptic strength and short-term plasticity together with recording of mEPSCs in autaptic neurons incubated with 15  $\mu\text{M}$  SBTub3 or 0.15% DMSO (Fig. 84A) showed comparable effects to that of PST-1 and 2 (Fig. 81 and 83). The number of cumulative mEPSCs raised in SB-Tub3-treated neurons only after receiving violet illumination following a power function (Fig. 84B). EPSC amplitude was not altered in SBTub3-treated neurons and neither in SCMs treated with DMSO (Fig. 84C). In both conditions PPR decreased equally as a

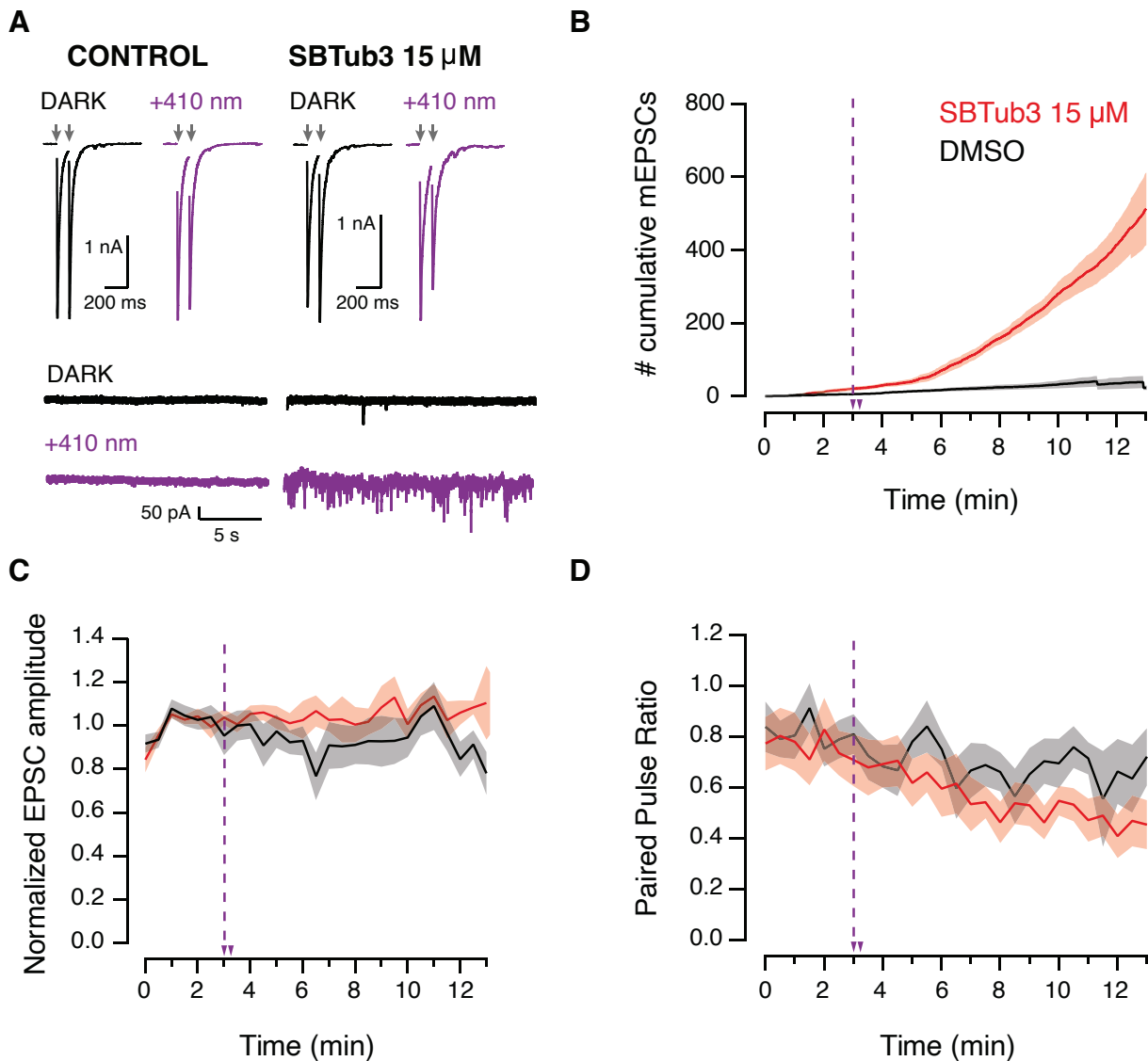


**Figure 84. The photocontrollable MT polymerization inhibitor SBTub3 triggers spontaneous synaptic vesicle release without affecting synaptic strength.** **A)** Neurons were either treated with 15  $\mu\text{M}$  SBTub3 or 0.15 % DMSO. Paired pulses and spontaneous release were recorded in dark conditions (black) and after applying 2 pulses of 3 s of violet light spaced 30 s (purple arrows and dotted line). **B)** Time-course of the mean number of cumulative mEPSCs, **C)** Normalized EPSC amplitude and **D)** Paired Pulse Ratio before and after 410 nm illumination in SCMs treated with SBTub3 (red,  $n = 9$ ) or DMSO (black,  $n = 7$ ). Notice how the number of mEPSCs increased steadily following a power function in neurons incubated with SBTub3 upon illumination ( $\text{mEPSC}(t)=0.99+t^{2.43}$ ) while it accumulated linearly in control conditions ( $\text{mEPSC}(t)=3.03t$ ). Solid line and shadowed areas indicate mean  $\pm$  s.e.m.

function of time (Fig. 84D), presumably due to rundown (Perez-Gonzalez et al., 2008). One possible explanation for the putative spontaneous release of synaptic vesicles entailed by MT depolymerization would be that MTs dynamics somehow increases basal calcium levels. To explore this hypothesis, and using SBTab3, we loaded the internal solution with high concentrations of the calcium chelating EGTA (10 mM and 20 mM, compared to the physiological concentration of 1 mM previously used). If an increase in spontaneous release of vesicles is linked to an increase in calcium levels triggered by MT depolymerization, we should not see increases in spontaneous vesicle release under basal concentrations of intracellular calcium. Like in the previous experiment, we observed that the cumulative number of mEPSCs increased steadily in neurons treated with SBTab3 after receiving 410 nm light pulses (Fig. 85A and B, up). Illumination of neurons treated with DMSO and recorded with 10 or 20 mM EGTA in the internal solution did not cause any effect in mEPSCs cumulative numbers. EPSC amplitude

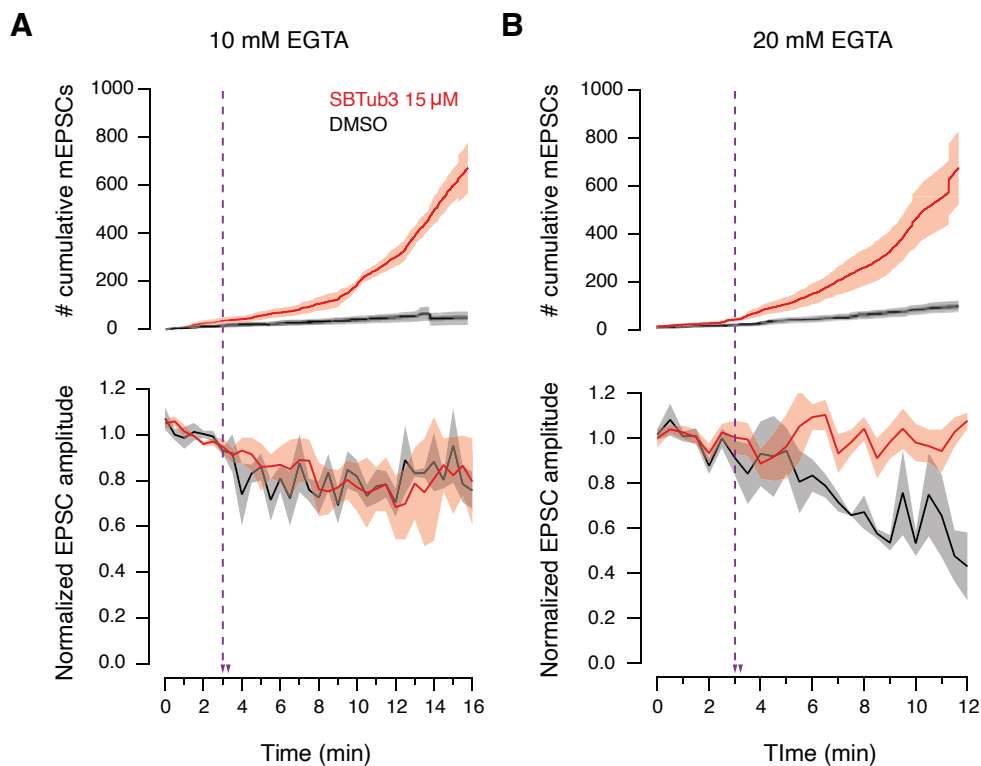


**Figure 85. Increase in the spontaneous release of synaptic vesicles triggered by microtubule depolymerization is a  $\text{Ca}^{2+}$ -independent process.** Spontaneous release (mEPSCs, up) and excitatory postsynaptic responses (EPSCs, down) were recorded in neurons incubated with 15  $\mu\text{M}$  SBTab3 or 0.15 % DMSO. **A)** The number of cumulative mEPSCs was well described by a power function in neurons incubated with SBTab3 when 10 mM EGTA ( $\text{mEPSC}(t)=0.34+t^{2.74}$ ;  $n = 4$ ) or **B)** 20 mM EGTA ( $\text{mEPSC}(t)=0.62+t^{2.64}$ ; SBTab3,  $n = 7$ ) were loaded in the internal solution and illuminated with violet light. mEPSCs accumulated linearly throughout the experiment in neurons incubated with DMSO both when **(A)** 10 mM EGTA ( $\text{mEPSC}(t)=3.65t$ ;  $n = 4$ ) and **(B)** 20 mM EGTA ( $\text{mEPSC}(t)=6.17t$ ;  $n = 10$ ) were loaded in the patch pipette. The number of cumulative mEPSCs and normalized EPSC amplitude is shown as mean  $\pm$  s.e.m. Dotted lines and arrows indicate 410 nm light pulses.



of both SBTub3- and DMSO-treated neurons slightly decreased when in presence of higher amounts of EGTA in the patch pipette (Fig. 85A and B, down).

These data indicate that MT depolymerization elicits the release of genuine mEPSCs, positing MT dynamics as a mechanism for generating spontaneous neurotransmitter release.

Next, to further validate that the enhancement of mEPSC release produced by treatment with photocontrollable MT-inhibitors was the result of a MT-targeted effect, we used combrestatin-A4 as a positive control. CA-4 is a MT-destabilizing molecule that binds to the colchicine-binding site of  $\beta$ -tubulin and alters microtubule dynamics by inhibiting tubulin assembly into microtubules (Gaspari et al., 2017).

Compared to CA-4, the use of CA-4-derived small photocontrollable molecules provide high temporal precision: a specific concentration of the inactive compound diffuses into SCMs for a determined time period and biological activity of the molecule is only achieved upon illumination at a particular time point. In contrast, since CA-4 is already an active biomolecule, its effect appears gradually and depends on the time it takes for the compound to reach its working concentration at synaptic sites. Consequently, electrophysiological recordings to determine the time course of the effect of CA-4 on synaptic transmission poses several challenges, such as the difficulty to maintain SCMs under whole-cell configuration for long periods of time, and inter-cellular variability that complicate the interpretation of the results due to differences in the concentration of CA-4 at the synapse among experiments. Hence, to assess the effect of CA-4 on synaptic transmission, instead of analyzing the time course of cumulative miniature events, basal mEPSC frequency of neurons incubated with 15  $\mu$ M CA-4 for 12 min was evaluated and compared to that of neurons incubated with inactive photoswitchable molecules in the dark or with DMSO.

Treatment of autaptic neurons with CA-4 resulted in significant increases of basal mEPSC frequency compared to that of control conditions ( $p < 0.0001$ ; one-way ANOVA followed by Bonferroni multiple comparisons test). In contrast, basal mEPSC frequency of neurons incubated with inactive photoswitchable molecules PST-1, PST-2 and SBTub3 in the dark were comparable to that of neurons treated with DMSO (Fig. 86). These results confirmed that the active isoform of combrestatin-derived photocontrollable molecules PST1, PST-2 and SBTub3, but not their inactive isoform, mimic the action of CA-4, and therefore can be considered genuine photocontrollable MT-inhibitors.

Collectively, the results obtained from electron micrographs, super-resolution microscopy and electrophysiology linked to photopharmacology reveal the participation of MTs in presynaptic function in which they may define a synaptic pool of vesicles involved in spontaneous neurotransmitter release.

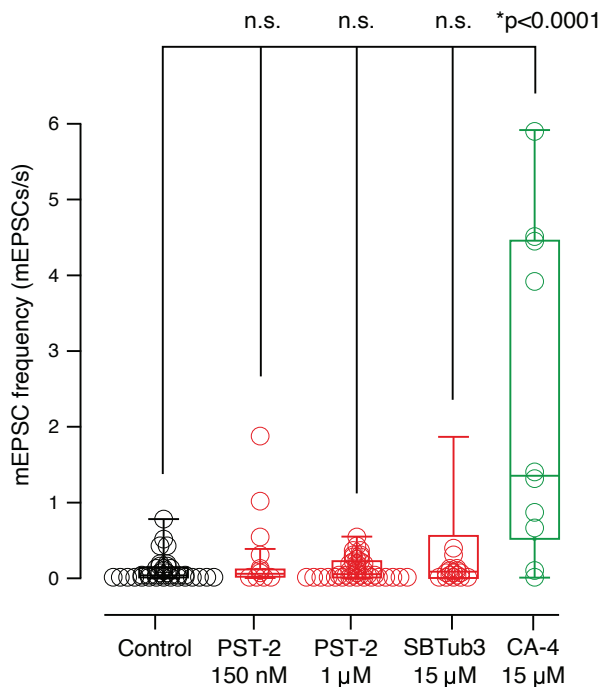


**Figure 86. The small microtubule-inhibitor combrestatinA-4 enhances spontaneous neurotransmitter release.** Box plots showing the median (horizontal line), 25–75% quartiles (boxes), and ranges (whiskers) of basal mEPSC frequency averaged from 3 min of recording of neurons treated with combrestatin A-4 (CA-4,  $n = 10$ ), or the inactive photocontrollable molecules PST-1 ( $n = 11$ ), PST-2 ( $n = 40$ ), SBTub3 ( $n = 16$ ) and DMSO ( $n = 36$ ). Single cell microcultures (SCMs) were incubated with  $15 \mu\text{M}$  CA-4 or photoswitchable molecules at the concentrations indicated for 12 min and were abundantly washed for 2 min. Notice how basal mEPSCs frequency of neurons incubated with CA-4 is significantly increased compared to that of control neurons. Statistical differences were evaluated using one-way ANOVA followed by Bonferroni multiple comparisons test.

## 6.2 Effect of MT depolymerization on postsynaptic function

Although modulation of postsynaptic function was shown to be controlled by MT polymerization (Fig. 79), the fact that synaptic strength was not modified by MT depolymerization triggered by photocontrollable MT-inhibitors suggests that the functional state of the postsynaptic compartment is not affected by MT catastrophe. To further evaluate this hypothesis, we analyzed the amplitude of miniature postsynaptic events before and after 410 nm illumination of neurons treated with SBTub3. Amplitude of mEPSCs remained unchanged in neurons treated with SBTub3 and illuminated with violet light (Fig. 87), indicating that the number of cholinergic postsynaptic receptors is not alte-

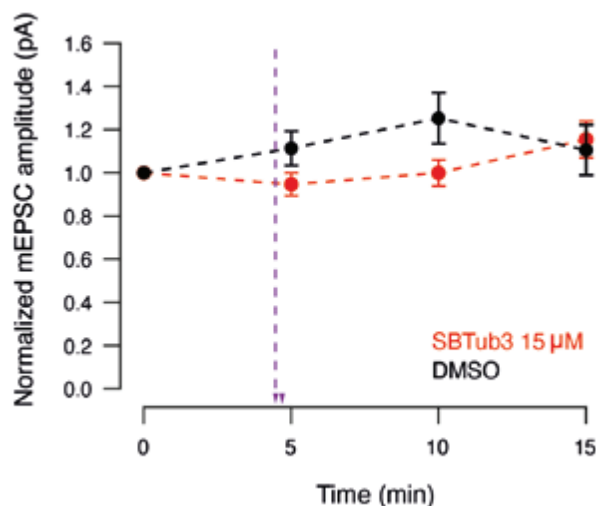


**Figure 87. Microtubule depolymerization does not alter postsynaptic function.** Amplitude of miniature postsynaptic currents (mEPSC) was analyzed as a function of experimental time in neurons treated with  $15 \mu\text{M}$  SBTub3 ( $n = 10$ ) or DMSO ( $n = 8$ ) before and after giving a pulse of 410 nm light for 3 s (dotted line). Differences were evaluated using the one-way repeated measures ANOVA followed by the Dunnett's multiple comparisons test.

red under enhancement of MT depolymerization produced by SBTub3. Illumination of non-treated neurons did not show any effect on mEPSC amplitude.

Accordingly, these results indicate that the hypothesis of MT depolymerization being a mechanism for scaling down the number of postsynaptic receptors is unlikely.

### 6.3 Study of the effect of MT depolymerization produced by KIF18A activity on synaptic transmission

To further investigate the effect of MT plus-end instability on presynaptic function, we sought another method to enhance MT depolymerization in a more physiological framework. KIF18A is a dual functional kinesin, which apart from its plus-end-directed motility common in the kinesin protein family, also displays microtubule depolymerizing activity (Mayr et al., 2007). KIF18A has been shown to accumulate in the plus-ends of kinetochore microtubules during mitosis and to be critical for chromosome segregation by controlling kinetochore microtubule dynamics (Stumpff et al., 2008). Not surprisingly, KIF18A is not expressed in neurons.

Here, we took advantage of the depolymerizing domain of KIF18A (Fig. 88A; Lin et al., 2020) to investigate the role of MT dynamics in spontaneous neurotransmitter release. The cumulative number of mEPSCs increased steadily when 90 nM KIF18A was loaded in the internal solution and dialyzed through the patch pipette (Fig. 88B). Lowering the amount of KIF18A for dialysis resulted in gradual decrease of the observed effect, indicating its concentration-dependance (Fig. 88C). The onset and kinetics of the increase, however, varied among experiments, most likely due to differences in neurons sizes and neuritic tree morphologies, which may affect the dialysis time of KIF18A from the patch pipette to axon terminals. When KIF18A 90 nM ( $p < 0.001$ ; one-way ANOVA followed by Bonferroni comparisons test) or 9 nM ( $p < 0.01$ ), but not 0.9 nM, were added to the internal solution, less time was required to reach 100 mEPSCs (Fig. 88D). Similar to the results obtained using photopharmacology, EPSC amplitude was not affected by dialysis with control buffer nor with any of the three KIF18A concentrations tested. PPR was slightly decreased in the four conditions (Fig. 88E), as seen in experiments with SBTub3 (Fig. 84D).

Overall, these results reinforce the idea of MTs entering synaptic boutons and support the existence of a functional Microtubule Bound Pool (MBP) of synaptic vesicles, which would be directly involved in spontaneous neurotransmission.

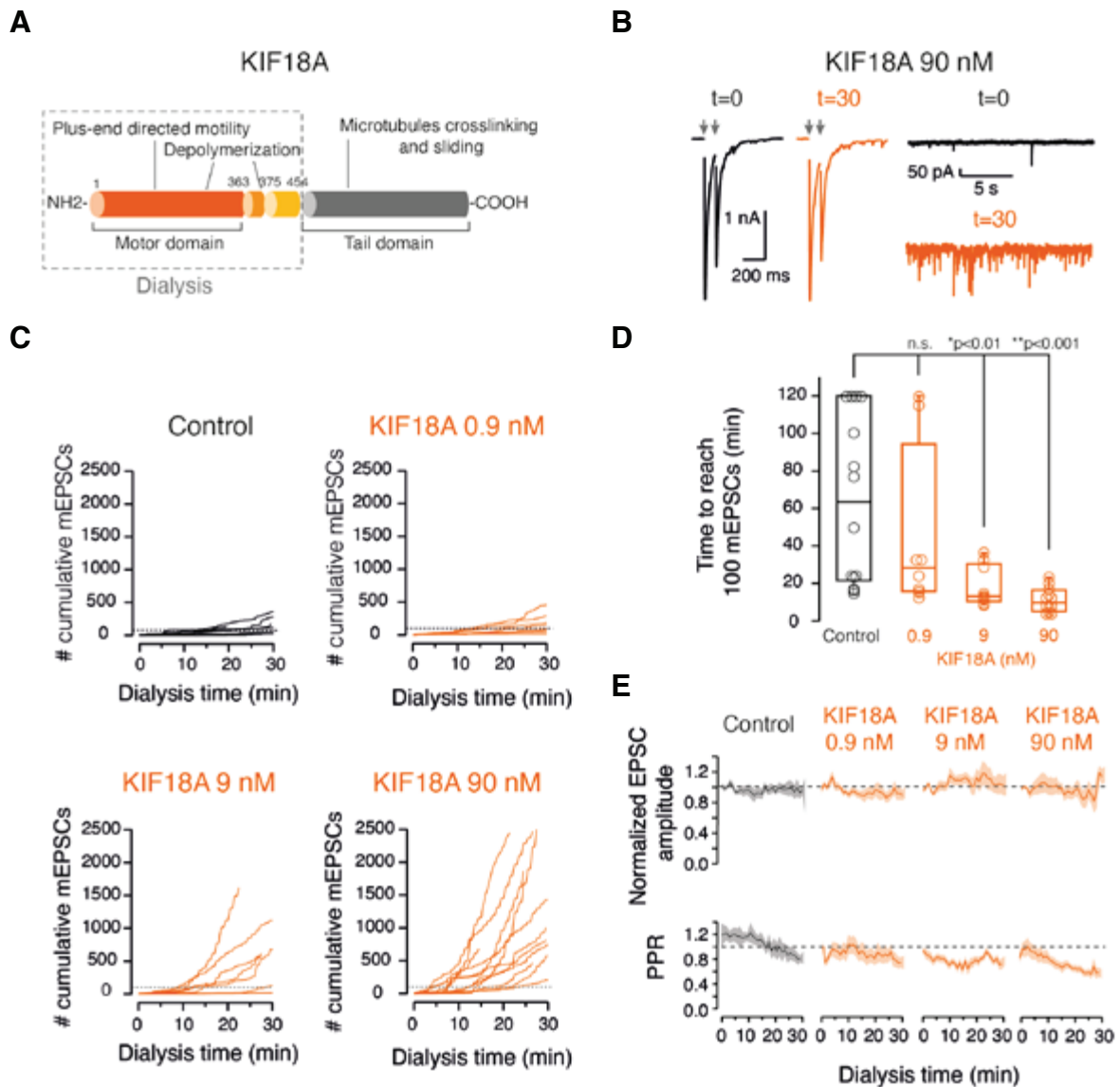


**Figure 88. Microtubule depolymerization by the kinesin family member 18A (KIF18A) increases spontaneous synaptic vesicle release.** **A)** Representation of KIF18A protein domains. The region of KIF18A containing the motor and depolymerization domains (1-453 amino acids) was loaded in the patch pipette at different concentrations to enhance MT depolymerization. **B)** Illustrative examples of the effect of KIF18A on evoked and spontaneous neurotransmission at times 0 (black) and 30 min (orange) of dialysis with KIF18A 90 nM. **C)** Number of cumulative mEPSCs as a function of experimental time in neurons dialyzed with control buffer (black,  $n = 14$ ) or KIF18A at ranging concentrations (orange): 0.9 nM ( $n = 8$ ), 9 nM ( $n = 8$ ) and 90 nM ( $n = 12$ ). Dotted line indicates 100 mEPSCs. **D)** Box plot showing the median (horizontal line), 25-75% quartiles (boxes), and ranges (whiskers) of the time required to reach 100 cumulative mEPSCs in recorded SCMs from **(C)**. If the time to reach 100 mEPSCs was out of the experimental time scope, the value was obtained by lineal regression with 120 min set as a maximum. Statistical differences were evaluated using one-way ANOVA followed by Bonferroni comparisons test. **E)** Time-course of normalized excitatory postsynaptic currents (EPSCs) amplitude and paired pulse ratio (PPR) as a function of experimental time of autaptic neurons recorded with control buffer (black,  $n = 14$ ) or KIF18A (orange) at 0.9 nM ( $n = 8$ ), 9 nM ( $n = 8$ ) or 90 nM ( $n = 12$ ) loaded in the intern solution. Solid lines and shadows indicate mean  $\pm$  s.e.m.

# 7 Characterization of the nature of synaptic vesicles released spontaneously upon microtubule depolymerization

Our results support that polymerization/depolymerization of dynamic microtubule plus-ends located at the presynaptic terminal contribute to spontaneous release of synaptic vesicles from the pool bound to microtubules.

Given the essential role of microtubules on the active transport of presynaptic components to axon terminals, one possibility is that the MBP is constituted by newly formed synaptic vesicles arriving from the cell body. Accordingly, spontaneous neurotransmitter release may mediate the entry of new vesicles into the synaptic vesicle cycle and serve as vesicle buffering of the local synaptic vesicle pool. If on the contrary, synaptic vesicles from the MBP are part of the local synaptic pool of vesicles, another intriguing question would be whether those vesicles from the MBP released spontaneously are also released in response to synaptic activity.

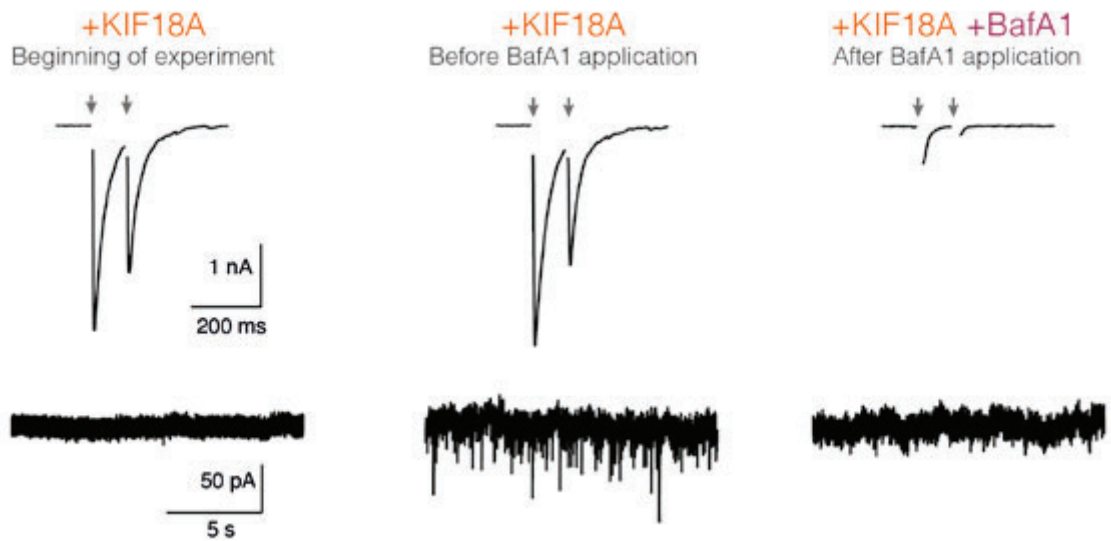
To investigate the nature of the synaptic vesicles belonging to the MBP, we used the ability of Bafilomycin A1 (BafA1) to block the v-type ATPase, a proton pump required for SV reacidification and neurotransmitter refilling (Fernandez-Alfonso & Ryan, 2008), while MTs were being depolymerized due to the KIF18A effect. BafA1 has been used in previous studies to determine the number of SVs contributing to evoked neurotransmission and has been shown to induce a rundown on EPSC amplitude dependent on frequency stimulation (Ikeda & Bekkers, 2009).

We recorded evoked and spontaneous neurotransmission in SCMs dialyzed with KIF18A, or control buffer, before and after acute application of 1  $\mu$ M BafA1 (Fig. 89A). Trains of 14 stimuli at 20 Hz were used to deplete the cytoplasmic pool of vesicles more efficiently upon BafA1 addition. To avoid increases in basal intracellular calcium concentration elicited by high-frequency stimulation, internal solution contained 10 mM EGTA. EPSC amplitude ran down to near 0 after  $\sim$ 15 min or  $\sim$ 5 min of BafA1 addition, in neurons loaded with control buffer (Fig. 89B) or KIF18A (Fig. 89C), respectively; thus confirming the action of BafA1 on blocking synaptic vesicle recycling and silencing SVs. Before the evoked response started to decay due to BafA1 effect, an increase in EPSC amplitude was observed in control conditions, as reported previously (Ikeda & Bekkers, 2009), but not in neurons dialyzed with KIF18A.

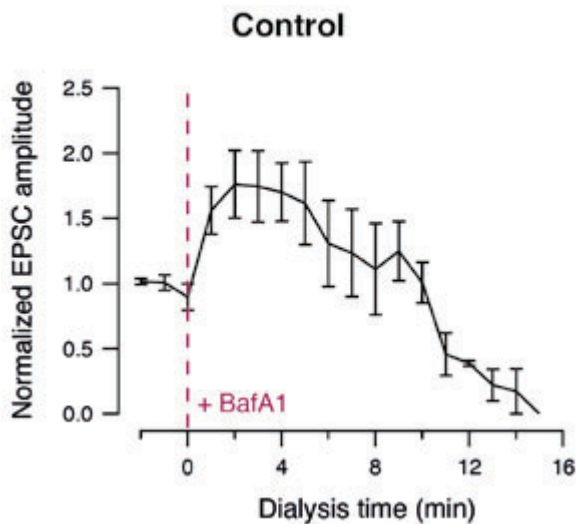
We found that upon application of BafA1, the amplitude of EPSCs and that of mEPSCs induced by the MT depolymerizing activity of KIF18A declined following an exponential function with comparable constant decays (EPSC amplitude,  $\lambda=0.45$  s $^{-1}$ ; mEPSC am-



A



B



C

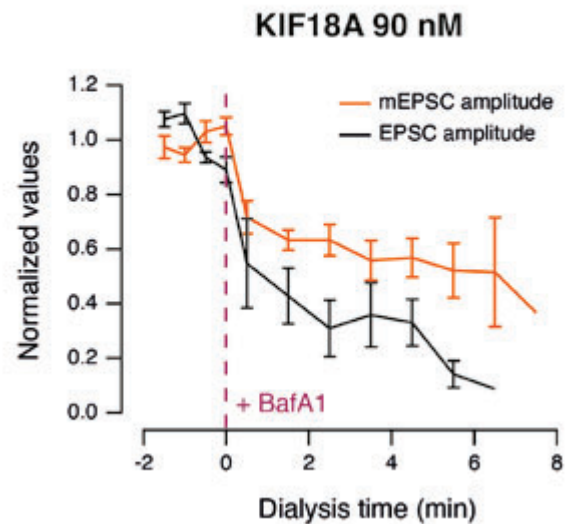


**Figure 89. Acute application of bafilomycin A1 decreases EPSC and mEPSC amplitude. A)** Spontaneous and evoked neurotransmission of single cell microcultures (SCMs) were recorded in control conditions and when 90 nM KIF18A was loaded in the patch pipette. Trains of 14 stimuli at 20 Hz to deplete synaptic vesicles more rapidly were combined with recording of paired pulses and mEPSCs after BafA1 addition. Internal solution contained 10 mM EGTA to maintain presynaptic basal calcium at low levels. Acute application of 1  $\mu$ M bafilomycin A1 (BafA1) was performed at time 0 (dotted line). **B)** Normalized evoked neurotransmission, measured as the amplitude of excitatory postsynaptic currents (EPSC), decreased to minimal values upon BafA1 addition in control conditions ( $n = 5$ ). Notice how the postsynaptic response increased right after BafA1 addition. **C)** Normalized EPSC and mEPSC amplitude of neurons dialyzed with 90 nM KIF18A ( $n = 6$ ) before and after addition of BafA1. Notice how depleting the cytoplasmic pool of synaptic vesicles by the action of BafA1 decreases both EPSC and mEPSC amplitude. Solid lines and shadows indicate mean  $\pm$  s.e.m.



plitude,  $\lambda=0.49 \text{ s}^{-1}$ ), indicating that both modes of synaptic transmission rely on the use of local recycled vesicles. It was not possible to evaluate the amplitude of mEPSCs in control condition due to the low rate of spontaneous neurotransmitter release.

These observations rule out the hypothesis of the MBP acting as a donor of newly formed synaptic vesicles, and reveal the recycling nature of synaptic vesicles from the MBP.

Despite the fact that synaptic strength was not affected by MT depolymerization while spontaneous release was (Fig. 81, 83, 84, 88), blocking synaptic vesicle recycling decreased both, EPSC and mEPSC amplitude, suggesting that synaptic vesicles engaged in both modes of neurotransmission are pulled from a common pool.

Taken together, our results uncover a functional role for the morphologically identified pool of vesicles bound to microtubules and reveal that MT dynamics are associated to spontaneous release of synaptic vesicles from this pool.





# DISCUSSION



The massive number of synapses formed during embryogenesis is refined during postnatal development by a process known as synaptic pruning. Despite the essential role of synaptic activity, increasing evidence involves the role of glial cells in this process by mediating debris clearance and secreting molecules that promote synapse disassembly. One example of these glial-secreted molecules is the protein SPARC, whose expression peaks during synaptic pruning. The SPARC-derived peptide p4.2 has been shown to recapitulate the activity of the full-length SPARC protein and to trigger a cell-autonomous program of synapse elimination (López-Murcia et al., 2015).

In the current thesis we have exploited the action of the peptide p4.2 to investigate how an autaptic network reacts to synapse loss (Fig. 55). We found that neurons grown in an autaptic circuit compensate for synapse elimination by activating a mechanism of presynaptic homeostatic plasticity without modifying the number of postsynaptic receptors. This compensatory response was driven by potentiation of presynaptic function and the assembly of new synaptic contacts (Fig. 89).

In agreement with previous results (López-Murcia et al., 2015), autaptic neurons grown in the absence of glial cells and exposed to p4.2 for ~6 h displayed decreases in synapse numbers and synaptic strength. Moreover, longer incubation times with p4.2 (~30 h) showed that neurons are able to compensate synapse elimination and bring synaptic transmission levels back to the original state (Fig. 56). In addition, we showed that the action of peptide p4.2 neither involves changes in synaptic excitability (Fig. 57) nor in the density of postsynaptic receptors (Figs. 67 and 68). These data suggest that during postnatal synaptic pruning, when correct processing of information concurs with massive synapse loss, neurons are able to sense and adjust synaptic strength to maintain a baseline level of synaptic activity within a given neuronal network.

Early studies on the effect of SPARC in endothelial cells already revealed the ability of peptide p4.2 to reorganize the F-actin cytoskeleton (Murphy-Ullrich et al., 1995). Our results confirm these observations and suggest that remodelling of the periodic actin skeleton found in neuronal processes (Figs. 70) might be key to disassemble synaptic contacts during synapse elimination. Although it is clear that peptide p4.2 binds to collagen present at the extracellular matrix (Kaufmann et al., 2004; Mayer et al., 1991; Sasaki et al., 1997, 1998), whether the effect observed on the actin cytoskeleton is an indirect consequence of the interaction of p4.2 to other candidate targets of SPARC, such as the previously reported  $\beta$ 3-integrin (Jones et al., 2011) or neuroligin/neurexin (Fan et al., 2021), needs further research.

PHP has been mainly studied using the alteration of postsynaptic receptors as a trigger (Davis & Müller, 2015; Frank et al., 2006). Here, we report that PHP can also be activated in response to synapse elimination. In contrast, synaptic scaling, a homeostatic synaptic mechanism driven by changes in the abundance of postsynaptic receptors, has been reported to participate during synapse formation, maturation, and elimination

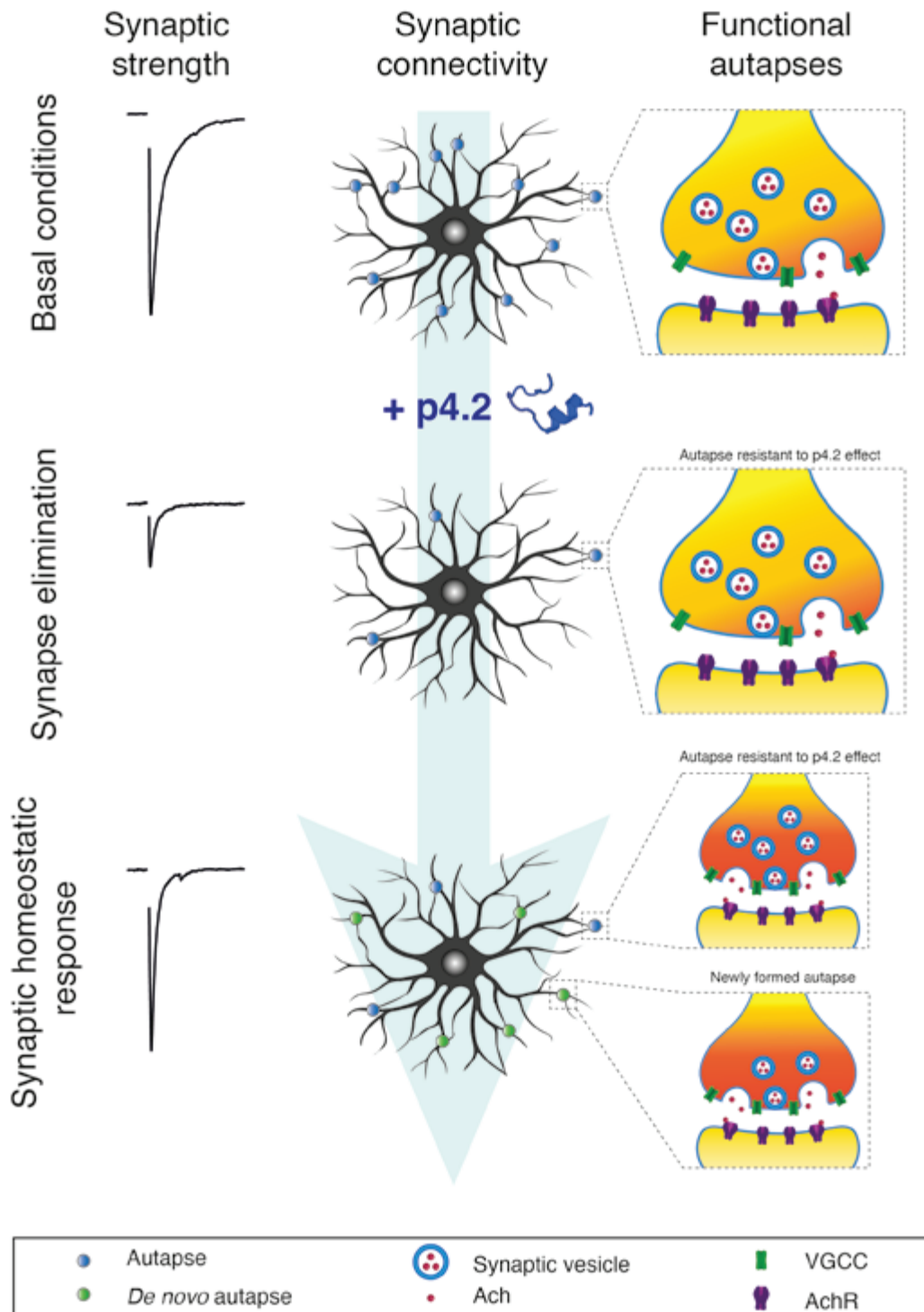


**Figure 89. Schematic representation of the presynaptic homeostatic plasticity response activated in response to synapse elimination in an autaptic circuit.** Synaptic strength, connectivity and functional autapses are represented in basal conditions, upon synapse elimination elicited by peptide p4.2 and at the end of the compensatory response. The number of autapses decreases upon exposure to p4.2 and *de novo* autapses are formed during the homeostatic response. Notice how presynaptic calcium entrance, represented in a red gradient colour, increases at the end of the homeostatic response, both in autapses resistant to p4.2 effect and those newly formed (containing fewer SVs). The number of cholinergic receptors is not modified during the homeostatic response. Abbreviations: acetylcholine (Ach), voltage-gated calcium channel (VGCC) and acetylcholine receptor (AchR).



(Desai et al., 2002; Hooks & Chen, 2006). In these studies, mEPSC amplitudes were scaled up or down as a function of developmental stage, revealing the participation of homeostatic synaptic plasticity in the refinement of synaptic connectivity. The fact that we did not observe changes in postsynaptic function during the compensatory response could be due to differences in the intrinsic properties of *in vitro* models versus *in vivo* models but could also reflect the variability of the *locus* (pre- or postsynaptic compartment) of the homeostatic synaptic plasticity mechanism activated depending on the cell type (Bartley et al., 2008; J. Kim & Tsien, 2008).

One important and yet unresolved question of synaptic homeostatic plasticity regards the signalling pathways by which a neuron senses changes in synaptic activity. Although the functional significance of autapses in neuronal networks is still controversial (John M. Bekkers, 1998), growing evidence support their implication in relevant network functions. For example, autapses in neocortical inhibitory interneurons have been shown to offer feedback inhibition to regulate AP generation (Bacci et al., 2003). Aligned with these findings, additional studies have also supported GABAergic autapses as self-inhibitory elements within neuronal circuits (Connelly & Lees, 2010; Karayannis et al., 2010). Less is known, however, about the physiology of excitatory autapses. A significant study performed in buccal ganglia of *Aplysia* provided the first evidence of a function for excitatory autapses in an intact tissue. In this experimental study it was shown that sustained depolarization in motor neurons, required during feeding behaviour (Hurwitz et al., 2000), is assisted by excitatory autaptic connections (Saada et al., 2009). The positive feedback loop of electrical activity needed to effect behavior may rely on the presence of autaptic neurons. Also, a recent study using dual soma-axon recording combined with 2-photon laser axotomy in acute brain slices, has shown that neocortical glutamatergic PCs form functional autaptic connections and represent an important circuit element in the neocortex by promoting neuronal responsiveness and burst firing (Yin et al., 2018). Our results suggest that excitatory neurons could use autaptic contacts to sense their synaptic output and take advantage of the mechanism here described to increase synaptic weight. As reported previously, synapse disassembly induced by p4.2 triggers the formation of multivesicular bodies and other endocytic structures containing presynaptic elements (López-Murcia et al., 2015). In light of our results, it is possible that retrograde transport of formed lysosomal degradation compartments could be part of the sensing mechanism used during PHP for determining neuron survival (Kononenko et al., 2017; Perlson et al., 2010) and reporting synapse loss. Accordingly, the coordinated potentiation of presynaptic terminal function with *de novo* synapse formation used for setting a correct level of neurotransmission might unmask a biologically relevant role of autapses. Future experiments using intact circuits should verify if excitatory autapses are indeed keepers of neuronal firing.

We found that the compensatory response involves an enhancement of presynaptic calcium influx (Figs. 65) and RRP size (Fig. 63), which are both hallmarks of presynaptic homeostatic plasticity (Davis & Müller, 2015). However, our results show that *de novo* synapse formation is also part of the presynaptic homeostatic mechanism activated to keep synaptic transmission at basal levels in response to synapse loss.

Although the molecular pathways underlying compensatory changes during PHP are still unclear, one possibility is that the homeostatic response is orchestrated from the cell body. If that were the case, the increase in presynaptic calcium entry observed was probably mediated by the insertion of VGCC copies at the synapse. Changes in the molecular composition of VGCCs, as well as, of certain accessory subunits or adhesion proteins present in the presynaptic terminal, could be important for establishing functional synapses in an altered neuronal cytoskeleton. By the end of the compensatory phase, however, all synapses experimented a comparable potentiation of presynaptic calcium entry (Fig. 65), indicating that any molecular modification was not determinant for setting functional differences among autaptic contacts resistant to the effect of p4.2 and those formed *de novo*. The widespread gain of function could be related to the use of cultured neurons (Pozo & Goda, 2010), but could also be reflecting a specific property of autaptic circuits.

In addition to the potentiation of presynaptic function in response to synapse elimination, the compensatory response also involved rapid synapse formation to bring neurotransmission to basal levels (Fig. 61). Our data show that, upon p4.2 exposure, autaptic neurons sensed which could have been excessive synapse loss and activated a compensatory mechanism to form a finite number of new synapses in a very little time (~2.5 h). The fact that synapse numbers were not completely restored to original levels while synaptic strength was, reflects the fine adjustment of synaptic transmission achieved by combining two mechanisms operating in parallel: presynaptic potentiation and *de novo* synapse formation. A quantitative estimate of synaptogenesis occurring during the homeostatic response can be drawn considering that a prototypical SCM contains ~200 synapses. Upon exposure to p4.2, the neuron would react to synapse elimination by forming ~75 new contacts in 10 h. If the assembly time of cholinergic autaptic synapses is found between ~1 (Bresler et al., 2004) and 2.5 h (Fig. 61), it would mean that SCMs establish 3–8 new contacts hour<sup>-1</sup> in response to synapse elimination. Considering a likelihood of finding the formation of a contact in cultured neurons of 0.4–1% (Friedman et al., 2000), basal synapse formation could increase by almost an order of magnitude during the homeostatic response. In other words, a neuron growing in a SCM takes a week to establish all its contacts (Albrecht et al., 2012) but, in front of a significant synapse loss, the neuron can recover one third of its synapses just in half a day. These observations highlight the fine regulation of synaptic connectivity to maintain neurotransmission at basal levels.

By the end of the homeostatic response, mature and recently assembled autapses coexist. Our results show that synapse formation allowed the re-establishment of synaptic strength to levels previous to synapse elimination and likely contributed to the observed increase in RRP size, which could be accomplished by the activation of certain regulatory mechanisms operating at the level of active zones (Müller et al., 2012). However, while synaptic strength recovered completely during p4.2 exposure, RRP did not (Fig. 63), which could be owed to the small RRP size found in immature contacts (Ahmari et al., 2000; Albrecht et al., 2012). In line with this observation, short-term plasticity was shifted towards a depressing phenotype at the end of the homeostatic response, but not during synapse elimination (Fig. 62), also reflecting the limited availability of synaptic vesicles in the immature contacts formed *de novo* as part of the homeostatic response.

Although it is an open question how presynaptic assembly could succeed to set functional synapses under a disrupted neuritic F-actin cytoskeleton (Fig. 70), what is certain is that presynaptic components had to be conveyed from the cell body to the synapse through microtubule active transport in order to assemble new synaptic contacts. The fact that a limited number of synapses were rapidly formed (Fig. 61) highlights the exquisite control of the homeostatic response and suggests the participation of microtubules in the maintenance of synapse numbers and synaptic strength. It is possible that the presynaptic homeostatic plasticity mechanism described here in response to synapse elimination relies on changes of MT active transport driven by increases in MT polymerization to rapidly assemble *de novo* synapses and to facilitate presynaptic calcium influx potentiation by means of increasing the number of VGCCs.

There is a long-standing debate on the role of microtubules in synaptic transmission. For many years, it was thought that microtubules provide structural support to the axon and dendrites necessary for MT active transport, with no direct contribution to synaptic transmission. This assumption has been questioned in the last two decades and it has been demonstrated that MTs play additional roles to synaptic function in both pre- and postsynaptic terminals (Adapted from Parato & Bartolini, 2021). Yet, the participation of MTs in synaptic function is still far from being understood.

To investigate the contribution of MTs to PHP it was first necessary to characterize what might be the role of dynamic MTs at the synaptic level. Previous observations from seminal EM studies showed that MTs are found at pre- and postsynaptic terminals (Gray, 1975; Westrum & Gray, 1977), and that a group of SVs are attached to MTs in synaptic boutons. Our findings support these observations (Fig. 75). Yet, for dynamic MTs to directly contribute to synaptic transmission, as it has been shown for actin filaments (Morales et al., 2000), MT plus-ends should be found at synaptic sites. Our results show that MT plus-ends are indeed associated with SVs and invade synaptic boutons (Figs. 76 and 77), suggesting a role for dynamic MTs at the presynaptic ter-

minal.

We first sought to investigate whether enhancement of MT polymerization might be used as a mechanism for regulating synaptic weight in an autaptic circuit by raising the free-tubulin pool. Although we did not directly visualize MT polymerization, it is expected that adding  $\alpha/\beta$ -tubulin heterodimers to the patch pipette during electrophysiological recordings resulted in more dynamic MTs undergoing polymerization. Enhancement of MT polymerization increased synaptic strength in a tubulin-concentration manner (Fig. 78) by potentiating postsynaptic function (Fig. 79) without altering the properties of the presynaptic terminal (Fig. 80). These results suggest that dynamic microtubules are not determinant for controlling presynaptic function in basal conditions. Nonetheless, how modifications in tubulin availability may impact the presynaptic homeostatic response observed upon synapse loss is an intriguing question. Due to time limitations, these experiments were out of the scope of this thesis.

Our observations are in line with previous studies showing that dynamic MTs direct cargo transport towards postsynaptic terminals (McVicker et al., 2016), enter dendritic spines in an activity-dependent manner and influence spine enlargement (Hu et al., 2008; Merriam et al., 2013). Invasion of MTs in dendritic spines during synaptic plasticity may be essential for MT-dependent motors to deliver specific cargoes, for example postsynaptic receptors or PSD95, and contribute to PSD molecular composition (Hu et al., 2011). Accordingly, either specific insertion of cholinergic receptors into the PSD or general insertion of AchR into both synaptic and extrasynaptic sites of the plasma membrane could account for the positive effect of MT polymerization on postsynaptic function. However, because the postsynaptic potentiation observed increased synaptic strength by  $\sim 20\%$  in a very short time ( $\sim 10$  min), a mechanism of massive non-specific insertion of AchR copies promoted by MT polymerization seems more likely. Enhanced MT polymerization could increase MT active transport and facilitate that more cholinergic receptors reach the postsynaptic membrane. In addition, mechanisms of lateral diffusion could mediate the clustering of newly inserted postsynaptic receptors to the PSD (Chiu et al., 2019; Choquet & Triller, 2013; Heine et al., 2008).

The fact that increases in synaptic strength induced by enhancing MT polymerization were tubulin concentration-dependent highlights the role of the free-tubulin pool as a key for regulating postsynaptic function through MT polymerization. If that were the case, one interesting possibility is that MT polymerization is used as a mechanism for regulating the number of PSD proteins reaching postsynaptic sides during synaptic scaling to rapidly compensate decreases in synaptic weight produced by unbalancing forces.

Overall, our results reinforce the idea of MTs invading postsynaptic terminals and associate MT dynamics to postsynaptic plasticity in which MT polymerization might underlie a powerful and non-specific mechanism for the insertion of postsynaptic receptors.

To further investigate the role of MTs in synaptic transmission, we induced MT depolymerization by different approaches, namely the use of CA-4-derived photocontrollable MT-inhibitors (Figs. 81,83,84) and the MT depolymerizing domain of the protein KIF18A (Fig. 88). On one hand, CA-4 is a MT-destabilizing drug whose mechanism of action relies on its binding to the colchicine domain of  $\beta$ -tubulin, thus preventing its assembly into MTs (Gaspari et al., 2017). On the other hand, the dual-function kinesin KIF18A accumulates at MT plus-ends and inhibits MT assembly (Du et al., 2010). In both cases, suppression of MT polymerization shifts MT dynamics into a depolymerizing state. Because promoting MT polymerization potentiated evoked responses, we expected enhancement of MT depolymerization to elicit the opposite outcome, synaptic depression, for example by impairing MT active transport of synaptic material to pre- and/or postsynaptic sites. That was not the case. Enhancement of MT depolymerization raised spontaneous synaptic vesicle release without altering synaptic strength (Figs. 81,83,84) or the properties of the postsynaptic terminal (Fig. 87), indicating that, at least on the timescale investigated, MT depolymerization solely affected spontaneous, and not evoked, neurotransmission. That might be explained by the excess of synaptic components required for synaptic activity at low frequency stimulation but could also be due to the fact that dynamic instability of postsynaptic MTs was not affected by the depolymerizing agents here used, for example due to the binding of MT associated proteins and posttranslational modifications that confer resistance to MT catastrophe (Janke & Magiera, 2020).

Although the morphologically identified pool of SVs bound to MTs had been previously identified (Gray, 1975), suggesting the involvement of MTs in SV pool organization, its functional relevance had remained a mystery. The fact that promoting depolymerization of presynaptic MTs fostered spontaneous neurotransmitter release is in line with the ultrastructural (Fig. 75) and morphological (Fig. 77) data shown here demonstrating the dynamic nature of presynaptic MTs entering presynaptic boutons.

Based on these findings, we aimed to investigate the impact of MT instability on synaptic transmission. Our electrophysiological results indicate that MT depolymerization is determinant for spontaneous neurotransmitter release. Spontaneous neurotransmission reflects the release of neurotransmitters from a single vesicle and occurs when the neuron is at rest. Although the discovery of spontaneous neurotransmission (Fatt & Katz, 1952) set the basis of the quantal theory, the mechanism by which synaptic vesicles are spontaneously released is still a matter of debate.

To reproduce the dynamic instability of MTs and promote MT depolymerization in our culture system, two types of photocontrollable MT-inhibitors were used: the bidirectional photoswitchable photostatins (PST-1 and PST-2) and the unidirectional photoswitchable SBTub3. Whereas photoswitching photostatins to their active state enhanced spontaneous SV release, photoswitch to their inactive isoform did not reverse this



effect (Figs. 81 and 83). That could be due to the remaining percentage of active photostatin that cannot be photoswitched by light but only spontaneous relaxation in the case of PST-1, but not PST-2, since its half-life is extremely short (45 s). It could also be that the metabolic instability inherent in azobenzenes-based molecules resulted in off-target effects, leading to stochastic SV release. However, this possibility was ruled out because CA-A1 (Fig. 86) and SBTub3 (Fig. 84) increased spontaneous neurotransmitter release, proving the specific MT-targeted effect of photostatins. In addition, MT depolymerization promoted by physiological means using the depolymerizing kinesin KIF18A (Fig. 88) further confirmed the pharmacological effect of combrestatin and its photoswitchable derivatives PST-1, PST-2 and SBTub3 on spontaneous synaptic transmission. Although SBTub3 showed to be a powerful and robust photocontrollable tool for promoting MT instability despite its unidirectional nature, forthcoming photoswitchable molecules may clarify whether the irreversibility observed in the effect of PSTs on spontaneous neurotransmitter release is owed to the lack of reversibility of these molecules or if the original state of MTs cannot be rescued by simply resuming MT polymerization but requires additional regulation factors.

Spontaneous neurotransmission occurs at low presynaptic calcium concentrations (reviewed in Kavalali, 2015). To rule out the possibility that MT depolymerization could be raising basal calcium levels that in turn would lead to asynchronous, and not spontaneous, release of synaptic vesicles, we kept calcium levels low by adding high concentrations of EGTA in the internal solution during MT depolymerization. We observed the same effect on spontaneous SV release (Fig. 85), supporting the hypothesis of MT instability as a mechanism for originating genuine spontaneous neurotransmitter release. Increase in the number of cumulative mEPSCs due to MT depolymerization was well described by a power function, which could be explained by a phenomenon of synchrony elicited by the MT depolymerizing agents used here. In other terms, in basal conditions, dynamic MTs assemble and disassemble at different times among different synapses, producing a lineal increase of cumulative miniature events as a function of time. By triggering MT depolymerization at a precise moment by photoactivating SBTub3, spontaneous neurotransmitter release is somehow "synchronized" in all autapses of the neuronal circuit, causing spontaneous NT release of all synapses to rise in unison.

Similar to the action of presynaptic calcium levels in controlling evoked neurotransmitter release probability, our results suggest that MT dynamics regulates spontaneous neurotransmitter release probability. According to that, it is expected that when MT dynamics is shifted to a depolymerizing state, for instance by the action of combrestatin-like molecules, MT catastrophe events are more likely to occur, and that raises the probability of spontaneous neurotransmitter release.

The steep increase in the number of cumulative mEPSCs observed during MT depoly-



merization reached ~400 mEPSCs in less than 9 min (Fig. 83 and 84). However, it is worth noting that this increase is not that exuberant if we account for the number of synaptic vesicles released at each release site. By measuring EPSC amplitude, and considering a quantal size of 70 pA and a constant release probability of 0.8, we can estimate the total number of release sites of a given autaptic neuron ( $EPSC = N \times Pr \times q$ ) and obtain an approximation of the cumulative number of mEPSCs per release site. An example is represented in Fig. 90. In control conditions, it is estimated that the cumulative number of mEPSCs per release site is below 2 after 9 min of illumination. In neurons incubated with SBTub3, however, each release site releases spontaneously ~10 synaptic vesicles within 9 min since the onset of SBTub3 photoactivation. This approximation shows that although MT depolymerization does increase mEPSC release more than 5 times, the relative number of miniature events released at each synapse is relatively low. This assumption supports the idea that synchronizing MT depolymerization in all autapses of the same neuron by photoactivating SBTub3 leads to the abrupt increase of cumulative mEPSCs observed.

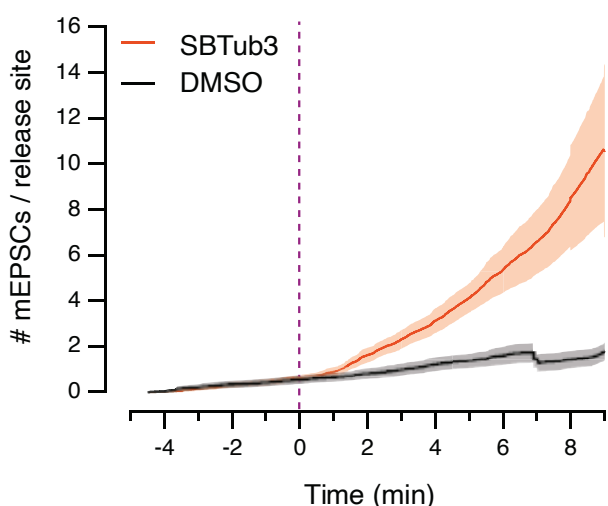


**Figure 90. Estimate of the cumulative number of mEPSCs per release site.** The number of release sites of an autaptic circuit can be estimated by measuring EPSC amplitude and considering a quantal size of 70 pA and a constant release probability of 0.8. Ratio of the cumulative number of mEPSCs and the estimated number of release sites provides an approximation of the number of vesicles released spontaneously at each release site as a function of time.

Generally, synaptic vesicles can be classified into the recycling pool and the non-recycling pool based on their intrinsic propensity to fuse upon stimulation (Alabi & Tsien, 2012). An intriguing and yet unresolved question is whether synaptic vesicles released spontaneously and those released upon stimulation belong to the same pool (reviewed in Chanaday & Kavalali, 2018). While some studies claim that spontaneous and evoked neurotransmitter release pull vesicles from the same pool (Groemer & Klingauf, 2007; Hua et al., 2010; Ikeda & Bekkers, 2009; Prange & Murphy, 1999; Wilhelm et al., 2010), others report they are drawn from different pools (Afuwape et al., 2017; Fredj & Burrone, 2009; Kavalali et al., 2011; Koenig & Ikeda, 1999; Mathew et al., 2008; Ramirez et al., 2012; Sara et al., 2005). These controversial results may be due in part to the type of synapses examined but also to the existence of distinct mechanisms underlying spontaneous neurotransmission, like the one described here.

Our results indicate that, although MT depolymerization boosts spontaneous neurotransmission without affecting evoked neurotransmission and short-term plasticity, synaptic vesicles released upon the arrival of an action potential and those released spontaneously originate from the same synaptic vesicle pool. Addition of bafilomycin A1, to prevent refilling of empty vesicles with acetylcholine during MT depolymerization, decreased both EPSC and mEPSC amplitude, indicating that both forms of synaptic transmission rely on synaptic vesicle recycling (Fig. 88). These data reveal that locally recycled vesicles, rather than *de novo* MT transported SVs, give rise to spontaneous neurotransmission produced by MT depolymerization.

As shown in a previous study, EPSC amplitude rundown during blockade of synaptic vesicle recycling depends on frequency stimulation (Ikeda & Bekkers, 2009), indicating that the more vesicles are released, the faster is the run down in synaptic strength. Interestingly, depletion of the recycling pool, displayed by the nearly complete elimination of the evoked response, occurred ~3 times faster when MT depolymerization was being exacerbated by KIF18A compared to control conditions. Enhanced spontaneous neurotransmission in these neurons could account for faster kinetics in the depletion of a common pool of synaptic vesicles, thus reinforcing the idea that SVs released during evoked and spontaneous synaptic transmission are drawn from the same pool.

Our results suggest that MTs might act as a brake to prevent spontaneous SV release (Fig. 91A). Yet, what might be the molecular mechanism underlying this process should be further investigated. One possibility is that MT disassembly leads to the detachment of synaptic vesicles bound to MTs observed in electron micrographs (Fig. 75). Without any constraints or brake exerted by the synaptic cytoskeleton, SVs can move freely throughout the presynaptic terminal and spontaneously merge with the plasma membrane, thus generating mEPSCs (Fig. 91B). At least two questions arise from this model: i) how are SVs from the MBP spontaneously released upon MT depolymerization? and, ii) how are recycled SVs sorted into what can be ultrastructurally recognized as the cytoplasmic pool and the MBP? Because SVs released during evoked and spontaneous neurotransmission are drawn from the recycling pool (Fig. 88), it is likely that vesicles from the MBP fuse with the plasma membrane using the same AZ machinery. Increase in the number of cumulative miniature events did not occur straight away after photoactivation of PSTs or SBTub3, but it took ~2-3 min (Figs. 81,83,84). Diffusion of MT-detached SVs scattered across the synaptic bouton towards the AZ could account for the delay between the enhancement of MT depolymerization and the boost of spontaneous neurotransmission observed. Yet, it is possible that other factors, such as the F-actin cytoskeleton or further regulatory mechanisms, might be involved in guiding free SVs from the MBP to the AZ. As it occurs with the replenishment of the RRP (Fig. 92, 1a and 1b), it is possible that vesicles of the MBP are pulled from the recycling pool when it has been exhausted (Fig. 92, 1a and 1c). On the contrary, it might also be that

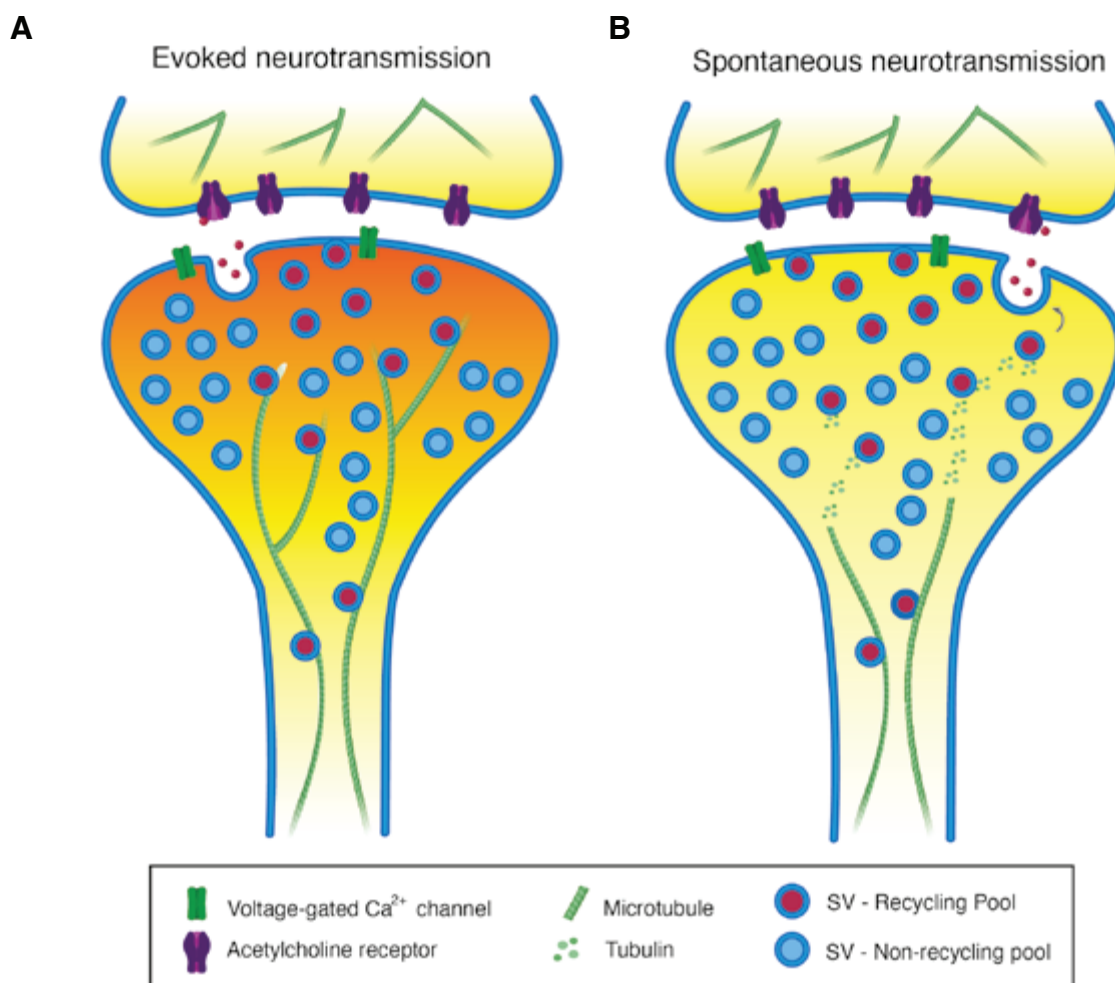


**Figure 91. Schematic representation for the model of spontaneous neurotransmitter release here proposed.** **A)** and **B)** synapses display evoked and spontaneous synaptic transmission, respectively. According to ultrastructural, morphological, and physiological findings we propose a model for spontaneous neurotransmitter release which involves the Microtubule Bound Pool (MBP), responsible for holding a set of synaptic vesicles from release (left). Upon microtubule depolymerization (right), synaptic vesicles can freely move through the presynaptic terminal and spontaneously fuse with the plasma membrane, thus producing miniature postsynaptic events. Notice how SVs released during evoked and spontaneous neurotransmission belong to the recycling pool, whereas those SVs reluctant to be released form the non-recycling pool. Orange colour of the presynaptic bouton indicates increase in presynaptic calcium influx.

recycled vesicles are directly segregated into the MBP after they have been refilled with neurotransmitters (Fig. 92, 2). Yet, what might be the mechanism by which SVs become attached to MTs to replenish the MBP, is to be investigated.

Although the functional role of spontaneous neurotransmission is still obscure, several studies have shown that spontaneous neurotransmitter release plays important roles in synaptic functions, including synaptic homeostasis (Andreae & Burrone, 2018; Kavalali, 2015; Truckenbrodt & Rizzoli, 2014). Of interest, activation of homeostatic synaptic plasticity mechanisms has been shown to occur in the absence of evoked activity (Frank et al., 2006; X. Wang et al., 2010). Consequently, it has been sugges-

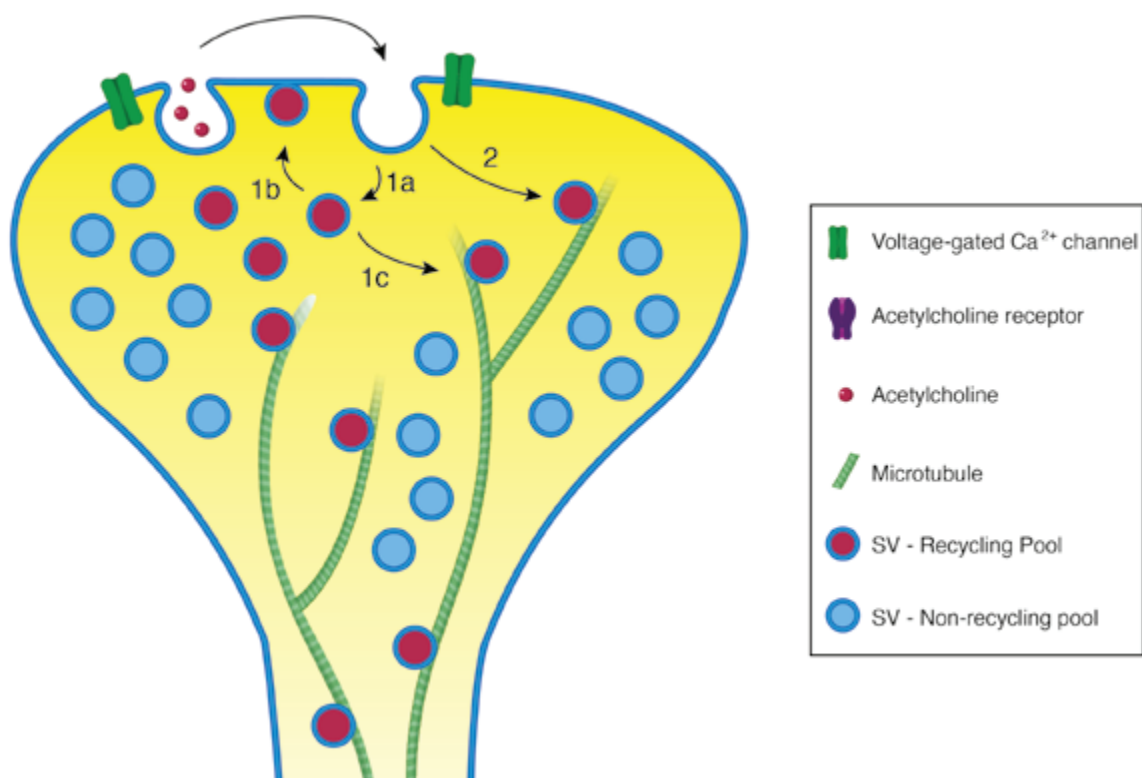


**Figure 92. Synaptic vesicle cycle of the microtubule bound pool (MBP).** Schematic representation of two possibilities that may mediate the replenishment of the MBP. 1) Spontaneous exocytosis of synaptic vesicles (SVs) elicited by microtubule (MT) depolymerization may be recycled and become a part of the cytoplasmic recycling pool (1a). Synaptic vesicles from the recycling pool are then used for replenishing the RRP (1b) or the MBP (1c) when they have been expended. 2) SVs may be recycled and incorporated directly into the MBP.

ted that spontaneous neurotransmission might be used to provide information about synaptic transmission levels. If that is indeed the case, and in the light of our observations, regulation of MT dynamics in autaptic neurons could be used as a mechanism for controlling spontaneous neurotransmitter release and be part of the sensing mechanism required to monitor synaptic weight. Future studies to identify the molecular mechanisms underlying the regulation of dynamic MTs at the synapse may contribute to deepen our knowledge into the function of spontaneous neurotransmission.

By providing ultrastructural, morphological, and physiological evidence we have proposed a concrete function for dynamic MTs at synaptic boutons in which they may act by regulating spontaneous neurotransmitter release probability. However, because our data are based on a culture system, further experiments using acute neuronal slices or *in vivo* models may further validate our findings.

Collectively, this project has contributed to gain a better understanding of the homeostatic synaptic mechanisms activated in response to synapse loss and has shed light on the role of dynamic MTs in both, evoked and spontaneous synaptic transmission.



# CONCLUSIONS





1. Single cell microcultures established in the absence of glial cells are a powerful experimental model for studying the effect of glial secreted molecules on synaptic transmission.
2. Exposure of autaptic circuits to the SPARC-derived peptide p4.2 eliminates a population of synaptic contacts.
3. Peptide p4.2 does not alter neuronal excitability or the properties of the postsynaptic terminal.
4. The presynaptic markers bassoon, synapsin-I and VAMP-2 can be used to estimate the number of synaptic contacts present in cultured neurons.
5. Autaptic neurons are able to sense and react to changes in synaptic connectivity by activating a mechanism of presynaptic homeostatic plasticity that maintains synaptic transmission at a baseline.
6. Presynaptic homeostatic plasticity in response to synapse elimination is driven by rapid *de novo* synapse formation and presynaptic potentiation.
7. Presynaptic potentiation as part of the presynaptic homeostatic response activated by synapse loss involves increases in presynaptic calcium influx and size of the readily releasable pool.
8. The action of peptide p4.2 to disassemble presynaptic contacts relies on changes in the distribution of the neuronal F-actin cytoskeleton.
9. Microtubule plus-ends invade presynaptic terminals and are associated to synaptic vesicles.
10. Increase of the free-tubulin pool enhances postsynaptic function without altering the properties of the presynaptic terminal.
11. Photocontrollable microtubule-inhibitors are a powerful tool for the study of MT dynamics in neurons.
12. Microtubule depolymerization enhances spontaneous neurotransmitter release in autaptic neurons.
13. The microtubule depolymerizing kinesin KIF18A can be used as a method for promoting miniature postsynaptic events.
14. MT dynamics regulate spontaneous neurotransmitter release probability.
15. Synaptic released spontaneously upon microtubule depolymerization belong to the same recycling pool of vesicles released during evoked neurotransmission.
16. Understanding how spontaneous neurotransmission is originated and regulated is essential to better understand its physiological function and improve our knowledge on how the nervous system processes information.





# REFERENCES



- Adler, C. E., Fetter, R. D., & Bargmann, C. I. (2006). UNC-6/Netrin induces neuronal asymmetry and defines the site of axon formation. *Nature Neuroscience*, 9(4), 511–518.
- Adler, E. M., Augustine, G. J., Duffy, S. N., & Charlton, M. P. (1991). Alien intracellular calcium chelators attenuate neurotransmitter release at the squid giant synapse. *Journal of Neuroscience*, 11(6), 1496–1507.
- Afuwape, O. A. T., Wasser, C. R., Schikorski, T., & Kavalali, E. T. (2017). Synaptic vesicle pool-specific modification of neurotransmitter release by intravesicular free radical generation. *Journal of Physiology*, 595(4), 1223–1238.
- Ahmari, S. E., Buchanan, J. A., & Smith, S. J. (2000). Assembly of presynaptic active zones from cytoplasmic transport packets. *Nature Neuroscience*, 3(5), 445–451.
- Alabi, A. R. A., & Tsien, R. W. (2012). Synaptic vesicle pools and dynamics. *Cold Spring Harbor Perspectives in Biology*, 4(8).
- Albrecht, D., López-Murcia, F. J., Pérez-González, A. P., Lichtner, G., Solsona, C., & Llobet, A. (2012). SPARC prevents maturation of cholinergic presynaptic terminals. *Molecular and Cellular Neuroscience*, 49(3), 364–374.
- Allen, N. J., Bennett, M. L., Foo, L. C., Wang, G. X., Chakraborty, C., Smith, S. J., & Barres, B. A. (2012). Astrocyte glypicans 4 and 6 promote formation of excitatory synapses via GluA1 AMPA receptors. *Nature*, 486(7403), 410–414.
- Allen, T. G. J. (2007). Preparation and maintenance of single-cell micro-island cultures of basal forebrain neurons. *Nature Protocols*, 1(6), 2543–2550.
- Allison, D. W., Gelfand, V. I., Spector, I., & Craig, A. M. (1998). Role of actin in anchoring postsynaptic receptors in cultured hippocampal neurons: Differential attachment of NMDA versus AMPA receptors. *Journal of Neuroscience*, 18(7), 2423–2436.
- Althof, D., Baehrens, D., Watanabe, M., Suzuki, N., Fakler, B., & Kulik, Á. (2015). Inhibitory and excitatory axon terminals share a common nano-architecture of their Cav2.1 (P/Q-type) Ca<sup>2+</sup> channels. *Frontiers in Cellular Neuroscience*, 9(315), 1–11.
- Alushin, G. M., Lander, G. C., Kellogg, E. H., Zhang, R., Baker, D., & Nogales, E. (2014). High-Resolution microtubule structures reveal the structural transitions in  $\alpha\beta$ -tubulin upon GTP hydrolysis. *Cell*, 157(5), 1117–1129.
- Andreae, L. C., & Burrone, J. (2018b). The role of spontaneous neurotransmission in synapse and circuit development. *Journal of Neuroscience Research*, 96(3), 354–359.
- Ango, F., Wu, C., Van Der Want, J. J., Wu, P., Schachner, M., & Huang, Z. J. (2008). Bergmann glia and the recognition molecule CHL1 organize GABAergic axons and direct innervation of Purkinje cell dendrites. *PLoS Biology*, 6(4), 739–756.
- Anwar, H., Li, X., Bucher, D., & Nadim, F. (2017). Functional roles of short-term synaptic plasticity with an emphasis on inhibition. *Current Opinion in Neurobiology*,

43, 71–78.

Araque, A., Sanzgiri, R. P., Parpura, V., & Haydon, P. G. (1999). Astrocyte-induced modulation of synaptic transmission. *Canadian Journal of Physiology and Pharmacology*, 77, 699–706.

Atasoy, D., Ertunc, M., Moulder, K. L., Blackwell, J., Chung, C., Su, J., & Kavalali, E. T. (2008). Spontaneous and evoked glutamate release activates two populations of NMDA receptors with limited overlap. *Journal of Neuroscience*, 28(40), 10151–10166.

Baas, P. W., Black, M. M., & Banker, G. A. (1989). Changes in microtubule polarity orientation during the development of hippocampal neurons in culture. *Journal of Cell Biology*, 109(6 I), 3085–3094.

Baas, P. W., Deitch, J. S., Black, M. M., & Banker, G. A. (1988). Polarity orientation of microtubules in hippocampal neurons: Uniformity in the axon and nonuniformity in the dendrite. *Proceedings of the National Academy of Sciences of the United States of America*, 85(21), 8335–8339.

Baas, Peter W., & Lin, S. (2011). Hooks and comets: The story of microtubule polarity orientation in the neuron. *Developmental Neurobiology*, 71(6), 403–418.

Babu, L. P. A., Wang, H. Y., Eguchi, K., Guillaud, L., & Takahashi, T. (2020). Microtubule and actin differentially regulate synaptic vesicle cycling to maintain high-frequency neurotransmission. *Journal of Neuroscience*, 40(1), 131–142.

Bacaj, T., Wu, D., Yang, X., Morishita, W., Zhou, P., Xu, W., Malenka, R. C., & Südhof, T. C. (2013). Synaptotagmin-1 and Synaptotagmin-7 Trigger Synchronous and Asynchronous Phases of Neurotransmitter Release. *Neuron*, 80(4), 947–959.

Bacci, A., Rudolph, U., Huguenard, J. R., & Prince, D. A. (2003). Major Differences in Inhibitory Synaptic Transmission onto Two Neocortical Interneuron Subclasses. *Journal of Neuroscience*, 23(29), 9664–9674.

Baines AJ, B. V. (1986). Synapsin I is a microtubule-bundling protein. *Nature*, 319(6049), 145–147.

Ballice-Gordon, R. J., & Lichtman, J. W. (1994). Long-term synapse loss induced by focal blockade of postsynaptic receptors. In *Nature* (Vol. 372, Issue 6506, pp. 519–524).

Banker, G. (1980). Trophic interactions between astroglial cells and hippocampal neurons in culture. *Science*, 209, 809–810.

Barber, M. J., & Lichtman, J. W. (1999). Activity-driven synapse elimination leads paradoxically to domination by inactive neurons. *Journal of Neuroscience*, 19(22), 9975–9985.

Bartley, A. F., Huang, Z. J., Huber, K. M., & Gibson, J. R. (2008). Differential activity-dependent, homeostatic plasticity of two neocortical inhibitory circuits. *Journal of Neurophysiology*, 100, 1983–1994.

Basnet, N., Nedozralova, H., Crevenna, A. H., Bodakuntla, S., Schlichthaerle,



- T., Taschner, M., Cardone, G., Janke, C., Jungmann, R., Magiera, M. M., Biertümpfel, C., & Mizuno, N. (2018). Direct induction of microtubule branching by microtubule nucleation factor SSNA1. *Nature Cell Biology*, 20(10), 1172–1180.
- Bear, M. F. (1996). A synaptic basis for memory storage in the cerebral cortex. *Proceedings of the National Academy of Sciences of the United States of America*, 93, 13453–13459.
- Beharry, A. A., & Woolley, G. A. (2011). Azobenzene photoswitches for biomolecules. *Chemical Society Reviews*, 40(8), 4422–4437.
- Bekkers, J. M., & Stevens, C. F. (1991). Excitatory and inhibitory autaptic currents in isolated hippocampal neurons maintained in cell culture. *Proceedings of the National Academy of Sciences of the United States of America*, 88(17), 7834–7838.
- Bekkers, John M. (1998). Neurophysiology: Are autapses prodigal synapses? *Current Biology*, 8(2), 52–55.
- Bekkers, John M. (2020). Autaptic Cultures: Methods and Applications. *Frontiers in Synaptic Neuroscience*, 12(18).
- Bekkers, John M., & Stevens, C. F. (1996). Cable properties of cultured hippocampal neurons determined from sucrose-evoked miniature EPSCs. *Journal of Neurophysiology*, 75(3), 1250–1255.
- Berg, D. K., & Hall, Z. W. (1975). Increased extrajunctional acetylcholine sensitivity produced by chronic post-synaptic neuromuscular blockade. *Journal of Physiology*, 244, 659–676.
- Bergles, D. E., Diamond, J. S., & Jahr, C. E. (1999). Clearance of glutamate inside the synapse and beyond. *Current Opinion in Neurobiology*, 9(3), 293–298.
- Betz, W. J. (1970). Depression of transmitter release at the neuromuscular junction of the frog. *Journal of Physiology*, 206, 629–644.
- Bharat, V., Siebrecht, M., Burk, K., Ahmed, S., Reissner, C., Kohansal-Nodehi, M., Steubler, V., Zweckstetter, M., Ting, J. T., & Dean, C. (2017). Capture of Dense Core Vesicles at Synapses by JNK-Dependent Phosphorylation of Synaptotagmin-4. *Cell Reports*, 21(8), 2118–2133.
- Bishop, D. L., Misgeld, T., Walsh, M. K., Gan, W. B., & Lichtman, J. W. (2004). Axon branch removal at developing synapses by axosome shedding. *Neuron*, 44(4), 651–661.
- Blakely, R. D., & Edwards, R. H. (2012). Vesicular and plasma membrane transporters for neurotransmitters. *Cold Spring Harbor Perspectives in Biology*, 4(2), a005595.
- Blatow, M., Caputi, A., Burnashev, N., Monyer, H., & Rozov, A. (2003).  $Ca^{2+}$  buffer saturation underlies paired pulse facilitation in calbindin-D28k-containing terminals. *Neuron*, 38, 79–88.
- Bliss, T. V. P., & Lomo, T. (1973). Long-lasting potentiation of synaptic trans-

mission in the dentate area of the unanaesthetized rabbit following stimulation of the perforant path. *The Journal of Physiology*, 232, 331–356.

Bloom, O., Evergren, E., Tomilin, N., Kjaerulff, O., Löw, P., Brodin, L., Pieribone, V. A., Greengard, P., & Shupliakov, O. (2003). Colocalization of synapsin and actin during synaptic vesicle recycling. *Journal of Cell Biology*, 161(4), 737–747.

Bollmann, J. H., Sakmann, B., & Borst, J. G. G. (2000). Calcium sensitivity of glutamate release in a calyx-type terminal. *Science*, 289, 953–957.

Bonhoeffer, T., & Yuste, R. (2002). Spine Motility. *Neuron*, 35(6), 1019–1027.

Borgdorff, A. J., & Choquet, D. (2002). Regulation of AMPA receptor lateral movements. *Nature*, 417, 649–653.

Borisy, G. G., & Taylor, E. W. (1967). The mechanism of action of colchicine. Colchicine binding to sea urchin eggs and the mitotic apparatus. *The Journal of Cell Biology*, 34(2), 535–548.

Borowiak, M., Nahaboo, W., Reynders, M., Nekolla, K., Jalinot, P., Hasserodt, J., Rehberg, M., Delattre, M., Zahler, S., Vollmar, A., Trauner, D., & Thorn-Seshold, O. (2015). Photoswitchable Inhibitors of Microtubule Dynamics Optically Control Mitosis and Cell Death. *Cell*, 162(2), 403–411.

Bourne, J. N., & Harris, K. M. (2008). Balancing structure and function at hippocampal dendritic spines. *Annual Review of Neuroscience*, 31, 47–67.

Boyden, E. S., Zhang, F., Bamberg, E., Nagel, G., & Deisseroth, K. (2005). Millisecond-timescale, genetically targeted optical control of neural activity. *Nature Neuroscience*, 8(9), 1263–1268.

Bradshaw, A. D., & Sage, E. H. (2001). SPARC, a matricellular protein that functions in cellular differentiation and tissue response to injury. *Journal of Clinical Investigation*, 107(9), 1049–1054.

Bredt, D. S., & Nicoll, R. A. (2003). AMPA receptor trafficking at excitatory synapses. *Neuron*, 40, 361–379.

Bresler, T., Shapira, M., Boeckers, T., Dresbach, T., Futter, M., Garner, C. C., Rosenblum, K., Gundelfinger, E. D., & Ziv, N. E. (2004). Postsynaptic Density Assembly Is Fundamentally Different from Presynaptic Active Zone Assembly. *Journal of Neuroscience*, 24(6), 1507–1520.

Buffelli, M., Burgess, R. W., Feng, G., Lobe, C. G., Lichtman, J. W., & Sanes, J. R. (2003). Genetic evidence that relative synaptic efficacy biases the outcome of synaptic competition. *Nature*, 424(6947), 430–434.

Burgalossi, A., Jung, S. Y., Man, K. M., Nair, R., Jockusch, W. J., Wojcik, S. M., Brose, N., & Rhee, J. S. (2012). Analysis of neurotransmitter release mechanisms by photolysis of caged Ca<sup>2+</sup> in an autaptic neuron culture system. *Nature Protocols*, 7(7), 1351–1365.

Burger, P. M., Mehl, E., Cameron, P. L., Maycox, P. R., Baumert, M., Lottspeich, F., De Camilli, P., & Jahn, R. (1989). Synaptic vesicles immunisolated from rat cere-

bral cortex contain high levels of glutamate. *Neuron*, 3, 715–720.

Busetto, G., Buffelli, M., Tognana, E., Bellico, F., & Cangiano, A. (2000). Hebbian mechanisms revealed by electrical stimulation at developing rat neuromuscular junctions. *Journal of Neuroscience*, 20(2), 685–695.

Cannon, W. (1932). *The wisdom of the body*. W.W. Norton.

Cartelli, D., Aliverti, A., Barbiroli, A., Santambrogio, C., Ragg, E. M., Casagrande, F. V. M., Cantele, F., Beltramone, S., Marangon, J., De Gregorio, C., Pandini, V., Emanuele, M., Chieriegatti, E., Pieraccini, S., Holmqvist, S., Bubacco, L., Roybon, L., Pezzoli, G., Grandori, R., Arnal, I., Cappelletti, G. (2016).  $\alpha$ -Synuclein is a Novel Microtubule Dynamase. *Scientific Reports*, 6(April), 1–13.

Castle, B. T., & Odde, D. J. (2015). Optical Control of Microtubule Dynamics in Time and Space. *Cell*, 162(2), 243–245.

Catterall, W. A., & Few, A. P. (2008). Calcium Channel Regulation and Presynaptic Plasticity. *Neuron*, 59(6), 882–901.

Ceccarelli, B., Hurlbut, W., & Mauro, A. (1973). Turnover of transmitter and vesicles at the frog neuromuscular junction. *The Journal of Cell Biology*, 57, 499–524.

Chanaday, N. L., Cousin, M. A., Milosevic, I., Watanabe, S., & Morgan, J. R. (2019). The synaptic vesicle cycle revisited: New insights into the modes and mechanisms. *Journal of Neuroscience*, 39(42), 8209–8216.

Chanaday, N. L., & Kavalali, E. T. (2018). Presynaptic origins of distinct modes of neurotransmitter release. *Curr Opin Neurobiol*, 51, 119–126.

Chen, C., & Tonegawa, S. (1997). Molecular genetic analysis of synaptic plasticity, activity-dependent neural development, learning, and memory in the mammalian brain. *Annual Review of Neuroscience*, 20, 157–184.

Chen, S. Y., & Cheng, H. J. (2009). Functions of axon guidance molecules in synapse formation. *Curr Opin Neurobiol*, 19(5), 471–478.

Chen, W. S., Chen, Y. J., Huang, Y. A., Hsieh, B. Y., Chiu, H. C., Kao, P. Y., Chao, C. Y., & Hwang, E. (2017). Ran-dependent TPX2 activation promotes acentrosomal microtubule nucleation in neurons. *Scientific Reports*, 7, 1–15.

Cheng, D., Hoogenraad, C. C., Rush, J., Ramm, E., Schlager, M. A., Duong, D. M., Xu, P., Wijayawardana, S. R., Hanfelt, J., Nakagawa, T., Sheng, M., & Peng, J. (2006). Relative and absolute quantification of postsynaptic density proteome isolated from rat forebrain and cerebellum. *Molecular and Cellular Proteomics*, 5(6), 1158–1170.

Chirwa, S. S., & Sastry, B. R. (1988). Asynchronous synaptic responses in hippocampal CA1 neurons during synaptic long-term potentiation. *Neuroscience Letters*, 89, 355–360.

Chiu, C. Q., Barberis, A., & Higley, M. J. (2019). Preserving the balance: diverse forms of long-term GABAergic synaptic plasticity. *Nature Reviews Neuroscience*, 20(5), 272–281.

- Cho, K.-O., Hunt, C. A., & Kennedy, M. B. (1992). The rat brain postsynaptic density fraction contains a homolog of the drosophila discs-large tumor suppressor protein. *Neuron*, 9, 929–942.
- Choquet, D., & Triller, A. (2013). The dynamic synapse. *Neuron*, 80(3), 691–703.
- Chowdhury, S., Shepherd, J. D., Okuno, H., Lyford, G., Petralia, R. S., Plath, N., Kuhl, D., Huganir, R. L., & Worley, P. F. (2006). Arc/Arg3.1 Interacts with the Endocytic Machinery to Regulate AMPA Receptor Trafficking. *Neuron*, 52, 445–459.
- Christopherson, K. S., Ullian, E. M., Stokes, C. C. A., Mallowney, C. E., Hell, J. W., Agah, A., Lawler, J., Mosher, D. F., Bornstein, P., & Barres, B. A. (2005). Thrombospondins are astrocyte-secreted proteins that promote CNS synaptogenesis. *Cell*, 120, 421–433.
- Chung, C., Barylko, B., Leitz, J., Liu, X., & Kavalali, E. T. (2010). Acute dynamin inhibition dissects synaptic vesicle recycling pathways that drive spontaneous and evoked neurotransmission. *Journal of Neuroscience*, 30(4), 1363–1376.
- Chung, S., Li, X., & Nelson, S. B. (2002). Short-term depression at thalamocortical synapses contributes to rapid adaptation of cortical sensory responses in vivo. *Neuron*, 34, 437–446.
- Chung, W.-S., Allen, N. J., & Eroglu, C. (2015). Astrocytes Control Synapse Formation, Function, and Elimination. *Cold Spring Harb Perspect Biol*, 7(9), a020370.
- Chung, W.-S., Clarke, L. E., Wang, G. X., Stafford, B. K., Sher, A., Chakraborty, C., Joung, J., Foo, L. C., Thompson, A., Chen, C., Smith, S. J., & Barres, B. A. (2013). Astrocytes mediate synapse elimination through MEGF10 and MERTK pathways. *Nature*, 504(7480), 394–400.
- Cingolani, L. A., Thalhammer, A., Yu, L. M. Y., Catalano, M., Ramos, T., Colicos, M. A., & Goda, Y. (2008). Activity-Dependent Regulation of Synaptic AMPA Receptor Composition and Abundance by  $\beta 3$  Integrins. *Neuron*, 58, 749–762.
- Clezardin, P., Malaval, L., Ehrensperger, A. -S, Delmas, P. D., Dechavanne, M., & McGregor, J. L. (1988). Complex formation of human thrombospondin with osteonectin. *European Journal of Biochemistry*, 175(2), 275–284.
- Cobb, S. R., Halasy, K., Vida, I., Nyíri, G., Tamás, G., Buhl, E. H., & Somogyi, P. (1997). Synaptic effects of identified interneurons innervating both interneurons and pyramidal cells in the rat hippocampus. *Neuroscience*, 79(3), 629–648.
- Cole, J. C., Villa, B. R. S., & Wilkinson, R. S. (2000). Disruption of actin impedes transmitter release in snake motor terminals. *Journal of Physiology*, 525(3), 579–586.
- Coles, C. H., & Bradke, F. (2015). Coordinating Neuronal Actin-Microtubule Dynamics. *Current Biology*, 25(15), R677–R691.
- Colicos, M. A., Collins, B. E., Sailor, M. J., & Goda, Y. (2001). Remodeling of synaptic actin induced by photoconductive stimulation. *Cell*, 107(5), 605–16
- Collingridge, G. L., Isaac, J. T. R., & Yu, T. W. (2004). Receptor trafficking and synaptic plasticity. *Nature Reviews Neuroscience*, 5, 952–962.

- Colman, H., & Lichtman, J. W. (1993). Interactions between Nerve and Muscle: Synapse Elimination at the Developing Neuromuscular Junction. *Developmental Biology*, 156(1), 1–10.
- Colón-Ramos, D. A. (2009). Chapter 2 Synapse Formation in Developing Neural Circuits. *Current Topics in Developmental Biology*, 87, 53–79.
- Colonnier, M. (1968). Synaptic patterns on different cell types in the different laminae of the cat visual cortex. An electron microscope study. *Brain Research*, 9(2), 268–287.
- Connelly, W. M., & Lees, G. (2010). Modulation and function of the autaptic connections of layer V fast spiking interneurons in the rat neocortex. *Journal of Physiology*, 588(12), 2047–2063.
- Couteaux, R., & Pécot-Dechavassine, M. (1970). Synaptic vesicles and pouches at the level of “active zones” of the neuromuscular junction. *C R Acad Hebd Seances Acad Sci D*, 271(25), 2346–2349.
- Crain, S. (1971). Intracellular recordings suggesting synaptic functions in chick embryo spinal sensory ganglion cells isolated in vitro. *Brain Research*, 26(1), 188–191.
- Cramer, L. P., Briggs, L. J., & Dawe, H. R. (2002). Use of fluorescently labelled deoxyribonuclease I to spatially measure G-actin levels in migrating and non-migrating cells. *Cell Motility and the Cytoskeleton*, 51, 27–38.
- Cull-Candy, S., Miledi, R., Trautmann, A., & Uchitel, O. (1980). On the release of transmitter at normal, myasthenia gravis and myasthenic syndrome affected human end-plates. *Journal of Physiology*, 299, 621–638.
- Cunha-Ferreira, I., Chazeau, A., Buijs, R. R., Stucchi, R., Will, L., Pan, X., Adolfs, Y., van der Meer, C., Wolthuis, J. C., Kahn, O. I., Schätzle, P., Altelaar, M., Pasterkamp, R. J., Kapitein, L. C., & Hoogenraad, C. C. (2018). The HAUS Complex Is a Key Regulator of Non-centrosomal Microtubule Organization during Neuronal Development. *Cell Reports*, 24(4), 791–800.
- Dahan, M., Lévi, S., Luccardini, C., Rostaing, P., Riveau, B., & Triller, A. (2003). Diffusion Dynamics of Glycine Receptors Revealed by Single-Quantum Dot Tracking. *Science*, 302, 442–445.
- Dale, H. H., Feldberg, W., & Vogt, M. (1936). Release of acetylcholine at voluntary motor nerve endings. *Journal of Physiology*, 86(4), 353–380.
- Danbolt, N. C. (2001). Glutamate uptake. *Progress in Neurobiology*, 65, 1–105.
- Darabid, H., Arbour, D., & Robitaille, R. (2013). Glial cells decipher synaptic competition at the mammalian neuromuscular junction. *Journal of Neuroscience*, 33(4), 1297–1313.
- Darcy, K. J., Staras, K., Collinson, L. M., & Goda, Y. (2006). Constitutive sharing of recycling synaptic vesicles between presynaptic boutons. *Nature Neuroscience*, 9(3), 315–321.

- Davis, G. W. (2006). Homeostatic control of neural activity: From phenomenology to molecular design. *Annual Review of Neuroscience*, 29, 307–323.
- Davis, G. W. (2013). Homeostatic signaling and the stabilization of neural function. *Neuron*, 80, 718–728.
- Davis, G. W., & Goodman, C. S. (1998). Synapse-specific control of synaptic efficacy at the terminals of a single neuron. *Nature*, 392, 82–86.
- Davis, G. W., & Müller, M. (2015). Homeostatic control of presynaptic neurotransmitter release. *Annual Review of Physiology*, 77, 251–270.
- Debanne, D., Campanac, E., Bialowas, A., Carlier, E., & Alcaraz, G. (2011). Axon physiology. *Physiological Reviews*, 91, 555–602.
- Deiters, A. (2010). Principles and Applications of the Photochemical Control of Cellular Processes. *ChemBioChem*, 11(1), 47–53.
- del Castillo, J., & Katz, B. (1954a). Quantal components of the end-plate potential. *The Journal of Physiology*, 124(3), 560–573.
- del Castillo, J., & Katz, B. (1954b). Statistical factors involved in neuromuscular facilitation and depression. *The Journal of Physiology*, 124(3), 574–585.
- Delvendahl, I., & Müller, M. (2019). Homeostatic plasticity—a presynaptic perspective. *Current Opinion in Neurobiology*, 54, 155–162.
- Delvendahl, I., Vyleta, N. P., von Gersdorff, H., & Hallermann, S. (2016). Fast, Temperature-Sensitive and Clathrin-Independent Endocytosis at Central Synapses. *Neuron*, 90, 492–498.
- Denker, A., Krohnert, K., Bucukers, J., Neher, E., & Rizzoli, S. O. (2011). The reserve pool of synaptic vesicles acts as a buffer for proteins involved in synaptic vesicle recycling. *Proceedings of the National Academy of Sciences of the United States of America*, 108(41), 17183–17188.
- Denker, A., & Rizzoli, S. O. (2010). Synaptic vesicle pools: An update. *Frontiers in Synaptic Neuroscience*, 2, 1–12.
- Dent, E. W., & Gertler, F. B. (2003). Cytoskeletal dynamics and transport in growth cone motility and guidance. *Neuron*, 40(2), 209–227.
- Desai, N. S., Cudmore, R. H., Nelson, S. B., & Turrigiano, G. G. (2002). Critical periods for experience-dependent synaptic scaling in visual cortex. *Nature Neuroscience*, 5(8), 783–789.
- Dickman, D. K., & Davis, G. W. (2009). The Schizophrenia Susceptibility Gene dysbindin Controls Synaptic Homeostasis. *Science*, 326, 1127–1130.
- Difiglia, M., Pasik, P., & Pasik, T. (1976). A golgi study of neuronal types in the neostriatum of monkeys. 114, 245–256.
- Dillon, C., & Goda, Y. (2005). The actin cytoskeleton: Integrating form and function at the synapse. *Annual Review of Neuroscience*, 28, 25–55.



Diniz, L. P., Almeida, J. C., Tortelli, V., Lopes, C. V., Setti-Perdigão, P., Stipursky, J., Kahn, S. A., Romão, L. F., De Miranda, J., Alves-Leon, S. V., De Souza, J. M., Castro, N. G., Panizzutti, R., & Gomes, F. C. A. (2012). Astrocyte-induced synaptogenesis is mediated by transforming growth factor  $\beta$  signaling through modulation of d-serine levels in cerebral cortex neurons. *Journal of Biological Chemistry*, 287(49), 41432–41445.

Dittman, J. S., Kreitzer, A. C., & Regehr, W. G. (2000). Interplay between facilitation, depression, and residual calcium at three presynaptic terminals. *Journal of Neuroscience*, 20(4), 1374–1385.

Dittman, J. S., & Ryan, T. A. (2019). The control of release probability at nerve terminals. *Nature Reviews Neuroscience*, 20, 177–186.

Dodge, F. A., & Rahamimoff, R. (1967). Co-operative action of calcium ions in transmitter release at the neuromuscular junction. *Journal of Physiology*, 193, 419–432.

Dolphin, A. C. (2013). The  $\alpha 2\delta$  subunits of voltage-gated calcium channels. *Biochimica et Biophysica Acta - Biomembranes*, 1828(7), 1541–1549.

Dreosti, E., Odermatt, B., Dorostkar, M. M., & Lagnado, L. (2009). A genetically-encoded reporter of synaptic activity in vivo. *6(12)*, 883–889.

Du, Y., English, C. A., & Ohi, R. (2010). The Kinesin-8 Kif18A Dampens Microtubule Plus-End Dynamics. *Current Biology*, 20, 374–380.

Dunaevsky, A., & Connor, E. A. (2000). F-actin is concentrated in nonrelease domains at frog neuromuscular junctions. *Journal of Neuroscience*, 20(16), 6007–6012.

Dunaevsky, A., Tashiro, A., Majewska, A., Mason, C., & Yuste, R. (1999). Developmental regulation of spine motility in the mammalian central nervous system. *Proceedings of the National Academy of Sciences of the United States of America*, 96(23), 13438–13443.

Dziadek, M., Pauksson, M., Aumailley, M., & Timpl, R. (1986). Purification and tissue distribution of a small protein (BM-40) extracted from a basement membrane tumor. *European Journal of Biochemistry*, 161, 455–464.

Eccles, J. C., & O'Connor, W. J. (1941). Abortive impulses at the neuromuscular junction. *Journal of Physiology*, 100, 318–328.

Emperador-Melero, J., & Kaeser, P. S. (2020). Assembly of the presynaptic active zone. *Current Opinion in Neurobiology*, 63, 95–103.

Engdahl, A. J., Torres, E. A., Lock, S. E., Engdahl, T. B., Mertz, P. S., & Streu, C. N. (2015). Synthesis, Characterization, and Bioactivity of the Photoisomerizable Tubulin Polymerization Inhibitor azo-Combretastatin A4. *Organic Letters*, 17(18), 4546–4549.

Eroglu, C., & Barres, B. A. (2010). Regulation of synaptic connectivity by glia. *Nature*, 468, 223–231.



- Evans, L. L., Lee, A. J., Bridgman, P. C., & Mooseker, M. S. (1998). Vesicle-associated brain myosin-V can be activated to catalyze actin-based transport. *Journal of Cell Science*, 111(14), 2055–2066.
- Fan, S., Gangwar, S. P., Machius, M., & Rudenko, G. (2021). Interplay between hevin, SPARC, and MDGAs: Modulators of neuroligin-neurexin transsynaptic bridges. *Structure*, 29(7), 664–678.
- Fasano, C., Thibault, D., & Trudeau, L. É. (2008). Culture of postnatal mesencephalic dopamine neurons on an astrocyte monolayer. *Current Protocols in Neuroscience*, SUPPL. 44, 1–19.
- Fatt, P., & Katz, B. (1951). An analysis of the end-plate potential recorded with an intra-cellular electrode. *The Journal of Physiology*, 115, 320–370.
- Fatt, P., & Katz, B. (1952). Spontaneous subthreshold activity at motor nerve endings. *Journal of Physiology*, 117, 109–128.
- Felmy, F., Neher, E., & Schneggenburger, R. (2003). Probing the intracellular calcium sensitivity of transmitter release during synaptic facilitation. *Neuron*, 37, 801–811.
- Fenske, P., Grauel, M. K., Brockmann, M. M., Dorn, A. L., Trimbuch, T., & Rosenmund, C. (2019). Autaptic cultures of human induced neurons as a versatile platform for studying synaptic function and neuronal morphology. *Scientific Reports*, 9(1), 1–12.
- Fernandez-Alfonso, T., & Ryan, T. (2008). A heterogeneous “resting” pool of synaptic vesicles that is dynamically interchanged across boutons in mammalian CNS synapses. *Neuron*, 36(1–4), 87–100.
- Fesce, R., Grohovaz, F., Valtorta, F., & Meldolesi, J. (1994). Neurotransmitter release: fusion or “kiss-and-run”? *Trends in Cell Biology*, 4(1), 1–4.
- Fiala, J. C., Feinberg, M., Popov, V., & Harris, K. M. (1998). Synaptogenesis Via Dendritic Filopodia in Developing Hippocampal Area CA1. *The Journal of Neuroscience*, 18(21), 8900–8911.
- Fields, R. D., & Burnstock, G. (2006). Purinergic signalling in neuron-glia interactions. *Nature Reviews Neuroscience*, 7(6), 423–436.
- Fischer, M., Kaech, S., Knutti, D., & Matus, A. (1998). Rapid actin-based plasticity in dendritic spines. *Neuron*, 20(5), 847–854.
- Foster, M., & Sherrington, C. S. (1897). *A textbook of physiology, part three: The central nervous system* (7th ed.). MacMillan & Co Ltd.
- Fox, K., & Stryker, M. (2017). Integrating Hebbian and homeostatic plasticity: Introduction. *Philosophical Transactions of the Royal Society B*, 372, 1–6.
- Frank, C. A., Kennedy, M. J., Goold, C. P. P., Marek, K. W., & Davis, G. W. W. (2006). Mechanisms Underlying the Rapid Induction and Sustained Expression of Synaptic Homeostasis. *Neuron*, 52, 663–677.

- Fredj, N. Ben, & Burrone, J. (2009). A resting pool of vesicles is responsible for spontaneous vesicle fusion at the synapse. *Nature Neuroscience*, 12(6), 751–758.
- Friedman, H. V., Bresler, T., Garner, C. C., & Ziv, N. E. (2000). Assembly of new individual excitatory synapses: Time course and temporal order of synaptic molecule recruitment. *Neuron*, 27(1), 57–69.
- Fuentes-Medel, Y., Ashley, J., Barria, R., Maloney, R., Freeman, M., & Budnik, V. (2012). Integration of a retrograde signal during synapse formation by glia-secreted TGF- $\beta$  ligand. *Current Biology*, 22, 1831–1838.
- Furshpan, E. J., MacLeish, P. R., O’Lague, P. H., & Potter, D. D. (1976). Chemical transmission between rat sympathetic neurons and cardiac myocytes developing in microcultures: evidence for cholinergic, adrenergic, and dual function neurons. *Proceedings of the National Academy of Sciences of the United States of America*, 73(11), 4225–4229.
- Furshpan, E. J., & Potter, D. D. (1958). Transmission at the giant motor synapses of the crayfish. *Journal of Physiology*, 145(2), 289–325.
- Gainey, M. A., Hurvitz-Wolff, J. R., Lambo, M. E., & Turrigiano, G. G. (2009). Synaptic scaling requires the GluR2 subunit of the AMPA receptor. *Journal of Neuroscience*, 29(20), 6479–6489.
- Galani, C., & Vlachos, A. (2020). Hebbian and Homeostatic Synaptic Plasticity—Do Alterations of One Reflect Enhancement of the Other? *Frontiers in Cellular Neuroscience*, 14(50), 1–8.
- Gan, W. B., Kwon, E., Feng, G., Sanes, J. R., & Lichtman, J. W. (2003). Synaptic dynamism measured over minutes to months: Age-dependent decline in an autonomic ganglion. *Nature Neuroscience*, 6(9), 956–960.
- Gao, L., Meiring, J. C. M., Heise, C., Rai, A., & Müller-deku, A. (2021). Photoswitchable epothilone-based microtubule stabilisers allow GFP imaging-compatible, optical control over the microtubule cytoskeleton. *BioRxiv Cell Biology*, 1–15.
- Gao, L., Meiring, J. C. M., Kraus, Y., Wranik, M., Weinert, T., Pritzl, S. D., Bingham, R., Ntoulou, E., Jansen, K. I., Olieric, N., Standfuss, J., Kapitein, L. C., Lohmüller, T., Ahlfeld, J., Akhmanova, A., Steinmetz, M. O., & Thorn-Seshold, O. (2021a). A Robust, GFP-Orthogonal Photoswitchable Inhibitor Scaffold Extends Optical Control over the Microtubule Cytoskeleton. *Cell Chemical Biology*, 28(2), 228-241.e6.
- Gao, L., Meiring, J. C. M., Kraus, Y., Wranik, M., Weinert, T., Pritzl, S. D., Bingham, R., Ntoulou, E., Jansen, K. I., Olieric, N., Standfuss, J., Kapitein, L. C., Lohmüller, T., Ahlfeld, J., Akhmanova, A., Steinmetz, M. O., & Thorn-Seshold, O. (2021b). A Robust, GFP-Orthogonal Photoswitchable Inhibitor Scaffold Extends Optical Control over the Microtubule Cytoskeleton. *Cell Chemical Biology*, 228–241.
- Gao, L., Meiring, J. C. M., Varady, A., Ruider, I. E., Heise, C., Wranik, M., Velasco, C. D., Taylor, J. A., Terni, B., Standfuss, J., Cabernard, C. C., Llobet, A., Steinmetz, M. O., Bausch, A. R., Distel, M., Thorn-seshold, J., Akhmanova, A., Thorn-Seshold, O., Andreas, R., ... Thorn-, O. (2021). In vivo photocontrol of microtubule dynamics and integrity, migration and mitosis, by the potent GFP-imaging-compatible photoswitchable

ble reagents SBTubA4P and SBTub2M. *BioRxiv*, 2021.03.26.437160.

Garner, C. C., Waites, C. L., & Ziv, N. E. (2006). Synapse development: Still looking for the forest, still lost in the trees. *Cell and Tissue Research*, 326(2), 249–262.

Gaspari, R., Prota, A. E., Bargsten, K., Cavalli, A., & Steinmetz, M. O. (2017). Structural Basis of cis- and trans-Combretastatin Binding to Tubulin. *Chem*, 2(1), 102–113.

Geppert, M., Goda, Y., Hammer, R. E., Li, C., Rosahl, T. W., Stevens, C. F., & Südhof, T. C. (1994). Synaptotagmin I: A major Ca<sup>2+</sup> sensor for transmitter release at a central synapse. *Cell*, 79, 717–727.

Goda, Y., & Stevens, C. F. (1994). Two components of transmitter release at a central synapse. *Proceedings of the National Academy of Sciences of the United States of America*, 91, 12942–12946.

Goldstein, A. Y., Wang, X., & Schwarz, T. L. (2008). Axonal transport and the delivery of pre-synaptic components. *Current Opinion in Neurobiology*, 18(5), 495–503.

González Inchauspe, C., Martini, F. J., Forsythe, I. D., & Uchitel, O. D. (2004). Functional compensation of P/Q by N-type channels blocks short-term plasticity at the calyx of Held presynaptic terminal. *Journal of Neuroscience*, 24(46), 10379–10383.

Goold, C. P., & Nicoll, R. A. (2010). Single-Cell Optogenetic Excitation Drives Homeostatic Synaptic Depression. *Neuron*, 68, 512–528.

Gordon-Weeks, P. R., Burgoyne, R. D., & Gray, E. G. (1982). Presynaptic microtubules: Organisation and assembly/disassembly. *Neuroscience*, 7(3).

Gotow, T., Miyaguchi, K., & Hashimoto, P. H. (1991). Cytoplasmic architecture of the axon terminal: Filamentous strands specifically associated with synaptic vesicles. *Neuroscience*, 40(2), 587–598.

Graffe, M., Zenisek, D., & Taraska, J. W. (2015). A marginal band of microtubules transports and organizes mitochondria in retinal bipolar synaptic terminals. *Journal of General Physiology*, 146(1), 109–117.

Grael, M. K., Maglione, M., Reddy-Alla, S., Willmes, C. G., Brockmann, M. M., Trimbuch, T., Rosenmund, T., Pangalos, M., Vardar, G., Stumpf, A., Walter, A. M., Rost, B. R., Eickholt, B. J., Haucke, V., Schmitz, D., Sigrist, S. J., & Rosenmund, C. (2016). Rim-binding protein 2 regulates release probability by fine-tuning calcium channel localization at murine hippocampal synapses. *Proceedings of the National Academy of Sciences of the United States of America*, 113(41), 11615–11620.

Gray, E. G. (1963). Electron microscopy of presynaptic organelles of the spinal cord. *Journal of Anatomy*, 97, 101–106.

Gray, E. G. (1969). Electron Microscopy of Excitatory and Inhibitory Synapses: A Brief Review. *Progress in Brain Research*, 31(C), 141–155.

Gray, E. G. (1975). Presynaptic microtubules and their association with synaptic vesicles. *Proceedings of the Royal Society of London - Biological Sciences*, 190(1100), 369–372.

- Gray, E. G. (1978). Synaptic vesicles and microtubules in frog motor endplates. *Proc. R. Soc. Lond. B*, 203, 219–227.
- Groemer, T. W., & Klingauf, J. (2007a). Synaptic vesicles recycling spontaneously and during activity belong to the same vesicle pool. *Nature Neuroscience*, 10(2), 145–147.
- Groemer, T. W., & Klingauf, J. (2007b). Synaptic vesicles recycling spontaneously and during activity belong to the same vesicle pool. *Nature Neuroscience*, 10(2), 145–147.
- Guedes-Dias, P., & Holzbaur, E. L. F. (2019). Axonal transport: Driving synaptic function. *Science*, 366(199), 1–13.
- Guedes-dias, P., Nirschl, J. J., Abreu, N. C., Tokito, M. K., Magiera, M. M., Holzbaur, E. L. F., & Sud, P. (2019). Kinesin-3 responds to local microtubule dynamics to target synaptic cargo delivery to the presynapse. *Neuron*, 29(2), 268–282.
- Gupta, K. K., Li, C., Duan, A., Alberico, E. O., Kim, O. V., Alber, M. S., & Goodson, H. V. (2013). Mechanism for the catastrophe-promoting activity of the microtubule destabilizer Op18/stathmin. *Proceedings of the National Academy of Sciences of the United States of America*, 110(51), 20449–20454.
- Haghighi, A. P., McCabe, B. D., Fetter, R. D., Palmer, J. E., Hom, S., & Goodman, C. S. (2003). Retrograde control of synaptic transmission by postsynaptic CaMKII at the *Drosophila* neuromuscular junction. *Neuron*, 39, 255–267.
- Halassa, M. M., Fellin, T., Takano, H., Dong, J. H., & Haydon, P. G. (2007). Synaptic islands defined by the territory of a single astrocyte. *Journal of Neuroscience*, 27(24), 6473–6477.
- Hall, D. H., & Hedgecock, E. M. (1991). Kinesin-related gene *unc-104* is required for axonal transport of synaptic vesicles in *C. elegans*. *Cell*, 65, 837–847.
- Han, B., Zhou, R., Xia, C., & Zhuang, X. (2017). Structural organization of the actin-spectrin-based membrane skeleton in dendrites and soma of neurons. *Proceedings of the National Academy of Sciences of the United States of America*, 114(32), E6678–E6685.
- Han, Y., Kaeser, P. S., Südhof, T. C., & Schneggenburger, R. (2011). RIM determines Ca<sup>2+</sup> channel density and vesicle docking at the presynaptic active zone. *Neuron*, 69, 304–316.
- Harata, N., Ryan, T. A., Smith, S. J., Buchanan, J., & Tsien, R. W. (2001). Visualizing recycling synaptic vesicles in hippocampal neurons by FM 1-43 photoconversion. *Proceedings of the National Academy of Sciences of the United States of America*, 98(22), 12748–12753.
- Harris, K. M., & Sultan, P. (1995). Variation in the number, location and size of synaptic vesicles provides an anatomical basis for the nonuniform probability of release at hippocampal CA1 synapses. *Neuropharmacology*, 34(11), 1387–1395.
- Hebb, D. O. (1949). *The organization of behaviour*. NY: John Wiley and Sons.

- Heine, M., Groc, L., Frischknecht, R., Béïque, J. C., Lounis, B., Rumbaugh, G., Huganir, R. L., Cognet, L., & Choquet, D. (2008). Surface mobility of postsynaptic AMPARs tunes synaptic transmission. *Science*, 320(5873), 201–205.
- Henneberger, C., Papouin, T., Oliet, S. H. R., & Rusakov, D. A. (2010). Long-term potentiation depends on release of d-serine from astrocytes. *Nature*, 463(7278), 232–236.
- Herzog, E., Nadrigny, F., Silm, K., Biesemann, C., Helling, I., Bersot, T., Steffens, H., Schwartzmann, R., Valentin Nägerl, U., El Mestikawy, S., Rhee, J. S., Kirchhoff, F., & Brose, N. (2011). In vivo imaging of intersynaptic vesicle exchange using VGLUT1 Venus knock-in mice. *Journal of Neuroscience*, 31(43), 15544–15559.
- Heuser, J. E., & Reese, T. S. (1973). Evidence for recycling of synaptic vesicle membrane during transmitter release at the frog neuromuscular junction. *Journal of Cell Biology*, 57, 315–344.
- Heuser, J. E., & Reese, T. S. (1981). Structural changes after transmitter release at the frog neuromuscular junction. *Journal of Cell Biology*, 88(3), 564–580.
- Hirokawa, N., Sobue, K., Kanda, K., Harada, A., & Yorifuji, H. (1989). The cytoskeletal architecture of the presynaptic terminal and molecular structure of synapsin 1. *Journal of Cell Biology*, 108(1), 111–126.
- Hirokawa, Nobutaka, Noda, Y., Tanaka, Y., & Niwa, S. (2009). Kinesin superfamily motor proteins and intracellular transport. *Nature Reviews Molecular Cell Biology*, 10(10), 682–696.
- Hodgkin, A. L., & Huxley, A. F. (1939). Action Potentials Recorded from Inside a Nerve Fibre. *Nature*, 144, 710–711.
- Hoffman, R. E., & McGlashan, T. H. (1997). Synaptic elimination, neurodevelopment, and the mechanism of hallucinated “voices” in schizophrenia. *American Journal of Psychiatry*, 154(12), 1683–1689.
- Hohenester, E., Maurer, P., & Timpl, R. (1997). Crystal structure of a pair of follistatin-like and EF-hand calcium-binding domains in BM-40. *EMBO Journal*, 16(13), 3778–3786.
- Holderith, N., Lorincz, A., Katona, G., Rózsa, B., Kulik, A., Watanabe, M., & Nusser, Z. (2012). Release probability of hippocampal glutamatergic terminals scales with the size of the active zone. *Nature Neuroscience*, 15(7), 988–997.
- Holtmaat, A., & Svoboda, K. (2009). Experience-dependent structural synaptic plasticity in the mammalian brain. *Nature Reviews Neuroscience*, 10, 647–658.
- Honda, A., Yamada, M., Saisu, H., Takahashi, H., Mori, K. J., & Abe, T. (2002). Direct, Ca<sup>2+</sup>-dependent interaction between tubulin and synaptotagmin I: A possible mechanism for attaching synaptic vesicles to microtubules. *Journal of Biological Chemistry*, 277(23), 20234–20242.
- Hooks, B. M., & Chen, C. (2006). Distinct Roles for Spontaneous and Visual Activity in Remodeling of the Retinogeniculate Synapse. *Neuron*, 52(2), 281–291.

- Hosoi, N., Holt, M., & Sakaba, T. (2009). Calcium Dependence of Exo- and Endocytotic Coupling at a Glutamatergic Synapse. *Neuron*, 63, 216–229.
- Hu, X., Ballo, L., Pietila, L., Viesselmann, C., Ballweg, J., Lombard, D., Stevenson, M., Merriam, E., & Dent, E. W. (2011). Bdnf-induced increase of PSD-95 in dendritic spines requires dynamic microtubule invasions. *Journal of Neuroscience*, 31(43), 15597–15603.
- Hu, X., Viesselmann, C., Nam, S., Merriam, E., & Dent, E. W. (2008). Activity-dependent dynamic microtubule invasion of dendritic spines. *Journal of Neuroscience*, 28(49), 13094–13105.
- Hua, Y., Sinha, R., Martineau, M., Kahms, M., & Klingauf, J. (2010). A common origin of synaptic vesicles undergoing evoked and spontaneous fusion. *Nature Neuroscience*, 13(12), 1451–1453.
- Huberman, A. D., Feller, M. B., & Chapman, B. (2008). Mechanisms underlying development of visual maps and receptive fields. *Annual Review of Neuroscience*, 31, 479–509.
- Hurwitz, I., Cropper, E. C., Vilim, F. S., Alexeeva, V., Susswein, A. J., Kupfermann, I., & Weiss, K. R. (2000). Serotonergic and peptidergic modulation of the buccal mass protractor muscle (I2) in *Aplysia*. *Journal of Neurophysiology*, 84(6), 2810–2820.
- Ibata, K., Sun, Q., & Turrigiano, G. G. (2008). Rapid Synaptic Scaling Induced by Changes in Postsynaptic Firing. *Neuron*, 57, 819–826.
- Ikeda, K., & Bekkers, J. M. (2006). Autapses. *Current Biology*, 16(9), 308.
- Ikeda, K., & Bekkers, J. M. (2009). Counting the number of releasable synaptic vesicles in a presynaptic terminal. *Proceedings of the National Academy of Sciences of the United States of America*, 106(8), 2945–2950.
- Irie, M. (2000). Diarylethenes for Memories and Switches Masahiro. *Chemical Reviews*, 100, 1685–1716.
- Janke, C., & Magiera, M. M. (2020). The tubulin code and its role in controlling microtubule properties and functions. *Nature Reviews Molecular Cell Biology*, 21, 307–326.
- Jaworski, J., Kapitein, L. C., Gouveia, S. M., Dortland, B. R., Wulf, P. S., Grigoriev, I., Camera, P., Spangler, S. A., Di Stefano, P., Demmers, J., Krugers, H., Defilippi, P., Akhmanova, A., & Hoogenraad, C. C. (2009). Dynamic Microtubules Regulate Dendritic Spine Morphology and Synaptic Plasticity. *Neuron*, 61(1), 85–100.
- Johnson, M. D. (1994). Synaptic glutamate release by postnatal rat serotonergic neurons in microculture. *Neuron*, 12(2), 433–442.
- Johnston, J., Seibel, S. H., Darnet, L. S. A., Renninger, S., Orger, M., & Lagnado, L. (2019). A Retinal Circuit Generating a Dynamic Predictive Code for Oriented Features. *Neuron*, 102, 1211–1222.
- Jones, E. V., Bernardinelli, Y., Tse, Y. C., Chierzi, S., Wong, T. P., & Murai, K. K.



(2011). Astrocytes control glutamate receptor levels at developing synapses through SPARC -  $\beta$ -integrin interactions. *Journal of Neuroscience*, 31(11), 4154–4165.

Jontes, J. D., Buchanan, J. A., & Smith, S. J. (2000). Growth cone and dendrite dynamics in zebrafish embryos: Early events in synaptogenesis imaged in vivo. *Nature Neuroscience*, 3(3), 231–237.

Josa-Culleré, L., & Llebaria, A. (2021). In the Search for Photocages Cleavable with Visible Light: An Overview of Recent Advances and Chemical Strategies. *ChemPhotoChem*, 5(4), 298–316.

Jung, J., Loy, K., Schilling, E. M., Röther, M., Brauner, J. M., Huth, T., Schlötzer-Schrehardt, U., Alzheimer, C., Kornhuber, J., Welzel, O., & Groemer, T. W. (2014). The antidepressant fluoxetine mobilizes vesicles to the recycling pool of rat hippocampal synapses during high activity. *Molecular Neurobiology*, 49, 916–930.

Kaesler, P. S., & Regehr, W. G. (2014). Molecular Mechanisms for Synchronous, Asynchronous, and Spontaneous Neurotransmitter Release. *Annual Reviews of Physiology*, 76, 333–363.

Kaesler, P. S., & Regehr, W. G. (2017). The readily releasable pool of synaptic vesicles. *Current Opinion in Neurobiology*, 43, 63–70.

Kapitein, L. C., & Hoogenraad, C. C. (2015). Building the Neuronal Microtubule Cytoskeleton. *Neuron*, 87(3), 492–506.

Karabelas, A. B., & Purrura, D. P. (1980). Evidence for autapses in the substantia nigra. *Brain Research*, 200(2), 467–473.

Karayannis, T., Elfant, D., Huerta-Ocampo, I., Teki, S., Scott, R. S., Rusakov, D. A., Jones, M. V., & Capogna, M. (2010). Slow GABA transient and receptor desensitization shape synaptic responses evoked by hippocampal neurogliaform cells. *Journal of Neuroscience*, 30(29), 9898–9909.

Katz, B., & Miledi, R. (1968). The role of calcium in neuromuscular facilitation. *The Journal of Physiology*, 195, 481–492.

Katz, Bernard. (1969). *The Release of Neural Transmitter Substances*. In Liverpool University Press.

Katz, L., & Shatz, C. (1996). Synaptic Activity and the Construction of Cortical Circuits. *Science*, 274, 1133–1138.

Kaufmann, B., Müller, S., Hanisch, F. G., Hartmann, U., Paulsson, M., Maurer, P., & Zaucke, F. (2004). Structural variability of BM-40/SPARC/osteonectin glycosylation: Implications for collagen affinity. *Glycobiology*, 14(7), 609–619.

Kavalali, E. T. (2015). The mechanisms and functions of spontaneous neurotransmitter release. *Nature Reviews Neuroscience*, 16, 5–16.

Kavalali, E. T., Chung, C. H., Khvotchev, M., Leitz, J., Nosyreva, E., Raingo, J., & Ramirez, D. M. O. (2011). Spontaneous neurotransmission: An independent pathway for neuronal signaling? *Physiology*, 26(1), 45–53.



- Kennedy, T. E., & Tessier-Lavigne, M. (1995). Guidance and induction of branch formation in developing axons by target-derived diffusible factors. *Current Opinion in Neurobiology*, 5, 83–90.
- Kim, C. H., & Lisman, J. E. (1999). A role of actin filament in synaptic transmission and long-term potentiation. *Journal of Neuroscience*, 19(11), 4314–4324.
- Kim, E., & Sheng, M. (2004). PDZ domain proteins of synapses. *Nature Reviews Neuroscience*, 5, 771–781.
- Kim, J., & Tsien, R. W. (2008). Synapse-Specific Adaptations to Inactivity in Hippocampal Circuits Achieve Homeostatic Gain Control while Dampening Network Reverberation. *Neuron*, 58, 925–937.
- Kim, S. H., & Ryan, T. A. (2010). CDK5 Serves as a Major Control Point in Neurotransmitter Release. *Neuron*, 67, 797–809.
- Kim, S. H., & Ryan, T. A. (2013). Balance of calcineurin A $\alpha$  and CDK5 activities sets release probability at nerve terminals. *Journal of Neuroscience*, 33(21), 8937–8950.
- King, J. S., & Bishop, G. A. (1982). The synaptic features of horseradish peroxidase-labelled recurrent collaterals in the ganglionic plexus of the cat cerebellar cortex. *Journal of Neurocytology*, 11(6), 867–880.
- Kirov, S. A., & Harris, K. M. (1999). Dendrites are more spiny on mature hippocampal neurons when synapses are inactivated. *Neuron*, 2(10), 878–883.
- Kirsch, J., & Betz, H. (1995). The postsynaptic localization of the glycine receptor-associated protein gephyrin is regulated by the cytoskeleton. *Journal of Neuroscience*, 15(6), 4148–4156.
- Klintsova, A. Y., & Greenough, W. T. (1999). Synaptic plasticity in cortical systems. *Current Opinion in Neurobiology*, 9(2), 203–208.
- Knowles, G. C., & McCulloch, C. A. G. (1992). Simultaneous localization and quantification of relative G and F actin content: Optimization of fluorescence labeling methods. *Journal of Histochemistry and Cytochemistry*, 40(10), 1605–1612.
- Koenig, J. H., & Ikeda, K. (1999). Contribution of active zone subpopulation of vesicles to evoked and spontaneous release. *Journal of Neurophysiology*, 81(4), 1495–1505.
- Kononenko, N. L., Claßen, G. A., Kuijpers, M., Puchkov, D., Maritzen, T., Tempes, A., Malik, A. R., Skalecka, A., Bera, S., Jaworski, J., & Haucke, V. (2017). Retrograde transport of TrkB-containing autophagosomes via the adaptor AP-2 mediates neuronal complexity and prevents neurodegeneration. *Nature Communications*, 8, 14819.
- Kononenko, N. L., & Haucke, V. (2015). Molecular mechanisms of presynaptic membrane retrieval and synaptic vesicle reformation. *Neuron*, 85, 484–496.
- Korobova, F., & Svitkina, T. (2010). Molecular Architecture of Synaptic Actin Cytoskeleton in Hippocampal Neurons Reveals a Mechanism of Dendritic Spine Mor-

phogenesis. *Molecular Biology of the Cell*, 21, 165–176.

Krueger, S. R., Kolar, A., & Fitzsimonds, R. M. (2003). The Presynaptic Release Apparatus Is Functional in the Absence of Dendritic Contact and Highly Mobile within Isolated Axons. *Neuron*, 40, 945–957.

Kucukdereli, H., Allen, N. J., Lee, A. T., Feng, A., Ozlu, M. I., Conatser, L. M., Chakraborty, C., Workman, G., Weaver, M., Sage, E. H., Barres, B. A., & Eroglu, C. (2011). Control of excitatory CNS synaptogenesis by astrocyte-secreted proteins hevin and SPARC. *Proceedings of the National Academy of Sciences of the United States of America*, 108(32), E440–E449.

Kummer, T. T., Misgeld, T., & Sanes, J. R. (2006). Assembly of the postsynaptic membrane at the neuromuscular junction: Paradigm lost. *Current Opinion in Neurobiology*, 16, 74–82.

Kupprion, C., Motamed, K., & Sage, E. H. (1998). SPARC (BM-40, osteonectin) inhibits the mitogenic effect of vascular endothelial growth factor on microvascular endothelial cells. *Journal of Biological Chemistry*, 273(45), 29635–29640.

Kuriu, T., Inoue, A., Bito, H., Sobue, K., & Okabe, S. (2006). Differential control of postsynaptic density scaffolds via actin-dependent and -independent mechanisms. *Journal of Neuroscience*, 26(29), 7693–7706.

Kuromi, H., & Kidokoro, Y. (1998). Two distinct pools of synaptic vesicles in single presynaptic boutons in a temperature-sensitive *Drosophila* mutant, *shibire*. *Neuron*, 20(5), 917–925.

Kusano, K., & Landau, E. M. (1975). Depression and recovery of transmission at the squid giant synapse. *The Journal of Physiology*, 245, 13–22.

Landis, D. M. D., Hall, A. K., Weinstein, L. A., & Reese, T. S. (1988). The organization of cytoplasm at the presynaptic active zone of a central nervous system synapse. *Neuron*, 1(3), 201–209.

Landis, S. C. (1976). Rat sympathetic neurons and cardiac myocytes developing in microcultures: Correlation of the fine structure of endings with neurotransmitter function in single neurons. *Proc Natl Acad Sci U S A*, 73(11), 4220–4224.

Lane, T. F., & Sage, E. H. (1990). Functional mapping of SPARC: Peptides from two distinct Ca<sup>++</sup>-binding sites modulate cell shape. *Journal of Cell Biology*, 111(6 II), 3065–3076.

Ledda, F. M., Adris, S., Bravo, A. I., Kairiyama, C., Bover, L., Chernajovsky, Y., Mordoh, J., & Podhajcer, O. L. (1997). Suppression of SPARC expression by antisense RNA abrogates the tumorigenicity of human melanoma cells. *Nature Medicine*, 3, 171–176.

Lee, A., Westenbroek, R. E., Haeseleer, F., Palczewski, K., Scheuer, T., & Catterall, W. A. (2002). Differential modulation of Cav2.1 channels by calmodulin and Ca<sup>2+</sup>-binding protein 1. *Nature Neuroscience*, 5(3), 210–217.

Lee, A., Wong, S. T., Gallagher, D., Li, B., Storm, D. R., Scheuer, T., & Catterall,

W. A. (1999).  $\text{Ca}^{2+}$ /calmodulin binds to and modulates P/Q-type calcium channels. *Nature*, 399, 155–159.

Lee, H.-K., & Kirkwood, A. (2019). Mechanisms of Homeostatic Synaptic Plasticity in vivo. *Frontiers in Cellular Neuroscience*, 13(520), 1–7.

Lee, S. H., & Sheng, M. (2000). Development of neuron-neuron synapses. *Current Opinion in Neurobiology*, 10, 125–131.

Lepicard, S., Franco, B., de Bock, F., & Parmentier, M. L. (2014). A presynaptic role of microtubule-associated protein 1/Futsch in *Drosophila*: Regulation of active zone number and neurotransmitter release. *Journal of Neuroscience*, 34(20), 6759–6771.

Li, C., Ullrich, B., Zhang, J. Z., Anderson, R. G. W., Brose, N., & Südhof, T. C. (1995).  $\text{Ca}^{2+}$ -dependent and -independent activities of neural and non-neural synaptotagmins. In *Nature* (Vol. 375, pp. 594–599).

Li, L., Chin, L. S., Shupliakov, O., Brodin, L., Sihra, T. S., Hvalby, Ø., Jensen, V., Zheng, D., Mcnamara, J. O., Greengard, P., & Andersen, P. (1995). Impairment of synaptic vesicle clustering and of synaptic transmission, and increased seizure propensity, in synapsin I-deficient mice. *Proceedings of the National Academy of Sciences of the United States of America*, 92(20), 9235–9239.

Li, X., Newbern, J. M., Wu, Y., Morgan-Smith, M., Zhong, J., Charron, J., & Snider, W. D. (2012). MEK Is a Key Regulator of Gliogenesis in the Developing Brain. *Neuron*, 75, 1035–1050.

Li, Y. C., Bai, W. Z., Zhou, L., Sun, L. K., & Hashikawa, T. (2010). Nonhomogeneous distribution of filamentous actin in the presynaptic terminals on the spinal motoneurons. *Journal of Comparative Neurology*, 518(16), 3184–3192.

Li, Y., Schmid, G., Hänggi, P., & Schimansky-Geier, L. (2010). Spontaneous spiking in an autaptic Hodgkin-Huxley setup. *Physical Review E - Statistical, Nonlinear, and Soft Matter Physics*, 82(6), 1–8.

Lin, Y., Wei, Y. L., & She, Z. Y. (2020). Kinesin-8 motors: regulation of microtubule dynamics and chromosome movements. *Chromosoma*, 129, 99–110.

Llinás, R., Steinberg, I. Z., & Walton, K. (1981). Relationship between presynaptic calcium current and postsynaptic potential in squid giant synapse. *Biophysical Journal*, 33(3), 323–352.

López-Muñoz, F., Boya, J., & Alamo, C. (2006). Neuron theory, the cornerstone of neuroscience, on the centenary of the Nobel Prize award to Santiago Ramón y Cajal. *Brain Research Bulletin*, 70, 391–405.

López-Murcia, F. J., Terni, B., & Llobet, A. (2015). SPARC triggers a cell-autonomous program of synapse elimination. *Proceedings of the National Academy of Sciences of the United States of America*, 112(43), 13366–13371.

Loss, Van Der, H., & Glaser, E. (1972). Autapses in neocortex cerebri: synapses between a pyramidal cell's axon and its own dendrites. *Brain Research*, 48, 355–360.

- Lu, T., & Trussell, L. O. (2000). Inhibitory transmission mediated by asynchronous transmitter release. *Neuron*, 26, 683–694.
- Lübke, J., Markram, H., Frotscher, M., & Sakmann, B. (1996). Frequency and dendritic distribution of autapses established by layer 5 pyramidal neurons in the developing rat neocortex: Comparison with synaptic innervation of adjacent neurons of the same class. *Journal of Neuroscience*, 16(10), 3209–3218.
- Lüders, J. (2021). Nucleating microtubules in neurons: Challenges and solutions. *Developmental Neurobiology*, 81(3), 273–283.
- Luo, F., Bacaj, T., & Südhof, T. C. (2015). Synaptotagmin-7 is essential for Ca<sup>2+</sup>-triggered delayed asynchronous release but not for Ca<sup>2+</sup>-dependent vesicle priming in retinal ribbon synapses. *Journal of Neuroscience*, 35(31), 11024–11033.
- Luo, F., Dittrich, M., Stiles, J. R., & Meriney, S. D. (2011). Single-pixel optical fluctuation analysis of calcium channel function in active zones of motor nerve terminals. *Journal of Neuroscience*, 31(31), 11268–11281.
- Lynch, G., & Baudry, M. (1984). The biochemistry of memory: A new and specific hypothesis. *Science*, 224, 1057–1063.
- Magleby, K. L., & Zengel, J. E. (1976). Augmentation: a process that acts to increase transmitter release at the frog neuromuscular junction. *Journal of Physiology*, 257, 449–470.
- Marder, E., & Prinz, A. A. (2003). Current compensation in neuronal homeostasis. *Neuron*, 37(1), 2–4.
- Marra, V., Burden, J. J., Thorpe, J. R., Smith, I. T., Smith, S. L., Häusser, M., Branco, T., & Staras, K. (2012). A Preferentially Segregated Recycling Vesicle Pool of Limited Size Supports Neurotransmission in Native Central Synapses. *Neuron*, 76(3), 579–589.
- Martínez San Segundo, P., Terni, B., Burgueño, J., Monroy, X., Dordal, A., Merlos, M., & Llobet, A. (2020). Outside-in regulation of the readily releasable pool of synaptic vesicles by  $\alpha\delta$ -1. *FASEB Journal*, 34(1), 1362–1377.
- Mathew, S. S., Pozzo-Miller, L., & Hablitz, J. J. (2008). Kainate modulates presynaptic GABA release from two vesicle pools. *Journal of Neuroscience*, 28(3), 725–731.
- Matveev, V., Zucker, R. S., & Sherman, A. (2004). Facilitation through Buffer Saturation: Constraints on Endogenous Buffering Properties. *Biophysical Journal*, 86, 2691–2709.
- Maurer, P., Hohenadl, C., Hohenester, E., Göhring, W., Timpl, R., & Engel, J. (1995). The C-terminal portion of BM-40 (SPARC/osteonectin) is an autonomously folding and crystallisable domain that binds calcium and collagen IV. *Journal of Molecular Biology*, 253(2), 347–357.
- Mayer, U., Aumailley, M., Mann, K., Timpl, R., & Engel, J. (1991). Calcium-dependent binding of basement membrane protein BM-40 (osteonectin, SPARC) to basement membrane collagen type IV. *European Journal of Biochemistry*, 198(1),

141–150.

Mayr, M. I., Hümmer, S., Bormann, J., Grüner, T., Adio, S., Woehlke, G., & Mayer, T. U. (2007). The Human Kinesin Kif18A Is a Motile Microtubule Depolymerase Essential for Chromosome Congression. *Current Biology*, 17(6), 488–498.

McVicker, D. P., Awe, A. M., Richters, K. E., Wilson, R. L., Cowdrey, D. A., Hu, X., Chapman, E. R., & Dent, E. W. (2016). Transport of a kinesin-cargo pair along microtubules into dendritic spines undergoing synaptic plasticity. *Nature Communications*, 7, 1–13.

Melkov, A., & Abdu, U. (2018). Regulation of long-distance transport of mitochondria along microtubules. *Cellular and Molecular Life Sciences*, 75(2), 163–176.

Merriam, E. B., Millette, M., Lombard, D. C., Saengsawang, W., Fothergill, T., Hu, X., Ferhat, L., & Dent, E. W. (2013). Synaptic regulation of microtubule dynamics in dendritic spines by calcium, F-actin, and Drebrin. *Journal of Neuroscience*, 33(42), 16471–16482.

Meyer-Franke, A., Kaplan, M. R., Pfeifer, F. W., & Barres, B. A. (1995). Characterization of the signaling interactions that promote the survival and growth of developing retinal ganglion cells in culture. *Neuron*, 15, 805–819.

Michel, F. J., & Trudeau, L. E. (2000). Clozapine inhibits synaptic transmission at GABAergic synapses established by ventral tegmental area neurones in culture. *Neuropharmacology*, 39(9), 1536–1543.

Miki, T., Kaufmann, W. A., Malagon, G., Gomez, L., Tabuchi, K., Watanabe, M., Shigemoto, R., & Marty, A. (2017). Numbers of presynaptic Ca<sup>2+</sup> channel clusters match those of functionally defined vesicular docking sites in single central synapses. *Proceedings of the National Academy of Sciences of the United States of America*, 114(26), E5246–E5255.

Miller, K. D., & MacKay, D. J. C. (1994). The Role of Constraints in Hebbian Learning. *Neural Computation*, 6, 100–126.

Milosevic, I. (2018). Revisiting the role of clathrin-mediated endocytosis in synaptic vesicle recycling. *Frontiers in Cellular Neuroscience*, 12(February), 1–13.

Mitchison, T., & Kirschner, M. (1984). Dynamic instability of microtubules. *Nature*, 312–15, 237–242.

Mitra, A., Mitra, S. S., & Tsien, R. W. (2012). Heterogeneous reallocation of presynaptic efficacy in recurrent excitatory circuits adapting to inactivity. *Nature Neuroscience*, 15(2), 250–257.

Mochida, S., Few, A. P., Scheuer, T., & Catterall, W. A. (2008). Regulation of Presynaptic CaV2.1 Channels by Ca<sup>2+</sup> Sensor Proteins Mediates Short-Term Synaptic Plasticity. *Neuron*, 57, 210–216.

Moechars, D., Weston, M. C., Leo, S., Callaerts-Vegh, Z., Goris, I., Daneels, G., Buist, A., Cik, M., Van Der Spek, P., Kass, S., Meert, T., D’Hooge, R., Rosenmund, C., & Hampson, R. M. (2006). Vesicular glutamate transporter VGLUT2 expression levels control quantal size and neuropathic pain. *Journal of Neuroscience*, 26(46),

12055–12066.

Morales, M., Colicos, M. A., & Goda, Y. (2000). Actin-dependent regulation of neurotransmitter release at central synapses. *Neuron*, 27(3), 539–550.

Motanis, H., Seay, M. J., & Buonomano, D. V. (2018). Short-Term Synaptic Plasticity as a Mechanism for Sensory Timing. *Trends Neurosci*, 41(10), 701–711.

Müller-Deku, A., Meiring, J. C. M., Loy, K., Kraus, Y., Heise, C., Bingham, R., Jansen, K. I., Qu, X., Bartolini, F., Kapitein, L. C., Akhmanova, A., Ahlfeld, J., Trauner, D., & Thorn-Seshold, O. (2020). Photoswitchable paclitaxel-based microtubule stabilizers allow optical control over the microtubule cytoskeleton. *Nature Communications*, 11(1), 1–12.

Müller, M., & Davis, G. W. (2012). Trans-Synaptic Control of Presynaptic Ca<sup>2+</sup> Influx Achieves Homeostatic Potentiation of Neurotransmitter Release. *Current Biology*, 22(12), 1102–1108.

Müller, M., Liu, K. S. Y., Sigrist, S. J., & Davis, G. W. (2012). RIM controls homeostatic plasticity through modulation of the readily-releasable vesicle pool. *Journal of Neuroscience*, 32(47), 16574–16585.

Müller, M., Pym, E. C. G., Tong, A., & Davis, G. W. (2011). Rab3-GAP Controls the Progression of Synaptic Homeostasis at a Late Stage of Vesicle Release. *Neuron*, 69, 749–762.

Murphy-Ullrich, J. E., Lane, T. F., Pallero, M. A., & Sage, E. H. (1995). SPARC mediates focal adhesion disassembly in endothelial cells through a follistatin-like region and the Ca<sup>2+</sup>-binding EF-hand. *Journal of Cellular Biochemistry*, 57(2), 341–350.

Murthy, V. N., Schikorski, T., Stevens, C. F., & Zhu, Y. (2001). Inactivity produces increases in neurotransmitter release and synapse size. *Neuron*, 32, 673–682.

Murthy, V. N., & Stevens, C. F. (1999). Reversal of synaptic vesicle docking at central synapses. *Nature Neuroscience*, 2(6), 503–507.

Nägler, K., Mauch, D. H., & Pfrieger, F. W. (2001). Glia-derived signals induce synapse formation in neurones of the rat central nervous system. *Journal of Physiology*, 533(3), 665–679.

Neher, E. (1998). Usefulness and limitations of linear approximations to the understanding of Ca<sup>++</sup> signals. *Cell Calcium*, 24(5–6), 345–357.

Neher, E., & Sakaba, T. (2008). Multiple Roles of Calcium Ions in the Regulation of Neurotransmitter Release. *Neuron*, 59, 861–872.

Neniskyte, U., & Gross, C. T. (2017). Errant gardeners: Glial-cell-dependent synaptic pruning and neurodevelopmental disorders. *Nature Reviews Neuroscience*, 18(11), 658–670.

Nerbonne, J. M., Gerber, B. R., Norris, A., & Burkhalter, A. (2008). Electrical remodelling maintains firing properties in cortical pyramidal neurons lacking KC-ND2-encoded A-type K<sup>+</sup> currents. *Journal of Physiology*, 586(6), 1565–1579.



- Nguyen, M. M., Stone, M. C., & Rolls, M. M. (2011). Microtubules are organized independently of the centrosome in *Drosophila* neurons. *6*(38), 1–16.
- Nishimune, A., Isaac, J. T. R., Molnar, E., Noel, J., Nash, S. R., Tagaya, M., Collingridge, G. L., Nakanishi, S., & Henley, J. M. (1998). NSF Binding to GluR2 Regulates Synaptic Transmission. *21*, 87–97.
- O'Brien, R. J., Kamboj, S., Ehlers, M. D., Rosen, K. R., Fischbach, G. D., & Huganir, R. L. (1998). Activity-dependent modulation of synaptic AMPA receptor accumulation. *Neuron*, *21*, 1067–1078.
- Ori-McKenney, K. M., Jan, L. Y., & Jan, Y. N. (2012). Golgi Outposts Shape Dendrite Morphology by Functioning as Sites of Acentrosomal Microtubule Nucleation in Neurons. *Neuron*, *76*(5), 921–930.
- Osterweil, E., Wells, D. G., & Mooseker, M. S. (2005). A role for myosin VI in postsynaptic structure and glutamate receptor endocytosis. *Journal of Cell Biology*, *168*(2), 329–338.
- Otis, T., Zhang, S., & Trussell, L. O. (1996). Direct measurement of AMPA receptor desensitization induced by glutamatergic synaptic transmission. *Journal of Neuroscience*, *16*(23), 7496–7504.
- Otsu, Y., Shahrezaei, V., Li, B., Raymond, L. A., Delaney, K. R., & Murphy, T. H. (2004). Competition between Phasic and Asynchronous Release for Recovered Synaptic Vesicles at Developing Hippocampal Autaptic Synapses. *Journal of Neuroscience*, *24*(2), 420–433.
- Pack-Chung, E., Kurshan, P. T., Dickman, D. K., & Schwarz, T. L. (2007). A *Drosophila* kinesin required for synaptic bouton formation and synaptic vesicle transport. *Nature Neuroscience*, *10*(8), 980–989.
- Palay, S. L. (1956). Synapses in the central nervous system. *The Journal of Biophysical and Biochemical Cytology*, *2*(4), 193–202.
- Pan, B., & Zucker, R. S. (2009). A General Model of Synaptic Transmission and Short-Term Plasticity. *Neuron*, *62*, 539–554.
- Paradis, S., Sweeney, S. T., & Davis, G. W. (2001). Homeostatic control of presynaptic release is triggered by postsynaptic membrane depolarization. *Neuron*, *30*, 737–749.
- Parato, J., & Bartolini, F. (2021). The microtubule cytoskeleton at the synapse. *Neuroscience Letters*, *753*(March), 135850.
- Parkhurst, C. N., Yang, G., Ninan, I., Savas, J. N., Yates, J. R., Lafaille, J. J., Hempstead, B. L., Littman, D. R., & Gan, W. B. (2013). Microglia promote learning-dependent synapse formation through brain-derived neurotrophic factor. *Cell*, *155*, 1596–1609.
- Parrish, J. Z., Kim, C. C., Tang, L., Bergquist, S., Wang, T., DeRisi, J. L., Jan, L. Y., Jan, Y. N., & Davis, G. W. (2014). Krüppel Mediates the Selective Rebalancing of Ion Channel Expression. *Neuron*, *82*, 537–544.



- Payton, J. E., Perrin, R. J., Clayton, D. F., & George, J. M. (2001). Protein-protein interactions of alpha-synuclein in brain homogenates and transfected cells. *Molecular Brain Research*, 95(1–2), 138–145.
- Penn, A. A., Riquelme, P. A., Feller, M. B., & Shatz, C. J. (1998). Competition in retinogeniculate patterning driven by spontaneous activity. *Science*, 279(5359), 2108–2112.
- Penney, J., Tsurudome, K., Liao, E. H., Elazzouzi, F., Livingstone, M., Gonzalez, M., Sonenberg, N., & Haghighi, P. A. (2012). TOR Is Required for the Retrograde Regulation of Synaptic Homeostasis at the *Drosophila* Neuromuscular Junction. *Neuron*, 74, 166–178.
- Perez-Gonzalez, A. P., Albrecht, D., Blasi, J., & Llobet, A. (2008). Schwann cells modulate short-term plasticity of cholinergic autaptic synapses. *The Journal of Physiology*, 586(Pt 19), 4675–4691.
- Perez, F., Diamantopoulos, G. S., Stalder, R., & Kreis, T. E. (1999). CLIP-170 highlights growing microtubule ends in vivo. *Cell*, 96, 517–527.
- Perlson, E., Maday, S., Fu, M., Moughamian, A. J., & Holzbaur, E. L. F. (2010). Retrograde Axonal Transport: Pathways To Cell Death? *Trends in Neurosciences*, 33(7), 335–344.
- Peters, A., & Proskauer, C. C. (1980). Smooth or sparsely spined cells with myelinated axons in rat visual cortex. *Neuroscience*, 5, 2079–2092.
- Petersen, S. A., Fetter, R. D., Noordermeer, J. N., Goodman, C. S., & DiAntonio, A. (1997). Genetic analysis of glutamate receptors in *drosophila* reveals a retrograde signal regulating presynaptic transmitter release. *Neuron*, 19, 1237–1248.
- Peterson, B. Z., DeMaria, C. D., & Yue, D. T. (1999). Calmodulin is the Ca<sup>2+</sup> sensor for Ca<sup>2+</sup>-dependent inactivation of L-type calcium channels. *Neuron*, 22, 549–558.
- Phillips, G. R., Huang, J. K., Wang, Y., Tanaka, H., Shapiro, L., Zhang, W., Shan, W. S., Arndt, K., Frank, M., Gordon, R. E., Gawinowicz, M. A., Zhao, Y., & Colman, D. R. (2001). The presynaptic particle web: Ultrastructure, composition, dissolution, and reconstitution. *Neuron*, 32(1), 63–77.
- Pieribone, V. A., Shupliakov, O., Brodin, L., Hilfiker-Rothenfluh, S., Czernik, A. J., & Greengard, P. (1995). Distinct pools of synaptic vesicles in neurotransmitter release. In *Nature* (Vol. 375, Issue 6531, pp. 493–497).
- Plomp, J., van Kempen, G., & Molenaar, P. (1992). Adaptation of Quantal Content To Decreased postsynaptic sensitivity at single endplates in alpha-bungarotoxin-treated rats. *Journal of Physiology*, 458, 487–499.
- Pozo, K., & Goda, Y. (2010). Unraveling mechanisms of homeostatic synaptic plasticity. *66(3)*, 337–351.
- Prange, O., & Murphy, T. H. (1999). Correlation of miniature synaptic activity and evoked release probability in cultures of cortical neurons. *Journal of Neuroscience*, 19(15), 6427–6438.

- Prekeris, R., & Terrian, D. M. (1997). Brain myosin V is a synaptic vesicle-associated motor protein: Evidence for a Ca<sup>2+</sup>-dependent interaction with the synaptobrevin-synaptophysin complex. *Journal of Cell Biology*, 137(7), 1589–1601.
- Preston, R., Bishop, G., & Kitai, S. (1980). Medium spiny neuron projection from the rat striatum: an intracellular horseradish peroxidase study. *Brain Research*, 183(4), 253–263.
- Prokop, A., Landgraf, M., Rushton, E., Broadie, K., & Bate, M. (1996). Presynaptic development at the *Drosophila* neuromuscular junction: Assembly and localization of presynaptic active zones. *Neuron*, 17, 617–626.
- Prota, A. E., Magiera, M. M., Kuijpers, M., Bargsten, K., Frey, D., Wieser, M., Jaussi, R., Hoogenraad, C. C., Kammerer, R. A., Janke, C., & Steinmetz, M. O. (2013). Structural basis of tubulin tyrosination by tubulin tyrosine ligase. *Journal of Cell Biology*, 200(3), 259–270.
- Pulido, C., & Marty, A. (2017). Quantal fluctuations in central mammalian synapses: Functional role of vesicular docking sites. *Physiological Reviews*, 97(4), 1403–1430.
- Qiang, L., Yu, W., Andreadis, A., Luo, M., & Baas, P. W. (2006). Tau protects microtubules in the axon from severing by katanin. *Journal of Neuroscience*, 26(12), 3120–3129.
- Qu, X., Kumar, A., Blockus, H., Waites, C., & Bartolini, F. (2019). Activity-Dependent Nucleation of Dynamic Microtubules at Presynaptic Boutons Controls Neurotransmission. *Current Biology*, 29(24), 4231-4240.e5.
- Raines, E. W., Lane, T. F., Iruela-Arispe, M. L., Ross, R., & Sage, E. H. (1992). The extracellular glycoprotein SPARC interacts with platelet-derived growth factor (PDGF)-AB and -BB and inhibits the binding of PDGF to its receptors. *Proceedings of the National Academy of Sciences of the United States of America*, 89(4), 1281–1285.
- Raino, J., Khvotchev, M., Liu, P., Darios, F., Li, Y. C., Ramirez, D. M. O., Adachi, M., Lemieux, P., Toth, K., Davletov, B., & Kavalali, E. T. (2012). VAMP4 directs synaptic vesicles to a pool that selectively maintains asynchronous neurotransmission. *Nature Neuroscience*, 15(5), 738–745.
- Ramirez, D. M. O., Khvotchev, M., Trauterman, B., & Kavalali, E. T. (2012a). Vti1a Identifies a Vesicle Pool that Preferentially Recycles at Rest and Maintains Spontaneous Neurotransmission. *Neuron*, 73(1), 121–134.
- Newman, E. A., Araque, A., & Dubinsky, J. M. (Eds.). (2017). *The beautiful brain: The drawings of Santiago Ramón Y Cajal.* (L. W. Swanson, L. King & E. Himmel, Contributors). Abrams Books.
- Rao, A., Kim, E., Sheng, M., & Craig, A. M. (1998). Heterogeneity in the molecular composition of excitatory postsynaptic sites during development of hippocampal neurons in culture. *Journal of Neuroscience*, 18(4), 1217–1229.
- Rastogi, S. K., Zhao, Z., Gildner, M. B., Shoulders, B. A., Velasquez, T. L., Blumenthal, M. O., Wang, L., Li, X., Hudnall, T. W., Betancourt, T., Du, L., & Brittain, W. J.

(2021). Synthesis, optical properties and in vitro cell viability of novel spiropyrans and their photostationary states. *Tetrahedron*, 80, 131854.

Ravelli, R. B. G., Gigant, B., Curmi, P. A., Jourdain, I., Lachkar, S., Sobel, A., & Knossow, M. (2004). Insight into tubulin regulation from a complex with colchicine and a stathmin-like domain. *Nature*, 428(6979), 198–202.

Reddy, L. V., Koirala, S., Sugiura, Y., Herrera, A. A., & Ko, C. P. (2003). Glial cells maintain synaptic structure and function and promote development of the neuromuscular junction in vivo. *Neuron*, 40, 563–580.

Regehr, W. G. (2012). Short-term presynaptic plasticity. *Cold Spring Harbor Perspectives in Biology*, 4(7), 1–19.

Reichardt, L., & Patterson, P. (1977). Neurotransmitter synthesis and uptake by isolated sympathetic neurones in microcultures. *Nature*, 270, 147–151.

Revenu, C., Athman, R., Robine, S., & Louvard, D. (2004). The co-workers of actin filaments: From cell structures to signals. *Nature Reviews Molecular Cell Biology*, 5(8), 635–646.

Riccomagno, M. M., & Kolodkin, A. L. (2015). Sculpting Neural Circuits by Axon and Dendrite Pruning. *Annual Review of Cell and Developmental Biology*, 31, 779–805.

Richards, D. A., Rizzoli, S. O., & Betz, W. J. (2004). Effects of wortmannin and latrunculin A on slow endocytosis at the frog neuromuscular junction. *Journal of Physiology*, 557(1), 77–91.

Ridge, R. M. A. P., & Betz, W. J. (1984). The effect of selective, chronic stimulation on motor unit size in developing rat muscle. *Journal of Neuroscience*, 4(10), 2614–2620.

Riveros, N., Fiedler, J., Lagos, N., Muñoz, C., & Orrego, F. (1986). Glutamate in rat brain cortex synaptic vesicles: influence of the vesicle isolation procedure. *Brain Research*, 386, 405–408.

Rizalar, F. S., Roosen, D. A., & Haucke, V. (2021). A Presynaptic Perspective on Transport and Assembly Mechanisms for Synapse Formation. *Neuron*, 109, 27–41.

Rizzoli, S. O., & Betz, W. J. (2005). Synaptic vesicle pools. *Nature Reviews Neuroscience*, 6, 57–69.

Roberts, W. M. (1993). Spatial calcium buffering in saccular hair cells. *Nature*, 363, 74–76.

Romberg, R. W., Werness, P. G., Lollar, P., Riggs, B. L., & Mann, K. G. (1985). Isolation and characterization of native adult osteonectin. *Journal of Biological Chemistry*, 260(5), 2728–2736.

Rosenblatt, S., Bassuk, J. A., Alpers, C. E., Sage, E. H., Timpl, R., & Preissner, K. T. (1997). Differential modulation of cell adhesion by interaction between adhesive and counter-adhesive proteins: Characterization of the binding of vitronectin to osteonectin (BM40, SPARC). *Biochemical Journal*, 324(1), 311–319.

Rosenmund, C., & Stevens, C. F. (1996). Definition of the readily releasable pool of vesicles at hippocampal synapses. *Neuron*, 16, 1197–1207.

Rost, B. R., Breustedt, J., Schoenherr, A., Grosse, G., Ahnert-Hilger, G., & Schmitz, D. (2010). Autaptic cultures of single hippocampal granule cells of mice and rats. *European Journal of Neuroscience*, 32(6), 939–947.

Rostaing, P., Real, E., Siksou, L., Lechaire, J. P., Boudier, T., Boeckers, T. M., Gertler, F., Gundelfinger, E. D., Triller, A., & Marty, S. (2006). Analysis of synaptic ultrastructure without fixative using high-pressure freezing and tomography. *European Journal of Neuroscience*, 24(12), 3463–3474.

Rozov, A., Burnashev, N., Sakmann, B., & Neher, E. (2001). Transmitter release modulation by intracellular Ca<sup>2+</sup> buffers in facilitating and depressing nerve terminals of pyramidal cells in layer 2/3 of the rat neocortex indicates a target cell-specific difference in presynaptic calcium dynamics. *Journal of Physiology*, 531(3), 807–826.

Saada, R., Miller, N., Hurwitz, I., & Susswein, A. J. (2009). Autaptic Excitation Elicits Persistent Activity and a Plateau Potential in a Neuron of Known Behavioral Function. *Current Biology*, 19(6), 479–484.

Saadat, S., Sendtner, M., & Rohrer, H. (1989). Ciliary neurotrophic factor induces cholinergic differentiation of rat sympathetic neurons in culture. *Journal of Cell Biology*, 108(5), 1807–1816.

Sage, H., Johnson, C., & Bornstein, P. (1984). Characterization of a novel serum albumin-binding glycoprotein secreted by endothelial cells in culture. *Journal of Biological Chemistry*, 259(6), 3993–4007.

Sage, H., Vernon, R. B., Funk, S. E., Everitt, E. A., & Angello, J. (1989). SPARC, a secreted protein associated with cellular proliferation, inhibits cell spreading in vitro and exhibits Ca<sup>2+</sup>-dependent binding to the extracellular matrix. *Journal of Cell Biology*, 109(1), 341–356.

Saheki, Y., & De Camilli, P. (2012). Synaptic Vesicle Endocytosis. *Cold Spring Harbor Perspectives in Biology*, 4(9), a005645–a005645.

Sailer, A., Ermer, F., Kraus, Y., Bingham, R., Lutter, F. H., Ahlfeld, J., & Thorn-Seshold, O. (2020). Potent hemithioindigo-based antimetabolites photocontrol the microtubule cytoskeleton in cellulose. *Beilstein Journal of Organic Chemistry*, 16, 125–134.

Sailer, A., Ermer, F., Kraus, Y., Lutter, F. H., Donau, C., Bremerich, M., Ahlfeld, J., & Thorn-Seshold, O. (2019). Hemithioindigos for Cellular Photopharmacology: Desymmetrised Molecular Switch Scaffolds Enabling Design Control over the Isomer-Dependency of Potent Antimetabolic Bioactivity. *ChemBioChem*, 20(10), 1305–1314.

Sakaba, T., Schneggenburger, R., & Neher, E. (2002). Estimation of quantal parameters at the calyx of Held synapse. *Neuroscience Research*, 44(4), 343–356.

Sakers, K., Lake, A. M., Khazanchi, R., Ouwenga, R., Vasek, M. J., Dani, A., & Dougherty, J. D. (2017). Astrocytes locally translate transcripts in their peripheral processes. *Proceedings of the National Academy of Sciences of the United States of*

America, 114(19), E3830–E3838.

Salvatierra, E., Alvarez, M. J., Leishman, C. C., Baquero, E. R., Lutzky, V. P., Chuluyan, H. E., & Podhajcer, O. L. (2015). SPARC controls melanoma cell plasticity through Rac1. *PLoS ONE*, 10(8), 1–20.

Sánchez-Huertas, C., Freixo, F., Viais, R., Lacasa, C., Soriano, E., & Lüders, J. (2016). Non-centrosomal nucleation mediated by augmin organizes microtubules in post-mitotic neurons and controls axonal microtubule polarity. *Nature Communications*, 7, 12187.

Sanes, J. R., & Zipursky, S. L. (2020). Synaptic Specificity, Recognition Molecules, and Assembly of Neural Circuits. *Cell*, 181, 536–556.

Sanes, R. J., & Lichtman, J. W. (1999). Development of the vertebrate neuromuscular junction. *Annu Rev. Neurosci.*, 22, 389–442.

Sankaranarayanan, S., Atluri, P. P., & Ryan, T. A. (2003). Actin has a molecular scaffolding, not propulsive, role in presynaptic function. *Nature Neuroscience*, 6(2), 127–135.

Sara, Y., Bal, M., Adachi, M., Monteggia, L. M., & Kavalali, E. T. (2011). Use-dependent AMPA receptor block reveals segregation of spontaneous and evoked glutamatergic neurotransmission. *Journal of Neuroscience*, 31(14), 5378–5382.

Sara, Y., Virmani, T., Deák, F., Liu, X., & Kavalali, E. T. (2005). An isolated pool of vesicles recycles at rest and drives spontaneous neurotransmission. *Neuron*, 45(4), 563–573.

Sasaki, T., Göhring, W., Mann, K., Maurer, P., Hohenester, E., Knäuper, V., Murphy, G., & Timpl, R. (1997). Limited cleavage of extracellular matrix protein BM-40 by matrix metalloproteinases increases its affinity for collagens. *Journal of Biological Chemistry*, 272(14), 9237–9243.

Sasaki, T., Hohenester, E., Göhring, W., & Timpl, R. (1998). Crystal structure and mapping by site-directed mutagenesis of the collagen-binding epitope of an activated form of BM-40/SPARC/osteonectin. *EMBO Journal*, 17(6), 1625–1634.

Sasaki, T., Miosge, N., & Timpl, R. (1999). Immunochemical and tissue analysis of protease generated neopeptides of BM-40 (osteonectin, SPARC) which are correlated to a higher affinity binding to collagens. *Matrix Biology*, 18(5), 499–508.

Schafer, D. P., Lehrman, E. K., Kautzman, A. G., Koyama, R., Mardinly, A. R., Yamasaki, R., Ransohoff, R. M., Greenberg, M. E., Barres, B. A., & Stevens, B. (2012). Microglia Sculpt Postnatal Neural Circuits in an Activity and Complement-Dependent Manner. *Neuron*, 74(4), 691–705.

Schätzle, P., Esteves da Silva, M., Tas, R. P., Katrukha, E. A., Hu, H. Y., Wierenga, C. J., Kapitein, L. C., & Hoogenraad, C. C. (2018). Activity-Dependent Actin Remodeling at the Base of Dendritic Spines Promotes Microtubule Entry. *Current Biology*, 28(13), 2081–2093.e6.

Scheibel, M., & Scheibel, A. (1971). Inhibition and the Renshaw Cell. A Structu-

ral Critique. *Brain Behav Evol*, 4(1), 53–93.

Scheiffele, P., Fan, J., Choih, J., Fetter, R., & Serafini, T. (2000). Neuroligin expressed in nonneuronal cells triggers presynaptic development in contacting axons. *Cell*, 101(6), 657–669.

Scheuss, V., Schneggenburger, R., & Neher, E. (2002). Separation of presynaptic and postsynaptic contributions to depression by covariance analysis of successive EPSCs at the calyx of held synapse. *Journal of Neuroscience*, 22(3), 728–739.

Schikorski, T., & Stevens, C. F. (1997). Quantitative Ultrastructural Analysis of Hippocampal. *J. Neurosci.*, 17(15), 5858–5867.

Schneggenburger, R., Meyer, A. C., & Neher, E. (1999). Released Fraction and Total Size of a Pool of Immediately Available Transmitter Quanta at a Calyx Synapse. *Neuron*, 23, 399–409.

Schneggenburger, R., & Neher, E. (2000). Intracellular calcium dependence of transmitter release rates at fast central synapse. *Nature*, 406, 889–893.

Schneggenburger, R., & Neher, E. (2005). Presynaptic calcium and control of vesicle fusion. *Current Opinion in Neurobiology*, 15, 266–274.

Schuyler, S. C., & Pellman, D. (2001). Microtubule “plus-end-tracking proteins”: The end is just the beginning. *Cell*, 105, 421–424.

Sengpiel, F., & Kind, P. C. (2002). The role of activity in development of the visual system. *Current Biology*, 12(23), 818–826.

Seung, H. S., Lee, D. D., Reis, B. Y., & Tank, D. W. (2000). The autapse: A simple illustration of short-term analog memory storage by tuned synaptic feedback. *Journal of Computational Neuroscience*, 9(2), 171–185.

Shapira, M., Zhai, R. G., Dresbach, T., Bresler, T., Torres, V. I., Gundelfinger, E. D., Ziv, N. E., & Garner, C. C. (2003). Unitary assembly of presynaptic active zones from Piccolo-Bassoon transport vesicles. *Neuron*, 38, 237–252.

Sharpless, S. (1975). Supersensitivity-like phenomena in the central nervous system. *Fed Proc*, 34(10), 1990–1997.

Sheng, M., & Kim, E. (2011). The postsynaptic organization of synapses. *Cold Spring Harbor Perspectives in Biology*, 3(12), 1–20.

Shepherd, J. D., Rumbaugh, G., Wu, J., Chowdhury, S., Plath, N., Kuhl, D., Huganir, R. L., & Worley, P. F. (2006). Arc/Arg3.1 Mediates Homeostatic Synaptic Scaling of AMPA Receptors. *Neuron*, 52, 475–484.

Shi, W. X., & Rayport, S. (1994). GABA synapses formed in vitro by local axon collaterals of nucleus accumbens neurons. *Journal of Neuroscience*, 14(7), 4548–4560.

Shupliakov, O., Bloom, O., Gustafsson, J. S., Kjaerulff, O., Löw, P., Tomilin, N., Pieribone, V. A., Greengard, P., & Brodin, L. (2002). Impaired recycling of synaptic vesicles after acute perturbation of the presynaptic actin cytoskeleton. *Proceedings*



of the National Academy of Sciences of the United States of America, 99(22), 14476–14481.

Sigler, A., Oh, W. C., Imig, C., Altas, B., Kawabe, H., Cooper, B. H., Kwon, H. B., Rhee, J. S., & Brose, N. (2017). Formation and Maintenance of Functional Spines in the Absence of Presynaptic Glutamate Release. *Neuron*, 94, 304–311.

Skwarczynski, M., Noguchi, M., Hirota, S., Sohma, Y., Kimura, T., Hayashi, Y., & Kiso, Y. (2006). Development of first photoresponsive prodrug of paclitaxel. *Bioorganic and Medicinal Chemistry Letters*, 16(17), 4492–4496.

Song, J. W., Misgeld, T., Kang, H., Knecht, S., Lu, J., Cao, Y., Cotman, S. L., Bishop, D. L., & Lichtman, J. W. (2008). Lysosomal activity associated with developmental axon pruning. *Journal of Neuroscience*, 28(36), 8993–9001.

Song, Y., & Brady, S. T. (2015). Posttranslational Modifications of Tubulin: Pathways to Functional Diversity of Microtubules. *Trends Cell Biol*, 25(3), 125–136.

Soykan, T., Kaempf, N., Sakaba, T., Vollweiter, D., Goerdeler, F., Puchkov, D., Kononenko, N. L., & Haucke, V. (2017). Synaptic Vesicle Endocytosis Occurs on Multiple Timescales and Is Mediated by Formin-Dependent Actin Assembly. *Neuron*, 93, 854-866.e4.

Star, E. N., Kwiatkowski, D. J., & Murthy, V. N. (2002). Rapid turnover of actin in dendritic spines and its regulation by activity. *Nature Neuroscience*, 5(3), 239–246.

Staras, K., Branco, T., Burden, J. J., Pozo, K., Darcy, K., Marra, V., Ratnayaka, A., & Goda, Y. (2010). A Vesicle Superpool Spans Multiple Presynaptic Terminals in Hippocampal Neurons. *Neuron*, 66, 37–44.

Steinmetz, M. O., & Prota, A. E. (2018). Microtubule-Targeting Agents: Strategies To Hijack the Cytoskeleton. *Trends in Cell Biology*, 28(10), 776–792.

Stepanova, T., Slemmer, J., Hoogenraad, C. C., Lansbergen, G., Dortland, B., De Zeeuw, C. I., Grosveld, F., Van Cappellen, G., Akhmanova, A., & Galjart, N. (2003). Visualization of microtubule growth in cultured neurons via the use of EB3-GFP (end-binding protein 3-green fluorescent protein). *Journal of Neuroscience*, 23(7), 2655–2664.

Stevens, B., Allen, N. J., Vazquez, L. E., Howell, G. R., Christopherson, K. S., Nouri, N., Micheva, K. D., Mehalow, A. K., Huberman, A. D., Stafford, B., Sher, A., Litke, A. M. M., Lambris, J. D., Smith, S. J., John, S. W. M., & Barres, B. A. (2007). The Classical Complement Cascade Mediates CNS Synapse Elimination. *Cell*, 131(6), 1164–1178.

Stevens, C. F., & Wesseling, J. F. (1999). Identification of a novel process limiting the rate of synaptic vesicle cycling at hippocampal synapses. *Neuron*, 24, 1017–1028.

Stevens, C. F., & Williams, J. H. (2007). Discharge of the readily releasable pool with action potentials at hippocampal synapses. *Journal of Neurophysiology*, 98, 3221–3229.

- Stevens, T. H., & Forgac, M. (1997). Structure, function and regulation of the vacuolar (H<sup>+</sup>)-ATPases. *Annu. Rev. Cell. Dev. Biol.*, 1, 779–808.
- Stogsdill, J. A., & Eroglu, C. (2017). The interplay between neurons and glia in synapse development and plasticity. *Curr Opin Neurobiol*, 42, 1–8.
- Stumpff, J., von Dassow, G., Wagenbach, M., Asbury, C., & Wordeman, L. (2008). The Kinesin-8 Motor Kif18A Suppresses Kinetochore Movements to Control Mitotic Chromosome Alignment. *Developmental Cell*, 14(2), 252–262.
- Südhof, T. C. (2004). the Synaptic Vesicle Cycle. *Annual Review of Neuroscience*, 27, 509–547.
- Südhof, T. C. (2012). The Presynaptic Active Zone. *Neuron*, 75(1), 11–25.
- Sudo, H., & Baas, P. W. (2010). Acetylation of microtubules influences their sensitivity to severing by katanin in neurons and fibroblasts. *Journal of Neuroscience*, 30(21), 7215–7226.
- Sulzer, D., Joyce, M. P., Lin, L., Geldwert, D., Haber, S. N., Hattori, T., & Rayport, S. (1998). Dopamine neurons make glutamatergic synapses in vitro. *Journal of Neuroscience*, 18(12), 4588–4602.
- Sun, Q., & Turrigiano, G. G. (2011). PSD-95 and PSD-93 play critical but distinct roles in synaptic scaling up and down. *Journal of Neuroscience*, 31(18), 6800–6808.
- Tai, C. Y., Kim, S. A., & Schuman, E. M. (2008). Cadherins and synaptic plasticity. *Current Opinion in Cell Biology*, 20, 567–575.
- Takamori, S., Holt, M., Stenius, K., Lemke, E. A., Grønborg, M., Riedel, D., Urlaub, H., Schenck, S., Brügger, B., Ringler, P., Müller, S. A., Rammner, B., Gräter, F., Hub, J. S., De Groot, B. L., Mieskes, G., Moriyama, Y., Klingauf, J., Grubmüller, H., ... Jahn, R. (2006). Molecular Anatomy of a Trafficking Organelle. *Cell*, 127, 831–846.
- Tamás, G., Buhl, E. H., & Somogyi, P. (1997). Massive autaptic self-innervation of GABAergic neurons in cat visual cortex. *Journal of Neuroscience*, 17(16), 6352–6364.
- Tang, G., Gudsnuk, K., Kuo, S. H., Cotrina, M. L., Rosoklija, G., Sosunov, A., Sonders, M. S., Kanter, E., Castagna, C., Yamamoto, A., Yue, Z., Arancio, O., Peterson, B. S., Champagne, F., Dwork, A. J., Goldman, J., & Sulzer, D. (2014). Loss of mTOR-Dependent Macroautophagy Causes Autistic-like Synaptic Pruning Deficits. *Neuron*, 83, 1131–1143.
- Tao-Cheng, J. H. (2007). Ultrastructural localization of active zone and synaptic vesicle proteins in a preassembled multi-vesicle transport aggregate. *Neuroscience*, 150, 575–584.
- Tardin, C., Cognet, L., Bats, C., Lounis, B., & Choquet, D. (2003). Direct imaging of lateral movements of AMPA receptors inside synapses. *The EMBO Journal*, 22(18), 4556–4665.
- Tashiro, A., & Yuste, R. (2003). Structure and molecular organization of dendritic spines. *Histology and Histopathology*, 18, 617–634.

- Taylor, E. W. (1965). The mechanism of colchicine inhibition of mitosis. *J Cell Biol.*, 25(1), 145–160.
- Temporal, S., Desai, M., Khorkova, O., Varghese, G., Dai, A., Schulz, D. J., & Golowasch, J. (2012). Neuromodulation independently determines correlated channel expression and conductance levels in motor neurons of the stomatogastric ganglion. *Journal of Neurophysiology*, 107, 718–727.
- Termine, J. D., Kleinman, H. K., Whitson, S. W., Conn, K. M., McGarvey, M. L., & Martin, G. R. (1981). Osteonectin, a bone-specific protein linking mineral to collagen. *Cell*, 26(Part 1), 99–105.
- Terni, B., López-Murcia, F. J., & Llobet, A. (2017). Role of neuron-glia interactions in developmental synapse elimination. *Brain Research Bulletin*, 129, 74–81.
- Thiery, J. P., Brackenbury, R., Rutishauser, U., & Edelman, G. M. (1977). Adhesion among neural cells of the chick embryo. II. Purification and characterization of a cell adhesion molecule from neural retina. *Journal of Biological Chemistry*, 252(19), 6841–6845.
- Thomson, A. M., Deuchars, J., & West, D. C. (1993). Large, deep layer pyramidal-pyramid single axon EPSPs in slices of rat motor cortex display paired pulse and frequency-dependent depression, mediated presynaptically and self-facilitation, mediated postsynaptically. *Journal of Neurophysiology*, 70(6), 2354–2369.
- Thomson, Alex M., West, D. C., Hahn, J., & Deuchars, J. (1996). Single axon IPSPs elicited in pyramidal cells by three classes of interneurons in slices of rat neocortex. *Journal of Physiology*, 496(1), 81–102.
- Toei, M., Saum, R., & Forgac, M. (2010). Regulation and Isoform Function of the V-ATPases Masashi. *Biochemistry*, 49(23), 4715–4723.
- Trachtenberg, J. T., Chen, B. E., Knott, G. W., Feng, G., Sanes, J. R., Welker, E., & Svoboda, K. (2002). Long-term in vivo imaging of experience-dependent synaptic plasticity in adult cortex. *Nature*, 420, 788–794.
- Truckenbrodt, S., & Rizzoli, S. O. (2014). Spontaneous vesicle recycling in the synaptic bouton. *Frontiers in Cellular Neuroscience*, 8, 409.
- Trussell, L. O., Zhang, S., & Ramant, I. M. (1993). Desensitization of AMPA receptors upon multiquantal neurotransmitter release. *Neuron*, 10(6), 1185–1196.
- Tsai, N. P., Wilkerson, J. R., Guo, W., Maksimova, M. A., Demartino, G. N., Cowan, C. W., & Huber, K. M. (2012). Multiple autism-linked genes mediate synapse elimination via proteasomal degradation of a synaptic scaffold PSD-95. *Cell*, 151(7), 1581–1594.
- Turrigiano, G., Abbott, L. F., & Marder, E. (1994). Activity-dependent changes in the intrinsic properties of cultured neurons. *Science*, 264, 974–977.
- Turrigiano, G. G., Leslie, K. R., Desai, N. S., Rutherford, L. C., & Nelson, S. B. (1998). Activity-dependent scaling of quantal amplitude in neocortical neurons. *Nature*, 391, 892–896.

- Turrigiano, Gina G., & Nelson, S. B. (2004). Homeostatic plasticity in the developing nervous system. *Nature Reviews Neuroscience*, 5, 97–107.
- Turrigiano, Gina G. (2008). The Self-Tuning Neuron: Synaptic Scaling of Excitatory Synapses. *Cell*, 135, 422–435.
- Turrigiano, Gina G. (2012). Homeostatic synaptic plasticity: Local and global mechanisms for stabilizing neuronal function. *Cold Spring Harbor Perspectives in Biology*, 4(1), 1–17.
- Ulrich, D., & Luscher, H. R. (1993). Miniature excitatory synaptic currents corrected for dendritic cable properties reveal quantal size and variance. *Journal of Neurophysiology*, 69(5), 1769–1773.
- Vale, R. D., Schnapp, B. J., Reese, T. S., & Sheetz, M. P. (1985). Movement of organelles along filaments dissociated from the axoplasm of the squid giant axon. *Cell*, 40(2), 449–454.
- Vallee, R. B. (1982). A Taxol-dependent Procedure for the Isolation of Microtubules and Microtubule-associated Proteins (MAPs). *The Journal of Cell Biology*, 92, 435–442.
- Van Haren, J., Charafeddine, R. A., Ettinger, A., Wang, H., Hahn, K. M., & Wittmann, T. (2018). Local control of intracellular microtubule dynamics by EB1 photodissociation. *Nature Cell Biology*, 20(3), 252–261.
- Velema, W. A., Szymanski, W., & Feringa, B. L. (2014). Photopharmacology: Beyond proof of principle. *Journal of the American Chemical Society*, 136(6), 2178–2191.
- Vere-Jones, D. (1966). Simple stochastic models for the release of quanta of transmitter from a nerve terminal. *Aust. J. Statist.*, 8, 53–63.
- Vincent, A. J., Lau, P. W., & Roskams, A. J. (2008). SPARC is expressed by macroglia and microglia in the developing and mature nervous system. *Developmental Dynamics*, 237(5), 1449–1462.
- Vukoja, A., Rey, U., Petzoldt, A. G., Ott, C., Vollweiler, D., Quentin, C., Puchkov, D., Reynolds, E., Lehmann, M., Hohensee, S., Rosa, S., Lipowsky, R., Sigrist, S. J., & Haucke, V. (2018). Presynaptic Biogenesis Requires Axonal Transport of Lysosome-Related Vesicles. *Neuron*, 99, 1–17.
- Wadiche, J. I., & Jahr, C. E. (2001). Multivesicular release at climbing fiber-Purkinje cell synapses. *Neuron*, 32, 301–313.
- Walsh, M. K., & Lichtman, J. W. (2003). In vivo time-lapse imaging of synaptic takeover associated with naturally occurring synapse elimination. *Neuron*, 37(1), 67–73.
- Wang, X. H., Zheng, J. Q., & Poo, M. M. (1996). Effects of cytochalasin treatment on short-term synaptic plasticity at developing neuromuscular junctions in frogs. *Journal of Physiology*, 491(1), 187–195.
- Wang, X., Wang, Q., Engisch, K. L., & Rich, M. M. (2010). Activity-dependent

- regulation of the binomial parameters  $p$  and  $n$  at the mouse neuromuscular junction in vivo. *Journal of Neurophysiology*, 104, 2352–2358.
- Watanabe, S., Rost, B. R., Camacho-Pérez, M., Davis, M. W., Söhl-Kielczynski, B., Rosenmund, C., & Jorgensen, E. M. (2013). Ultrafast endocytosis at mouse hippocampal synapses. *Nature*, 504, 242–247.
- Watanabe, S., Trimbuch, T., Camacho-Pérez, M., Rost, B. R., Brokowski, B., Söhl-Kielczynski, B., Felies, A., Davis, M. W., Rosenmund, C., & Jorgensen, E. M. (2014). Clathrin regenerates synaptic vesicles from endosomes. *Nature*, 515(7526), 228–233.
- Weiner, A. T., Thyagarajan, P., Shen, Y., & Rolls, M. M. (2021). To nucleate or not, that is the question in neurons. *Neuroscience Letters*, 751(March), 135806.
- Westrum, L. E., & Gray, E. G. (1977). Microtubules associated with postsynaptic “thickenings.” *Journal of Neurocytology*, 6(5), 505–518.
- Weyhersmüller, A., Hallermann, S., Wagner, N., & Eilers, J. (2011). Rapid active zone remodeling during synaptic plasticity. *Journal of Neuroscience*, 31(16), 6041–6052.
- Wienisch, M., & Klingauf, J. (2006). Vesicular proteins exocytosed and subsequently retrieved by compensatory endocytosis are nonidentical. *Nature Neuroscience*, 9(8), 1019–1027.
- Wierenga, C. J., Walsh, M. F., & Turrigiano, G. G. (2006). Temporal regulation of the expression locus of homeostatic plasticity. *Journal of Neurophysiology*, 96, 2127–2133.
- Wilhelm, B. G., Groemer, T. W., & Rizzoli, S. O. (2010). The same synaptic vesicles drive active and spontaneous release. *Nature Neuroscience*, 13(12), 1454–1456.
- Wilhelm, B. G., Mandad, S., Truckenbrodt, S., Kröhnert, K., Schäfer, C., Rammner, B., Koo, S. J., Claßen, G. A., Krauss, M., Haucke, V., Urlaub, H., & Rizzoli, S. O. (2014). Composition of isolated synaptic boutons reveals the amounts of vesicle trafficking proteins. *Science*, 344(6187), 1023–1028.
- Wilton, D. K., Dissing-Olesen, L., & Stevens, B. (2019). Neuron-Glia Signaling in Synapse Elimination. *Annual Review of Neuroscience*, 42, 107–127.
- Witte, H., Neukirchen, D., & Bradke, F. (2008). Microtubule stabilization specifies initial neuronal polarization. *Journal of Cell Biology*, 180(3), 619–632.
- Wittmann, T., Dema, A., & van Haren, J. (2020). Lights, cytoskeleton, action: Optogenetic control of cell dynamics. *Current Opinion in Cell Biology*, 66, 1–10.
- Wong, W. T., Faulkner-Jones, B. E., Sanes, J. R., & Wong, R. O. L. (2000). Rapid dendritic remodeling in the developing retina: Dependence on neurotransmission and reciprocal regulation by Rac and Rho. *Journal of Neuroscience*, 20(13), 5024–5036.
- Xu-Friedman, M. A., & Regehr, W. G. (2004). Structural Contributions to Short-Term Synaptic Plasticity. *Physiological Reviews*, 84, 69–85.

- Yamagata, M., Duan, X., & Sanes, J. R. (2018). Cadherins interact with synaptic organizers to promote synaptic differentiation. *Frontiers in Molecular Neuroscience*, 11(142), 1–15.
- Yamauchi, A., Lever, J. D., & Kemp, K. W. (1973). Catecholamine loading and depletion in the rat superior cervical ganglion. A formal fluorescence and enzyme histochemical study with numerical assessments. *Journal of Anatomy*, 114(2), 271–282.
- Yang, J., Yang, H., Liu, Y., Li, X., Qin, L., Lou, H., Duan, S., & Wang, H. (2016). Astrocytes contribute to synapse elimination Via type 2 inositol 1,4,5-trisphosphate receptor-dependent release of ATP. *ELife*, 5(APRIL2016), 1–17.
- Yin, L., Zheng, R., Ke, W., He, Q., Zhang, Y., Li, J., Wang, B., Mi, Z., Long, Y. sheng, Rasch, M. J., Li, T., Luan, G., & Shu, Y. (2018). Autapses enhance bursting and coincidence detection in neocortical pyramidal cells. *Nature Communications*, 9(1).
- Yonekawa, V., Harada, A., Okada, Y., Funakoshi, T., Kanai, Y., Takei, Y., Tera-da, S., Noda, T., & Hirokawa, N. (1998). Defect in synaptic vesicle precursor transport and neuronal cell death in KIF1A motor protein-deficient mice. *Journal of Cell Biology*, 141(2), 431–441.
- Younger, M. A., Müller, M., Tong, A., Pym, E. C., & Davis, G. W. (2013). A presynaptic ENaC channel drives homeostatic plasticity. *Neuron*, 79, 1–14.
- Zemelman, B. V., Lee, G. A., Ng, M., & Miesenböck, G. (2002). Selective photostimulation of genetically chARGed neurons. *Neuron*, 33(1), 15–22.
- Zhang, W., & Benson, D. L. (2001). Stages of synapse development defined by dependence on F-actin. *Journal of Neuroscience*, 21(14), 5169–5181.
- Zhang, Wandong, & Benson, D. L. (2002). Developmentally regulated changes in cellular compartmentation and synaptic distribution of actin in hippocampal neurons. *Journal of Neuroscience Research*, 69(4), 427–436.
- Zhang, Wandong, Vazquez, L., Apperson, M., & Kennedy, M. B. (1999). Citron binds to PSD-95 at glutamatergic synapses on inhibitory neurons in the hippocampus. *Journal of Neuroscience*, 19(1), 96–108.
- Zhao, C. J., Dreosti, E., & Lagnado, L. (2011). Homeostatic synaptic plasticity through changes in presynaptic calcium influx. *Journal of Neuroscience*, 31(20), 7492–7496.
- Zhou, Q., Xiao, M. Y., & Nicoll, R. A. (2001). Contribution of cytoskeleton to the internalization of AMPA receptors. *Proceedings of the National Academy of Sciences of the United States of America*, 98(3), 1261–1266.
- Ziv, N. E., & Garner, C. C. (2004). Cellular and molecular mechanisms of presynaptic assembly. *Nature Reviews Neuroscience*, 5(5), 385–399.
- Zucker, R. S., & Regehr, W. G. (2002). Short-term synaptic plasticity. *Annual Review of Physiology*, 64, 355–405.







# ANNEXES



# 1 Collagen production

Contrary to agarose, which is a non-permissive substrate, collagen type I was used as a growing-permissive substrate for the establishment of microcultures. Collagen was obtained from Sprague Dawley rat tail tendons as described (Lumsden AG et al., 1983) and stored at 4°C for a maximum of 5 months.

Collagen microdots were made by mixing the collagen with RPMI medium and subsequently spraying the mixture with an atomizer on the coverslips.

## Materials and solutions

- » 10 L of MQ-water at 4°C
- » Ethanol 70% (v/v)
- » Acetic acid 3% (v/v), prepared from Glacial acetic acid (ref. UN2789, AppliChem, Panreac, Germany)
- » Glass beaker of 5 L, 600 ml and 250 ml, sterile
- » 4 magnetic stirrers
- » Graduated cylinder of 100 ml
- » 5 sterile 10-cm-diameter Petri dishes
- » Haemostats
- » Scissors
- » Tweezers
- » Dialysis tubing cellulose membrane (ref. D9527, Sigma-Aldrich, St. Louis, MO)
- » 15 ml conical tubes

## Procedure

### *1st day*

- » 4-5 rat tails were collected and sterilized in ethanol 70% for 20 min. Tails can be stored frozen at -20°C and thawed in ethanol.
- » The proximal end of the tail was fixed using a straight haemostat while a second haemostat was closely placed (1-1.5 cm) from the first one. By a sharp and fast twist, tail bones were fractured so they could be carefully removed, leaving the tendons loose.
- » Using the scissors, tendons were cut and placed in sterile MQ-water inside a Petri dish.
- » This process was repeated until all tendons were extracted from the tail.
- » Using the tweezers, tendons were cleaned by separating the fibres from any tissue debris and placed in sterile MQ-water inside a Petri dish. This process was repeated.

ted twice so that the tendons were completely clean.

- » Tendons were drained and approximately 4 g of tendons were placed in 150 ml of prechilled acetic acid 3% (v/v) in a glass beaker.
- » Tendons were dissolved by slow agitation for 24h at 4°C.

As collagen began to dissolve, the solution became viscous, stopping the movement of the magnetic stirrer. Thus, it is important to check that the solution is in constant agitation during the first hours. To prevent dissolution of other proteins, stirring set was as slow as possible.

#### *2nd day*

- » The acetic acid solution containing the dissolved fibres was centrifuged for 90 min at 20000 g and at 4°C (Centrifuge Himac, model CR 22N, rotor Hitachi 47, R15A).
- » Supernatant was collected under the laminar flow hood and placed into the dialysis mesh, which had been previously boiled for 10 min in a 1 mM EDTA solution (pH 8) and washed 5 times with sterile MQ-water. The pellet containing undissolved fibres was discarded.
- » The mesh containing the collagen solution was placed into a 5 L glass beaker filled with 4 L of prechilled MEM 0.1X, pH 4 without carbonate (see the Solutions section) for dialysis.

#### *3rd and 4th day*

- » Dialysis was performed at 4°C in constant agitation for 3 days. Medium was changed every 24 h.
- » Dialysis removes the excess of acid while maintaining a low pH to prevent collagen from gelling, which occurs at an alkaline pH.

#### *5th day*

- » After 72 h, collagen was collected, mixed with 1% (v/v) Penicillin/Streptomycin and distributed in 5 ml aliquots using 15-ml conical sterile tubes. Aliquots were kept at 4°C for up to 5 months.

Because the collagen solution obtained was highly concentrated, its viscosity did not allow proper pulverization to produce collagen microdrops. In addition, collagen becomes solid under alkaline pH, a property we benefited from to generate microdrops and establish SCMs.

Accordingly, the collagen solution obtained was diluted in RPMI-1640 Medium 10x, pH 7.5-8.5 (ref. R1383, Sigma-Aldrich, St. Louis, MO) before spraying onto the 12-well tissue plate.

Because collagen viscosity varies among distinct collagen stocks, the amount of RPMI added needed to be assayed for each stock before use. Typically, collagen:RPMI ratios ranged between 1:5 and 1:10.

## 2 Solutions

### **Agarose II-A 0.15% (w/v)**

This solution was used to coat the coverslips used for the establishment of single cell microcultures from rat superior cervical ganglia. Agarose generates a non-permissive growing substrate in which neurons cannot survive.

-0.06 g of agarose II-A (ref. A9918, Sigma-Aldrich, St. Louis, MO) are diluted in 40 ml of sterile MQ water

-The solution is heated in the microwave and agitated to dissolve the agarose

-500 µl of the agarose solution were added to each well where the coverslips were. Before it became viscous, agarose was removed only leaving a thin coat on the coverslip.

-Agarose was left to dry and sterilize under the laminar flow hood with UV light.

### **Minimum Essential Medium Eagle**

This solution was prepared to produce collagen type I from rat tails

- Minimum Essential Medium Eagle (MEM) (ref. M0644, Sigma-Aldrich, St. Louis, MO) was diluted in 100 ml of sterile MQ water, resulting in a concentration of 10x.

-40 ml of MEM 10x were diluted in 4 L of MQ water to obtain a final concentration of 0.1x that is used for dialysis.

### **Tris-EDTA solution**

This solution was used to chelate calcium ions from the dialysis mesh during collagen production.

-0.088 g of EDTA were diluted in 300 ml of MQ water and pH was adjusted at 8.

Since EDTA acidifies the solution, but its dissolution requires a basic pH, NaOH had to be added to dilute the EDTA while it was in constant agitation.

### **Buffered water, pH 7.3**

This solution was used during lentivirus production to prepare the HEK293T cell transfection mix.

-2.5 mM HEPES was prepared in 50 ml of MQ water and pH was adjusted to 7.3

-The solution was filtered with a 22 µm pore size vacuum filter and kept at 4°C for up to 6 months

### **HeBS 2x saline buffer**

This solution was used during lentivirus production to prepare the HEK293T cell transfection mix.



- 0.28 M NaCl, 0.05 M HEPES and 1.5 M Na<sub>2</sub>HPO<sub>4</sub> were prepared in 500 ml of MQ water
- pH was adjusted to 7 with 10 M NaOH
- The solution was filtered with a 22 µm pore size vacuum filter and kept at 4°C or at -80°C for up to 2 years

### **TE Buffer (Tris-EDTA) 10x**

This solution was used during lentivirus production to prepare the HEK293T cell transfection mix.



- 0.1 M Tris-HCl and 0.01 M EDTA were diluted in 1 L of MQ water producing a 10x stock that had to be diluted to 0.1x for HEK293T transfection.
- The solution was kept at 4°C



# PUBLICATIONS



# Synapse elimination activates a coordinated homeostatic presynaptic response in an autaptic circuit

Cecilia D. Velasco <sup>1,2</sup> & Artur Llobet <sup>1,2</sup>✉

The number of synapses present in a neuronal circuit is not fixed. Neurons must compensate for changes in connectivity caused by synaptic pruning, learning processes or pathological conditions through the constant adjustment of the baseline level of neurotransmission. Here, we show that cholinergic neurons grown in an autaptic circuit in the absence of glia sense the loss of half of their synaptic contacts triggered by exposure to peptide p4.2, a C-terminal fragment of SPARC. Synaptic elimination is driven by a reorganization of the periodic F-actin cytoskeleton present along neurites, and occurs without altering the density of postsynaptic receptors. Neurons recover baseline neurotransmission through a homeostatic presynaptic response that consists of the coordinated activation of rapid synapse formation and an overall potentiation of presynaptic calcium influx. These results demonstrate that neurons establishing autaptic connections continuously sense and adjust their synaptic output by tweaking the number of functional contacts and neurotransmitter release probability.

<sup>1</sup>Department of Pathology and Experimental Therapy, Faculty of Medicine and Health Science, Institute of Neurosciences, University of Barcelona, 08907 L'Hospitalet de Llobregat, Barcelona, Spain. <sup>2</sup>Laboratory of Neurobiology, Bellvitge Biomedical Research Institute (IDIBELL), 08907 L'Hospitalet de Llobregat, Barcelona, Spain. ✉email: [allobet@ub.edu](mailto:allobet@ub.edu)

Synapses must adapt their strength to a constantly changing environment. As a result, synaptic transmission is finely tuned through gain and loss of function mechanisms, which allow the correct function of neuronal circuits<sup>1</sup>. The adaptive properties of synapses can, however, be altered by conditions that modify basal neurotransmission. Changes in excitability, post-synaptic receptor expression, or neurotransmitter release need to be compensated by homeostatic mechanisms that actively return synaptic transmission to the baseline level in order to maintain the stability of neuronal networks<sup>2–4</sup>. The correction of transient unbalances of basal neurotransmission must also take into account that the number of synapses of a given neuronal circuit is not fixed. Synaptic connectivity varies as a function of the developmental stage, learning processes, or certain disease conditions, implying that homeostatic mechanisms have to somehow be able to account for changes in the functional number of contacts present in a given neuronal circuit<sup>5</sup>.

During postnatal development there is a pruning of synapses formed exuberantly during embryogenesis, therefore, the correct processing of information must concur with a massive synapse loss. So far it is unclear how neurons adjust a correct number of connections and what are the mechanisms used to balance formation and elimination<sup>6</sup>. This is in part due to the incomplete understanding of mechanisms causing postnatal elimination of synapses<sup>7</sup>. Despite the determinant role of neuronal activity<sup>8</sup>, there are growing evidences invoking the participation of glial cells<sup>9</sup>. For example, astrocytes appear to cooperate with the complement system to phagocytose selected synapses<sup>10</sup> or secrete ATP to decrease synapse numbers<sup>11</sup>. Microglia, Schwann cells, or satellite cells also participate in the refinement of synaptic connectivity in the central and peripheral nervous system<sup>9,12</sup>. These evidences together illustrate the important role of neuron–glia interactions in the pruning of neuronal connectivity and bring forward the possible implications of their deregulation.

Among the many molecules released by glia, secreted protein acidic and rich in cysteine (SPARC) emerges as an important cue capable of decreasing synapse numbers<sup>13</sup>. In the nervous system SPARC is exclusively produced by glial cells<sup>14</sup>. It is found enriched in the peripheral processes of astrocytes<sup>15</sup> and its production peaks postnatally<sup>14</sup>. Hence, the enhanced secretion of SPARC could contribute to the developmental pruning of synaptic contacts, as well as, to the elimination of synapses found in certain pathological conditions.

The current work investigates how a neuron establishing an autaptic circuit reacts to the elimination of connectivity driven by SPARC. Although autapses are normally established by certain excitatory and inhibitory neurons<sup>16–18</sup>, it is yet unclear how they participate in the processing of information. Taking advantage of the ability of superior cervical ganglion neurons to form cholinergic autaptic contacts in the absence of glial cells<sup>19,20</sup>, we investigated the neuronal reaction to synapse elimination caused by exposure to a C-terminal fragment of SPARC. The finding of a compensatory response based in the addition of new release sites coordinated with a potentiation of presynaptic calcium influx sheds light on how autaptic circuits maintain a constant synaptic output.

## Results

### Peptide p4.2 induces a biphasic change in synaptic strength.

Previous observations showed that exposure of cholinergic single cell microcultures (SCMs) for 2–5 h to 200 nM p4.2, a 20 amino acid peptide derived from the EC-domain of SPARC, activates a process of synapse elimination<sup>13</sup>. To find out if all autaptic contacts established by a single neuron could be disassembled or, if in contrast, there were synapses resistant to elimination, the

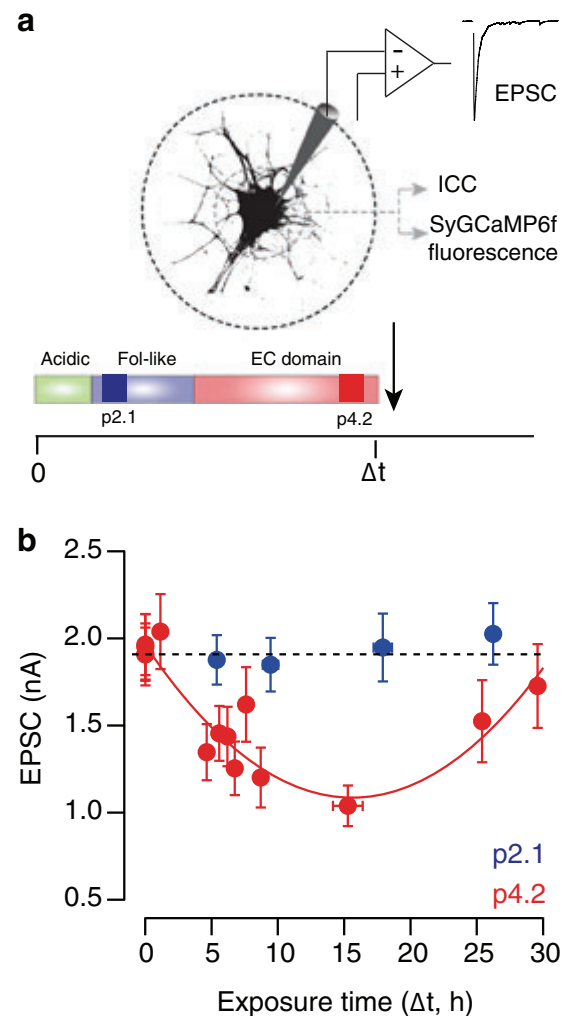


**Fig. 1 Exposure to p4.2 induces a biphasic response in synaptic strength.**

**a** Experimental setup. Evoked excitatory postsynaptic currents (EPSCs) were recorded from cholinergic single cell microcultures (SCMs). Electrophysiological recordings were associated to immunocytochemistry (ICC) for synaptic markers or to imaging of presynaptic calcium influx using synaptophysin::GCaMP6f (SyGCaMP6f). SCMs were exposed for variable time intervals to p4.2, a 20 amino acid peptide derived from the EC-domain of SPARC, which triggers a cell-autonomous mechanism of synapse elimination. The 20 amino acid peptide p2.1, derived from the SPARC follistatin-like domain, was used as control. **b** A parabolic fit,  $EPSC(t) = 3.49t^2 - 109.4t + 1960$ , described changes in EPSC amplitude (pA) as a function of p4.2 exposure (t, hours). EPSCs decayed maximally after 15.4 h of exposure to 200 nM p4.2. Longer application times induced a compensatory response that returned EPSCs to control values within 30 h. Each bin indicates the average EPSC amplitude of ten individual neurons. Error bars show s.e.m. ( $n = 280$  SCMs, 50 different cultures). Exposure to p2.1 ( $n = 72$  SCMs, nine different cultures) did not induce any change in basal synaptic strength (dotted line). Each bin shows the average EPSC amplitude of 18 neurons. Error bars indicate s.e.m.

incubation time with p4.2 was prolonged up to 30 h (Fig. 1a). Synapse loss was estimated by quantifying the decay in synaptic strength, measured as the amplitude of excitatory postsynaptic currents (EPSCs). Neither a complete suppression of synaptic transmission, nor a stabilization at a steady-state phase was observed. Synaptic strength reached a maximum decrease followed by a compensatory increase that was complete within ~30 h. Changes in EPSC amplitude were well described by a parabolic fit

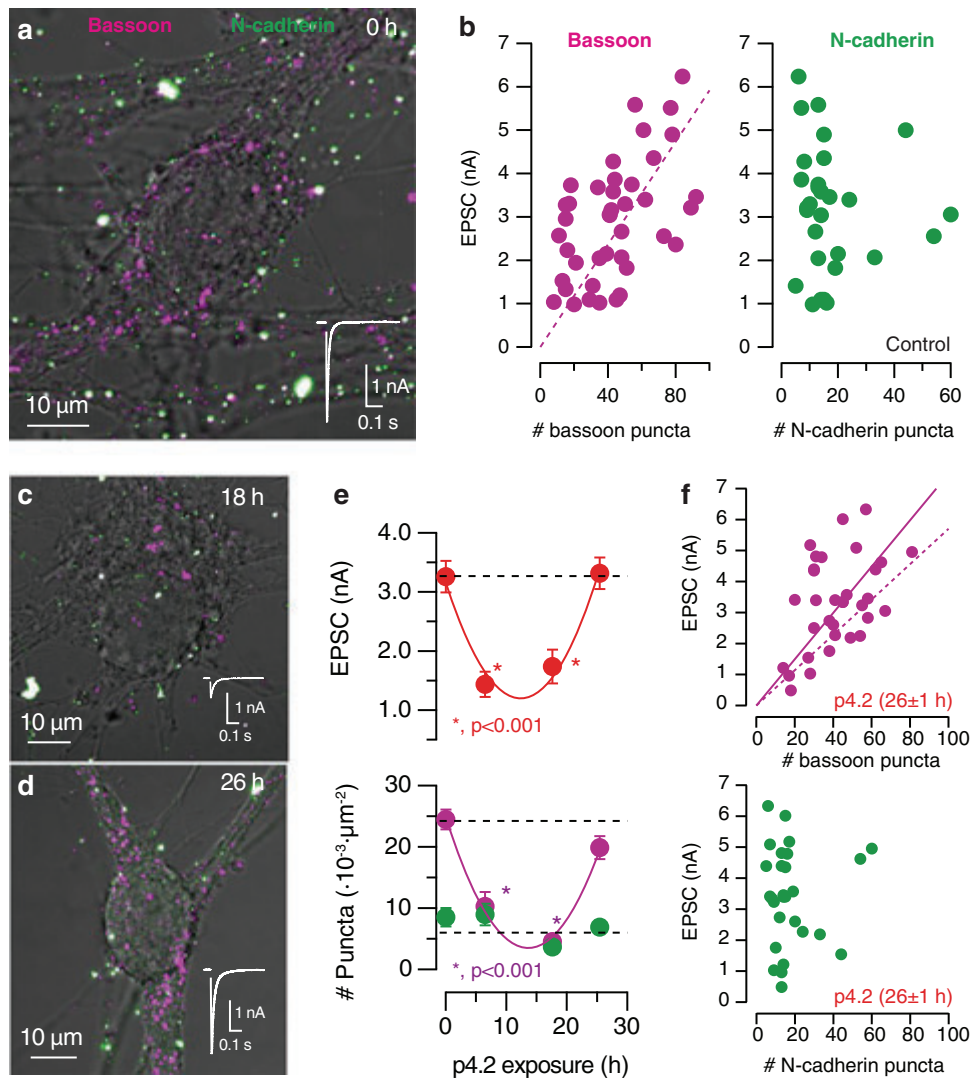


**Fig. 2 Rapid synapse formation compensates synaptic elimination caused by p4.2.** Correlative electrophysiology and immunocytochemistry experiments evaluated how changes in the density of synaptic puncta affected neurotransmission. **a** Image of the somatic and perisomatic region (soma + 20  $\mu\text{m}$  radius) of a SCM stained for bassoon (magenta) and N-cadherin (green). Puncta found within the imaged area were evaluated as putative synapses contributing to the recorded excitatory postsynaptic current (EPSC, white trace). **b** Plots showing the relationship between EPSC amplitude and the number of bassoon or N-cadherin puncta detected in control SCMs ( $n = 41$ ). Only bassoon puncta were linearly related to synaptic strength (59  $\text{pA}\cdot\text{bassoon puncta}^{-1}$ , Pearson correlation coefficient = 0.54). **c, d** Images of the somatic and perisomatic region (soma + 20  $\mu\text{m}$  radius) of two SCMs exposed to p4.2 for 18 and 26 h, respectively. Both images display the associated EPSCs. **e** Relationship of EPSC amplitude as well as density of bassoon and N-cadherin puncta with p4.2 exposure time. Dots indicate mean  $\pm$  s.e.m. Experimental groups: 0 h p4.2 (control),  $n = 28$ ; 6 h p4.2,  $n = 19$ ; 17.6 h p4.2,  $n = 18$ ; 26 h p4.2,  $n = 33$ . Synaptic strength (expressed in pA) and the density of bassoon puncta were both related to p4.2 exposure time by two parabolic functions ( $\text{EPSC}(t) = 13t^2 - 317t + 3162$ ,  $\text{Puncta}(t) = 0.11t^2 - 3.14t + 25$ ). They showed minimum values at 12.4 and 15 h, respectively. Asterisks indicate significant differences relative to control values using one-way ANOVA followed by Bonferroni multiple comparisons test. **f** EPSC amplitude was linearly related (solid line) to the number of bassoon puncta after exposure to p4.2 for 26 h ( $n = 33$ , 72  $\text{pA}\cdot\text{bassoon puncta}^{-1}$ , Pearson correlation coefficient = 0.45). The dotted line indicates the relationship obtained for control SCMs (as in **b**), for comparison purposes. No relationship between synaptic strength and the number of N-cadherin puncta was found after exposure to p4.2 for 26 h ( $n = 33$ ).

(Fig. 1b,  $n = 280$ ). The alterations observed in neurotransmission were not related to changes in neuronal excitability, which was unaffected by exposure to p4.2 (Supplementary Fig. 1). Peptide p2.1, which also contains 20 amino acids but is derived from the SPARC follistatin-like domain, did not modify EPSC amplitude and was used as control (Fig. 1b,  $n = 72$ )<sup>13</sup>.

The biphasic change in synaptic strength observed during exposure to 200 nM p4.2 suggested the activation of a homeostatic, compensatory mechanism of synapse elimination. To investigate this possibility, we carried out correlative electrophysiology and immunocytochemistry experiments. SCMs were

fixed and stained for bassoon and N-cadherin, a presynaptic active zone component and a synaptic adhesion protein, respectively (Fig. 2a). Although both markers showed a punctate staining, only 35% of bassoon labels co-localized with N-cadherin, suggesting the tagging of different structures. Bassoon labeling showed above 80% co-localization with the presynaptic markers synapsin-I and VAMP-2, suggesting a bona fide identification of synaptic terminals (Supplementary Fig. 2). The number of bassoon puncta located in the cell body and nearby dendritic tree (see “Methods” for details) was linearly related to synaptic strength, implying each identified contact contributed

with 59 pA to the recorded EPSC (Fig. 2b). Considering a quantal size of approximately 70 pA, the average probability of neurotransmitter release in a given autapse would be  $\sim 0.8$ , which is in agreement with previous observations<sup>21</sup>. Puncta identified by N-cadherin staining were, however, not linearly related to synaptic strength. This result could arise from the labeling of non-synaptic structures, or, could also reflect the dispensability of N-cadherin in the formation and stabilization of autapses present in SCMs, contrary to those formed by CNS neurons on dendritic spines<sup>22</sup>.

The changes experimented in the density of bassoon puncta during exposure to 200 nM p4.2 paralleled variations in synaptic strength (Fig. 2c–e). Parabolic fits showed that the minimum EPSC amplitude and density of bassoon puncta were reached upon 12.4 and 15 h of p4.2 exposure, respectively. Changes in synaptic strength thus preceded the compensatory increase in the number of bassoon puncta and supported that synapse formation took place in a time window of  $\sim 2.5$  h. New release sites were probably not the unique contributors to the homeostatic response because the original density of bassoon puncta was not completely recovered when EPSCs reached control values (Fig. 2e). The compensatory response likely involved a potentiation of synapses resistant to elimination. The slope of the linear relationship found between EPSC amplitude and the number of bassoon puncta of SCMs exposed to 200 nM p4.2 for more than 24 h (Fig. 2f) indicated that each synapse contributed with approximately 72 pA to neurotransmission, which represented approximately a 25% increase from control neurons. Synaptic strength found at the end of the homeostatic response continued being unrelated to the number of N-cadherin puncta. Altogether, correlative electrophysiology and immunocytochemistry experiments showed that autapses responded to elimination triggered by p4.2 through a coordinated potentiation of synaptic transmission and de novo synapse formation.

### Increased presynaptic calcium influx compensates synapse loss.

To evaluate the mechanisms accounting for the gain in synaptic function, we first investigated the size of the Readily Releasable Pool (RRP) of synaptic vesicles using high frequency stimulation<sup>19,23,24</sup>. The RRP is defined by those vesicles located at active zones that are ready to be released upon the arrival of an action potential. An increase in the RRP size, and thus, in the availability of synaptic vesicles could favor the enhancement of synaptic strength as reported in previous studies<sup>25,26</sup>. The RRP size experimented a biphasic change during exposure to p4.2, reaching the minimum value after 16 h (Fig. 3a). The compensatory response was, however, incomplete in the time interval explored, resembling results obtained for bassoon puncta (Fig. 2e). The study of RRP size was complemented by investigating short-term plasticity. The lower is the number of synaptic vesicles available for release, the higher is the depression assayed by paired pulse stimuli<sup>1</sup>. Depression evoked for a time interval of 50 ms was not modified during the phase of net synapse elimination but, it was enhanced during the compensatory response (Fig. 3b). Paired pulse depression increased by  $\sim 25\%$  in SCMs treated for  $>24$  h with p4.2, which could be explained by the participation of newly formed synapses. Immature contacts contain a low number of synaptic vesicles in their active zones<sup>27</sup> and tend to display short-term depression<sup>28</sup>. An alternative explanation for the increase in paired pulse depression could also be an increase in neurotransmitter release probability driven by the enhancement of presynaptic calcium influx.

To evaluate this possibility, we recorded EPSCs concomitantly to imaging of presynaptic calcium entry using SyGCaMP6f (Fig. 4a, Supplementary movie 1). The indicator accumulated in discrete puncta, which responded to the application of a train of five stimuli

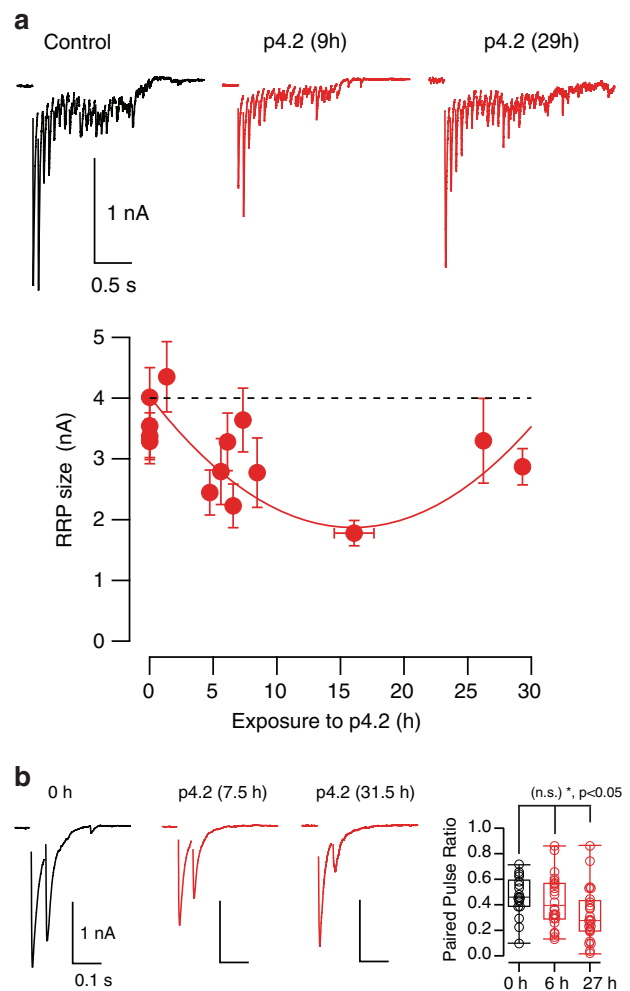


**Fig. 3** Changes in the size of the RRP and paired pulse plasticity during exposure to peptide p4.2. **a** Trains of 20 stimuli delivered at 14 Hz were used to calculate the size of the RRP. Changes in the Ready Releasable Pool (RRP) size were biphasic and were described by a parabolic fit expressed in pA ( $RRP(t) = 8.5t^2 - 270t + 4028$ ). The minimum value was found after 16 h of exposure to peptide p4.2 ( $n = 224$ , each bin shows the mean  $\pm$  s.e.m. of 16 different neurons). **b** Paired pulse plasticity was assayed by delivering two pulses at a time interval of 50 ms at the indicated times of p4.2 exposure. The characteristic depression observed in control neurons was increased at the end of the homeostatic response. Box plot shows the median (horizontal line), 25–75% quartiles (boxes), and ranges (whiskers) of the paired pulse ratio obtained in control neurons ( $n = 18$ ), neurons exposed to p4.2 for  $6.4 \pm 1$  h (mean  $\pm$  s.e.m.,  $n = 26$ ) and neurons exposed to p4.2 for  $27 \pm 1$  h (mean  $\pm$  s.e.m.,  $n = 25$ ). Statistical differences were evaluated using one-way ANOVA followed by Bonferroni multiple comparisons test.

delivered at 20 Hz. The identity of putative synaptic contacts identified with SyGCaMP6f was confirmed after application of 1  $\mu$ M TTX, which suppressed transient changes in fluorescence (Fig. 4b). The distribution of presynaptic calcium increases was well described by three gaussian functions showing mean  $\pm$  SD  $\Delta F/F_0$  changes of  $0.022 \pm 0.01$ ,  $0.100 \pm 0.05$  and  $0.277 \pm 0.02$ , respectively. The three populations were considered to represent terminals of low, medium, and high calcium influx, respectively (Fig. 4c). Since the classification of a given terminal could fluctuate as a result of changes in the open probability of calcium channels, we next evaluated the variability of SyGCaMP6f responses to single stimuli. It was not possible to resolve fluorescence increases in contacts that displayed low presynaptic calcium entry. Only



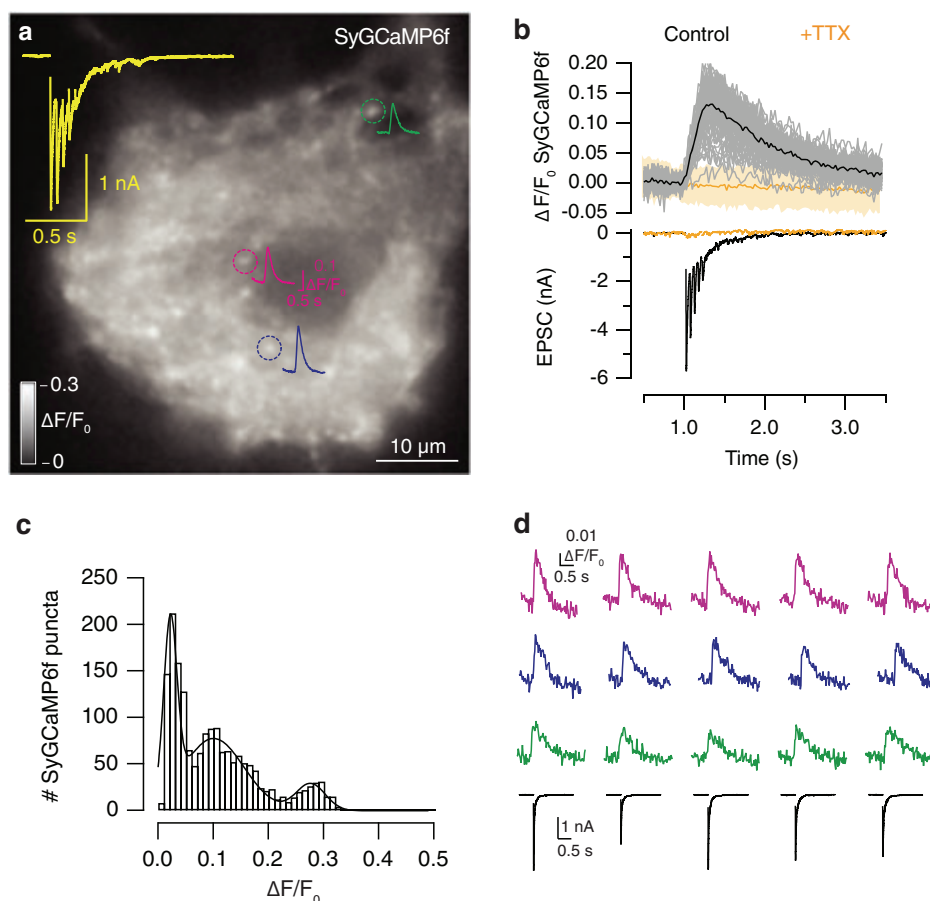


**Fig. 4 Characterization of presynaptic calcium influx in individual autaptic contacts using SyGCaMP6f.** **a** Increase in SyGCaMP6f fluorescence experimented by a SCM upon application of a train of five stimuli delivered at 20 Hz. The image is an average of 32 frames acquired at 40 Hz from the beginning of stimulation. Discrete, round  $\sim 1 \mu\text{m}$  spots that appeared as changes larger than three standard deviations of basal  $\Delta F/F_0$  were considered as functional presynaptic terminals. Dotted circles show the responses of three different synapses. **b** ROIs displaying increases in SyGCaMP6f fluorescence during stimulation (individual synapses, gray traces; average, black trace) did not respond in the presence of  $1 \mu\text{M}$  TTX (orange). The solid orange trace indicates the average response of identified synaptic contacts and shadowed area shows three times the SD. Notice that EPSCs were suppressed in the presence of TTX. **c** Distribution of peak  $\Delta F/F_0$  changes detected in individual puncta in response to a train of five stimuli. Bars show data from control SCMs ( $n = 1755$ , 27 neurons). Fit to gaussian functions identified three population of responses with mean  $\Delta F/F_0$  values of 0.02, 0.1, and 0.28, respectively. **d** Five consecutive responses of the presynaptic terminals identified in **a** to a single depolarization applied at 0.03 Hz. Notice that the increases in SyGCaMP6f fluorescence remained constant while the amplitude of the associated excitatory postsynaptic currents (EPSCs) varied.

synapses showing medium and high presynaptic calcium influx were analyzed. The amplitude of detected SyGCaMP6f transients was stable ( $\text{CV} = 8\%$ ,  $n = 3$  SCMs), compared to the larger variability found in associated EPSCs ( $\text{CV} = 20\%$ ,  $n = 3$  SCMs, Fig. 4d). This result indicates that: (i) a reliable opening of voltage gated calcium channels occurred independently of the intrinsic variations in neurotransmitter release probability, and (ii) global presynaptic calcium influx was an inherent property of identified contacts. Altogether, these results validated the presence of three different populations of synapses.

The characteristic biphasic response in synaptic strength to 200 nM p4.2 was also observed in SCMs expressing SyGCaMP6f (Fig. 5a) but, it was faster than in non-infected neurons (compare to Fig. 1b). The minimum EPSC amplitude was found at 9.4 h and the accomplishment of the compensatory response was observed upon  $\sim 18$  h exposure. SCMs infected with lentiviruses were treated with maximal concentrations of CNTF (see “Methods” for details) to facilitate maximal synapse formation<sup>29</sup>, which could explain the different kinetics of the homeostatic response. Treatment with p2.1 did not cause any alteration in synaptic strength and neither modify the probability of finding terminals with low, medium, or high calcium influx (Fig. 5b). The

amplitude of presynaptic calcium transients in response to a train of five stimuli also remained unaffected after 6 h of p4.2 exposure, however, it was modified during the compensatory response to synapse elimination. There was an overall increase in presynaptic calcium influx after 19 h of exposure to 200 nM p4.2 (Fig. 5c). The populations of contacts showing low, medium and high calcium responses were identified at mean  $\pm$  SD  $\Delta F/F_0$  changes of  $0.054 \pm 0.02$ ,  $0.177 \pm 0.04$ , and  $0.36 \pm 0.04$  (Fig. 5d), which suggested a broad potentiation of synapses resistant to p4.2. The increase in presynaptic calcium influx was also evident in responses evoked by single stimuli. For example, Fig. 5e illustrates a neuron exposed for 19 h to p4.2 that displayed a comparable synaptic strength to a control neuron but, showed larger presynaptic calcium transients. On average the amplitude of  $\Delta F/F_0$  SyGCaMP6f changes evoked by single stimulation raised from  $3.8 \pm 0.4\%$  ( $n = 13$ ) to  $5.6 \pm 0.4$  (mean  $\pm$  s.e.m.,  $n = 15$ ,  $p = 0.009$ , unpaired  $t$ -test) by the end of the compensatory response, thus confirming a gain in presynaptic calcium entry.

**Synapse loss does not alter the density of nicotinic receptors.** To find out whether the compensatory increase of synaptic

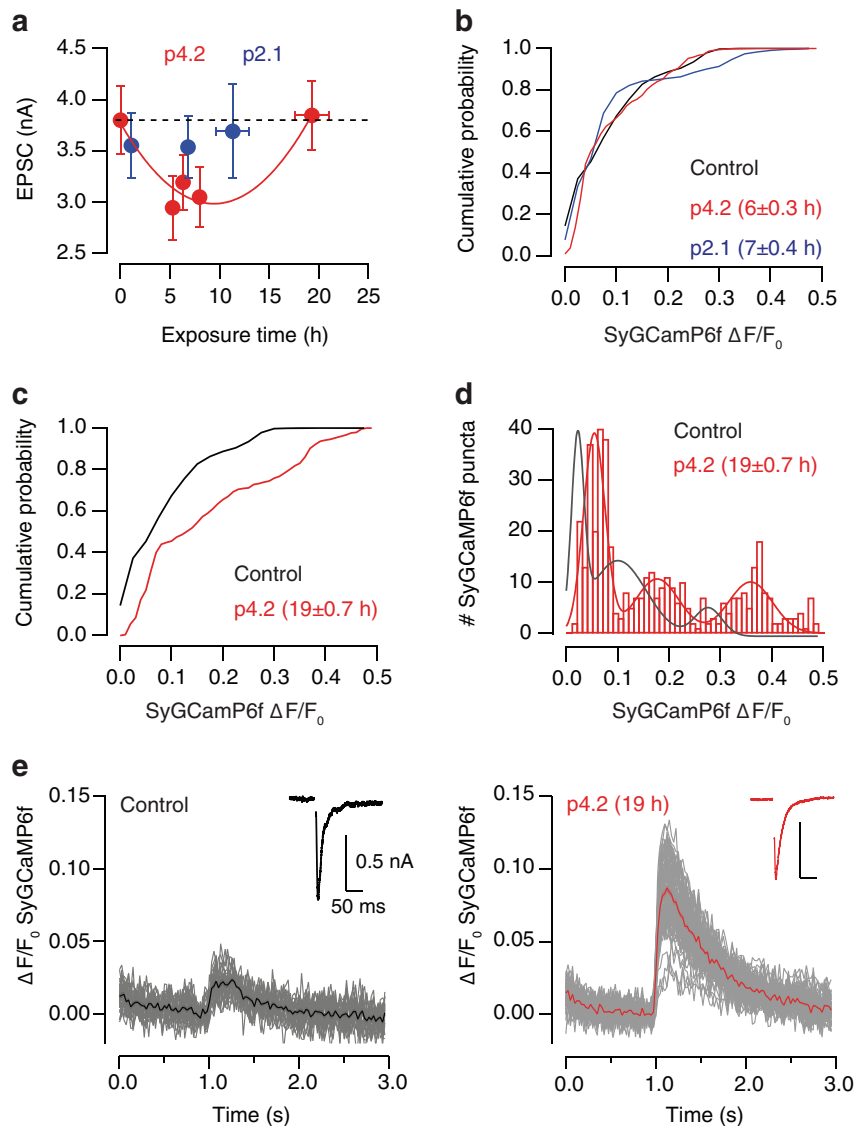


**Fig. 5 Exposure to p4.2 causes an increase in presynaptic calcium influx.** **a** Changes in EPSC amplitude during exposure of SCMs expressing SyGCaMP6f to 200 nM p4.2 or 200 nM p2.1. Changes in synaptic strength during treatment with peptide p4.2 followed a parabolic function showing a minimum value at 9.4 h ( $EPSC(t) = 3.6t^2 - 112t + 1961$ , expressed in pA). Bins indicate mean  $\pm$  s.e.m. of 11 SCMs, ( $n = 55$ ). Notice that exposure to p2.1 did not modify EPSC size (bins indicate mean  $\pm$  s.e.m. of 8 SCMs,  $n = 24$ ). **b, c** Cumulative probability of increases in SyGCaMP6f  $\Delta F/F_0$  found in individual puncta upon application of a train of five stimuli delivered at 20 Hz. Data are illustrated for two time intervals of p4.2 exposure, which correspond to the minimum value of synaptic strength (**b**  $6 \pm 0.3$  h,  $n = 847$ , 20 SCMs) and to the completion of the compensatory response (**c**  $19 \pm 0.7$  h,  $n = 521$ , 10 SCMs), respectively. Time of exposure to p4.2 is indicated as mean  $\pm$  s.e.m. Responses obtained in control conditions or in cells treated with p2.1 ( $n = 647$ ) are displayed for comparison purposes. **d** Histogram showing individual peak  $\Delta F/F_0$  changes obtained upon stimulation with a train of five stimuli delivered at 20 Hz ( $n = 521$ , 10 SCMs) in cells exposed to p4.2 for  $19 \pm 0.7$  h (mean  $\pm$  s.e.m.). They were described by three gaussian functions showing mean  $\Delta F/F_0$  values of 0.05 and 0.18 and 0.36. The gray trace shows the scaled profile of the distribution of control responses for comparison purposes. **e** SyGCaMP6f responses of two different SCMs that showed comparable synaptic strength. Left, control neuron. The average response is shown in black. Right, presynaptic calcium increases recorded at the end of the compensatory response to synapse elimination. The average response is shown in red.

strength had also a postsynaptic component, we evaluated the contribution of nicotinic receptors to neurotransmission. Recordings obtained by electrical stimulation followed by the application of a local puff of 50  $\mu$ M acetylcholine showed that the amplitude of EPSCs was comparable to the amplitude of chemically evoked nicotinic currents (Fig. 6a). The relationship between both types of postsynaptic currents was altered by p4.2 exposure. The characteristic decrease in synaptic strength was not followed by a reduction in the amplitude of nicotinic currents, which remained constant throughout the period investigated (Fig. 6b). Exposure to peptide p2.1 did not modify the response to

chemical or electrical stimulation (Fig. 6c). This result suggested that peptide p4.2 caused synapse elimination by driving the removal of the presynaptic element without affecting the density of postsynaptic cholinergic receptors.

Since local delivery of acetylcholine acts on both synaptic and extrasynaptic nicotinic receptors, we next investigated the role of synaptic receptors by analysing quantal size. The amplitude of miniature excitatory postsynaptic currents (mEPSCs) remained unaltered in SCMs exposed to p4.2 for different time intervals (Fig. 6d, e). A uniform average quantal size of  $\sim 70$  pA, which was similar to previously reported values<sup>19,30</sup>, demonstrated that the

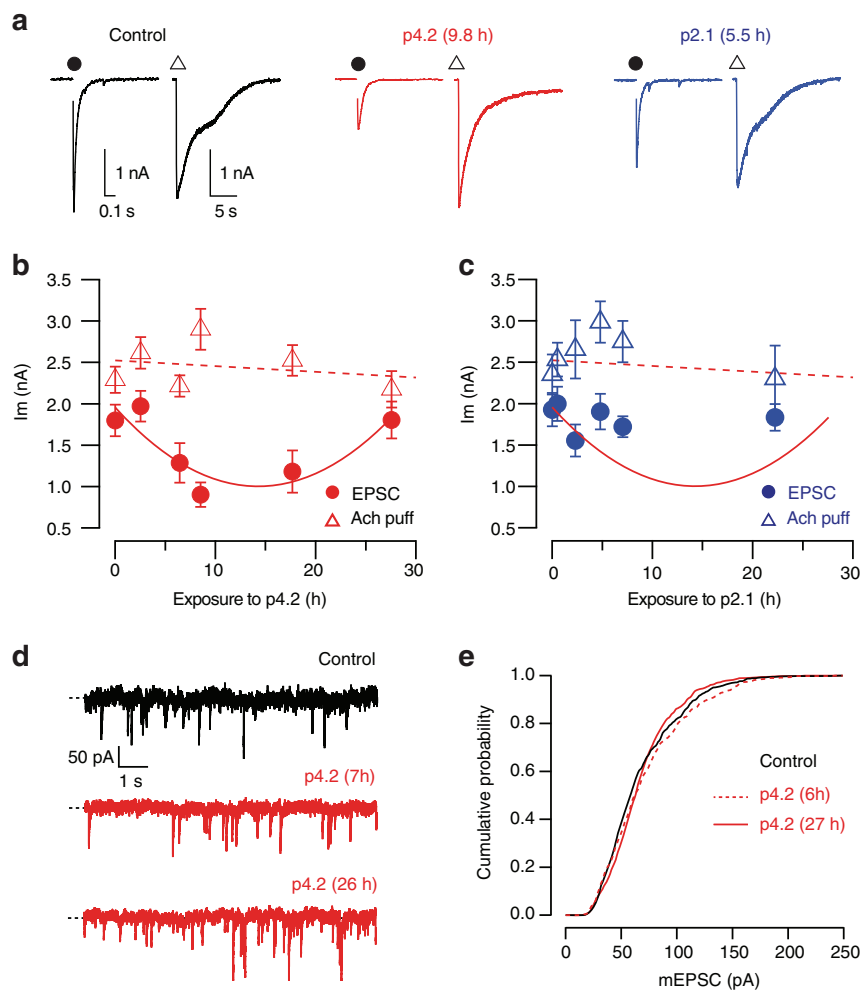


**Fig. 6** Separation of the pre and postsynaptic components of the compensatory response to p4.2 action. **a** Recordings of evoked neurotransmission obtained by a sequential depolarization (dot) and a local puff of 50  $\mu$ M acetylcholine (triangle). Time interval between electrical and chemical stimulation was 1 min. The examples illustrate the characteristic responses obtained in control SCMs or, upon exposure to p4.2 and p2.1. **b** Whilst the amplitude of EPSCs decayed during exposure to p4.2 following a parabolic fit (solid line), postsynaptic responses to acetylcholine remained unaltered (dotted line). Each bin indicates the mean  $\pm$  s.e.m of ten different neurons ( $n = 60$ ). **c** Neither EPSC amplitudes nor responses to an acetylcholine puff were modified by exposure to p2.1. Each bin shows the mean  $\pm$  s.e.m of 8 different SCMs ( $n = 48$ ). **d** Examples of miniature excitatory postsynaptic currents (mEPSCs) recorded in a control neuron and at the indicated times of exposure to 200 nM p4.2. **e** Cumulative probability of mEPSC amplitudes obtained in control neurons ( $n = 574$ , 12 SCMs) and in neurons exposed to p4.2 for an average time of 6 h ( $n = 605$ , 12 SCMs) or 27 h ( $n = 607$ , 10 SCMs).

number of synaptic nicotinic receptors was essentially unaffected by p4.2 action. The absence of an obvious postsynaptic alteration makes unlikely that cholinergic receptors were the trigger of the homeostatic response, as it occurs in other neuronal types<sup>31</sup>. Moreover, the maintenance of a constant density of cholinergic receptors in the plasma membrane could facilitate the assembly of new contacts during the compensatory response to synapse loss.

#### Peptide p4.2 remodels the neuronal F-actin cytoskeleton.

Peptide p4.2 displays counteradhesive properties on cultured endothelial cells due to its ability to disrupt focal adhesions<sup>32,33</sup> by presumably recapitulating the ability of SPARC to redistribute F-actin<sup>34</sup>. To investigate if p4.2 was capable of altering the organization of F-actin in other cell types, we exposed CHO cells to 200 nM p4.2 for 16 h (Fig. 7a). As a result, there was an enrichment of filamentous actin in the periphery of cells (Fig. 7b, c), which was not related to depolymerization. Exposure to latrunculin-A increased soluble actin monomers in the cell cytoplasm, however, peptide p4.2 failed to do so and confirmed its ability to reorganize the F-actin cytoskeleton without

disrupting it (Fig. 7d). Comparable results were obtained using HEK-293 cells and confirmed the capacity of peptide p4.2 to induce a reorganization of the F-actin cytoskeleton.

We next assessed if peptide p4.2 displayed a similar action on the actin network found in neurons. STED microscopy revealed the characteristic periodic F-actin skeleton of neuronal processes (Fig. 8a–c). Actin ring-like structures showed a periodicity of 195 nm, which is comparable to values described for cultured hippocampal neurons<sup>35–37</sup>. Exposure of SCMs to 200 nM peptide p4.2 for 15 or 27 h disrupted actin organization: F-actin appeared distributed in patches rather than in regularly spaced bands (Fig. 8d, e). Although there was no obvious organization of F-actin, some neuritic regions showed periodic structures located at a distance between 250 and 300 nm.

To estimate the time course of changes in the organization of the F-actin cytoskeleton present along the axon and dendrites, we took advantage of the ability of latrunculin-A to increase neurotransmitter release probability<sup>38</sup>. The analysis of responses to paired pulse stimuli showed that disruption of presynaptic F-actin by local application of 20  $\mu$ M latrunculin-A<sup>39</sup> enhanced

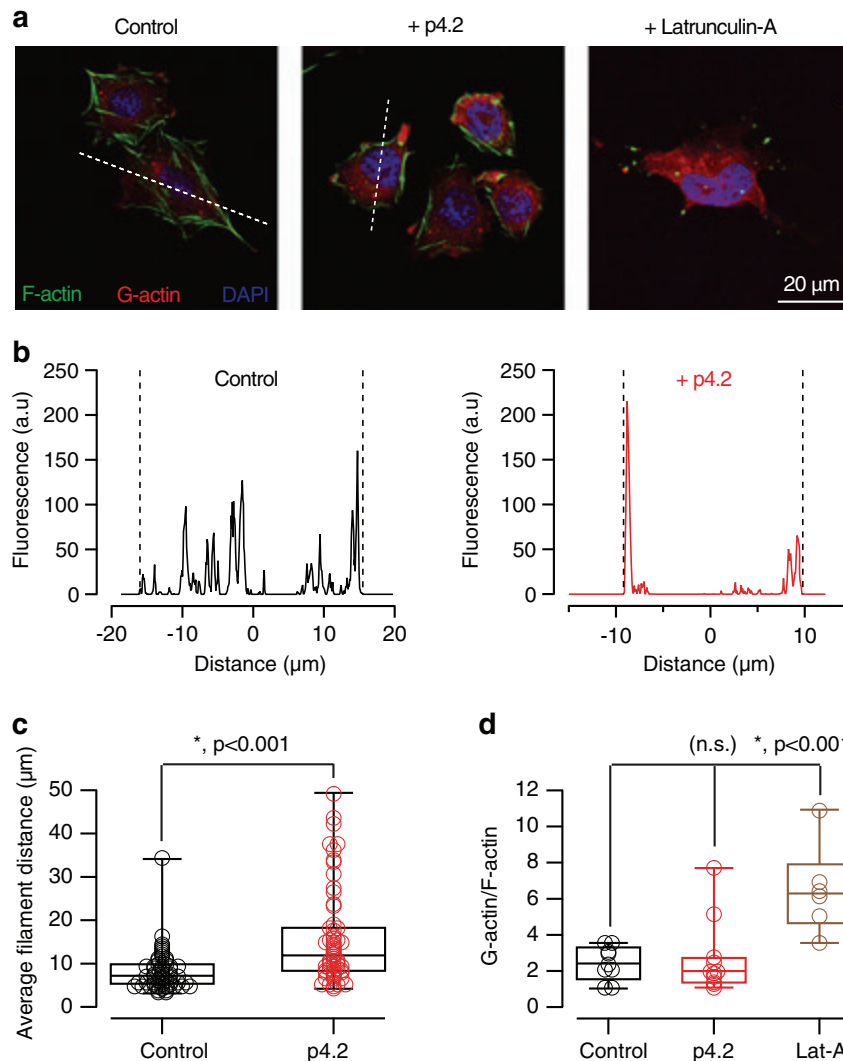


**Fig. 7 Exposure to p4.2 causes a reorganization of the F-actin cytoskeleton.** **a** Images of CHO cells labeled with phalloidin-Alexa Fluor 488 and deoxyribonuclease I-Alexa Fluor 594 to show the distribution of F-actin and G-actin, respectively. Cells were treated for 16 h with 200 nM p4.2 or 1  $\mu$ M latrunculin-A. **b** A line profile (dotted line in **a**) was drawn through the longest cell axis (see “Methods” for details) to evaluate the distribution of F-actin. Fluorescence peaks indicate the distribution of actin filaments. The cell center is set to a distance of 0  $\mu$ m and cell borders are indicated by dotted lines. The examples show that F-actin concentrated in the periphery as a result of p4.2 treatment. **c** Box plot showing the median (horizontal line), 25–75% quartiles (boxes), and ranges (whiskers) of distance among F-actin filaments in control cells ( $n = 58$ ) and cells exposed to p4.2 ( $n = 60$ ). Statistical differences were evaluated using unpaired two-tailed Student’s *t*-test. **d** The relationship between G-actin and F-actin was studied on a single cell basis by integrating the fluorescence of deoxyribonuclease I-Alexa Fluor 594 and phalloidin-Alexa Fluor 488. Box plot shows the median (horizontal line), 25–75% quartiles (boxes), and ranges (whiskers) of G-actin/F-actin in control cells ( $n = 9$ ), cells exposed to p4.2 ( $n = 11$ ) and cells treated with latrunculin-A ( $n = 6$ ). Evaluation of statistical differences using one-way ANOVA followed by Bonferroni multiple comparisons test showed that exposure to p4.2 did not modify the relationship between G-actin and F-actin. Latrunculin-A was used as a control for F-actin depolymerization.

synaptic strength and, consequently, increased short-term depression by  $\sim 40\%$  (Fig. 9a). Although basal paired pulse plasticity assayed in a 100 ms interval was not significantly decreased by exposure to p4.2, depression evoked by latrunculin-A was indeed enhanced (Fig. 9b and c). In 3 out of 7 cells treated for  $19 \pm 1$  h (mean  $\pm$  s.e.m.) with p4.2, the second EPSC was almost absent, due to a maximum increase of release probability. Taking into account that short-term depression is essentially determined presynaptically<sup>1</sup>, we used the potentiation of latrunculin-A effect as a readout of F-actin remodeling induced by p4.2. The decrease in paired pulse ratio as a result of F-actin depolymerization decayed exponentially as a function of p4.2 exposure (Fig. 9d), suggesting that the peptide instructed a reorganization of presynaptic actin with a time constant of 5.5 hours. A complete rearrangement of the F-actin cytoskeleton

could be expected after three time constants, which coincides with the maximum synapse loss found at  $\sim 16$  h (Fig. 2e).

**F-actin stabilization prevents synapse elimination.** To investigate whether reorganization of the F-actin cytoskeleton was driving synapse elimination and the consequent homeostatic response, the action of p4.2 was impeded by simultaneous exposure to jaspilakinolide, an F-actin stabilizing drug<sup>13,40</sup>. Quantification of the number of SyGCaMP6f puncta responding to a train of five stimuli confirmed the ability of jaspilakinolide to prevent synapse loss. Control SCMs contained  $(2.23 \pm 0.30) \times 10^{-3}$  puncta- $\mu\text{m}^{-2}$  ( $n = 27$ , mean  $\pm$  s.e.m.), while neurons exposed for 6 h to p4.2 presented a lower density of  $(1.26 \pm 0.17) \times 10^{-3}$  puncta- $\mu\text{m}^{-2}$  ( $n = 20$ ; Fig. 10a,  $p < 0.05$ ). As for correlative electrophysiology and immunocytochemistry



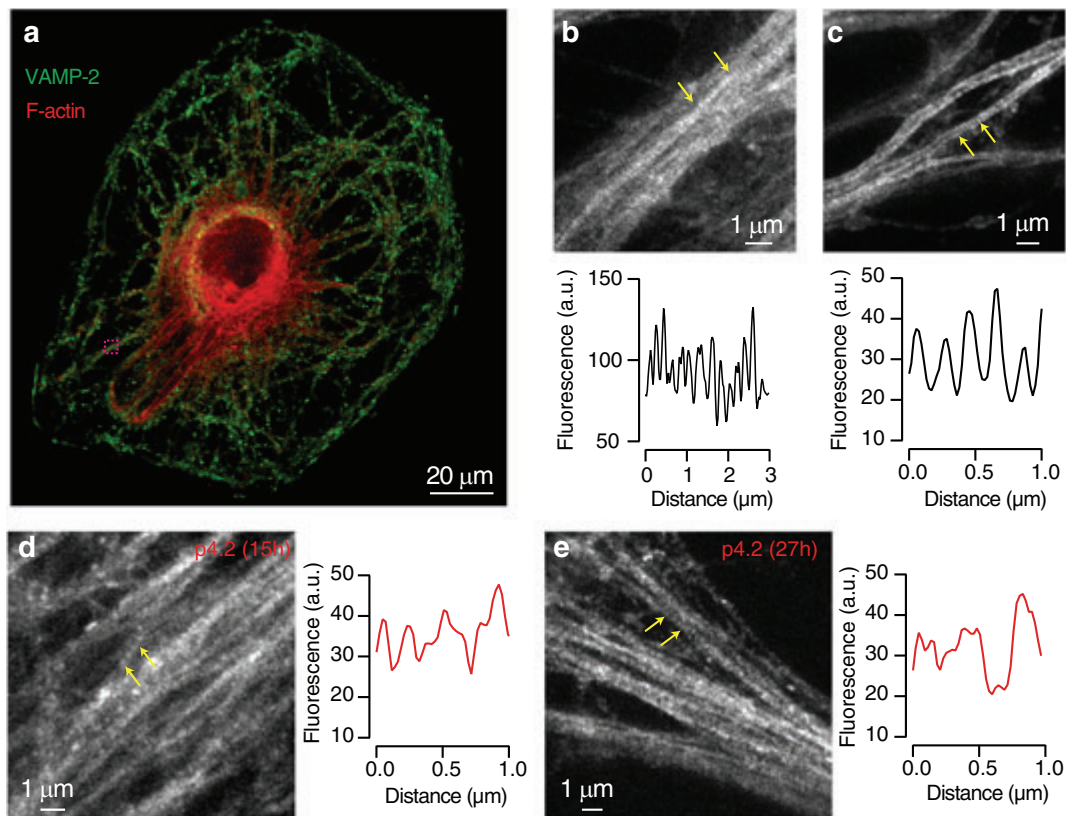


**Fig. 8 Peptide p4.2 disrupts the periodic actin skeleton present in neurites.** **a** Image of a SCM showing the distribution of VAMP-2 and F-actin stained with phalloidin-Atto 647 N. The boxed region was selected for visualization with STED microscopy (shown in **b**). **b, c** Up, periodic actin structures are present along neurites of control SCMs. Images were obtained in two different neurons. Down, plot of line profiles drawn between arrows. The presence of actin-ring like structures is illustrated by peaks of fluorescence, which are regularly spaced at a distance of  $\sim 190$  nm. **d, e** The overall appearance of the periodic actin skeleton is altered by exposure to 200 nM peptide p4.2 for 15 h (**d**) or 27 h (**e**). Most neurites do not show obvious actin-ring like structures, however, plot profiles in selected neuronal processes (arrows) display regularly spaced peaks at 250–300 nm distance.

experiments (Fig. 2), the density of SyGCaMP6f puncta paralleled changes in synaptic strength, increasing to  $(1.86 \pm 0.30) \times 10^{-3}$  puncta  $\mu\text{m}^{-2}$  ( $n = 10$ ) after 19 h of p4.2 treatment. The relationship found between synaptic strength and the density of SyGCaMP6f puncta was maintained when p4.2 was applied concomitantly to jasplakinolide. Neither EPSC amplitude, nor the density of  $(2.12 \pm 0.28) \times 10^{-3}$  puncta  $\mu\text{m}^{-2}$  ( $n = 16$ ) were different from control neurons. The distribution of changes in SyGCaMP6f fluorescence was also comparable to controls (Fig. 10b). These data suggest that the stabilization of the actin cytoskeleton precluded synaptic elimination induced by p4.2 and the consequent potentiation of presynaptic calcium influx.

## Discussion

In the current work, we characterize the neuronal response activated to counterbalance the cell-autonomous elimination of synaptic contacts triggered by p4.2, a peptide derived from the C-terminal region of SPARC<sup>13</sup>. Neurons grown in an autaptic circuit are capable of maintaining baseline neurotransmission without modifying their number of postsynaptic receptors. The homeostatic response exclusively invokes presynaptic mechanisms that combine the potentiation of presynaptic terminal function with the assembly of new synaptic contacts. Presynaptic calcium influx and RRP size increase, which are both hallmarks of presynaptic homeostatic plasticity<sup>26,31</sup>, moreover, the rapid formation of a finite number of synapses demonstrates the ability of neurons to carry out synapse assembly as part of the compensatory response. These evidences together show that neurons

establishing an autaptic circuit set a baseline level of neurotransmission by sensing and finely adjusting the number and properties of neurotransmitter release sites.

The molecular mechanisms responsible for presynaptic homeostatic plasticity have been previously investigated using the alteration of postsynaptic receptors as a trigger (reviewed in the ref. 2). In the current work, compensatory presynaptic mechanisms are not activated by the impairment of postsynaptic terminal function but, by the retraction of the presynaptic element in an autaptic circuit<sup>13</sup>. Yet, part of the homeostatic response can be considered classical because it involves the potentiation of presynaptic calcium influx (see for example ref. 41), the participation of rapid synapse formation must also be accounted for. What signal could act as a trigger for the gain of presynaptic function as well as for the addition of new neurotransmitter release sites? The participation of trans-synaptic communication pathways is unlikely because the compensatory response is not activated by an alteration of the density of postsynaptic receptors<sup>42</sup>. An alternative must come from other signaling pathways. The modification of the periodic actin skeleton found in neuronal processes might be a key to de-stabilize synaptic contacts and trigger the formation of multivesicular bodies and other endocytic structures containing presynaptic elements<sup>13</sup>. Retrograde transport of formed lysosomal degradation compartments could be important for determining neuron survival<sup>43,44</sup> and in the light of our observations, could also be used for reporting synapse loss.

A quantitative estimate of the intensification of synaptogenesis occurring during the homeostatic response can be drawn

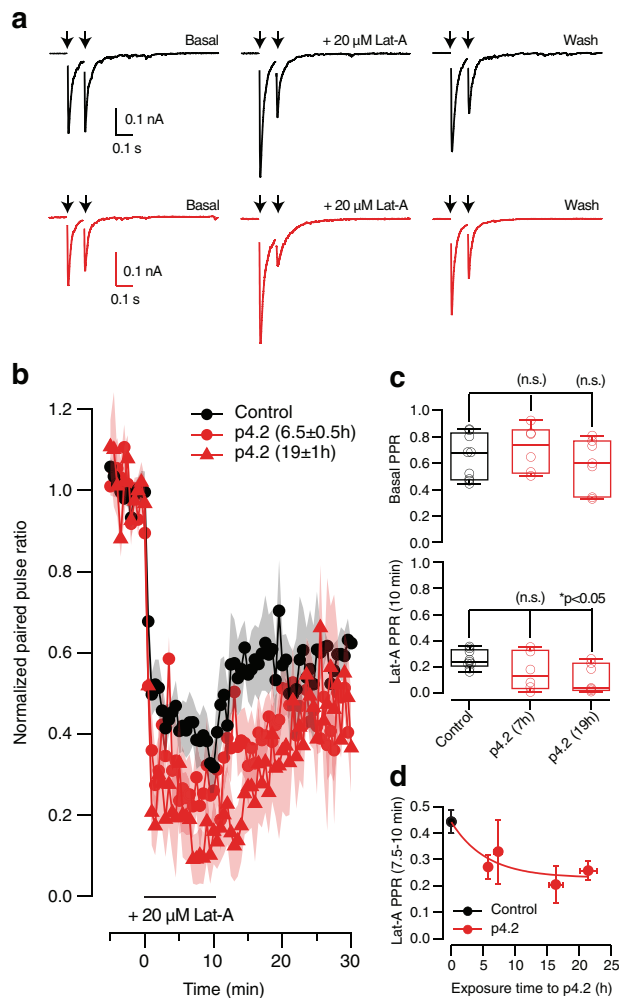


**Fig. 9 Time course of presynaptic F-actin cytoskeleton reorganization induced by peptide p4.2.** **a** Changes in short-term plasticity caused by latrunculin-A were used to evaluate the timescale of F-actin reorganization induced by p4.2. Application of 20  $\mu$ M latrunculin-A enhanced paired-pulse depression measured in a 100 ms interval by increasing the amplitude of the first EPSC. A partial recovery of depression was observed after washing out latrunculin-A. Black traces show paired-pulse plasticity recorded in a control SCM. Red traces illustrate the effect of 20  $\mu$ M latrunculin-A in a cell exposed to 200 nM p4.2 for 19 h. **b** Normalized paired-pulse ratio as a function of experiment time. Notice that depression was immediately enhanced upon application of latrunculin-A. **c** Paired pulse ratio (PPR) recorded in basal conditions (up) and 10 min after application of 20  $\mu$ M latrunculin-A (down) in the indicated experimental conditions. Box plots show the median (horizontal line), 25–75% quartiles (boxes), and ranges (whiskers) of PPR values obtained in control conditions ( $n = 9$ ) and 7 h ( $n = 6$ ) or 19 h ( $n = 7$ ) after application of 200 nM p4.2. **d** Decay in PPR caused by latrunculin-A as a function of exposure time to peptide p4.2. Each bin shows the mean  $\pm$  s.e.m. of three different neurons ( $n = 12$ ). Individual PPR values correspond to the average decrease observed between 7.5 and 10 min of latrunculin-A exposure. PPR obtained in control SCMs is indicated in black (mean  $\pm$  s.e.m.,  $n = 9$ ). Bins are fitted to a single exponential function, providing a time constant of 5.5 h.

considering that a prototypical SCM contains  $\sim$ 200 synapses. Upon exposure to p4.2, the neuron would react to synapse elimination by forming  $\sim$ 75 new contacts in 10 h. If the assembly time of cholinergic autaptic synapses is found between  $\sim$ 1<sup>45</sup> and 2.5 h (see Fig. 2e), it would mean SCMs establish 3–8 new contacts  $\text{hour}^{-1}$  in response to synapse elimination. Considering a

likelihood of finding the formation of a contact in cultured neurons of 0.4–1%<sup>46</sup>, basal synapse formation could increase by almost an order of magnitude during the homeostatic response. In other terms, a neuron growing in a SCM takes a week to establish all its contacts<sup>21</sup> but, in front of a significant synapse loss, the neuron can recover one third of its synapses just in half a day.

By the end of the homeostatic response mature and recently assembled autapses coexist. Newly formed contacts likely contributed to the observed increase in RRP size, which could also be accomplished by the activation of certain regulatory mechanisms operating at the level of active zones<sup>26</sup>. The small RRP size of immature contacts<sup>21,27</sup> explains why synaptic strength recovers completely during p4.2 exposure, whilst RRP does not. Fast synapse formation allows the re-establishment of neurotransmitter release sites, which can efficiently support synaptic transmission but with a limited availability of synaptic vesicles. Short-term plasticity is consequently affected, shifted towards a depressing phenotype.

Assuming that the homeostatic response is orchestrated from the cell body, the increase in presynaptic calcium entry is probably mediated by the insertion of voltage gated calcium channel copies at the synapse. However, it remains an open question how is it possible to achieve the functional assembly of synaptic contacts upon disruption of neuritic ring-like F-actin structures. Changes in the molecular composition of voltage-gated calcium channels as well as, of certain accessory subunits or adhesion proteins present in the presynaptic terminal, could be important for establishing functional synapses in an altered neuronal cytoskeleton. Any molecular modification was, however, not determinant for setting functional differences among synaptic contacts. By the end of the compensatory phase, all synapses experienced a comparable potentiation of presynaptic calcium entry. This widespread gain of function could be related to the use of cultured neurons<sup>4</sup> but could also be reflecting a specific property of autaptic circuits.

Autaptic contacts are commonly established by excitatory and inhibitory neurons, such as pyramidal neurons of the neocortex, cerebellar interneurons or spiny neurons of the striatum<sup>16–18,47,48</sup>. Although the specific roles of autapses have been a matter of debate<sup>49</sup>, there are growing evidences that support their implication in relevant network functions. For example, excitatory autapses are important to maintain persistent activation of B31/B32 neurons in *Aplysia*<sup>50</sup>, or, to enhance bursting in layer 5-pyramidal neurons<sup>51</sup>. The coordinated potentiation of presynaptic terminal function with *de novo* synapse formation used for setting a correct level of neurotransmission might unmask a biologically relevant role of autapses. Excitatory neurons could use autaptic contacts to sense their synaptic output and take advantage of the mechanism here described to increase gain and, consequently enhance excitability. Future experiments should verify if excitatory autapses are indeed keepers of neuronal firing.

## Methods

**Molecular biology.** The synaptophysin::GCaMP6f (SyGCaMP6f) construct was provided by Dr. Leon Lagnado as an improved version of syGCaMP2<sup>52,53</sup>. The coding sequence of SyGCaMP6f was cloned into pWPXL (Addgene plasmid # 12257; <http://n2t.net/addgene:12257>; RRID:Addgene\_12257) by replacing EGFP using BamHI and NdeI. For lentivirus production, HEK 293T cells were transfected by the calcium phosphate technique following methods described by Didier Trono (<http://tronolab.epfl.ch/lentivectors>) with pMD2G (Addgene plasmid # 12259; <http://n2t.net/addgene:12259>; RRID:Addgene\_12259), pCMV8.74 (Addgene plasmid # 22036; <http://n2t.net/addgene:22036>; RRID:Addgene\_22036), and pWPXL. Two days later, culture medium containing lentiviral particles was collected in three rounds at 8 h intervals, kept at 4  $^{\circ}$ C, and centrifuged at 500 $\times$ g. Supernatants were distributed in aliquots and stored at  $-80$   $^{\circ}$ C.

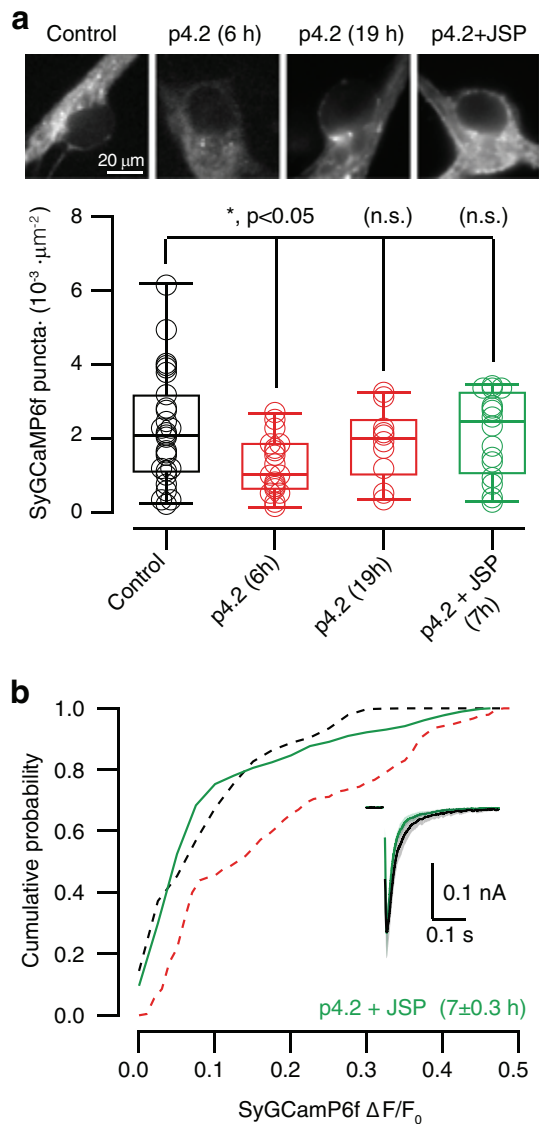


**Fig. 10 Stabilization of the presynaptic F-actin cytoskeleton prevents the action of p4.2.** **a** The transient decay of SyGCaMP6f puncta caused by exposure to 200 nM p4.2 was not observed when the peptide was incubated in the presence of 1  $\mu\text{M}$  jasplakinolide. Examples of difference images obtained during stimulation with five stimuli delivered at 20 Hz in the indicated conditions. Notice that the density of putative synaptic contacts is transiently reduced during p4.2 exposure but remains unaltered if neurons are treated concomitantly with jasplakinolide. Box plots show the median (horizontal line), 25–75% quartiles (boxes), and ranges (whiskers) of the density of SyGCaMP6f puncta in control conditions ( $n = 27$ ), after 6 h of exposure to p4.2 ( $n = 20$ ), after 19 h of exposure to p4.2 ( $n = 10$ ) and after 7 h incubation of p4.2 and jasplakinolide ( $n = 16$ ). Statistical differences were evaluated using one-way ANOVA followed by Bonferroni multiple comparisons test. Only exposure to p4.2 for 6 h induced a significant decrease of SyGCaMP6f puncta. **b** Cumulative probability of SyGCaMP6f  $\Delta F/F_0$  increases observed after application of a train of five stimuli delivered at 20 Hz in neurons exposed to 200 nM p4.2 and 1  $\mu\text{M}$  jasplakinolide for  $7 \pm 0.3$  h (mean  $\pm$  s.e.m.,  $n = 1030$ , 16 SCMs). Dotted lines show the distributions obtained in control conditions (black) and after exposure to peptide p4.2 for 19 h (as shown in Fig. 5c) for comparison purposes. The inset displays the profile of the average EPSC (solid line  $\pm$  shadowed area indicate mean  $\pm$  s.e.m.) obtained in control SCMs (black,  $n = 12$ ) and in neurons treated with 200 nM peptide p4.2 and 1  $\mu\text{M}$  jasplakinolide (green,  $n = 11$ ).

**Cell culture.** Experimental procedures were approved by the Department of Environment from the Generalitat de Catalunya. SCMs from superior cervical ganglion neurons were prepared following previously described methods using postnatal day 0 (P0) to P2 Sprague Dawley rats<sup>19,30</sup>. Briefly, medium containing all dissociated ganglionic cells was placed in a 100-mm-diameter culture dish for 60 min at 37 °C. At the end of this preplating period,  $\geq 95\%$  of non-neuronal cells were found to be adhered to the dish, but most neurons remained in suspension. Medium was then collected, and neurons seeded at 2500 cells  $\text{mL}^{-1}$  on 15 mm coverslips containing 10–20 collagen microdrops of 100–400  $\mu\text{m}$  diameter. Culture medium was DMEM/F12 [1:1] containing 2.5% fetal bovine serum, 2.5% rat serum (prepared in the animal care facility of the Campus of Bellvitge, University of Barcelona), 5 nM NGF, 1–2 nM CNTF (Alomone Labs, Jerusalem, Israel), and 25 U/ml penicillin/streptomycin at 37 °C and 8%  $\text{CO}_2$ . To genetically modify SCMs, lentiviral infection was applied at 13 days in vitro (D.I.V.) during a 1:2 overnight incubation of the appropriate viral stock. Fluorescence was evident at 4–6 days after infection. SCMs were exposed for time intervals ranging from 0 to 30 h to p2.1 (CQNHHCCKHGKVCCELDESNTTP) or p4.2 (TCDLNDNKYIALEEWAGCFG). Peptides p2.1 and p4.2 were synthesized by GL Biochem (Shanghai, China). Stocks were prepared at 2 mM using MQ water and aliquots were stored at  $-80$  °C. Peptide solutions were thawed and diluted in culture medium.

CHO cells were grown on coverslips coated with the collagen used for establishing microcultures. Cells from passages 8–12 were seeded at a density of 20,000 cells  $\text{mL}^{-1}$ . Culture medium was DMEM/F12 [1:1] containing 10% fetal bovine serum and 10 U/ml penicillin/streptomycin. CHO cells were maintained at 37 °C and 5%  $\text{CO}_2$ .

**Immunocytochemistry and STED microscopy.** For immunocytochemistry, coverslips containing SCMs were fixed in 4% PFA prepared in phosphate buffer 0.1 M. They were incubated overnight at 4 °C with a monoclonal anti-bassoon primary antibody (1:1000, Enzo Life Sciences, ADI-VAM-PS003) combined with one of the following polyclonal antibodies: anti-N-cadherin (10  $\mu\text{g}/\text{mL}$ , R&D Systems, AF6426), anti-VAMP-2 (1:500, Synaptic Systems, 104202), or, anti-Synapsin-I (1:1000, Millipore, AB1543P). Appropriate secondary antibodies labeled with Alexa Fluor 488 and Alexa Fluor 555 were used for fluorescent staining. Cells were visualized in a Zeiss LSM 880 confocal microscope (Carl Zeiss AG, Oberkochen, Germany). Optical sections were acquired using a 63 $\times$  oil immersion objective PL-APO (1.4 N.A.).

For visualization by STED microscopy, SCMs were immersed for 15 min in a 4% PFA solution prepared in phosphate buffer 0.1 M. Overnight incubation at 4 °C with a primary antibody anti-VAMP-2 (1:1000, Synaptic Systems 104211) was followed by application of an anti-mouse secondary antibody labeled with Alexa Fluor 488. SCMs were subsequently incubated with 0.165  $\mu\text{M}$  phalloidin-Atto 647N (Sigma-Aldrich, 65906) for 2.5 h at room temperature, followed by an overnight period at 4 °C.

Single plane STED images were acquired on a Leica TCS SP8 STED 3 $\times$  (Leica Microsystems, Mannheim, Germany) on a DMI8 stand using a 100 $\times$ /1.4NA HCS2 PL APO objective. A pulsed supercontinuum light source set at 644 nm was used for excitation and a pulsed depletion laser at 775 nm was added with no pulse delay at 20% intensity. Detection was performed with a hybrid detector (HyD) between 652 and 750 nm and gating between 0, 3, and 6 ns. Scanner speed was set to 600 Hz and images were taken with 8 $\times$  frame accumulation and 2 $\times$  frame average. Pixel size was set according to the depletion power to 23 nm.

**Electrophysiological recordings.** All experiments were performed in the whole-cell configuration of patch-clamp mode using neurons microcultured for 18–22 D. I.V. Typical resistances of pipettes used for recordings were 3–5 M $\Omega$  when filled with internal solution composed of the following (in mM): 130 K-gluconate, 4  $\text{MgCl}_2$ , 1 EGTA, 10 HEPES, 3  $\text{Na}_2\text{ATP}$ , 1 NaGTP, pH 7.2, 290 mOsm/kg. External solution contained (in mM): 130 NaCl, 5 KCl, 2  $\text{MgCl}_2$ , 10 HEPES-hemisodium salt, and 10 glucose, pH 7.4. The final 2 mM  $\text{CaCl}_2$  concentration was always achieved by dilution from a 1 M stock. All salts were from Sigma-Aldrich (St. Louis, MO). Before the addition of glucose and  $\text{CaCl}_2$ , the osmolality of the external solution was adjusted to 290 mOsm/kg. Experiments were performed at room temperature (23 °C).

Recordings were made using an Axopatch-1D patch-clamp amplifier (Molecular Devices, San Jose, CA) under the control of an ITC-18 board (Instrutech Corp, Port Washington, NY) driven by WCP software (Dr. John Dempster, University of Strathclyde, UK) or mafPC (courtesy of M. A. Xu-Friedman, University at Buffalo, NY). Neurons were clamped at  $-60$  mV and stimulated by a 1–2 ms depolarization step that drove membrane potential to 0 mV. The presence of functional autaptic synapses was identified by the generation of excitatory postsynaptic currents (EPSCs). Further details of neurotransmission in SCMs are described elsewhere<sup>13,19,21,30</sup>. To test the contribution of postsynaptic nicotinic receptors, a local puff of 50  $\mu\text{M}$  acetylcholine was locally applied using a fused-silica capillary (Microfil, #MF-28G, World Precision Instruments, Sarasota, FL). Timing of application was set to 30 ms using a TTL pulse.

**Simultaneous electrophysiological recording and imaging.** To associate presynaptic calcium influx to neurotransmission, SCMs expressing SyGCaMP6f were



imaged and simultaneously recorded electrophysiologically (Fig. 1a), see also ref. <sup>54</sup>. Coverslips were mounted on an RC-25 imaging chamber (Warner Instruments, Hamden, CT) and observed in an inverted Olympus IX-50 microscope. Cells were illuminated with blue light, using an ET480/20x excitation filter. Fluorescence was acquired using a q505LP dichroic and a HQ535/50 nm emission filter (Chroma Technology Corp., VT). Images were collected through a 60× UPlanFLN objective (1.25 N.A., Olympus, Tokyo, Japan) and visualized on an ImageEM camera controlled by HClImage (Hamamatsu). Images from a 256 × 256 pixels box located on the perisomatic region were acquired at 40 Hz. TTL pulses generated by mafPC controlled the exposure time of the camera, as well as the timing of light illumination, which was adjusted via a shutter (Uniblitz, NY), to minimize photobleaching.

**Analysis of electrophysiological and imaging data.** Electrophysiological recordings were analyzed using custom-made macros written in Igor Pro software (Wavemetrics, Lake Oswego, OR) versions 6.0–8.0. Image analysis was carried out combining Image J and macros written in Igor Pro software. SyGCaMP6f fluorescence (F) was obtained after subtracting the background fluorescence found in regions of interest drawn outside of the microculture. Calcium increases were reported as relative changes of SyGCaMP6f fluorescence, measured as  $(F - F_0)/F_0$ . Putative synapses were identified on difference images that illustrated the location of stimulation dependent changes in fluorescence (see examples in Fig. 10a). 1.3 × 1.3 μm ROIs were drawn on the center of mass of identified puncta, which were typically round, ~1 μm diameter structures. A given punctum was considered a synapse when exhibited a  $\Delta F/F_0$  increase above three standard deviations of baseline values recorded before stimulation. This criterion avoided the contribution of synapses found out of focus. Block of depolarization with 1 μM TTX ( $n = 4$ ) demonstrated that changes in SyGCaMP6f fluorescence were exclusively related to neurotransmission (see the example in Fig. 4b).

**Correlative electrophysiology and immunocytochemistry.** SCMs displaying a representative morphology were recorded, micrographed, fixed, and stained by immunocytochemistry (Fig. 1a) for the expression of the presynaptic marker bassoon (Enzo Life Sciences, ADI-VAM-PS003) and the synaptic adhesion protein N-cadherin (R&D Systems, AF6426). Appropriate secondary antibodies labeled with Alexa Fluor 488 and Alexa Fluor 555 were used to visualize N-cadherin and bassoon labeling, respectively. Images of recorded SCMs were used to identify stained microcultures in a Zeiss LSM 880 confocal microscope. Confocal sections were acquired using a 63× oil immersion objective PL-APO (1.4 N.A.). The procedure for obtaining an estimate of synapses contributing to recorded EPSCs was based in the quantification of the density of bassoon and N-cadherin puncta located in the somatic region and nearby dendritic tree. Specifically, only somatic and dendritic puncta found ≤20 μm away from the edge of the soma were considered. Synaptic contacts more distally located were not considered because the cable-filtering properties of dendrites in cultured neurons attenuate their contribution to recorded EPSCs<sup>55</sup>. A punctum was considered as a putative synapse if it spanned from three to five consecutive confocal Z-sections (0.33 μm optical thickness), had a diameter ranging from 0.2 to 0.5 μm and was stained with bassoon or N-cadherin. Density was calculated by dividing the number of bassoon and N-cadherin puncta by the analyzed area.

**Quantification of F-actin and G-actin stainings.** Simultaneous labeling of G-actin and F-actin was carried out following previously described methods<sup>56,57</sup>. Briefly, CHO cells were fixed in PFA 4% and stained with phalloidin-Alexa Fluor 488 (A12379, Thermofisher, Waltham, MA) and deoxyribonuclease I-Alexa Fluor 594 (D12372, Invitrogen, Carlsbad, CA). Cells were visualized under a Leica TCS-SL confocal microscope using a 63× immersion oil objective PL-APO (1.4 N.A.). Images were analyzed in Image J.

The distance among F-actin filaments was calculated using a line profile drawn along the longest cell axis estimated by Image J (Feret's diameter). Only the basal region of the cell (~1.5 μm optical thickness) was considered for analysis. To estimate the quantity of G-actin and F-actin in a single cell, the fluorescence of all pixels found in the maximum intensity projection were summed (RawIntDen command in Image J) after background subtraction. The relationship between G-actin and F-actin was calculated by dividing values obtained in the red and green channel, respectively.

F-actin structures present in SCMs were revealed by STED microscopy and analyzed by plotting changes in fluorescence intensity along line profiles (1–3 μm length) drawn in Image J. Values were exported to Igor Pro 8.0 to quantify periodicity. The average distance between peaks found within an analyzed segment (see for example Fig. 8b–e) was considered as representative of a given neurite.

**Statistics and reproducibility.** Control experiments certifying the action of peptide p4.2<sup>13</sup> were carried out for each culture, considering a culture as a group of SCMs established from a litter of rat pups. The neurons of a given culture were distributed between two or more different experimental protocols. Experimental groups used for evaluating statistical differences passed the Kolmogorov-Smirnov normality test. Data from averages were always expressed as mean ± s.e.m. Comparisons between two groups were established using unpaired two-tailed

Student's *t*-test. When comparing more than two groups one-way ANOVA followed by Bonferroni multiple comparison test was applied. The number of independent observations, as well as the type of statistical test applied and the degree of significance, are indicated in the figures.

**Reporting summary.** Further information on research design is available in the Nature Research Reporting Summary linked to this article.

## Data availability

The data that support the findings of this study are included in the article and supplementary information, and, are available from the corresponding author upon reasonable request.

Received: 4 November 2019; Accepted: 21 April 2020;

Published online: 22 May 2020

## References

- Regehr, W. G. Short-term presynaptic plasticity. *Cold Spring Harb. Perspect. Biol.* **4**, a005702 (2012).
- Davis, G. W. & Müller, M. Homeostatic control of presynaptic neurotransmitter release. *Annu. Rev. Physiol.* **77**, 251–270 (2015).
- Turrigiano, G. Homeostatic synaptic plasticity: local and global mechanisms for stabilizing neuronal function. *Cold Spring Harb. Perspect. Biol.* **4**, a005736 (2012).
- Pozo, K. & Goda, Y. Unraveling mechanisms of homeostatic synaptic plasticity. *Neuron* **66**, 337–351 (2010).
- Turrigiano, G. G. & Nelson, S. B. Homeostatic plasticity in the developing nervous system. *Nat. Rev. Neurosci.* **5**, 97–107 (2004).
- Colón-Ramos, D. A. Synapse formation in developing neural circuits. *Curr. Top. Dev. Biol.* **87**, 53–79 (2009).
- Kano, M. & Watanabe, T. Developmental synapse remodeling in the cerebellum and visual thalamus. *Fl000Res* **8** <https://doi.org/10.12688/fl000research.18903.1> (2019).
- Colman, H., Nabekura, J. & Lichtman, J. W. Alterations in synaptic strength preceding axon withdrawal. *Science* **275**, 356–361 (1997).
- Wilton, D. K., Dissing-Olesen, L. & Stevens, B. Neuron-Glia signaling in synapse elimination. *Annu. Rev. Neurosci.* **42**, 107–127 (2019).
- Stephan, A. H., Barres, B. A. & Stevens, B. The complement system: an unexpected role in synaptic pruning during development and disease. *Annu. Rev. Neurosci.* **35**, 369–389 (2012).
- Yang, J. et al. Astrocytes contribute to synapse elimination via type 2 inositol 1,4,5-trisphosphate receptor-dependent release of ATP. *Elife* **5**, e15043 (2016).
- Terni, B., López-Murcia, F. J. & Llobet, A. Role of neuron-glia interactions in developmental synapse elimination. *Brain Res. Bull.* **129**, 74–81 (2017).
- Lopez-Murcia, F. J., Terni, B. & Llobet, A. SPARC triggers a cell-autonomous program of synapse elimination. *Proc. Natl Acad. Sci. USA* **112**, 13366–13371 (2015).
- Vincent, A., Lau, P. & Roskams, A. SPARC is expressed by macroglia and microglia in the developing and mature nervous system. *Dev. Dyn.* **237**, 1449–1462 (2008).
- Sakers, K. et al. Astrocytes locally translate transcripts in their peripheral processes. *Proc. Natl Acad. Sci. USA* **114**, E3830–E3838 (2017).
- Lübke, J., Markram, H., Frotscher, M. & Sakmann, B. Frequency and dendritic distribution of autapses established by layer 5 pyramidal neurons in the developing rat neocortex: comparison with synaptic innervation of adjacent neurons of the same class. *J. Neurosci.* **16**, 3209–3218 (1996).
- Van der Loos, H. & Glaser, E. M. Autapses in neocortex cerebri: synapses between a pyramidal cell's axon and its own dendrites. *Brain Res.* **48**, 355–360 (1972).
- Tamás, G., Buhl, E. H. & Somogyi, P. Massive autaptic self-innervation of GABAergic neurons in cat visual cortex. *J. Neurosci.* **17**, 6352–6364 (1997).
- Perez-Gonzalez, A. P., Albrecht, D., Blasi, J. & Llobet, A. Schwann cells modulate short-term plasticity of cholinergic autaptic synapses. *J. Physiol.* **586**, 4675–4691 (2008).
- Furshpan, E., Landis, S., Matsumoto, S. & Potter, D. Synaptic functions in rat sympathetic neurons in microcultures. I. Secretion of norepinephrine and acetylcholine. *J. Neurosci.* **6**, 1061–1079 (1986).
- Albrecht, D. et al. SPARC prevents maturation of cholinergic presynaptic terminals. *Mol. Cell Neurosci.* **49**, 364–374 (2012).
- Benson, D. L. & Tanaka, H. N-cadherin redistribution during synaptogenesis in hippocampal neurons. *J. Neurosci.* **18**, 6892–6904 (1998).
- Thanawala, M. S. & Regehr, W. G. Determining synaptic parameters using high-frequency activation. *J. Neurosci. Methods* **264**, 136–152 (2016).

24. Sakaba, T., Schneggenburger, R. & Neher, E. Estimation of quantal parameters at the calyx of Held synapse. *Neurosci. Res.* **44**, 343–356 (2002).
25. Wang, X., Pinter, M. J. & Rich, M. M. Reversible recruitment of a homeostatic reserve pool of synaptic vesicles underlies rapid homeostatic plasticity of quantal content. *J. Neurosci.* **36**, 828–836 (2016).
26. Müller, M., Liu, K. S., Sigrist, S. J. & Davis, G. W. RIM controls homeostatic plasticity through modulation of the readily-releasable vesicle pool. *J. Neurosci.* **32**, 16574–16585 (2012).
27. Ahmari, S. E., Buchanan, J. & Smith, S. J. Assembly of presynaptic active zones from cytoplasmic transport packets. *Nat. Neurosci.* **3**, 445–451 (2000).
28. Taschenberger, H. & von Gersdorff, H. Fine-tuning an auditory synapse for speed and fidelity: developmental changes in presynaptic waveform, EPSC kinetics, and synaptic plasticity. *J. Neurosci.* **20**, 9162–9173 (2000).
29. Saadat, S., Sendtner, M. & Rohrer, H. Ciliary neurotrophic factor induces cholinergic differentiation of rat sympathetic neurons in culture. *J. Cell Biol.* **108**, 1807–1816 (1989).
30. Lopez-Murcia, F. J., Royle, S. J. & Llobet, A. Presynaptic clathrin levels are a limiting factor for synaptic transmission. *J. Neurosci.* **34**, 8618–8629 (2014).
31. Frank, C. A., Kennedy, M. J., Goold, C. P., Marek, K. W. & Davis, G. W. Mechanisms underlying the rapid induction and sustained expression of synaptic homeostasis. *Neuron* **52**, 663–677 (2006).
32. Lane, T. F. & Sage, E. H. Functional mapping of SPARC: peptides from two distinct Ca<sup>2+</sup>-binding sites modulate cell shape. *J. Cell Biol.* **111**, 3065–3076 (1990).
33. Murphy-Ullrich, J. E., Lane, T. F., Pallero, M. A. & Sage, E. H. SPARC mediates focal adhesion disassembly in endothelial cells through a follistatin-like region and the Ca<sup>2+</sup>-binding EF-hand. *J. Cell Biochem.* **57**, 341–350 (1995).
34. Goldblum, S. E., Ding, X., Funk, S. E. & Sage, E. H. SPARC (secreted protein acidic and rich in cysteine) regulates endothelial cell shape and barrier function. *Proc. Natl Acad. Sci. USA* **91**, 3448–3452 (1994).
35. Han, B., Zhou, R., Xia, C. & Zhuang, X. Structural organization of the actin-spectrin-based membrane skeleton in dendrites and soma of neurons. *Proc. Natl Acad. Sci. USA* **114**, E6678–E6685 (2017).
36. Xu, K., Zhong, G. & Zhuang, X. Actin, spectrin, and associated proteins form a periodic cytoskeletal structure in axons. *Science* **339**, 452–456 (2013).
37. Bär, J., Kobler, O., van Bommel, B. & Mikhaylova, M. Periodic F-actin structures shape the neck of dendritic spines. *Sci. Rep.* **6**, 37136 (2016).
38. Morales, M., Colicos, M. A. & Goda, Y. Actin-dependent regulation of neurotransmitter release at central synapses. *Neuron* **27**, 539–550 (2000).
39. Sankaranarayanan, S., Atluri, P. P. & Ryan, T. A. Actin has a molecular scaffolding, not propulsive, role in presynaptic function. *Nat. Neurosci.* **6**, 127–135 (2003).
40. Holzinger, A. Jasplakinolide: an actin-specific reagent that promotes actin polymerization. *Methods Mol. Biol.* **586**, 71–87 (2009).
41. Jeans, A. F., van Heusden, F. C., Al-Mubarak, B., Padamsey, Z. & Emptage, N. J. Homeostatic presynaptic plasticity is specifically regulated by P/Q-type Ca. *Cell Rep.* **21**, 341–350 (2017).
42. Goel, P., Li, X. & Dickman, D. Disparate postsynaptic induction mechanisms ultimately converge to drive the retrograde enhancement of presynaptic efficacy. *Cell Rep.* **21**, 2339–2347 (2017).
43. Kononenko, N. L. et al. Retrograde transport of TrkB-containing autophagosomes via the adaptor AP-2 mediates neuronal complexity and prevents neurodegeneration. *Nat. Commun.* **8**, 14819 (2017).
44. Perlson, E., Maday, S., Fu, M. M., Moughamian, A. J. & Holzbaur, E. L. Retrograde axonal transport: pathways to cell death? *Trends Neurosci.* **33**, 335–344 (2010).
45. Bresler, T. et al. Postsynaptic density assembly is fundamentally different from presynaptic active zone assembly. *J. Neurosci.* **24**, 1507–1520 (2004).
46. Friedman, H. V., Bresler, T., Garner, C. C. & Ziv, N. E. Assembly of new individual excitatory synapses: time course and temporal order of synaptic molecule recruitment. *Neuron* **27**, 57–69 (2000).
47. Preston, R. J., Bishop, G. A. & Kitai, S. T. Medium spiny neuron projection from the rat striatum: an intracellular horseradish peroxidase study. *Brain Res.* **183**, 253–263 (1980).
48. Pouzat, C. & Marty, A. Autaptic inhibitory currents recorded from interneurons in rat cerebellar slices. *J. Physiol.* **509**, 777–783 (1998).
49. Bekkers, J. M. Neurophysiology: are autapses prodigal synapses? *Curr. Biol.* **8**, R52–R55 (1998).
50. Saada, R., Miller, N., Hurwitz, I. & Susswein, A. J. Autaptic excitation elicits persistent activity and a plateau potential in a neuron of known behavioral function. *Curr. Biol.* **19**, 479–484 (2009).
51. Yin, L. et al. Autapses enhance bursting and coincidence detection in neocortical pyramidal cells. *Nat. Commun.* **9**, 4890 (2018).
52. Dreosti, E., Odermatt, B., Dorostkar, M. M. & Lagnado, L. A genetically encoded reporter of synaptic activity in vivo. *Nat. Methods* **6**, 883–889 (2009).
53. Johnston, J. et al. A retinal circuit generating a dynamic predictive code for oriented features. *Neuron* **102**, 1211–1222 (2019).
54. Martínez San Segundo, P. et al. Outside-in regulation of the readily releasable pool of synaptic vesicles by  $\alpha 2\delta$ -1. *FASEB J.* **34**, 1362–1377 (2020).
55. Bekkers, J. & Stevens, C. Cable properties of cultured hippocampal neurons determined from sucrose-evoked miniature EPSCs. *J. Neurophysiol.* **75**, 1250–1255 (1996).
56. Knowles, G. C. & McCulloch, C. A. Simultaneous localization and quantification of relative G and F actin content: optimization of fluorescence labeling methods. *J. Histochem. Cytochem.* **40**, 1605–1612 (1992).
57. Cramer, L. P., Briggs, L. J. & Dawe, H. R. Use of fluorescently labelled deoxyribonuclease I to spatially measure G-actin levels in migrating and non-migrating cells. *Cell Motil. Cytoskelet.* **51**, 27–38 (2002).

### Acknowledgements

This work was sponsored by the Spanish government (Ministerio de Ciencia e Innovación), grant RTI2018-096948-B-I00 (A.L.), co-funded by the European Regional Development Fund (ERDF). We also thank CERCA Program/Generalitat de Catalunya for institutional support. A.L. is a Serra Hünter fellow. C.V. was contracted by a MICINN predoctoral fellowship (FPI - BES-2016-076551).

### Author contributions

A.L. conceived the study. C.V. performed experiments and analysed data. A.L. wrote the manuscript.

### Competing interests

The authors declare no competing interests.

### Additional information

Supplementary information is available for this paper at <https://doi.org/10.1038/s42003-020-0963-8>.

Correspondence and requests for materials should be addressed to A.L.

Reprints and permission information is available at <http://www.nature.com/reprints>

Publisher's note Springer Nature remains neutral with regard to jurisdictional claims in published maps and institutional affiliations.



**Open Access** This article is licensed under a Creative Commons Attribution 4.0 International License, which permits use, sharing, adaptation, distribution and reproduction in any medium or format, as long as you give appropriate credit to the original author(s) and the source, provide a link to the Creative Commons license, and indicate if changes were made. The images or other third party material in this article are included in the article's Creative Commons license, unless indicated otherwise in a credit line to the material. If material is not included in the article's Creative Commons license and your intended use is not permitted by statutory regulation or exceeds the permitted use, you will need to obtain permission directly from the copyright holder. To view a copy of this license, visit <http://creativecommons.org/licenses/by/4.0/>.

© The Author(s) 2020

